NASA Contractor Report 165829

NASA-CR-165829-VOL-2
19820024469

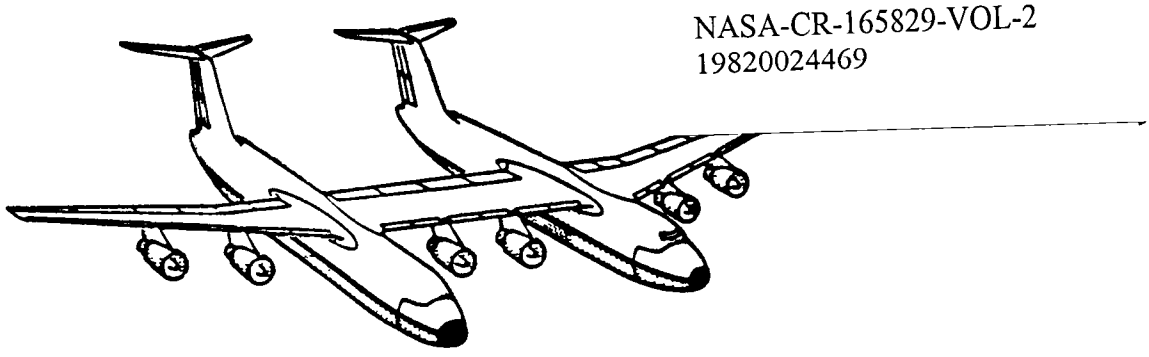

MULTIBODY AIRCRAFT STUDY APPENDIXES-VOLUME II

J. W. Moore; E. P. Craven;
B. T. Farmer; J. F. Honrath;
R. E. Stephens; R. T. Meyer

LOCKHEED-GEORGIA COMPANY
A Division of Lockheed Corporation
Marietta, Georgia 30063

Contract No. NAS1-15927
JULY 1982

National Aeronautics and
Space Administration

Langley Research Center
Hampton, Virginia 23665

NASA Contractor Report 165829

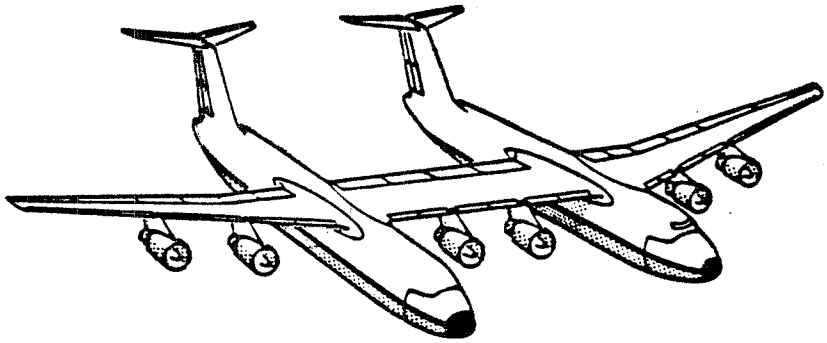

MULTIBODY AIRCRAFT STUDY APPENDIXES-VOLUME II

J. W. Moore; E. P. Craven;
B. T. Farmer; J. F. Honrath;
R. E. Stephens; R. T. Meyer

LOCKHEED-GEORGIA COMPANY
A Division of Lockheed Corporation
Marietta, Georgia 30063

Contract No. NAS1-15927
JULY 1982

National Aeronautics and
Space Administration

Langley Research Center
Hampton, Virginia 23665

This Page Intentionally Left Blank

NASA
NASA

This Page Intentionally Left Blank

TABLE OF CONTENTS

TABLE OF CONTENTS (Cont'd)

TABLE OF CONTENTS (Cont'd)

TABLE OF CONTENTS (Cont'd)

TABLE OF CONTENTS (Cont'd)

This Page Intentionally Left Blank

LIST OF FIGURES

(APPENDIXES)

LIST OF FIGURES Cont'd)

(APPENDIXES)

LIST OF FIGURES Cont'd)

(APPENDIXES)

LIST OF FIGURES Cont'd)

(APPENDIXES)

LIST OF FIGURES Cont'd)

(APPENDIXES)

LIST OF FIGURES Cont'd)

(APPENDIXES)

LIST OF FIGURES Cont'd)

(APPENDIXES)

LIST OF FIGURES Cont'd)

(APPENDIXES)

LIST OF FIGURES Cont'd)

(APPENDIXES)

LIST OF FIGURES Cont'd)

(APPENDIXES)

LIST OF FIGURES Cont'd)

(APPENDIXES)

LIST OF FIGURES Cont'd)

(APPENDIXES)

LIST OF FIGURES Cont'd)

(APPENDIXES)

LIST OF FIGURES Cont'd)

(APPENDIXES)

APPENDIX A

FUSELAGE SIZING AND SELECTION

A.1 INTRODUCTION

The initial analysis required in the definition of the point design aircraft is the fuselage sizing and selection. Although the point design aircraft are analyzed at a payload of 350,000 kg (771,618 lb), payload values of 75,000 kg (165,347 lb), 167,000 kg (368,172 lb), and 258,000 kg (568,793 lb) are also included in this analysis for subsequent use in the payload sensitivity studies.

A.2 SIZING REQUIREMENTS

The four payloads noted above are to be transported in 2.44m x 2.44m x 3.05m or 6.10m (8 x 8 x 10 ft or 20 ft) containers at a net payload density of 160.2 kg/m^3 (10.0 lb/ft^3). Sufficient clearance is required between containers and between containers and structure for a cargo restraint system. A walkway is required at each end of the cargo floor. Pressurization requirements are as specified in section 2.1, Design Requirements.

A.3 MULTIBODY FUSELAGE SIZING

Initially, conventional C-5 type fuselage cross sections, with external corners being formed by two intersecting circular arcs, are developed for one, two, three, and four rows (sticks) of containers with structural clearances and floor beam depths based on previous fuselage cross section development experience. This initial estimation of fuselage characteristics permits fuselage development to continue while computer programs are designed and basic loads determined for a structural analysis of minimum structural clearances and beam depths required for each of the stick arrangements.

Lateral clearance between containers and between containers and structure is 15.2 cm (6 in) to permit installation of cargo restraint systems. Cargo floor width and fuselage constant section perimeter, cross-sectional area, and equivalent diameter are determined for each stick arrangement and are shown in Figure A-1.

Cargo floor lengths are determined based on cargo floor width, fuselage payload, cargo density, linear container spacing of 7.6 cm (3 in), and the 2.44m x 2.44m x 3.05m (8 x 8 x 10 ft) container.

Each container has an empty weight of 499.0 kg (1100 lb) and an internal

NO. OF STICKS	FLOOR WIDTH m (FT)	FUSELAGE EFFICIENCY	FUSELAGE CONSTANT SECTION		
			PERIMETER m (FT)	EQUIVALENT DIA. - m (FT)	X-SECTION AREA SQ. m. (SQ. FT)
1	2.74 (9)	0.394	13.78 (45.2)	4.39 (14.4)	15.09 (162.4)
2	5.33 (17.5)	0.363	20.36(66.8)	6.46 (21.2)	32.72 (352.2)
3	7.92 (26)	0.309	27.34 (89.7)	8.56 (28.1)	57.65 (620.5)
4	10.52 (34.5)	0.258	34.69 (113.8)	10.85 (35.6)	92.29 (993.4)

Figure A-1. Fuselage Constant Dimensions

volume of 16.4 m^3 (580 ft^3). This results in a loaded container weight of 3129.8 kg (6900 lb) using the prescribed payload density. The payload density is allowed to vary slightly for all payloads to avoid fractional containers in any fuselage.

Rectangular cargo floor lengths are determined for each fuselage payload and for one through four sticks of containers. It is recognized that some of the wider cargo floors will possibly permit tapering into the fore and afterbody to reduce fuselage length, with the attendant reductions in weight and drag. This aspect is investigated in the final design phase.

The rectangular cargo floor length is established as the fuselage constant section length. Fuselage lengths are then a result of the constant section lengths, plus fineness ratios of 1.5 for the forebody and 2.5 for the afterbody, multiplied by the equivalent fuselage diameter shown in Figure A-1.

Wetted areas are calculated for each fuselage based on the perimeter and length of the constant section and on an empirical formula for the fore and afterbody. This procedure yields fairly accurate results and eliminates the time and cost of fully developing the entire matrix of fuselages.

Lastly, a total fuselage fineness ratio (L/D_e) is calculated for each fuselage. These fineness ratios, along with the other foregoing fuselage data, are shown in Figure A-2.

A.4 PRELIMINARY FUSELAGE SELECTION

The selection of the stick arrangement for a given payload is predicated primarily on wetted area and total fuselage L/D_e, although fuselage efficiency (container(s) cross section area/fuselage cross section area) is also considered. As shown in Figure A-1, fuselage efficiency increases as cargo floor width decreases. This

AIRCRAFT PAYLOAD - kg (LB)	75,000 (165,347)							
NUMBER OF FUSELAGES	3				2			
FUSELAGE PAYLOAD - kg (LB)	25,002 (55,120)				37,503 (82,680)			
NUMBER OF STICKS	1	2	3	4	1	2	3	4
NUMBER OF CONTAINERS*	8	8	9	8	12	12	12	12
CONSTANT SECTION FLOOR LENGTH - m (FT)	25.30 (83)	12.80 (42)	9.45 (31)	6.40 (21)	37.19 (122)	19.51 (64)	13.11 (43)	10.06 (33)
FUSELAGE LENGTH - m (FT)	42.98 (141)	38.71 (127)	43.89 (144)	49.99 (164)	54.56 (179)	45.11 (148)	47.55 (156)	53.64 (176)
WETTED AREA - SQ. m (SQ. FT.)	514 (5530)	621 (6680)	898 (9670)	1251 (13,470)	677 (7290)	757 (8150)	999 (10,750)	1379 (14,840)
FUSELAGE FINENESS RATIO - L/D_e	9.8	6.0	5.1	4.6	12.4	6.9	5.6	4.9
SELECTED STICK ARRANGEMENT	X				X			

AIRCRAFT PAYLOAD - kg (LB)	167,000 (368,172)							
NUMBER OF FUSELAGES	3				2			
FUSELAGE PAYLOAD - kg (LB)	55,669 (122,730)				83,502 (184,090)			
NUMBER OF STICKS	1	2	3	4	1	2	3	4
NUMBER OF CONTAINERS*	18	18	18	20	27	28	27	28
CONSTANT SECTION FLOOR LENGTH - m (FT)	55.47 (182)	28.04 (92)	18.59 (61)	15.54 (51)	85.04 (279)	44.20 (145)	28.65 (94)	22.56 (74)
FUSELAGE LENGTH - m (FT)	73.15 (240)	53.95 (177)	53.04 (174)	59.13 (194)	102.72 (337)	70.10 (230)	63.09 (207)	66.14 (217)
WETTED AREA - SQ. m. (SQ. FT.)	930 (10,010)	929 (10,000)	1149 (12,370)	1568 (16,880)	1337 (14,390)	1260 (13,560)	1424 (15,330)	1812 (19,500)
FUSELAGE FINENESS RATIO - L/D_e	16.7	8.3	6.2	5.4	23.4	10.9	7.4	6.1
SELECTED STICK ARRANGEMENT		X				X		

* 2.44 m x 2.44 m x 3.05 m (8 FT x 8 FT x 10 FT)

Figure A-2. Fuselage Sizing and Selection - Multibody (Sheet 1 of 2)

AIRCRAFT PAYLOAD - kg (LB)	258,000 (568,793)							
NUMBER OF FUSELAGES	3				2			
FUSELAGE PAYLOAD - kg (LB)	86,001 (189,600)				129,002 (284,400)			
NUMBER OF STICKS	1	2	3	4	1	2	3	4
NUMBER OF CONTAINERS*	28	28	27	28	42	42	42	44
CONSTANT SECTION FLOOR LENGTH - m (FT)	87.48 (287)	43.89 (144)	28.04 (92)	21.64 (71)	131.06 (430)	66.75 (219)	44.50 (146)	37.19 (122)
FUSELAGE LENGTH - m (FT)	105.16 (345)	69.80 (229)	62.48 (205)	65.23 (214)	148.74 (488)	92.66 (304)	78.94 (259)	80.77 (265)
WETTED AREA - SQ. m. (SQ.FT.)	1370 (14,750)	1253 (13,490)	1407 (15,150)	1780 (19,160)	1971 (21,220)	1719 (18,500)	1857 (19,990)	2319 (24,960)
FUSELAGE FINENESS RATIO - L/D_e	23.9	10.8	7.3	6.0	33.9	14.3	9.2	7.4
SELECTED STICK ARRANGEMENT		X					X	

AIRCRAFT PAYLOAD - kg (LB)	350,000 (771,618)							
NUMBER OF FUSELAGES	3				2			
FUSELAGE PAYLOAD - kg (LB)	116,664 (257,200)				175,000 (385,810)			
NUMBER OF STICKS	1	2	3	4	1	2	3	4
NUMBER OF CONTAINERS*	37	36	36	36	56	56	57	56
CONSTANT SECTION FLOOR LENGTH - m (FT)	117.96 (387)	56.08 (184)	37.49 (123)	28.35 (93)	174.96 (574)	88.09 (289)	58.83 (193)	44.50 (146)
FUSELAGE LENGTH - m (FT)	135.64 (445)	81.99 (269)	71.93 (236)	71.93 (236)	192.63 (632)	114.00 (374)	92.66 (304)	88.09 (289)
WETTED AREA - SQ m. (SQ. Ft.)	1790 (19,270)	1501 (16,160)	1666 (17,930)	2012 (21,660)	2575 (27,720)	2153 (23,180)	2249 (24,210)	2573 (27,700)
FUSELAGE FINENESS RATIO - L/D_e	30.9	12.7	8.4	6.6	43.9	17.6	10.8	8.1
SELECTED STICK ARRANGEMENT			X				X	

* 2.44 m x 2 44 m x 3.05 m (8 Ft x 8 Ft x 10 FT)

Figure A-2. Fuselage Sizing and Selection - Multibody (Sheet 2 of 2)

alone dicates selection of the single stick configuration in all cases; however, as noted in Figure A-2, the other selection parameters can have a much more significant impact. Cargo floor lengths are also considered since previous experience has shown that rectangular floor lengths in excess of 61.0m (200 ft) dictate fuselage lengths which limit the desired aircraft rotation on takeoff. This, in turn, can cause excessive cargo floor heights and restrictions on side force turns (tip over angles).

Figure A-3 shows forebody, afterbody, and total fuselage fineness ratios versus Mach number. These data are used as a guide for the multibody fuselage design; however, total fuselage L/D_e is not a "design to" absolute to the exclusion of the other design requirements. In addition, the forebody fineness ratio of the multibody fuselages is increased to 1.5, relative to the 1.25 shown for Mach 0.80, due to the protrusion of the flight deck considerably outside of fuselage contour for nose loading/unloading of cargo. Figure A-3 also shows that the preferred total fuselage L/D_e for the Mach 0.80 speed is in the area of 9.25. It is of note that the C-5, C-141, and 747 are all in close agreement with this curve.

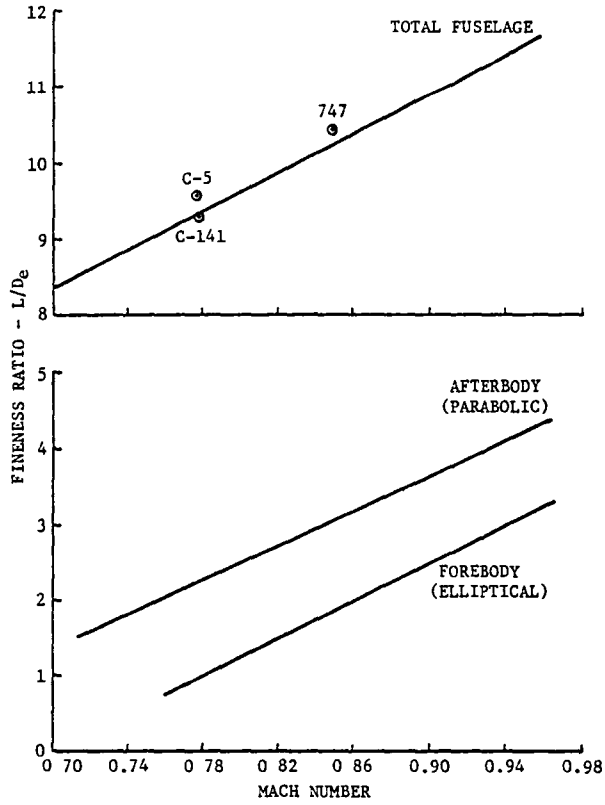

Figure A-3. Effect of Mach Number on Fuselage Fineness Ratio (Uncambered)

Referring again to Figure A-2, the bottom row shows the selected stick arrangement, for all fuselage payloads, which is based on an evaluation of the previously noted selection parameters. Since the four-stick arrangement is shown to generally have an undesirable L/D_e, invariably the largest wetted area and lowest fuselage efficiency, it is dropped from further consideration.

A.5 FINAL FUSELAGE SELECTION

Structural clearance and floor beam depth analyses are performed on two fuselage cross sections. One is the conventional C-5 type cross section

previously described, and the other is identified as being "oval" with its external corners being defined by four intersecting arcs. The primary objective of the oval shape is to minimize the fuselage cross section area required to encompass the containerized payload. The reduced cargo compartment pressure altitude requirement of 5486.4 m (18,000 ft) up to 12,192.0 m (40,000 ft) for these aircraft, as compared to a requirement of 2438.4 m (8000 ft) up to an altitude of 12,192.0 m (40,000 ft) for current transport aircraft such as the C-5 and C-141, results in the feasibility of this fuselage shape.

The fuselage cross sections and the resulting payload/stick arrangement are given in Figures A-4 through A-6 for the conventional shape and in Figures A-7 through A-9 for the oval shape.

Since the 75,000 kg (165,347 lb) (1-stick) payload conventional fuselage constant section is nearly a perfect circle, it offers the lowest cross sectional area, wetted area, and pressure volume; therefore, a one stick oval fuselage offers no advantages and is not evaluated. This payload arrangement is the only one having a 2.7 m (9 ft) access to the cargo compartment. The three larger payloads all have a 5.33 m (17.5 ft) access and varying degrees of tapered floor plans to maximize the fuselage efficiency and minimize the fuselage wetted area.

Fuselage summary data resulting from the cross section and floor plan data of the previous figures are given in Figures A-10 and A-11 for the three and two-body aircraft, respectively. Fuselage lengths are derived by maintaining forebody and afterbody fineness ratios of 1.5 and 2.5, respectively, based on fuselage maximum cross section area equivalent diameter. Fuselage wetted area, pressure volume, and efficiency are determined for each fuselage alternative. From these data it is seen that not only do the oval shaped fuselages provide the maximum efficiency, both wetted surface area and pressure volume are minimized. Fuselage skin friction and weight decrease as wetted surface area decreases; therefore, it can be expected that the oval fuselage at all payload values will result in the minimum weight and drag aircraft.

Two and three-body aircraft are sized for each fuselage alternative using direct operating cost (DOC) as the optimizing parameter. Summary data for each of the resulting aircraft are given in Figures A-12 and A-13. It is noted that the DOC data contained in these figures are derived based upon a fuel cost of 15.1 ¢/l (57 ¢/gal) and 1979 dollars.

Results of the aircraft sizing indicate that the conventional fuselage shape provides the minimum DOC for the 167,000 kg (368,172 lb) payload air-

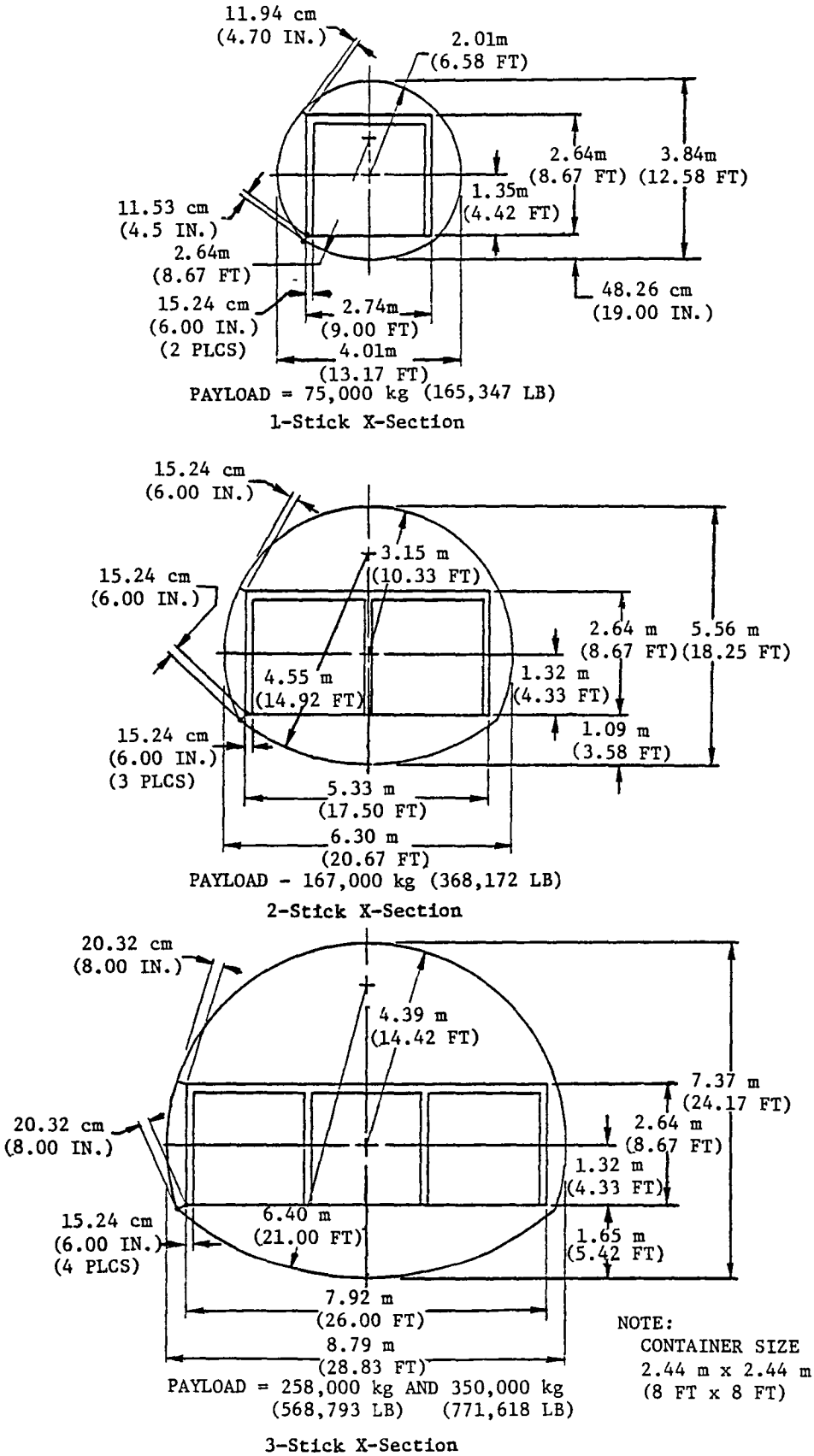

Figure A-4. Fuselage X-Sections - Conventional

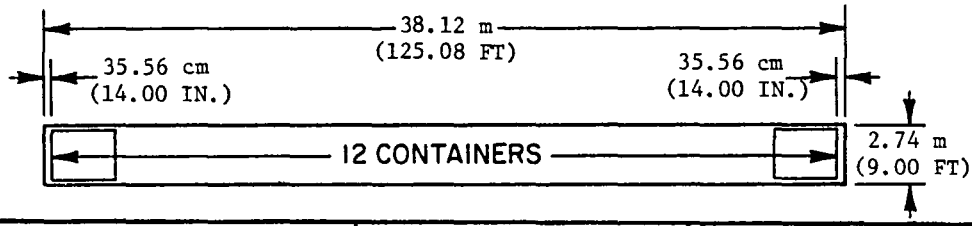

PAYLOAD kg (LB)		NO. OF CONTAINERS 2.44m x 2.44m x 3.05m (8 FT x 8 FT x 10 FT)		NET PAYLOAD DENSITY kg/m^3 (LB/FT^3)	FLOOR AREA m^2(FT^2)
PER A/C	PER FUS	PER A/C	PER FUS		
75,000 (165,349)	37,500 (82,674)	24	12	159.86 (9.98)	105 (1126)

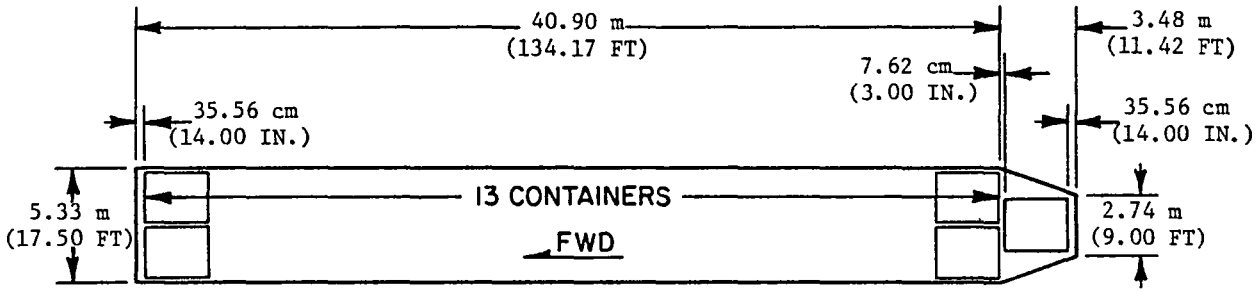

PAYLOAD kg (LB)		NO. OF CONTAINERS 2.44m x 2.44m x 3.05m (8 FT x 8 FT x 10 FT)		NET PAYLOAD DENSITY kg/m^3 (LB/FT^3)	FLOOR AREA	
					RECT m^2(FT^2)	TOTAL m^2(FT^2)
PER A/C	PER FUS	PER A/C	PER FUS			
167,000 (368,172)	83,500 (184,086)	54	27	157.94 (9.86)	220 (2368)	234 (2520)

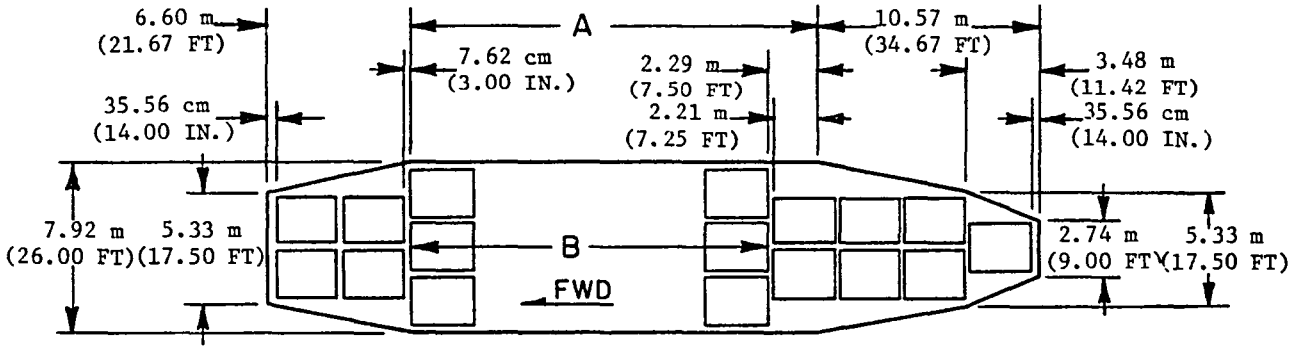

PAYLOAD kg (LB)		DIMENSION A-m (FT)	NO. OF CONTAINERS 2.44m x 2.44m x 3.05m (8 FT x 8 FT x 10 FT)			NET PAYLOAD DENSITY kg/m^3 (LB/FT^3)	FLOOR AREA	
							RECT. m^2(FT^2)	TOTAL m^2(FT^2)
PER A/C	PER FUS		B	PER A/C	PER FUS			
258,000 (568,793)	129,000 (284,397)	33.45 (109.75)	10	82	41	161.15 (10.06)	265 (2854)	370 (3982)
350,000 (771,618)	175,000 (385,809)	49.07 (161.00)	15	112	56	159.86 (9.98)	389 (4186)	494 (5314)

Figure A-5. Cargo Compartment - Two-Body Conventional Fuselage

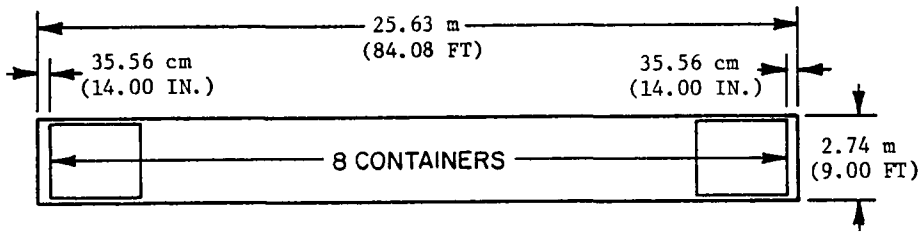

PAYLOAD kg (LB)		NO. OF CONTAINERS 2.44m x 2.44m x 3.05m (8 FT x 8 FT x 10 FT)		NET PAYLOAD DENSITY kg/m^3 (LB/FT^3)	FLOOR AREA m^2 (FT^2)
PER A/C	PER FUS	PER A/C	PER FUS		
75,000 (165,349)	25,000 (55,116)	24	8	159.86 (9.98)	70 (757)

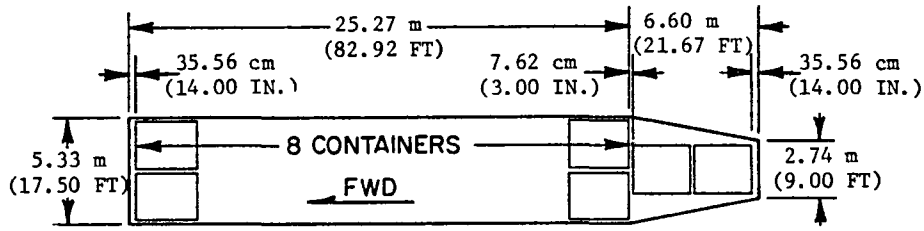

PAYLOAD kg (LB)		NO. OF CONTAINERS 2.44m x 2.44m x 3.05m (8 FT x 8 FT x 10 FT)		NET PAYLOAD DENSITY kg/m^3 (LB/FT^3)	FLOOR AREA	
					RECT m^2 (FT^2)	TOTAL m^2 (FT^2)
PER A/C	PER FUS	PER A/C	PER FUS			
167,000 (368,172)	55,667 (122,724)	54	18	157.94 (9.86)	135 (1451)	161 (1738)

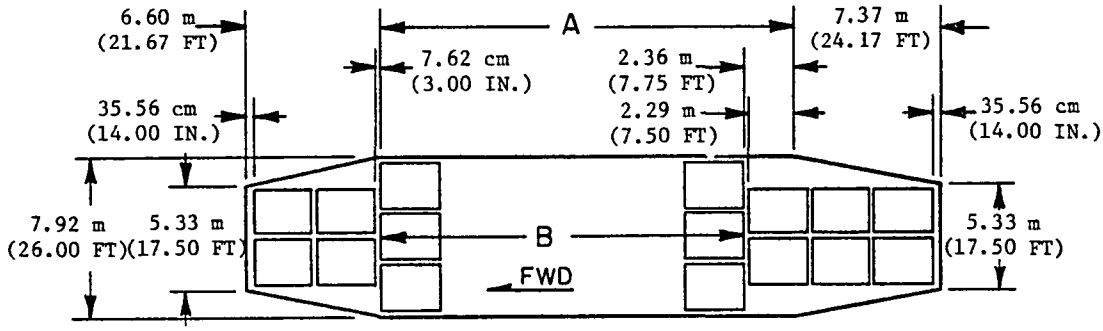

PAYLOAD kg (LB)		DIMENSION A-m (FT)	NO. OF CONTAINERS 2.44m x 2.44m x 3.05m (8 FT x 8 FT x 10 FT)			NET PAYLOAD DENSITY kg/m^3 (LB/FT^3)	FLOOR AREA	
							RECT. m^2 (FT^2)	TOTAL m^2 (FT^2)
PER A/C	PER FUS		B	PER A/C	PER FUS			
258,000 (568,793)	86,000 (189,598)	21.03 (69.00)	6	84	28	156.66 (9.78)	167 (1794)	259 (2791)
350,000 (771,618)	116,667 (257,206)	30.40 (99.75)	9	111	37	161.63 (10.09)	241 (2594)	334 (3591)

Figure A-6. Cargo Compartment - Three-Body Conventional Fuselage

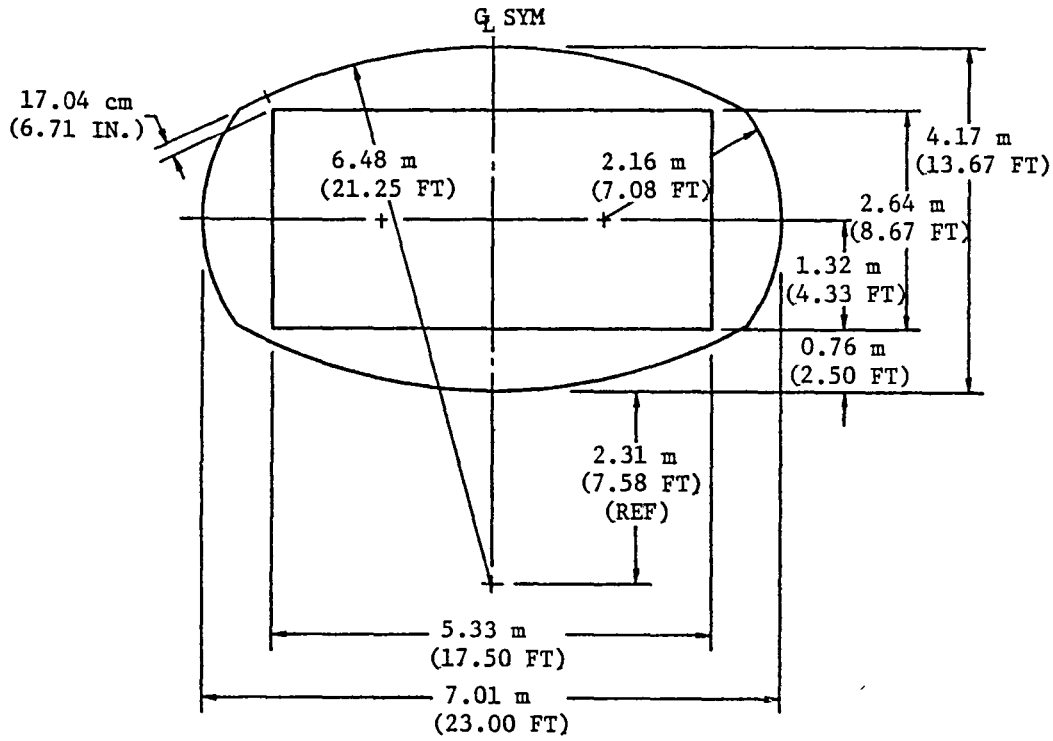

PAYLOAD = 167,000 kg (368,172 LB)

2-Stick X-Section

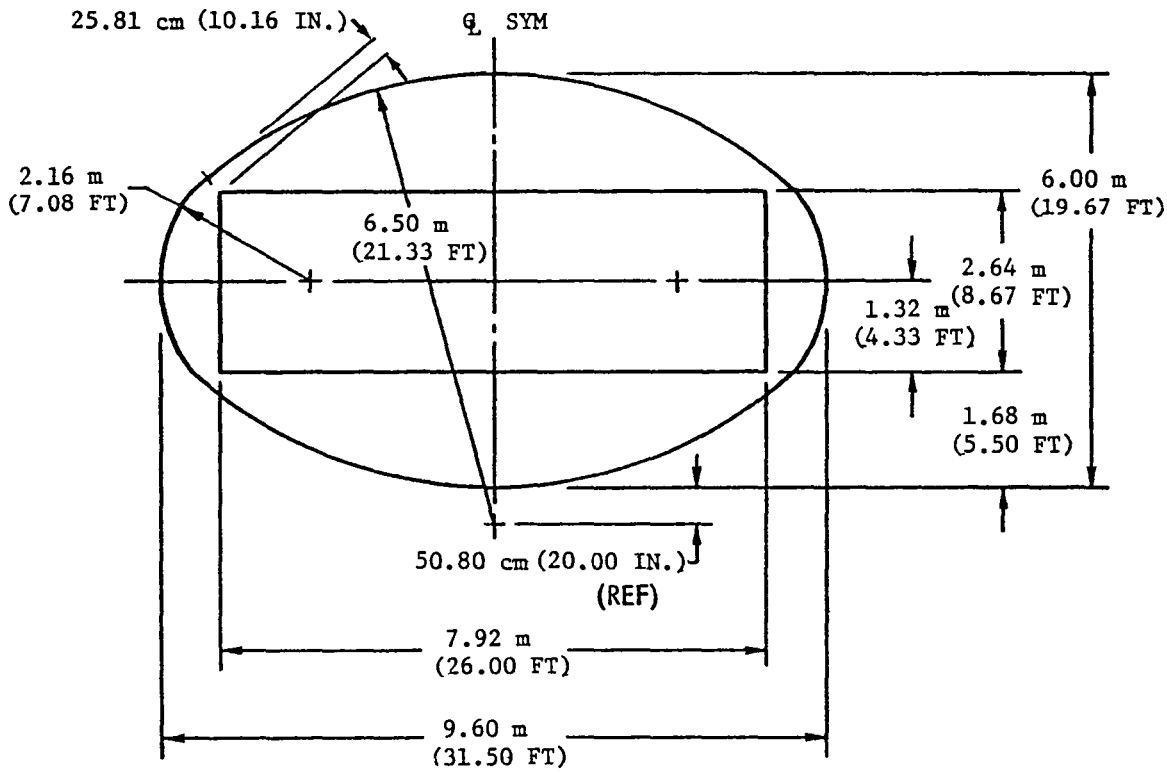

PAYLOAD = 258,000 kg AND 350,000 kg
(568,793 LB) (771,618 LB)

3-Stick X-Section

Figure A-7. Fuselage X-Sections - Oval

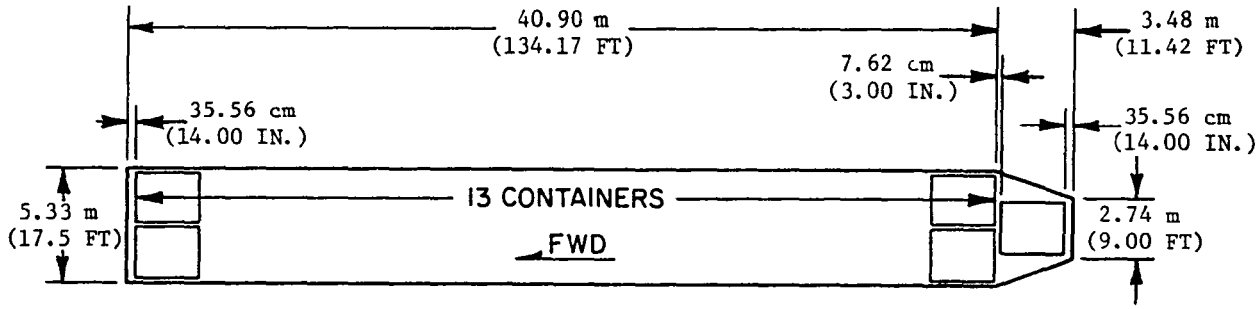

PAYLOAD kg (LB)		NO. OF CONTAINERS 2.44m x 2.44m x 3.05m (8 FT x 8 FT x 10 FT)		NET PAYLOAD DENSITY	FLOOR AREA	
PER A/C	PER FUS	PER A/C	PER FUS	kg/m^3 (LB/FT^3)	RECT. m^2 (FT^2)	TOTAL m^2 (FT^2)
167,000 (368,172)	83,500 (184,086)	54	27	157.94 (9.86)	220 (2368)	234 (2520)

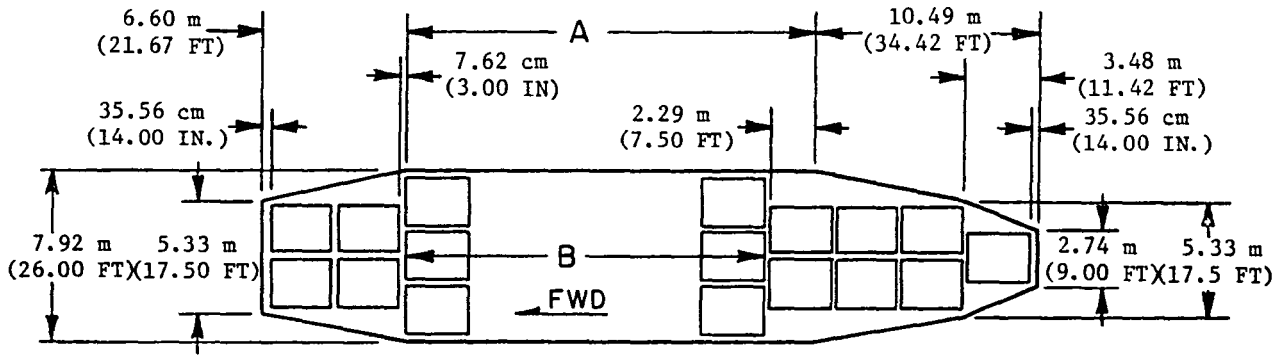

PAYLOAD kg (LB)		DIMENSION A-m (FT)	NO. OF CONTAINERS 2.44m x 2.44m x 3.05m (8 FT x 8 FT x 10 FT)			NET PAYLOAD DENSITY	FLOOR AREA	
PER A/C	PER FUS		B	PER A/C	PER FUS	kg/m^3 (LB/FT^3)	RECT. m^2 (FT^2)	TOTAL m^2 (FT^2)
258,000 (568,793)	129,000 (284,397)	33.53 (110.00)	10	82	41	161.15 (10.06)	266 (2861)	370 (3983)
350,000 (771,618)	175,000 (385,809)	49.15 (161.25)	15	112	56	159.86 (9.98)	390 (4193)	494 (5315)

Figure A-8. Cargo Compartment - Two-Body Oval Fuselage

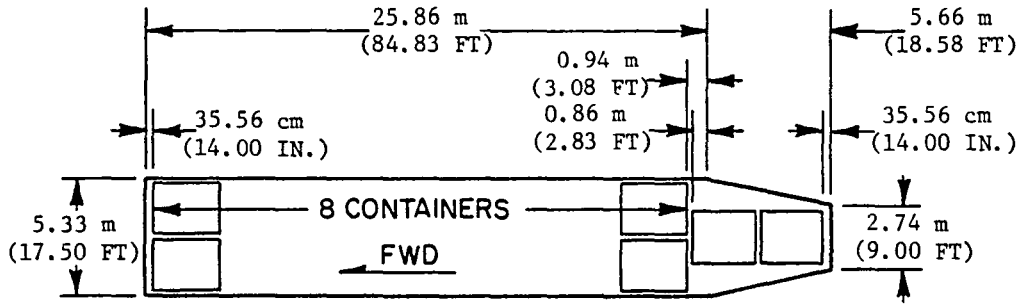

PAYLOAD kg (LB)		NO. OF CONTAINERS 2.44m x 2.44m x 3.05m (8 FT x 8 FT x 10 FT)		NET PAYLOAD DENSITY kg/m^3 (LB/FT^3)	FLOOR AREA	
					RECT m^2(FT^2)	TOTAL m^2(FT^2)
PER A/C	PER FUS	PER A/C	PER FUS			
167,000 (368,172)	55,667 (122,724)	54	18	157.94 (9.86)	140 (1505)	163 (1751)

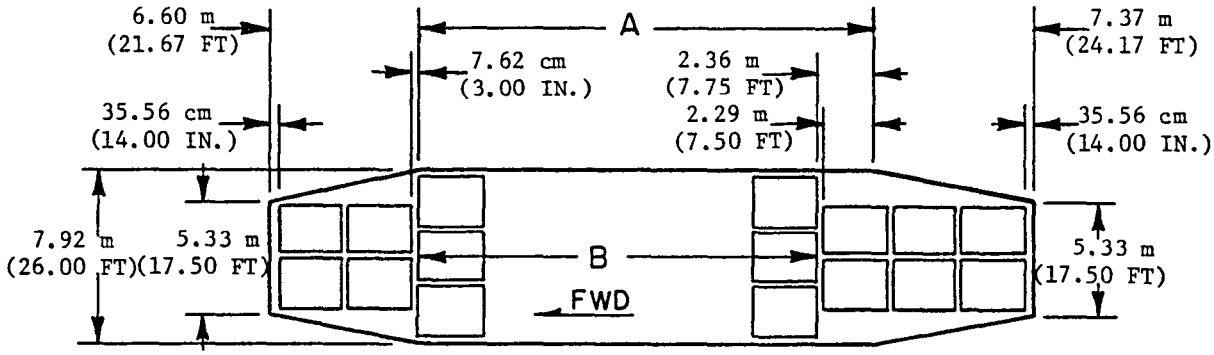

PAYLOAD kg (LB)		DIMENSION A-m (FT)	NO. OF CONTAINERS 2.44m x 2.44m x 3.05m (8 FT x 8 FT x 10 FT)			NET PAYLOAD DENSITY kg/m^3 (LB/FT^3)	FLOOR AREA	
							RECT. m^2(FT^2)	TOTAL m^2(FT^2)
PER A/C	PER FUS		B	PER A/C	PER FUS			
258,000 (568,793)	86,000 (189,598)	21.03 (69.00)	6	84	28	156.66 (9.78)	167 (1794)	259 (2791)
350,000 (771,618)	116,667 (257,206)	30.40 (99.75)	9	111	37	161.63 (10.09)	241 (2594)	334 (3591)

Figure A-9. Cargo Compartment - Three-Body Oval Fuselage

METRIC UNITS

PAYLOAD PER FUSELAGE-kg	25,000	55,667		86,000		116,667	
FUSELAGE SHAPE CONVENTIONAL (C) OVAL (O)	C	C	O	C	O	C	O
FUSELAGE DIMENSIONS - m							
LENGTH	42.34	49.45	48.56	53.49	51.49	62 87	60.86
WIDTH	4.01	6.30	7.01	8.79	9.60	8.79	9.60
HEIGHT	3.83	5 56	4.17	7.37	6.00	7.37	6.00
MAXIMUM X-SECT AREA-SQ.m	12.27	28.06	23.24	51.49	44.35	51.49	44.35
FUSELAGE EQUIVALENT DIA - m	3.95	5.98	5.44	8.10	7 52	8.10	7 52
WETTED AREA - SQ. m (AW)	484	799	788	1125	1014	1366	1246
PRESSURIZED VOLUME - CU. m	382	1033	904	1759	1534	2241	1950
TOTAL CONTAINERS (2.44m x 2.44m x 3.05m)	8	18	18	28	28	37	37
FUSELAGE EFFICIENCY AC/AF	0.4845	0.4238	0.5117	0.3464	0.4022	0.3464	0.4022
FUSELAGE PAYLOAD/AW	10.59	14.27	14.47	15.66	17.38	17.49	19.18
NUMBER OF STICKS	1	2	2	3	3	3	3

CUSTOMARY UNITS

PAYLOAD PER FUSELAGE-LB	55,116	122,724		189,598		257,206	
FUSELAGE SHAPE CONVENTIONAL (C) OVAL (O)	C	C	O	C	O	C	O
FUSELAGE DIMENSIONS-FT							
LENGTH	138.92	162.25	159.33	175.50	168.92	206.25	199.67
WIDTH	13.17	20.67	23.00	28.83	31.50	28.83	31.50
HEIGHT	12.58	18.25	13.67	24.17	19.67	24.17	19.67
MAXIMUM X-SECT AREA-SQ. FT.	132.10	302.00	250.17	554.20	477.43	554.20	477.43
FUSELAGE EQUIVALENT DIA-FT.	12.97	19.61	17.85	26.56	24.66	26.56	24.66
WETTED AREA-SQ. FT. (AW)	5,206	8,601	8,482	12,105	10,912	14,703	13,413
PRESSURIZED VOLUME - CU. FT.	13,496	36,488	31,943	62,131	54,193	79,173	68,874
TOTAL CONTAINERS-8'x8'x10'	8	18	18	28	28	37	37
FUSELAGE EFFICIENCY AC/AF	0.4845	0.4238	0.5117	0.3464	0.4022	0.3464	0.4022
FUSELAGE PAYLOAD/AW	10.59	14.27	14.47	15.66	17.38	17.49	19.18
NUMBER OF STICKS	1	2	2	3	3	3	3

Figure A-10. Fuselage Data Summary - Three-Body

METRIC UNITS

PAYLOAD PER FUSELAGE - kg	37,500	83,500		129,000		175,000	
FUSELAGE SHAPE CONVENTIONAL (C) OVAL (O)	C	C	O	C	O	C	O
FUSELAGE DIMENSIONS - m							
LENGTH	54.84	65.43	63.25	65.91	63.98	81.76	79.60
WIDTH	4.01	6.30	7.01	8 79	9.60	8.79	9.60
HEIGHT	3.83	5.56	4.17	7 37	6.00	7.37	6.00
MAXIMUM X-SECT AREA - SQ.m.	12.27	28.06	23.24	51.49	44.35	51.49	44.35
FUSELAGE EQUIVALENT DIA-M	3.95	5.98	5.44	8.10	7.52	8.10	7.52
WETTED AREA - SQ.m. (A_w)	639	1089	1058	1443	1324	1845	1711
PRESSURIZED VOLUME - CU m.	536	1413	1209	2548	2168	3351	2861
TOTAL CONTAINERS (2.44 m x 2.44 m x 3.05 m)	12	27	27	41	41	56	56
FUSELAGE EFFICIENCY (A_c/A_f)	0.4845	0.4238	0.5117	0.3464	0.4022	0.3464	0.4022
FUSELAGE PAYLOAD/A_w	12.02	15.70	16.16	18.32	19.96	19.43	20.95
NUMBER OF STICKS	1	2	2	3	3	3	3

CUSTOMARY UNITS

PAYLOAD PER FUSELAGE - LB	82,674	184,086		284,397		385,809	
FUSELAGE SHAPE CONVENTIONAL (C) OVAL (O)	C	C	O	C	O	C	O
FUSELAGE DIMENSIONS - FT							
LENGTH	179.92	214.67	207.50	216.25	209.92	268.25	261.17
WIDTH	13.17	20.67	23.00	28.83	31.50	28.83	31.50
HEIGHT	12.58	18.25	13.67	24.17	19.67	24.17	19.67
MAXIMUM X-SECT AREA - SQ.FT.	132.10	302.00	250.17	554.20	477.43	554.20	477.43
FUSELAGE EQUIVALENT DIA-FT	12.97	19.61	17.85	26.56	24.66	26.56	24.66
WETTED AREA - SQ.FT. (A_w)	6,879	11.727	11,388	15,527	14,246	19,858	18,414
PRESSURIZED VOLUME - CU.FT.	18,912	49,913	42,693	89,966	76,562	118,336	101,031
TOTAL CONTAINERS (8 FT x 8 FT x 10 FT)	12	27	27	41	41	56	56
FUSELAGE EFFICIENCY A_c/A_f	0.4845	0.4238	0.5117	0.3464	0.4022	0.3464	0.4022
FUSELAGE PAYLOAD/A_w	12.02	15.70	16.16	18.32	19.96	19.43	20.95
NUMBER OF STICKS	1	2	2	3	3	3	3

Figure A-11. Fuselage Data Summary - Two-Body

METRIC UNITS

PAYLOAD - kg	75,000	167,000		258,000		350,000	
FUSELAGE SHAPE CONVENTIONAL (C) OVAL (O)	C	C	O	C	O	C	O
GEOMETRY							
WING ASPECT RATIO	13 32	13 13	12 47	11 78	11 70	10 44	10 70
AREA - 10 SQ m	33 9	74 6	79 7	113 1	115 0	161 3	164 3
FUSELAGE BODY SEPARATION - m	25 9	38.1	38.4	44 4	44.7	50 0	51.0
WEIGHTS - 1000 kg							
STRUCTURE	67.9	143 3	150 1	207 9	202.2	283.5	284 0
WING	23 6	59 3	57 7	90 2	88.0	122 0	123 6
EMPENNAGE	2.4	6 1	5.9	10 3	10 4	13.3	13.6
FUSELAGE	32.5	58.6	66 8	78.3	75 1	110 8	107.6
LANDING GEAR	7 4	15.4	15 8	23 2	22 9	27 4	31 4
NACELLE & PYLON	2.0	3.9	3.9	5 9	5 8	5 9	7 8
PROPULSION SYSTEM	11.5	23.7	24.1	37 2	36.4	51 7	50 5
SYSTEMS & EQUIPMENT	11 7	16.3	16 2	20 1	19 9	24.0	23.8
WEIGHT EMPTY	91 1	183.3	190.4	265 2	258 5	359.2	358.3
OPERATING EQUIPMENT	1 8	3.9	4 1	6 1	6 1	9 6	9 7
OPERATING WEIGHT	92.9	187 2	194.5	271.3	264.6	368.8	368.0
PAYLOAD	75.0	167 0	167 0	258 0	258 0	350 0	350 0
FUEL MISSION	53 4	107 1	108 6	163 3	160 0	221.4	217 3
GROSS	221 3	461.3	470 1	692 6	682.6	940 2	935 3
PROPULSION							
THRUST/ENGINE - 1000 N	111.7	222.4	225.5	340 7	333 6	462 2	452 4
PERFORMANCE							
CRUISE L/D	22.04	23 04	23.16	22.59	22 75	22 61	22.98
BLOCK FUEL - 1000 kg	44 7	89.7	91 0	136 8	133.9	185.4	181 9
FUSELAGE DRAG	0 00795	0 00601	0 00541	0.00524	0 00478	0 00424	0.00393
EQUIVALENT PARASITE DRAG AREA-Sq m	2 00	3 32	3 23	4.50	4 15	5 49	5 11
ECONOMIC							
FUEL PRICE $/l	0 15	0.15	0 15	0 15	0 15	0 15	0 15
AIRCRAFT PRICE $M	41 3	93 9	95 3	154 1	150 0	226 6	225.0
DOC-¢/AMgkm	4 89	4 15	4 21	4 05	3 96	4 08	4.04
FUSELAGE WEIGHT/PAYLOAD	0.434	0.351	0 400	0.304	0 291	0 317	0.308
Mg-km/l	8.73	9.69	9 55	9 82	10 02	9 83	10.01

CUSTOMARY UNITS

PAYLOAD - LB	165,347	368,172		568,793		771,618	
FUSELAGE SHAPE CONVENTIONAL (C) OVAL (O)	C	C	O	C	O	C	O
GEOMETRY							
WING ASPECT RATIO	13.32	13 13	12.47	11.78	11.70	10.44	10.70
AREA - 100 SQ FT	36.5	80.3	85.8	121.7	123.8	173 6	176.8
FUSELAGE BODY SEPARATION-FT.	84 9	125.0	125.9	145.8	146.5	163.9	167.4
WEIGHTS-1000 LB							
STRUCTURE	149.7	316.0	330 9	458 3	445 8	625 0	626.1
WING	52.0	130 7	127 3	198 8	194.1	269 0	272.6
EMPENNAGE	5.2	13.4	12.9	22.8	23 0	29 3	30 0
FUSELAGE	71.7	129.2	147.3	172 7	165 6	244.3	237.3
LANDING GEAR	16 3	34 1	34 7	51.0	50 4	60 4	69 0
NACELLE & PYLON	4 5	8.6	8.7	13.0	12.7	13.0	17.2
PROPULSION SYSTEM	25.4	52.3	53 1	82.1	80.2	113.9	111.3
SYSTEMS & EQUIPMENT	25.7	35 8	35.8	44.3	43.8	52 9	52 4
WEIGHT EMPTY	200.8	404.1	419 8	584.7	569.8	791.8	790.0
OPERATING EQUIPMENT	4.0	8.5	8 9	13.5	13 6	21.3	21.2
OPERATING WEIGHT	204 8	412.6	428 7	598.2	583 4	813.1	811.2
PAYLOAD	165 3	368 2	368.2	568.8	568 8	771 6	771.6
FUEL MISSION	117.8	236.2	239.6	360 0	352.6	488 1	479.2
GROSS	487 9	1017 0	1036 5	1527 0	1504 8	2072.8	2062.0
PROPULSION							
THRUST/ENGINE-1000 LB	25 1	50.0	50 7	76.6	75.0	103.9	101.7
PERFORMANCE							
CRUISE L/D	22 04	23 04	23 16	22 59	22.75	22 61	22 98
BLOCK FUEL-1000 LB.	98.6	197 7	200 6	301.6	295 3	408.7	401.1
FUSELAGE DRAG	0 00795	0.00601	0 00541	0 00524	0 00478	0 00424	0.00393
EQUIVALENT PARASITE AREA-SQ FT	21.49	35 71	34.75	48 45	44 64	59 12	55 04
ECONOMIC							
FUEL PRICE - $ GAL	0 57	0 57	0 57	0 57	0 57	0 57	0 57
AIRCRAFT PRICE MILLION $	41.3	93.9	95 3	154 1	150 0	226 6	225 0
DOC ¢/ATNM	8 22	6 98	7 07	6 80	6 65	6 86	6 79
FUSELAGE WEIGHT/PAYLOAD	0.434	0 351	0 400	0 304	0.291	0.317	0 308
TON NM/GAL. FUEL	19.67	21 83	21 52	22.12	22 58	22.14	22.55

Figure A-12. Fuselage Study - Two-Body Aircraft Data Summary

METRIC UNITS

PAYLOAD - kg	75,000	167,000		258,000		350,000	
FUSELAGE SHAPE CONVENTIONAL (C) OVAL (O)	C	C	O	C	O	C	O
GEOMETRY							
WING ASPECT RATIO	12 03	11 05	11 00	10 13	10 46	9 05	9 57
AREA - 10 SQ m	37 1	81 2	88 9	132 1	132.4	175.6	184 0
FUSELAGE BODY SEPARATION - m	25 7	36 5	38 1	44 5	45.3	48 5	51.1
WEIGHTS-1000 kg							
STRUCTURE	77 3	158 4	173 7	248 4	249 2	325 2	317 7
WING	31 4	74 1	78 5	120 4	126 3	157 5	154 7
EMPENNAGE	2.6	7 3	7 4	12 9	13 0	15 8	17 4
FUSELAGE	33 2	56 5	66 4	83 0	78 1	109 2	104 1
LANDING GEAR	7 9	16 3	17 0	25 4	25 3	33 8	33 2
NACELLE & PYLON	2 2	4 3	4 4	6 7	6 4	8 8	8 4
PROPULSION SYSTEM	12 6	26 1	26 8	42 8	41 1	58 0	54 7
SYSTEMS & EQUIPMENT	12 2	17 1	17 3	21 9	21 7	25 4	25 3
WEIGHT EMPTY	102 1	201 5	217 8	313 1	311 9	408.5	397 7
OPERATING EQUIPMENT	1 9	4.1	4 2	6 7	6 5	10 0	9 1
OPERATING WEIGHT	13 2	205 5	221 9	319 8	318 4	418 5	406.9
PAYLOAD	75 0	167 0	167 0	258 0	258 0	350 0	350 0
FUEL-MISSION	57 9	116 5	119 7	203 5	179 0	244 8	233 8
GROSS	236 9	487 2	508 7	762 9	755 5	1013 3	990 6
PROPULSION							
THRUST/ENGINE-1000 N	121 4	243 3	249 5	388.3	373 7	514 2	488.0
PERFORMANCE							
CRUISE L/D	21 66	22.34	22 66	21.84	22 47	21.93	22 58
BLOCK FUEL - 1000 kg	48 5	97 4	100 1	154 8	149 6	204.7	195 4
FUSELAGE DRAG	0 00821	0 00590	0.00534	0 00518	0 00476	0 00437	0.00450
EQUIVALENT PARASITE DRAG AREA-SQ m	2 35	3 78	3.73	5 50	4.97	6.43	5 87
ECONOMIC							
FUEL PRICE $/l	0 15	0.15	0.15	0.15	0 15	0 15	0.15
AIRCRAFT PRICE $M	44 9	101.9	107 3	176.7	175.2	253 4	247 8
DOC-¢/ AMgkm	5 23	4.5	4 64	4 57	4 49	4 49	4 37
FUSELAGE WEIGHT/PAYLOAD	0 443	0 338	0.398	0 322	0 303	0 312	0 297
Mg-km/l	8.05	8.92	8.68	8.67	8.97	8.90	9.32

CUSTOMARY UNITS

PAYLOAD - LB	165,347	368,172		568,793		771,618	
FUSELAGE SHAPE CONVENTIONAL (C) OVAL (O)	C	C	O	C	O	C	O
GEOMETRY							
WING ASPECT RATIO	12.03	11 05	11 00	10.13	10.46	9 05	9.57
AREA - 100 SQ FT	39 9	87.4	95 7	142.2	142.5	189.0	198.1
FUSELAGE BODY SEPARATION-FT.	84.3	119 6	124.9	146.1	148 6	159 2	167 6
WEIGHTS-1000 LB							
STRUCTURE	170 4	349 3	382 9	547.6	549 3	717 0	700.3
WING	69.3	163 4	173 0	265 4	278.5	347.3	341.0
EMPENNAGE	5 7	16.1	16.3	28 5	28 7	34.9	38.4
FUSELAGE	73.2	124.5	146 4	183.0	172 1	240.8	229.4
LANDING GEAR	17 4	36 0	37 5	56.0	55.7	74.5	73.1
NACELLE & PYLON	4 8	9 4	9 6	14 8	14.2	19.5	18 5
PROPULSION SYSTEM	27 7	57.5	59.0	94 4	90.6	127 8	120 7
SYSTEMS & EQUIPMENT	27.0	37.7	38 2	48 3	47 9	55.9	55 8
WEIGHT EMPTY	225.1	444 2	480 1	690.3	687 7	900 6	876.8
OPERATING EQUIPMENT	4 1	9.0	9.3	14 7	14.3	22.0	20.1
OPERATING WEIGHT	229.2	453 1	489 3	705 0	702 0	922.6	897 0
PAYLOAD	165 3	368 2	368.2	568 8	568 7	771.6	771.6
FUEL MISSION	127.7	256 8	264.0	448.7	394 6	539.7	515.4
GROSS	522 2	1074.1	1121 5	1681 9	1665 5	2233 9	2184 0
PROPULSION							
THRUST/ENGINE-1000 LB	27 3	54.7	56.1	87 3	84 0	115 6	109 7
PERFORMANCE							
CRUISE L/D	21.66	22.34	22 66	21 84	22 47	21 93	22.58
BLOCK FUEL - 1000 LB	106 9	214.8	220 7	341 2	329 8	451.2	430 8
FUSELAGE DRAG	0 00821	0.00590	0 00534	0 00518	0 00476	0 00437	0.00450
EQUIVALENT PARASITE AREA - SQ FT.	25 25	40 67	40 18	59 24	53 55	69 16	63 21
ECONOMIC							
FUEL PRICE - $/GAL	0 57	0 57	0 57	0 57	0 57	0 57	0 57
AIRCRAFT PRICE $M	44 9	101 9	107 3	176 7	175 2	253 4	247 8
DOC-¢/ATNM	8 79	7.50	7 79	7 67	7 54	7 55	7 34
FUSELAGE WEIGHT/PAYLOAD	0 443	0 338	0 398	0 322	0 303	0 312	0 297
TON NM/GAL FUEL	18 14	20 10	19 56	19 54	20 22	20 05	21 00

Figure A-13. Fuselage Study - Three-Body Aircraft Data Summary

craft and the oval fuselage shape provides the minimum DOC for the 258,000 kg (568,793 lb) and 350,000 kg (771,618 lb) payload aircraft. Although the 167,000 kg (368,172 lb) payload oval fuselage aircraft has a lower wetted area and drag than the conventional fuselage aircraft, its weight is higher. For this two-stick arrangement the wetted area and drag advantages are offset by the decrease in structural efficiency of the oval shape compared to the conventional shape. The conventional shape has only two breaks in the external contour where pressure loads must be reacted by tension ties to prevent fuselage cover bending loads. The oval shape has four external contour breaks resulting in additional structural elements to react the pressure loads. From the aircraft sizing data it is shown that not until the three-stick arrangement of the two higher payloads is reached does the decrease in fuselage wetted area and drag offset the reduced structural efficiency of the oval shape.

Based upon the data presented, the following shape selections are made as a function of aircraft payload value for both the two-body and three-body configurations:

Payload - kg (lb)	Fuselage Shape	No. Sticks
75,000 (165,347)	Conventional	1
167,000 (368,172)	Conventional	2
258,000 (568,793)	Oval	3
350,000 (771,618)	Oval	3

A.6 OVAL SHAPE FUSELAGE ANALYSIS

The oval shape offered the advantages of minimizing cross sectional fuselage area to enclose a given cargo compartment while retaining the ability to react internal pressure as hoop tension in the skin. However, the design produces inefficiencies resulting from the kick loads generated at the intersections of the circular arcs and the presence of the high hoop tension stresses occurring in the large radius arcs. Tension ties are required to react the loads. Several additional variables which influence the fuselage structural weight are cabin pressure, underfloor depth, cargo floor width, and pressure skin curvature. The oval section weight factors derived for this study reflect the difference in oval and conventional shapes and are shown in Figure A-14. A section weight factor of 1.00 is assigned to conventional C-5 type shapes.

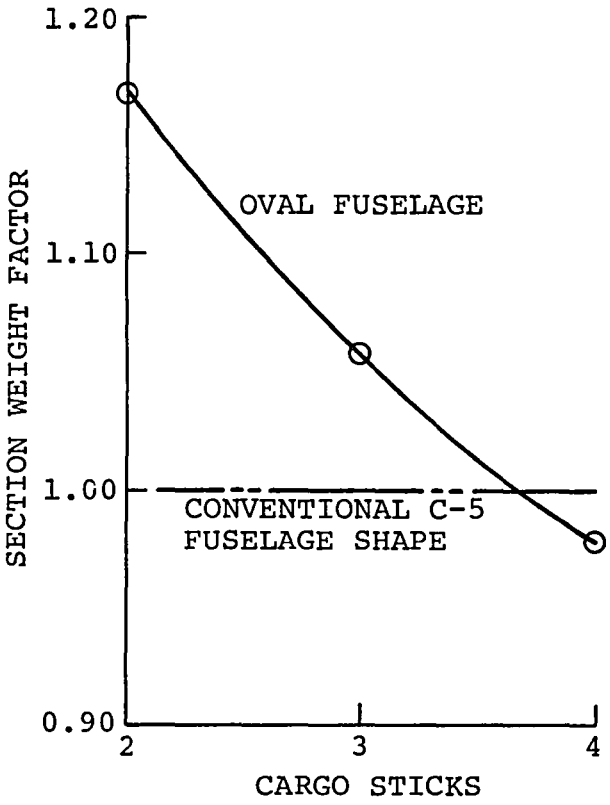

Figure A-14. Section Weight Factor vs Cargo Sticks

In the conventional fuselage, the enclosure above the cargo floor is a single circular cylinder with the radius defined to clear a predetermined cargo envelope. The region below the cargo floor is not constrained in cross sectional area by cargo envelope requirements and can be optimized for best structural depth. This is not true for the oval shape. The oval fuselage section for the two and three stick cargo arrangements are seventeen and six percent heavier, respectively, than conventional shapes. The fact that one section is heavier than another does not indicate a preference for selection. The data used for selection of either oval or conventional aircraft are presented in Section A.5.

The section weight factor for the four stick oval shape is two percent lighter than that for the conventional shape. Fuselages for wide cargo compartments result in considerable amounts of unusable volume above the compartment. In this case the disadvantage of the unusable volume of the conventional shape offsets the disadvantages previously discussed for the oval shape. The four stick container arrangement is required to minimize the length of the cargo compartment for very large payloads.

Three oval shape configuration options are analyzed as shown in Figure A-15. The primary variable defining each of these shapes is the underfloor beam depth. Each of the three configuration options has the same compartment cross section and fuselage width. Configuration 1 has the minimum beam depth and cross section area. This results in the highest fuselage efficiency, (ratio of container/ fuselage area). The only disadvantage associated with this configuration is that it has the highest section weight factor. Configuration 2 has an increased beam depth of 25 percent and a cross section area increase of 10 percent compared to configuration 1. This reduces the

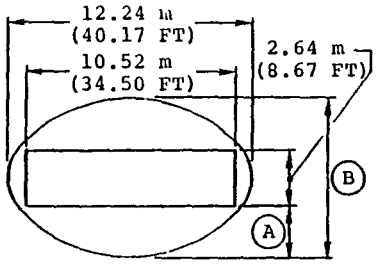

	CONFIGURATION OPTIONS		
	1	2	3
(A) BEAM DEPTH - cm (IN.)	203.20 (80.00)	254.00 (100.00)	330.20 (130.00)
(B) FUSELAGE HEIGHT - m (FT)	6.71 (22.00)	7.72 (25.33)	9.24 (30.33)
X-SECTION - SQ. m (SQ. FT)	65 (695)	71 (766)	84 (904)
EQUIVALENT DIA. - m (FT)	9.05 (29.70)	9.51 (31.20)	10.33 (33.90)
PERIMETER - m (FT)	30.48 (100.00)	31.09 (102.00)	33.22 (109.00)
FUSELAGE EFFICIENCY	0.368	0.334	0.283
SECTION WEIGHT FACTOR	1.07	0.98	0.97

Figure A-15. Oval Fuselage Cross-Section Shape Comparison

fuselage efficiency by 9 percent, and the section weight factor by 8.4 percent. Configuration 3 has the lowest fuselage efficiency and section weight factor as its beam depth of 330 cm (130 inches) approaches that of a full circular fuselage having a 480 cm (189 inch) beam depth.

To further evaluate the oval shapes, a fuselage was sized for each of the three section configurations. Summary data for each fuselage is shown in Figure A-16. Each fuselage has a forward body fineness ratio (λ) of 1.5, an aft λ of 2.5, and a total fuselage λ in excess of 11. All cargo floors are 94.5 m (310 feet) long and have access to permit simultaneous loading of two sticks of cargo. The container arrangement for options 1 and 2 is identical. Configuration option 3 has the minimum constant section length and accommodates more containers in the tapered areas, thus producing the minimum fuselage length and wetted area.

The three fuselages have a maximum length variation of only three percent, however, the increase in wetted area from configuration option 1 to 3 is nine percent. The changes in wetted areas for configurations 1 and 2 are not significant. A plot of the fuselage weight as related to the floor beam depth is shown in Figure A-17. The minimum weight fuselage has a constant section floor beam depth of 254 cm (100 inch) (Configuration No. 2). The fuselage weight is directly proportional to the aircraft gross weight; thus, configuration 2 fuselage is selected as one of the configurations

CONFIGURATION OPTION	1	2	3
BEAM DEPTH - cm (IN.)	203.20 (80.00)	254.00 (100.00)	330.20 (130.00)
CONSTANT SECTION LENGTH-m (FT)	76.17 (249.90)	73.49 (241.10)	73.15 (240.00)
TOTAL LENGTH - m (FT)	112.44 (368.90)	111.53 (365.90)	114.70 (376.30)
WETTED AREA - SQ. m (SQ. FT)	3057 (32,900)	3066 (33,000)	3335 (35,900)
FUSELAGE λ	12.4	11.7	11.1

Figure A-16. Fuselage Summary Data

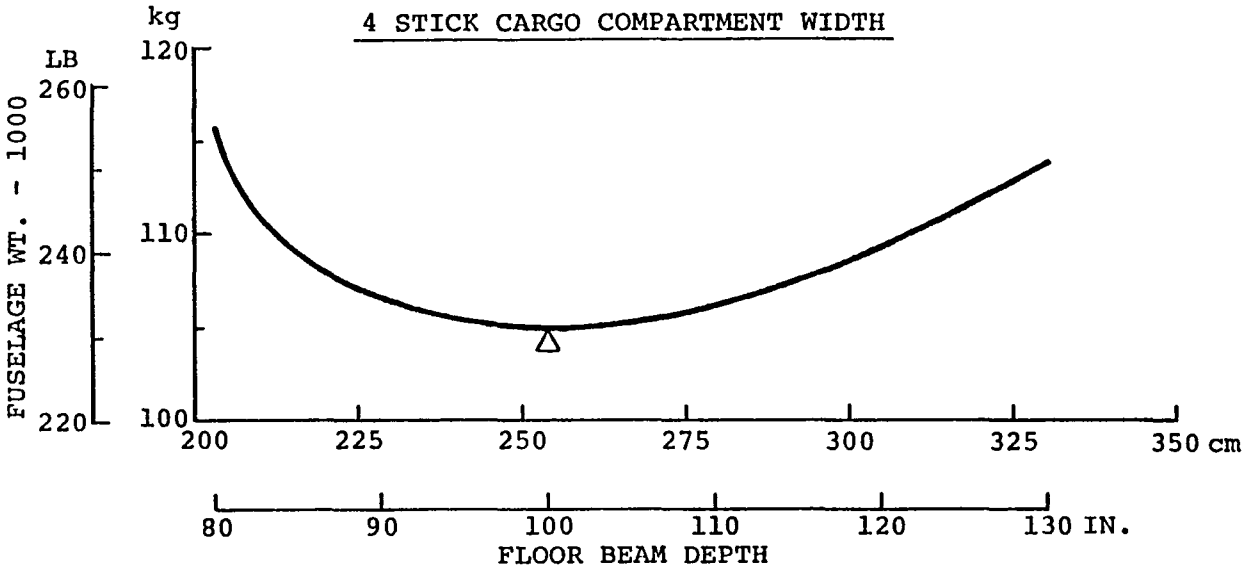

Figure A-17. Oval Fuselage Weight vs Constant Section Floor Beam Depth

used in the single body fuselage sizing and selection study (Section A-7).

A.7 SINGLEBODY FUSELAGE SIZING AND SELECTION

Payloads and sizing requirements for the single body reference aircraft fuselages are the same as those shown for the multibody fuselages, except that each payload herein is to be transported in a single fuselage. Since the payloads are accommodated in a single fuselage, certain fuselage cross sections are eliminated based on geometric data. For example, a 75,000 kg (165,347 lb) payload, 24 containers in a four-stick arrangement results in a total fuselage L/D_e of 4.7. Of this value, 4.0 is solely for the forebody and afterbody which results in a virtually nonexistent fuselage constant section. Conversely, a 350,000 kg (771,618 lb) payload, 112 containers, in a single-stick arrangement results in a fuselage 365.8 m (1200 ft) in

length. Evaluation of and selections from more reasonable combinations of payloads, cross sections, and stick arrangements are shown in Figure A-18.

For the 75,000kg (165,347 lb) payload, conventional fuselages are developed using the data previously shown in Figures A-4 and A-5. Corresponding data for the oval fuselages is shown in Figures A-7 and A-8. Although the 75,000 kg (165,347 lb) payload, two-stick oval fuselage has a lower wetted area (drag) than the corresponding conventional fuselage, as shown in Figure A-18, its weight is higher. For this two-stick arrangement, the wetted area advantage is offset by the decrease in structural efficiency of the oval shape compared to the conventional shape. The same effect is shown for the 167,000 kg (368,172 lb) payload for the multibody fuselage sizing and selection, along with an explanation for the structural efficiency decrease. The conventional fuselage with a two-stick arrangement is selected for the 75,000 kg (165,347 lb) payload single body reference aircraft for the above reason and because it has the preferred L/D_e, as it relates to Figure A-3, for Mach 0.80.

The conventional fuselage for the 167,000 kg (368,172 lb) payload is based on the three-stick arrangement shown in Figures A-4 and A-5. The oval fuselages are based on data shown in Figure A-7 and the corresponding floor plans shown in Figure A-8. The oval shape with a three-stick arrangement is selected for this payload since, as shown in Figure A-18, this fuselage has the better L/D_e and fuselage efficiency combination and the lower wetted area.

For the larger payloads, 258,000 kg (568,793 lb) and 350,000 kg (771,618 lb), a four-stick arrangement is required for the single body reference aircraft. It is evident from Figure A-18 that the three-stick arrangement has a very high L/D_e for the largest payload. The fuselage cross section and floor plan for the four-stick configuration are shown in Figure A-19. In Figures A-12 and A-13 the multibody three-stick oval fuselage aircraft are shown to have lower DOC than the three-stick conventional fuselage aircraft for the above payloads. Based on these data, the oval shape fuselage is selected for the four stick arrangement single body reference aircraft.

Stick arrangements greater than four are not evaluated. A five-stick arrangement has a fuselage width of approximately 15.2 m (50 ft) and a cargo floor width of 13.1 m (43 ft). This is believed to be excessive, due in part to the forebody fineness ratio as it relates to the nose visor door opening, to the structural span required for the cargo floor width, and to frontal area increases.

PAYLOAD - kg (LB)	75,000 (165,347)				
NUMBER OF CONTAINERS	24				
TYPE FUSELAGE C = CONVENTIONAL O = OVAL	C			O	
NUMBER OF STICKS	1	2	3	2	3
FUSELAGE LENGTH - m (FT)	91 (298)	62 (204)	48 (157)	60 (197)	46 (150)
WETTED AREA - m^2 (FT^2)	1,067 (11,487)	1,034 (11,130)	964 (10,372)	979 (10,542)	888 (9,557)
FUSELAGE FINENESS RATIO - L/D_e	22.9	10.4	5.9	11.0	6.0
FUSELAGE EFFICIENCY	0.484	0.424	0.346	0.512	0.402
SELECTED FUSELAGE SHAPE & STICK ARRANGEMENT		X			

PAYLOAD - kg (LB)	167,000 (368,172)			258,000 (568,793)		350,000 (771,618)	
NUMBER OF CONTAINERS	54			82		112	
TYPE FUSELAGE C = CONVENTIONAL O = OVAL	C	O		O		O	
NUMBER OF STICKS	3	2	3	3	4	3	4
FUSELAGE LENGTH - m (FT)	76 (250)	106 (348)	74 (243)	105 (345)	87 (284)	136 (447)	112 (366)
WETTED AREA - m^2 (FT^2)	1,702 (18,315)	1,825 (19,647)	1,598 (17,197)	2,368 (25,492)	2,302 (24,780)	3,139 (33,784)	3,064 (32,980)
FUSELAGE FINENESS RATIO - L/D_e	9.4	19.5	9.8	14.0	9.1	18.1	11.7
FUSELAGE EFFICIENCY	0.346	0.512	0.402	0.402	0.335	0.402	0.335
SELECTED FUSELAGE SHAPE & STICK ARRANGEMENT			X		X		X

Figure A-18. Fuselage Sizing and Selection - Single Body Reference

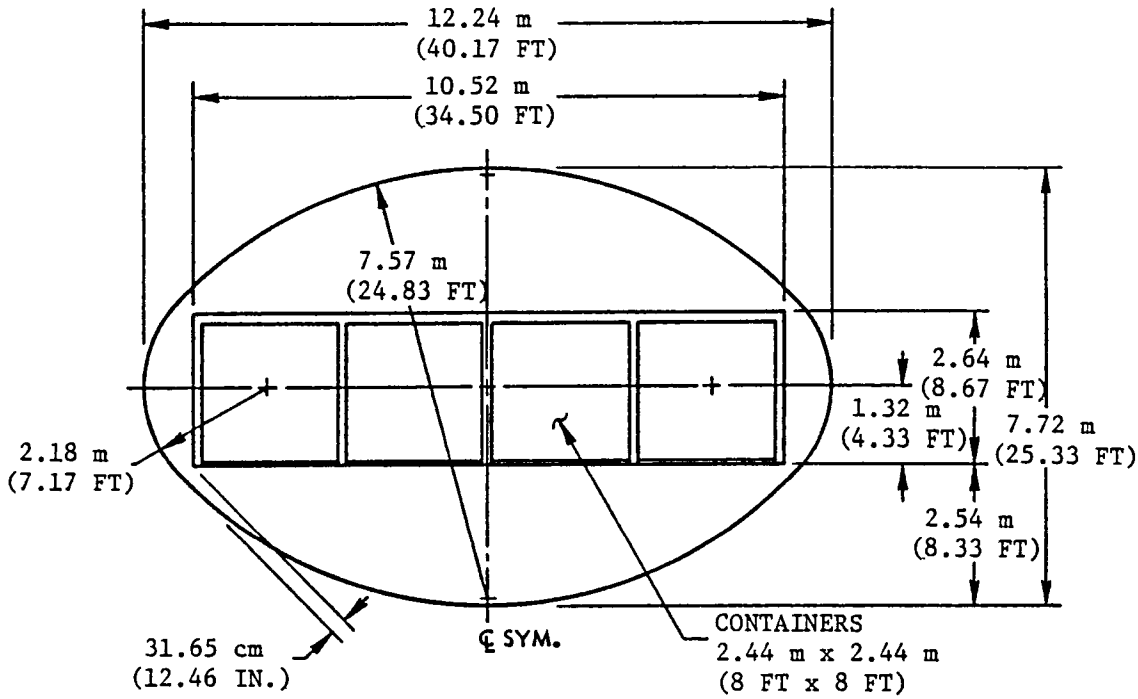

4-STICK OVAL FUSELAGE X-SECTION SBR

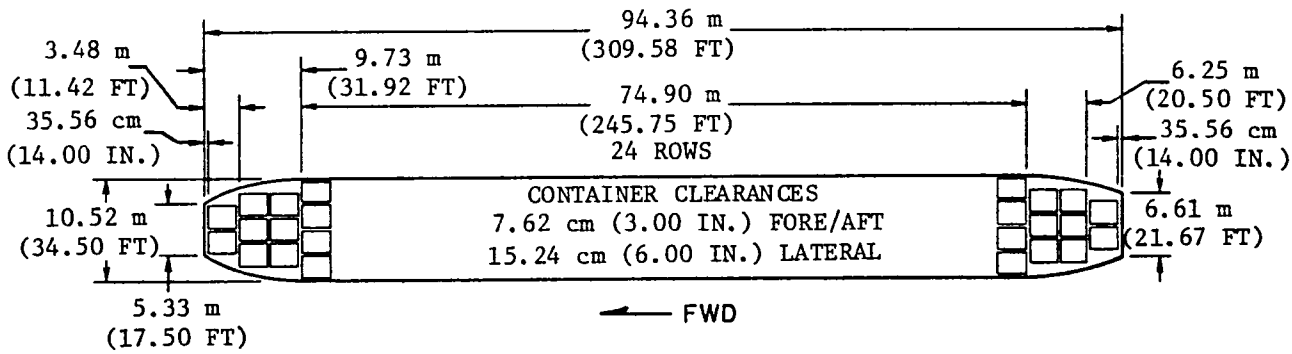

PAYLOAD kg (LB)	NO. OF CONTAINERS 2.44m x 2.44m x 3.05m (8 FT x 8 FT x 10 FT)	NET PAYLOAD DENSITY kg/m^3 (LB/FT^3)	FLOOR AREA	
			RECT. m^2(FT^2)	TOTAL m^2(FT^2)
350,000 (771,618)	112	159.86 (9.98)	788 (8,478)	957 (10,300)

Figure A-19. Oval Fuselage Data - Single Body Reference

Fuselages for the 258,000 kg (568,793 lb) payload are developed based on data shown in Figure A-7 and A-8 for the three-stick arrangement and Figure A-19 for the four-stick arrangement. Figure A-18 shows the four-stick arrangement to have the lower wetted area and the preferred L/D_e and is the selected configuration for this payload.

Since the 350,000 kg (771,618 lb) payload, three-stick arrangement, has an unacceptable L/D_e of 18.1, as shown in Figure A-18, and because stick arrangements greater than four are not evaluated, the four-stick oval is the only selection available for this payload. For these reasons, a double-lobe fuselage cross section is proposed for competitive evaluation with the four-stick oval, shown as the selected configuration in Figure A-18.

Fuselages for the 350,000 kg (771,618 lb) payload point design aircraft are developed based on data shown in Figure A-19 for the oval shape and in Figure A-20 for the double-lobe. Figure A-21 shows the double-lobe fuselage to have the lesser wetted area and greater fuselage efficiency; the oval fuselage, however, has the more desirable L/D_e, for Mach 0.80, as indicated in Figure A-3. This prevents a selection from being made based only upon these data, therefore, aicraft are sized for the two fuselage shapes and a competitive analysis is performed. The results of this analysis are shown in Figure A-22. As seen in this figure, the oval fuselage aircraft is less in weight and cost than the double-lobe configuration, though slightly higher in fuselage drag. The higher weight of the double-lobe aircraft is due primarily to the fuselage structural tie arrangement, which requires vertical tension ties at the intersection of the two lobes, and to the increased wing area and block fuel.

The selection criterion, DOC, shows the oval fuselage configuration to have the lower DOC of the two aircraft. Figure A-22 shows the oval fuselage aircraft has a DOC of 7.10¢/AMgkm (11.93¢/ATNM), versus 7.40¢/AMgkm (12.44¢ATNM) for the double-lobe aircraft, and therefore, remains the selected configuration for the 350,000 kg (771,618 lb) payload.

Selection of the single body reference aircraft fuselage type and number of sticks, versus payload, is summarized in Figure A-23.

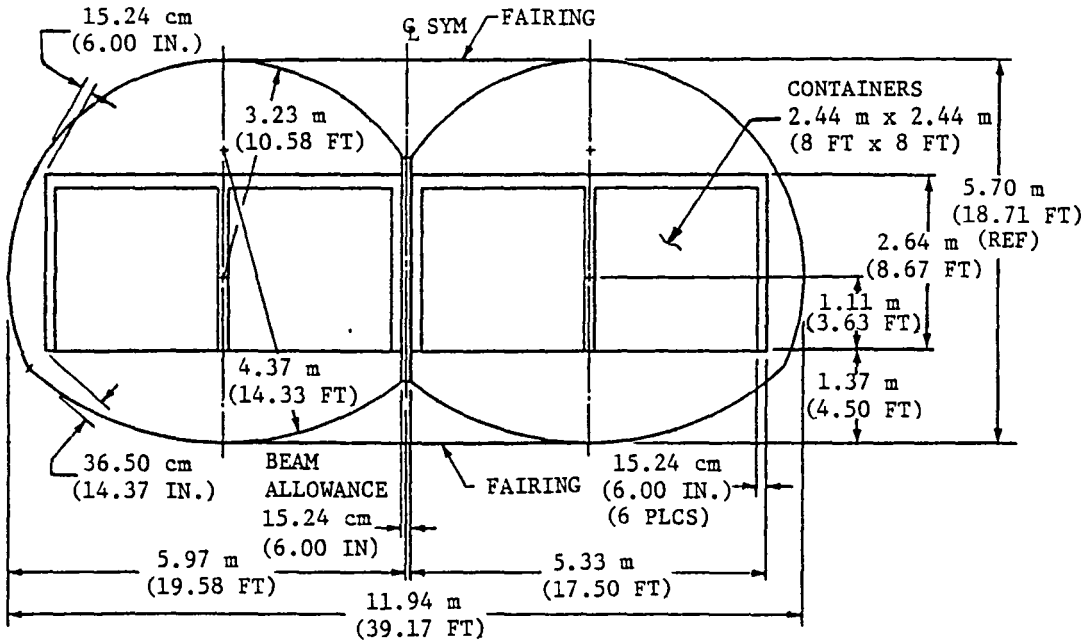

4-STICK HORIZONTAL DOUBLE-LOBE FUSELAGE X-SECTION

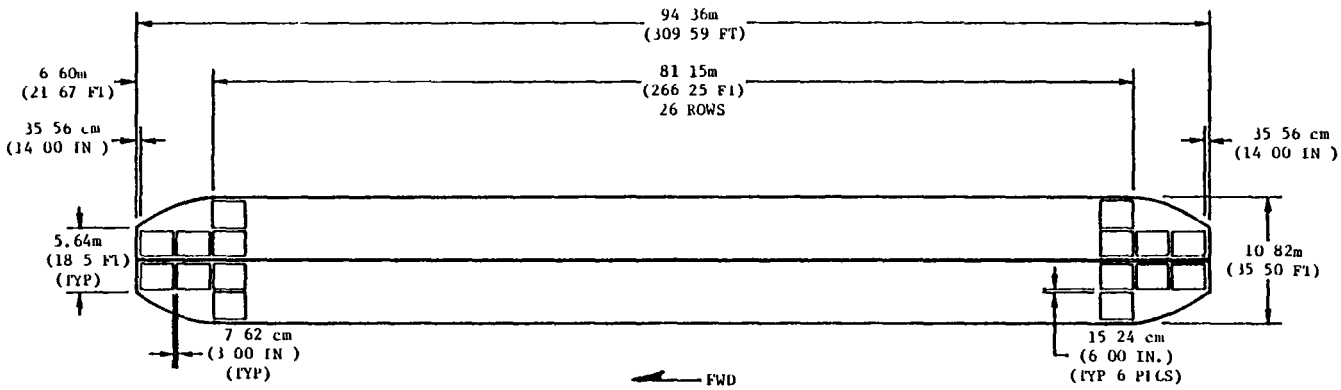

PAYLOAD kg (LB)	NO. OF CONTAINERS 2.44m x 2.44m x 3.05m (8 FT x 8 FT x 10 FT)	NET PAYLOAD DENSITY kg/m^3 (LB/FT^3)	FLOOR AREA	
			RECT. m^2(FT^2)	TOTAL m^2(FT^2)
350,000 (771,618)	112	159.86 (9.98)	878 (9,452)	1025 (11,028)

Figure A-20. Double-Lobe Fuselage Data - Single Body Reference

PAYLOAD PER FUSELAGE - kg (LB)	350,000 (771,618)	
FUSELAGE SHAPE	OVAL	HORIZONTAL DOUBLE-LOBE
FUSELAGE DIMENSIONS - m (FT)		
LENGTH	111.53 (365.91)	115.36 (378.49)
WIDTH	12.24 (40.17)	11.94 (39.17)
HEIGHT	7.72 (25.33)	5.70 (18.71)
MAX. X-SECT. AREA - SQ.m. (SQ. FT.)	71.02 (764.50)	57.45 (618.40)
FUSE. EQUIVALENT DIA. - m (FT)	9.51 (31.21)	8.55 (28.06)
WETTED AREA (A_W) - SQ.m. (SQ.FT.)	3,064 (32,983)	2,992 (32,208)
PRESSURIZED VOLUME - CU.m. (CU.FT.)	6,347 (224,156)	5,359 (189,255)
TOTAL CONTAINERS 2.44 m x 2.44 m x 3.05 m (8 FT x 8 FT x 10 FT)	112	112
FUSELAGE EFFICIENCY A_C/A_F	0.3347	0.4140
FUSELAGE PAYLOAD/A_W	23.39	23.96
NET PAYLOAD DENSITY - kg/m^3 (LB/FT^3)	159.86 (9.98)	159.86 (9.98)
FUSELAGE L/De	11.17	13.50

Figure A-21. Fuselage Data Summary - Single Body Reference

PAYLOAD - kg (LB)	350,000 (771,618)	
FUSELAGE SHAPE	OVAL	HORIZONTAL DOUBLE-LOBE
GEOMETRY		
WING ASPECT RATIO	8.93	8.93
AREA - 10 SQ.m. (100 SQ.FT.)	161.7 (174.1)	173.4 (186.6)
WEIGHTS -1000 kg (1000 LB)		
STRUCTURE	287.9 (634.8)	309.9 (683.3)
WING	122.9 (271.0)	129.0 (284.4)
EMPENNAGE	7.9 (17.4)	8.2 (18.0)
FUSELAGE	105.0 (231.5)	118.9 (262.1)
LANDING GEAR	42.0 (94.3)	44.1 (97.5)
NACELLE & PYLON	9.3 (20.6)	9.7 (21.3)
PROPULSION SYSTEM	53.4 (117.8)	55.4 (122.2)
SYSTEMS & EQUIPMENT	23.4 (51.4)	23.8 (52.4)
WEIGHT EMPTY	364.7 (804.0)	389.1 (857.8)
OPERATING EQUIPMENT	7.7 (16.9)	7.8 (17.1)
OPERATING WEIGHT	372.4 (820.9)	396.8 (874.9)
PAYLOAD	350.0 (771.6)	350.0 (771.6)
FUEL MISSION	235.5 (519.2)	243.7 (537.1)
GROSS	957.9 (2,111.7)	990.5 (2,183.6)
PROPULSION		
THRUST/ENGINE - 1000 N (1000 LB)	330.9 (74.4)	342.1 (76.9)
PERFORMANCE		
CRUISE L/D	21.48	21.47
BLOCK FUEL - 1000 kg (1000 LB)	196.9 (434.2)	203.8 (449.2)
FUSELAGE DRAG	0.00305	0.00298
EQUIV. PARISITE AREA - SQ.m. (SQ.FT.)	4.64 (49.90)	4.78 (51.43)
ECONOMIC		
FUEL PRICE - $/1 ($/GAL)	0.34 (1.30)	0.34 (1.30)
AIRCRAFT PRICE - MILLION $	303.8	321.9
DOC - ¢/AMgkm (ATNM)	7.10 (11.93)	7.40 (12.44)
FUSELAGE WEIGHT/PAYLOAD	0.300	0.340
Mg-km/1 (TON NM/GAL. FUEL)	9.25 (20.84)	8.94 (20.14)

Figure A-22. Aircraft Data Summary - Single Body Reference

PAYLOAD	75,000 kg (165,347 LB)	167,000 kg (368,172 LB)	258,000 kg (568,793 LB)	350,000 kg (771,618 LB)
TYPE FUSELAGE	CONVENTIONAL	OVAL	OVAL	OVAL
NUMBER OF STICKS	2	3	4	4

Figure A-23. Aircraft Fuselage Selection Summary - Single Body Reference

This Page Intentionally Left Blank

APPENDIX B

MULTIBODY AIRCRAFT WING EFFICIENCY AND SPANLOAD DISTRIBUTION

Studies of multibody aircraft require that an aerodynamic and structural analysis be made for a series of two-body and three-body aircraft configurations. To accomplish this analysis, the spanwise load distributions and induced drag efficiencies are required. Since experimental data for determining wing efficiencies and spanwise loads for multibody configurations are nonexistent, an analytical study is conducted to determine these effects. The investigation involves the use of two computer programs, L7 and Hess, in the determination of theoretical load distributions used for the parametric studies.

The HESS program is a subsonic, potential flow panel method program, which employs constant strength surface source panels to account for thickness effects, and superimposes a dipole lattice on lifting elements to account for circulation. While no corrections are made to include viscous effects, a first-order approximation for compressibility is made using the Gothert rule to shrink the lateral geometry by $\beta = \sqrt{1 - M^2}$. The L7 program uses a discrete vortex lattice method.

The first task involves the determination of a reasonable baseline wing. The general planform is derived from multibody preliminary wing designs which include a "batted" center wing (zero trailing-edge sweep) between the bodies. However, the basic, tapered wing is used to simplify the relocation of the bodies. As is typical in the manufacturing process, the wing is defined using linear lofting techniques with control stations at the root, tip, and mid-span location, or "break," at η=38.3 percent semispan, which corresponds to the initial fuselage location of the two and three-body configurations. Anhedral of 0.05 rad (3 degrees) is also incorporated for stability and control.

Once the planform is defined, a theoretical analysis is performed on the wing alone using the L7 program to determine a reasonable twist distribution. The analysis consists of performing a matrix of runs at a constant angle of attack, and using a constant C_L case to investigate the effects of inboard and outboard washout variations on span efficiencies. The final twist schedule is 0.07 rad (4 degrees) at

root, 0.05 rad (3 degrees) at "break," and zero rad (degrees) at tip.

The second task involves five configurations run on the HESS code. These consist of a wing-alone, a single body, two, two-bodies with different spanwise fuselage locations, and a three-body configuration. A constant fuselage model is used for all cases to provide a basis for comparison, and the relative vertical location between the fuselage and wing is governed by the height of the cargo box. No attempt is made to add fillets to the wing/fuselage intersection. Wing twist also remains unchanged for all configurations. The final HESS models are shown in Figure B-1.

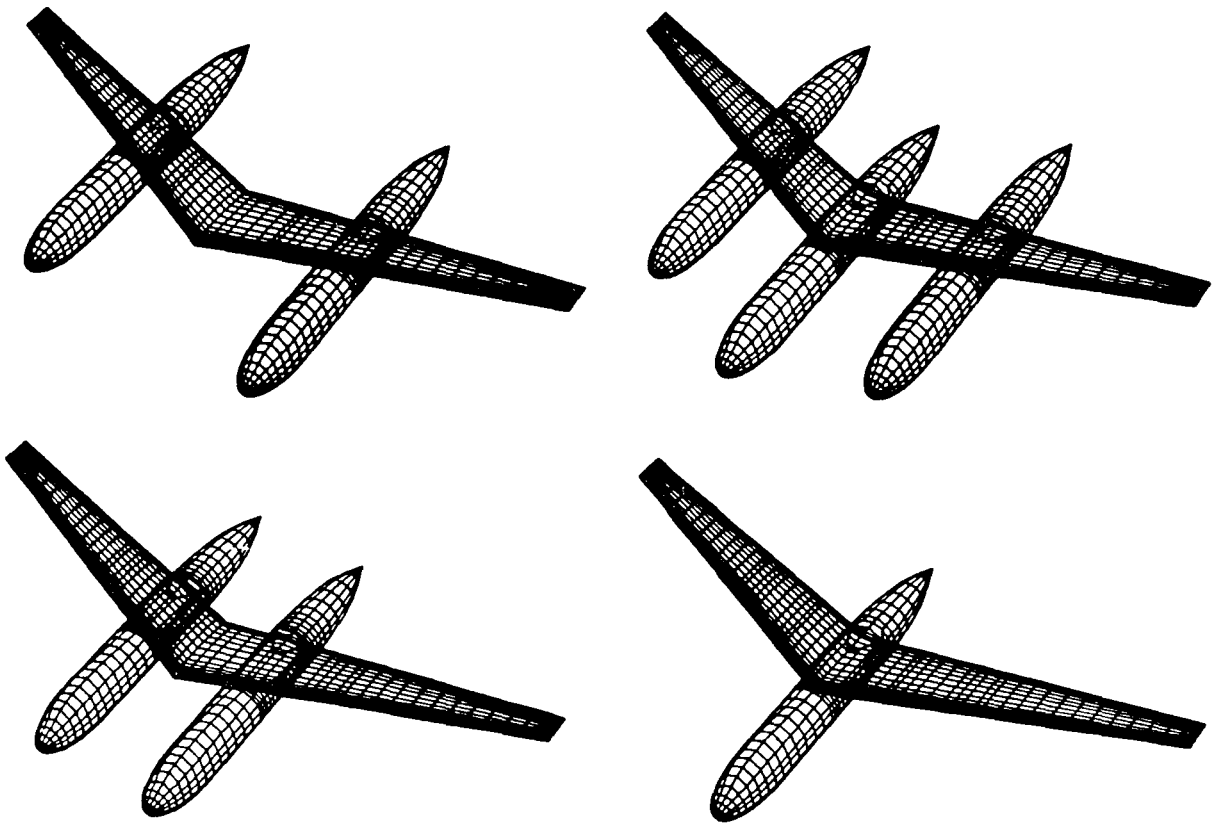

Figure B-1. Hess Models for Aerodynamic Loading Prediction

It is determined that a wing/fuselage cruise lift coefficient of 0.55 will define the design point at which comparisons of wing efficiencies will be made. The span loading data obtained from the HESS calculations are presented in Figure B-2 for all cases except the three-body aircraft. The tabulated data, showing span efficiencies for each case, include all five configurations.

The use of the HESS code to cover the entire spectrum of needed body combinations is prohibitive from a cost standpoint. The L7 vortex-lattice method (VLM) is chosen as the low-cost alternative. Initial efforts are aimed at finding a vortex-lattice configuration that will adequately simulate the more accurate HESS results.

Figure B-3 compares the span loading distribution results of the HESS rou-

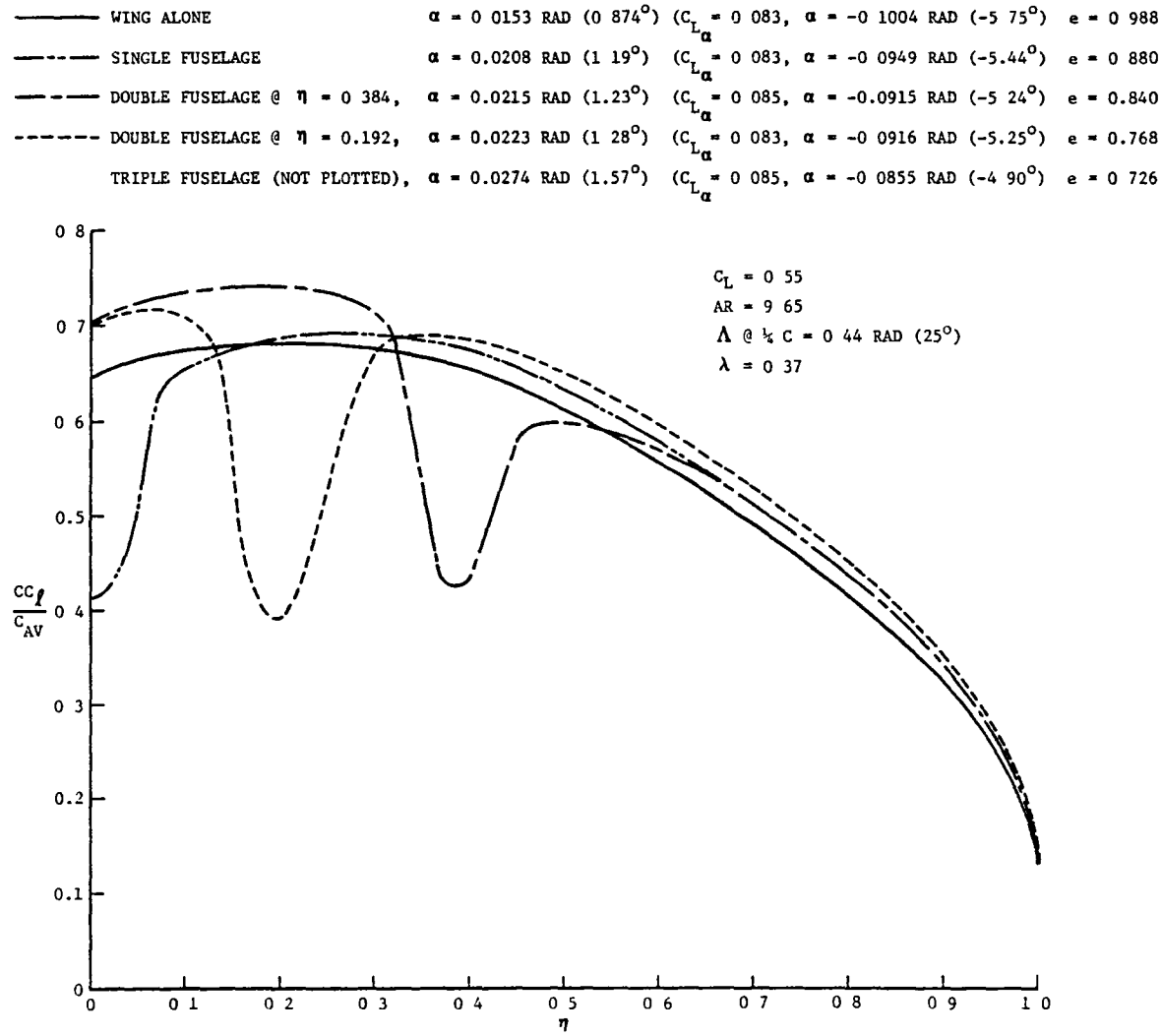

Figure B-2. Effect of Fuselage Location on Spanwise Loading

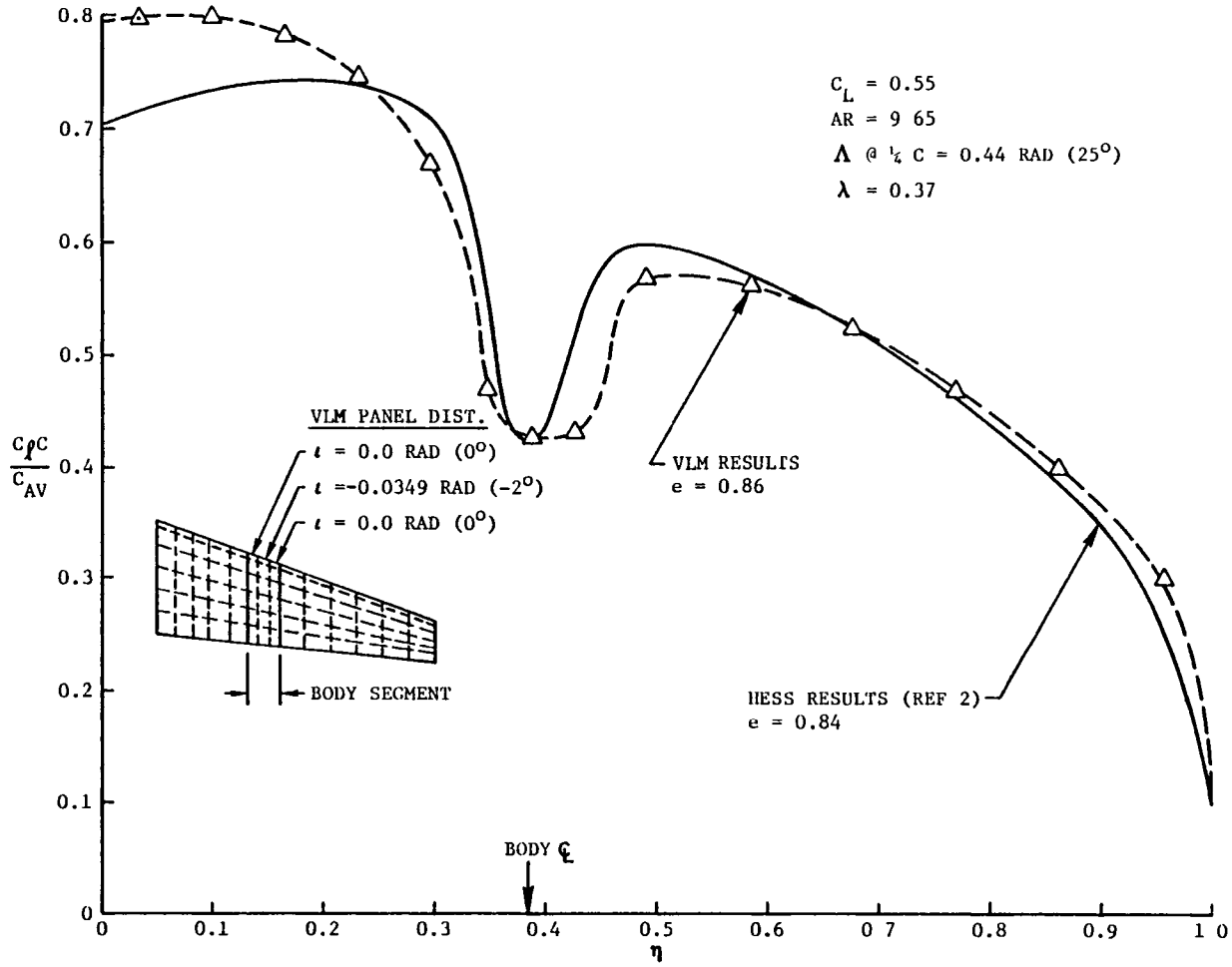

Figure B-3. Hess and Vortex Lattice Span Loading Comparison for Two-Body Configuration

tine and the VLM for the wide two-body configuration. The inset of this figure describes the vortex panel distribution and local incidence required for the VLM to simulate the HESS results. The VLM solution for this paneling, which is obtained through trial and error, shows fair to good agreement. However, the induced drag efficiencies for a series of two-body configurations, shown in Figure B-4 as a function of body spanwise location, do not satisfactorily represent the more rigorous solution obtained from the HESS routine. On this basis, the VLM approach is abandoned.

It is noted that the body influence on the span loading as calculated by HESS is similar in shape as body location is varied. Also, it appears that superposition of effects is valid, which indicates a relatively localized effect due to the bodies. The incremental span loading due to the body,

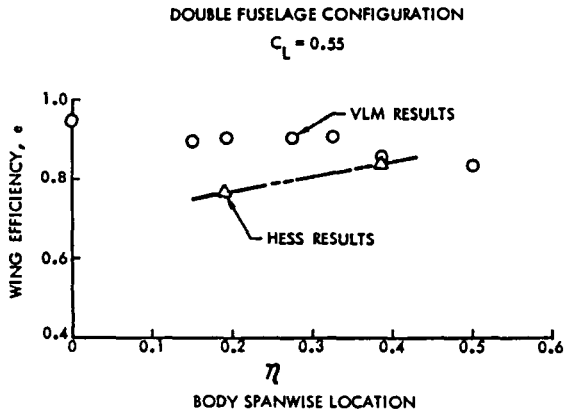

Figure B-4. Wing Efficiency Comparison - Hess and Vortex Lattice Derivation

i.e., the difference between the HESS results and the optimum loading, is presented in Figure B-5 at a C_L = 0.55 for the two-body locations. The net effect of this increment for both cases is zero by definition. Further examination of Figure B-5 shows a similar geometric shape of the incremental lift for each body location. This similarity led to the development of a proprietary method which provides a mathematical representation of the incremental lift effects for each body location in terms of configuration geometry and lift loss at the body centerline. A typical incremental loading produced by the mathematical expression is shown in Figure B-6 and compared with the HESS results for a body centerline location at η = 0.384. While the correlation between the mathematical representation and the actual HESS incremental lift is not exact, it is satisfactory for a general representation of the body effects of the wing span loading distribution as shown in Figure B-7. The total span load is determined to be the sum of the incremental body effects on lift and the optimum (or elliptical) wing loading.

The technique, as developed, is applicable to single and two-body configurations. By superposition of the single and two-body effects, the incremental span loading for three-body effects is available. By combining the incremental span loading effects for one, two, or three-body configurations with the optimum span loading distribution, the total span loading distribution for any wing-body combination can be developed. These results can then be used to establish the wing efficiency for the wing-body combination.

Presented in Figure B-8 are the wing efficiencies for a series of two-body configurations based on span loading distributions calculated using the developed technique. The good agreement between the wing efficiency from the HESS span loadings and the wing efficiency from the calculated span loadings confirms the applicability of the method to preliminary investigations of multibody configurations.

During the HESS analysis, no effort is made to obtain improved span efficiency through improved wing-body juncture design. Several design practices

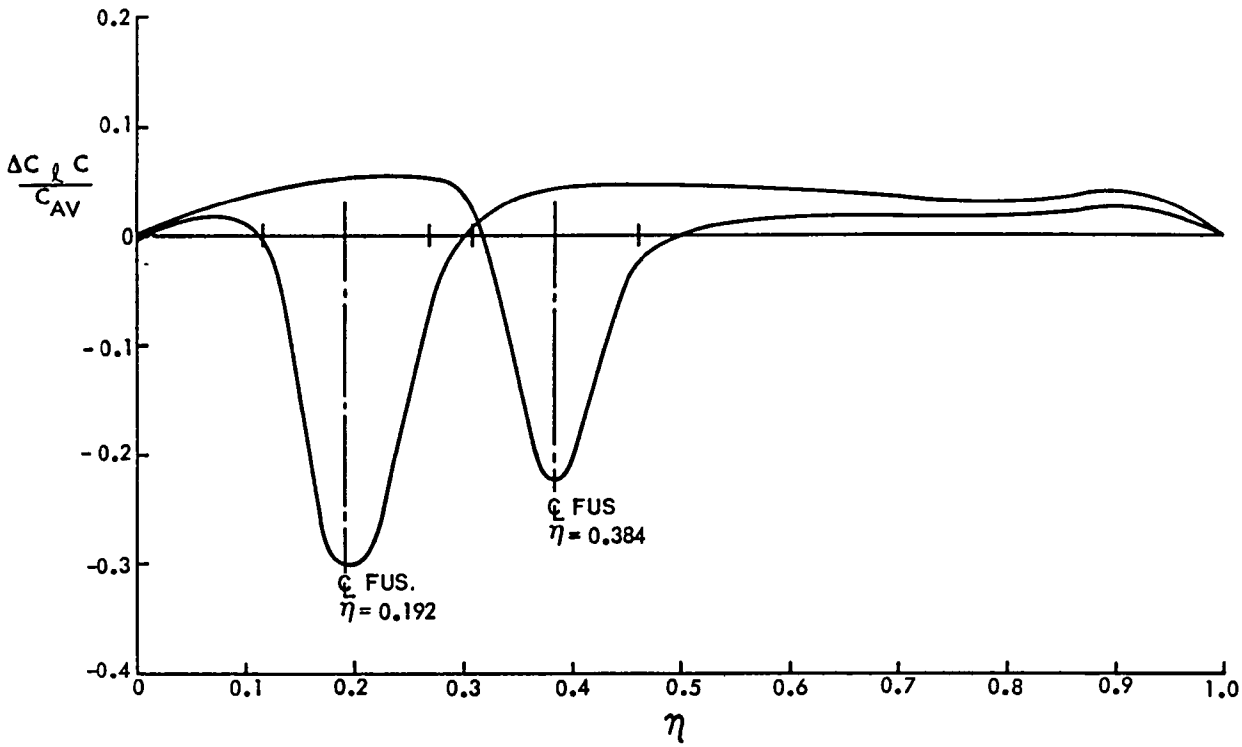

Figure B-5. Body Induced Incremental Span Loading Parameter - Two, Two-Body Configurations

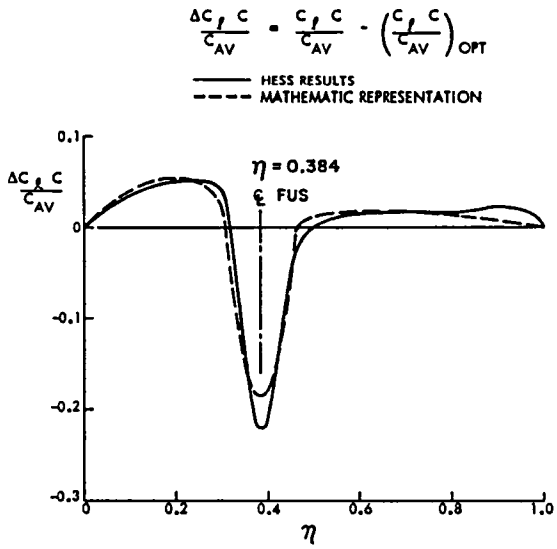

Figure B-6. Incremental Span Loading Parameter Comparison - Two-Body Configuration

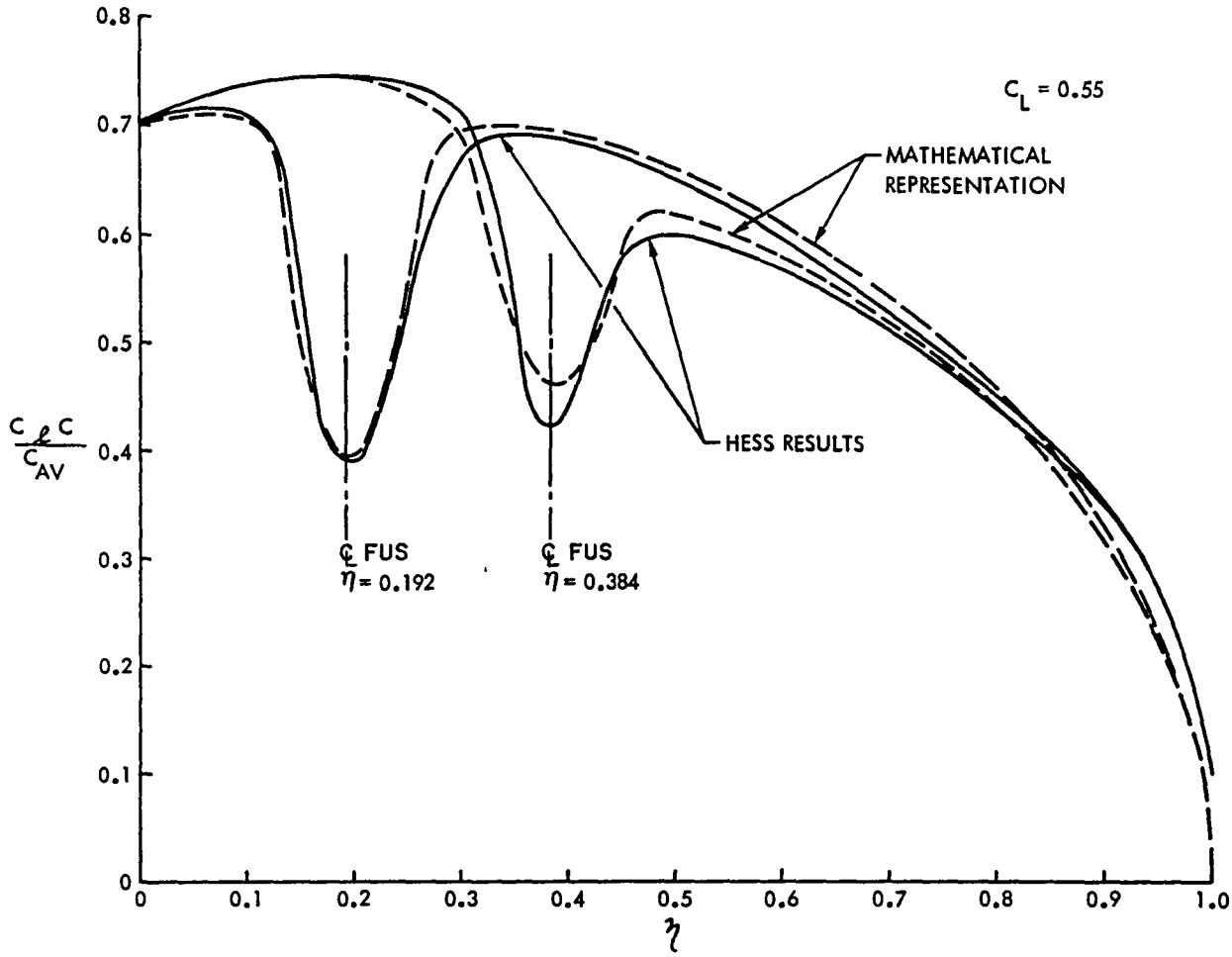

Figure B-7. Span Loading Comparisons - Two-Body Configurations

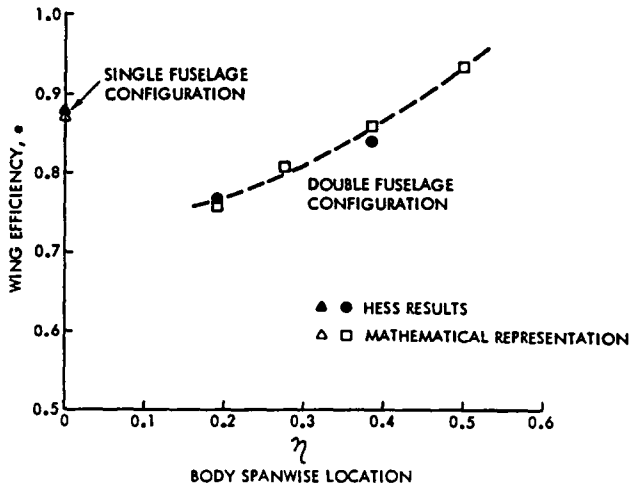

Figure B-8. Wing Efficiency Comparison - Single and Two-Body Configurations

are available for improved wing efficiency, including (1) exposed wing upper surface in the region of the fuselage for improved carryover effects, (2) fuselage shaping or cambering for improved body lift, and (3) wing-body filleting to reduce interference effects. The application of these specific design practices is not within the scope of this study; however, an estimate of the available benefits is in order.

By applying the design techniques mentioned above, it is assumed that various percentage improvements could be obtained in the lift-loss due to the body. A 100 percent improvement represents the clean wing. At 50 percent improvement, the wing efficiency of the single body configuration changes from 0.87 for the unimproved HESS results to 0.96. This level of efficiency is representative of that attained on conventional, single body aircraft. A similar improvement is achieved on the narrow two-body (η = 0.192) configuration for the same percentage change in body lift loss; that is, the efficiency changes from 0.76 to 0.925. Since these trends are compatible with normal design results, a 50 percent improvement in body lift loss is assumed for all multibody configurations.

Span load distributions are developed for a series of two and three-body configurations and the attendant efficiency factors determined. These results are presented in Figures B-9 and B-10 as a function of body location and diameter relative to wing span. These data are based on mathematical representation of the body-induced span loading increments and correlated with the results obtained from HESS for simple, multiple wing-body configurations. The results include the presumed effect of a 50 percent improvement in the incremental lift loss due to the body that is available through critical aerodynamic design. The data in Figures B-9 and B-10 are those used throughout the parametric study to define wing efficiency for various body locations and sizes. It is recognized that this procedure is correlated only with results from a more rigorous analytical tool, namely the HESS code, which has been shown to produce accurate interference effects. The mathematical model used here represents a low-cost alternative to HESS, and future efforts should include correlation with experimental results.

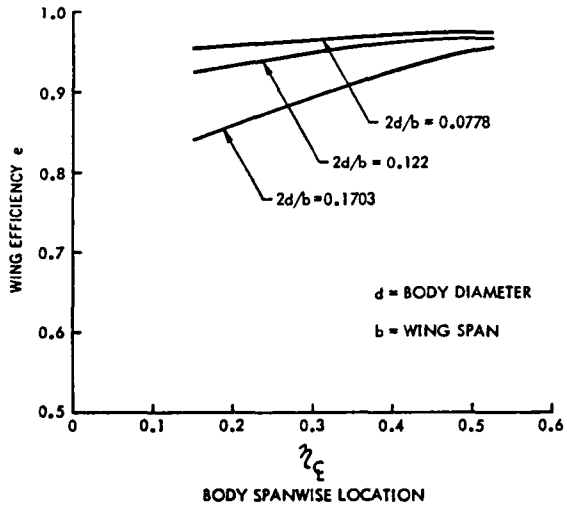

Figure B-9. Wing Efficiency - Two-Body Configuration

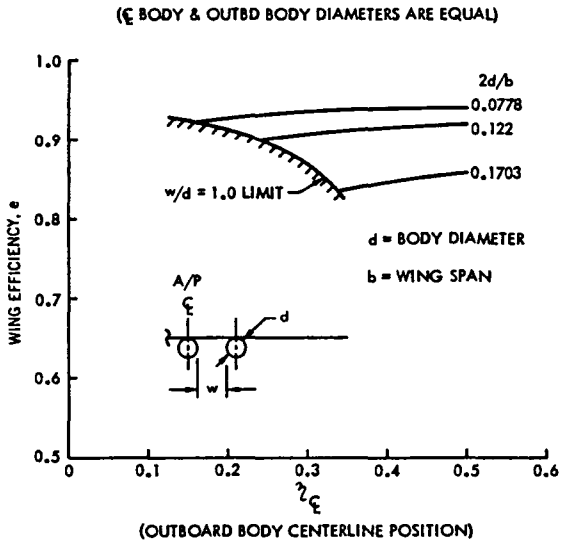

Figure B-10. Wing Efficiency - Three-Body Configuration

This Page Intentionally Left Blank

APPENDIX C

WING PLANFORM AND BODY SPANWISE LOCATION SELECTION

C.1 PRELIMINARY WING PLANFORM DEFINITION STUDIES

The initial studies of the multibody aircraft include investigations of four payload values; 75,000, 167,000, 258,000, and 350,000 kg (165,347, 368,172, 568,793, and 771,618 lb), and body wing semispan locations of 19, 38.5, and 50 percent. The results of these studies identify the existence of a number of performance, structural, and control problem. The 258,000 kg (568,793 lb) payload aircraft shown in Figures C-1 and C-2 with bodies located at 50 percent wing semispan will be used to illustrate these problems and their potential solutions.

The wing planform used for these aircraft has a swept straight leading edge and a zero swept trailing edge between the bodies. The sweep of the outer panel is 0.44 rad (25 degrees) at the quarter chord line. As shown by the wing planform data given in Figure C-3, 82 and 79 percent of the total wing area is encompassed by the wing inner panel for the two and three-body aircraft, respectively. Assuming an elliptical lift distribution over this wing area distribution results in relatively high section lift coefficients required over the outer panel when compared to those of the inner panel. In addition, this area distribution, in relationship to its influence on chord length in combination with the assumed thickness distribution, results in an inefficient wing structural arrangement. The relatively small outer wing panel also minimizes the magnitude of the control forces which can be produced. This control force problem is compounded by the location of the bodies at 50 percent semispan where the moment of inertia produced and required to be reacted by the control force will be very high. The two-body aircraft is used as a means to investigate these problems such that possible solutions and/or required additional studies can be identified.

C.1.1 Wing Performance

The basic aerodynamic data used, including the wing estimated span efficiency and load distribution, are based upon a Hess code model analysis. The analysis is generalized to apply to

SPEED	0.80 MACH
PAYLOAD	258,000 kg (568,793 LB)
RANGE	6,482 km (3,500 NM)
OPERATING WT.	250,973 kg (553,300 LB)
BLOCK FUEL	125,872 kg (277,500 LB)
GROSS WT.	659,342 kg (1,453,600 LB)
ENGINE THRUST	310,797 N (69,870 LB)
ASPECT RATIO	12.58

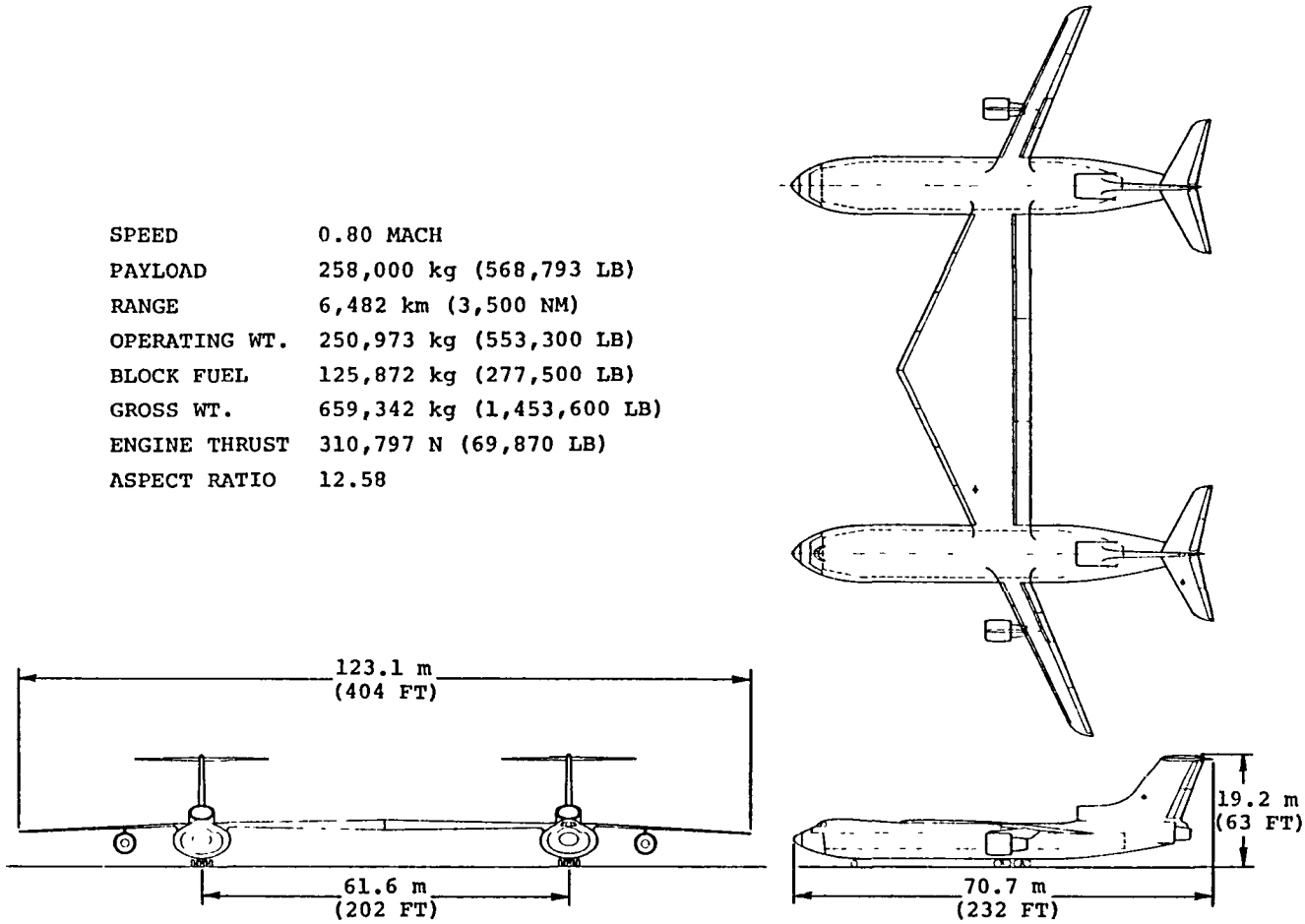

Figure C-1. General Arrangement - Two-Body Aircraft

SPEED	0.80 MACH
PAYLOAD	258,000 kg (568,793 LB)
RANGE	6,482 km (3,500 NM)
OPERATING WT.	307,218 kg (677,300 LB)
BLOCK FUEL	146,284 kg (322,500 LB)
GROSS WT.	740,263 kg (1,632,000 LB)
ENGINE THRUST	365,199 N (82,100 LB)
ASPECT RATIO	10.28

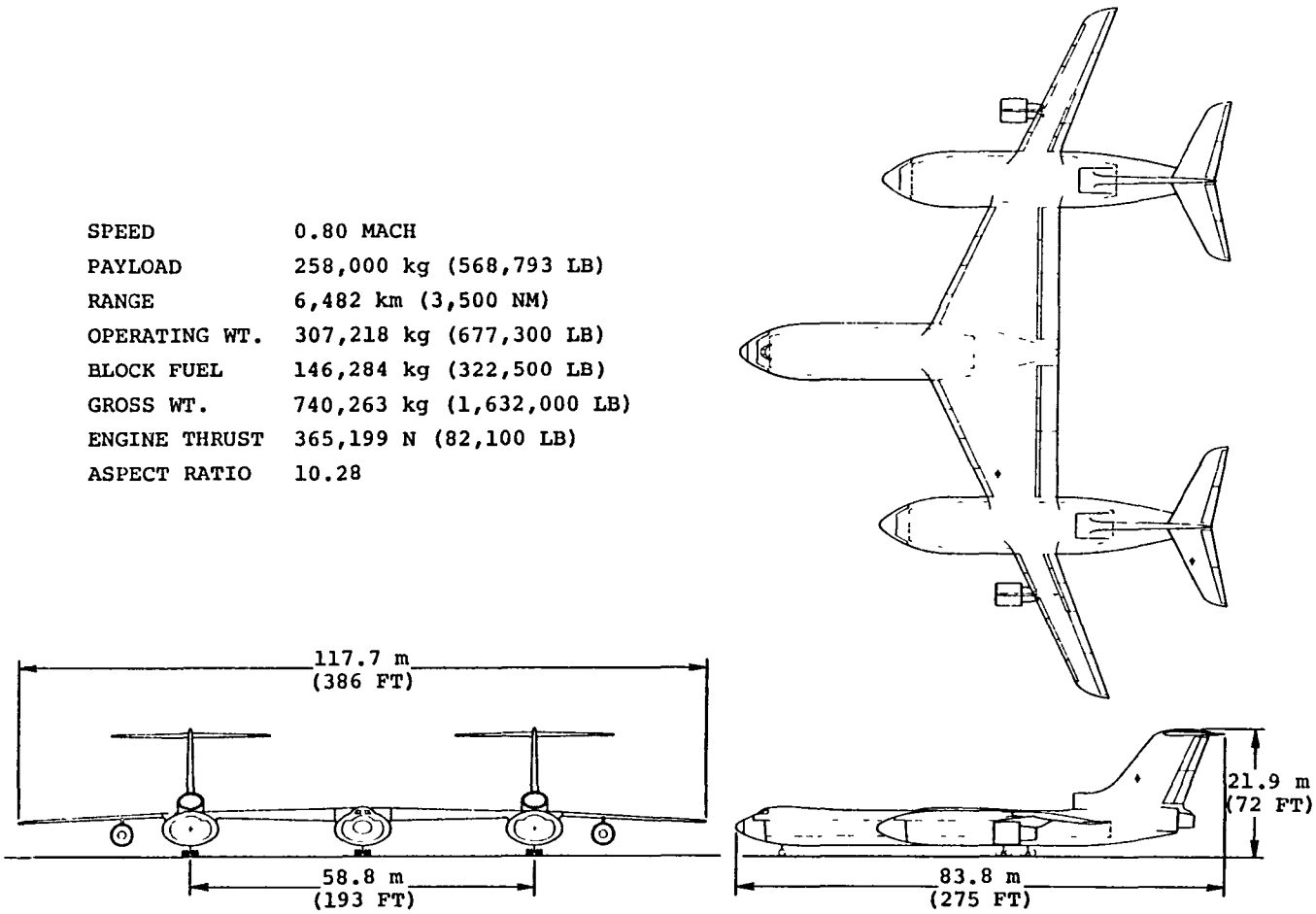

Figure C-2. General Arrangement - Three-Body Aircraft

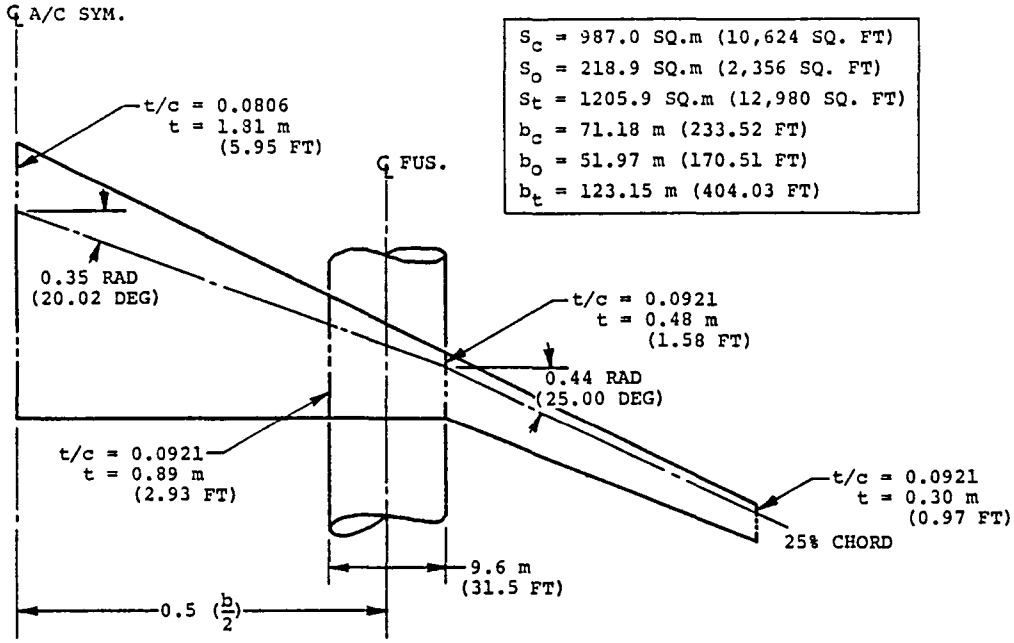

TWO-BODY WING PLANFORM

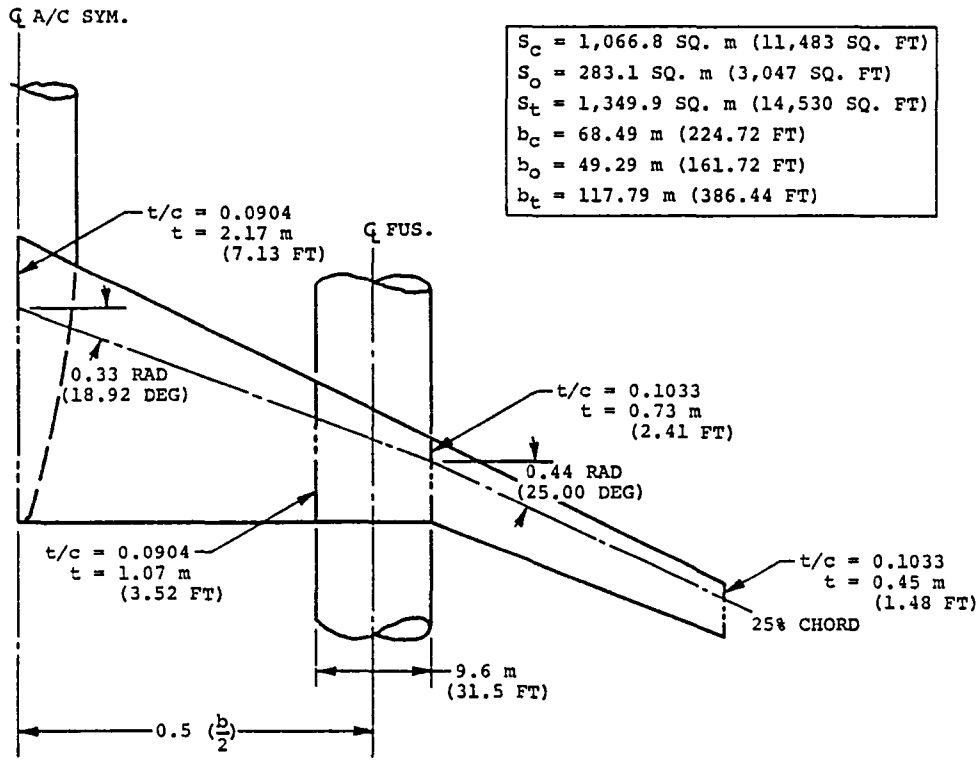

THREE-BODY WING PLANFORM

Figure C-3. Wing Planform Definition - Two-and-Three-Body Aircraft

various body locations assuming a wing elliptical loading is achieved. Although the Hess analysis was based upon a wing planform with full span leading and trailing edge sweep, it was assumed the results would be applicable to the study planform, if an equivalent span loading were maintained. However, the results of the analysis indicate a need to refine and/or apply additional constraints to the analysis. The areas of concern are illustrated by examining the wings which are optimized at each of three body semispan locations.

Figure C-4 shows the wing section lift coefficient (c_1) vs wing semispan location of the three selected body locations based on an elliptic span load distribution. Because of the trailing-edge bat between the fuselages, the wings are geometrically composed of two panels with the break station at the outer side of the fuselage. The increasingly large bat size as body spanwise location increases results in large local chords on the inner panel which require low local lift coefficient values to achieve an

TWO-BODY - 258,000 kg (568,793 LB) - OVAL				
η	GROSS WEIGHT	DATE	TIME	t/c REF
0.19	762,449 kg (1,680,912 LB)	1/11/80	14:08	0.1124
0.385	689,211 kg (1,519,451 LB)	1/9/80	13:43	0.1023
0.50	659,319 kg (1,453,549 LB)	1/29/80	14:50	0.0921

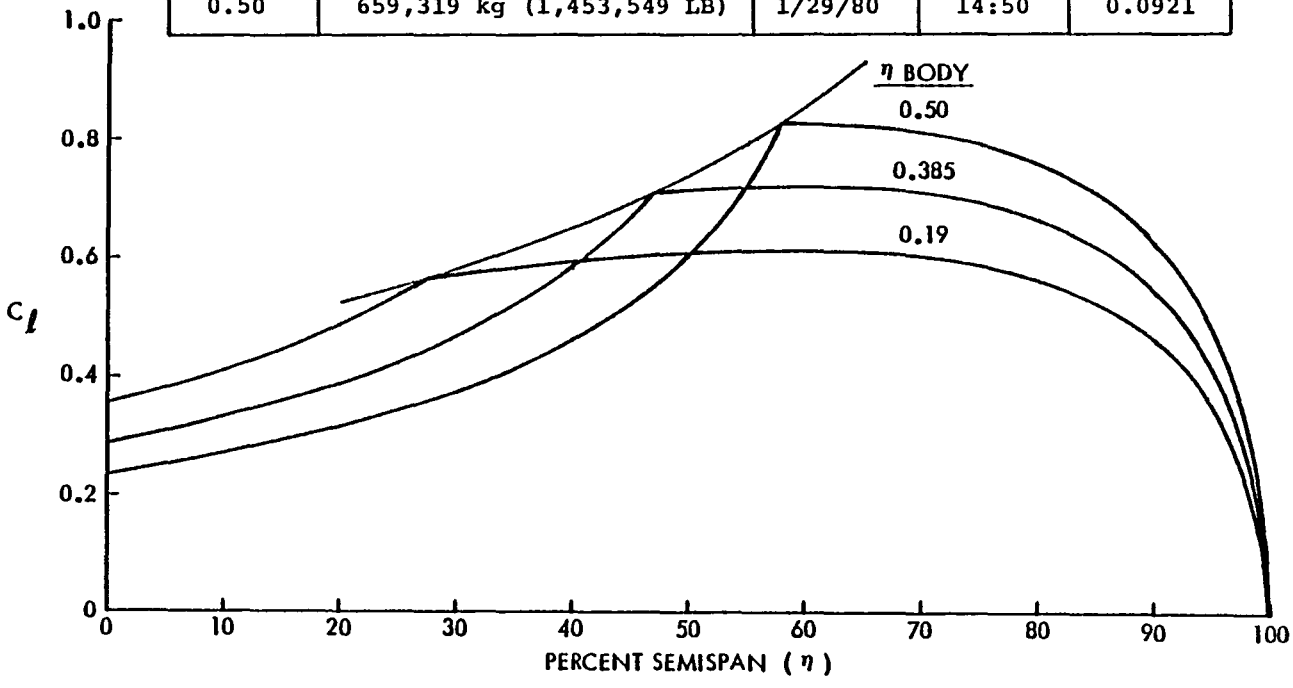

Figure C-4. Section Lift Coefficients - Estimated

elliptic loading. Achieving the elliptic load also implies increasingly higher local lift coefficients on the outer panel as the chord lengths on this panel, relative to the inner panel, become smaller. As shown in Figure C-4, the section lift coefficient projected for the outer panel for the configuration with the body located at 50 percent semispan is very high and probably unachievable.

The high local lift coefficient has an undesirable effect, since, if other pertinent parameters such as sweep angle, Mach number, and desired compressible drag level are fixed, the allowable thickness ratio varies inversely with lift coefficient. Hence, with the body at the most outer location, the thickness ratio of the outer panel is relatively low. When coupled with the short chord length of the wing outer panel, this results in insufficient wing thickness at the body for an efficient structural design.

C.1.2 Wing Structural Efficiency

The results of a preliminary structural analysis of the wing as defined by the planform geometry given in Figure C-3 indicate that the wing weight should be increased as much as 20 to 40 percent. This is due to several factors. The most significant factor is the wing planform geometric constraint. An optimum structural arrangement would locate the wing maximum thickness and chord length at the wing station where the maximum bending moment is developed. This maximum bending moment as shown in Figure C-5 occurs approximately at the body centerline. However, for these aircraft, the wing chord and thickness are constrained at the centerline location, as previously discussed, for aerodynamic reasons. The structural thickness at the point of maximum load is only 45.7 cm (18 in.) (refer to Figure C-3). As a result of this constrained thickness, the cover load is approximately 21,429 kg/cm (120,000 lb/in.) as shown in Figure C-6. For comparison, the C-5 loading is about 7143 kg/cm (40,000 lb/in.) and the C-141 is about 3572 kg/cm (20,000 lb/in.).

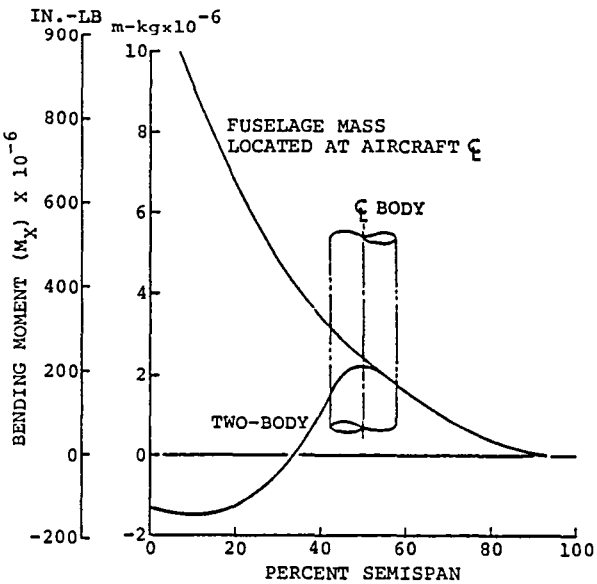

Figure C-5. Wing Bending Moment - 258,000 kg (568,793 lb) Two-Body Oval Fuselage

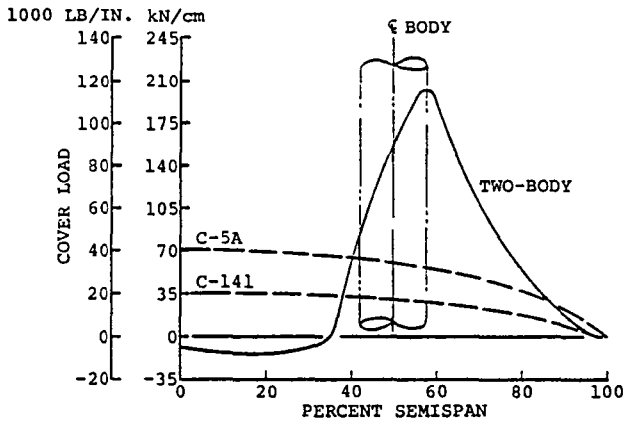

Figure C-6. Wing Cover Loads - 258,000 kg (568,793 lb) Two-Body Oval Fuselage

The wing cover material thickness required to react these cover loads is shown in Figure C-7. Wing cover thickness ($\bar{t}$) is defined as the total wing box cover cross-sectional area divided by the wing box chord. As shown in the figure, $\bar{t}$ for the multibody wing at the fuselage/wing junction is approximately 6.99 cm (2.75 in.) as compared to 1.91 cm (0.75 in.) for the C-5 aircraft.

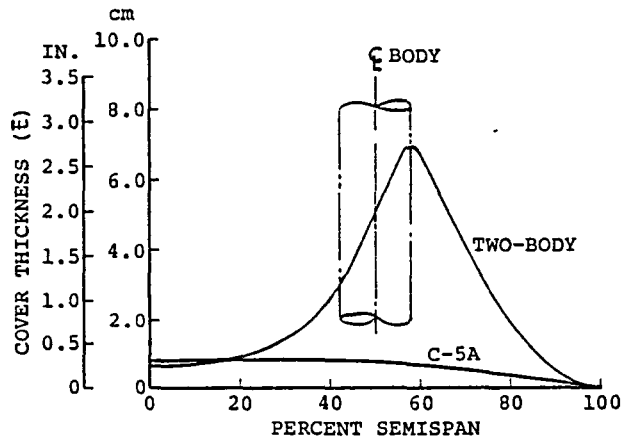

Figure C-7. Wing Cover Thickness Distribution - 258,000 kg (568,793 lb) Two-Body Oval Fuselage

Obviously, based upon the $\bar{t}$ required, the optimum wing structural arrangement has not been used.

C.1.3 Control Force Requirements

The two and three-body configurations as shown in Figures C-1 and C-2 would have obvious control problems. Since the two-body configuration would be most critical, comments are directed towards it. The same logic, but to a lesser degree, applies to the three-body.

Although exact roll requirements are unknown, preliminary studies of very large aircraft show that desired levels of roll capability are similar to those of the largest flying aircraft - the C-5A. The two-body aircraft, as shown, using available conventional spoilers and ailerons has only 20 percent of the desired level.

At $1.3V_S$, for example, it would take three seconds of maximum control to bank the aircraft 0.16 rad (9 degrees). The tremendous inertia and the lack of control area combine to compound the problem. Weight of the aircraft is double that of a C-5, but the inertia in roll as given in Figure C-8 is increased by a factor of 10. Total wing area and span are doubled to increase roll availability, but the area distribution is unusual. Only 18 percent of the area is outboard of the fuselage.

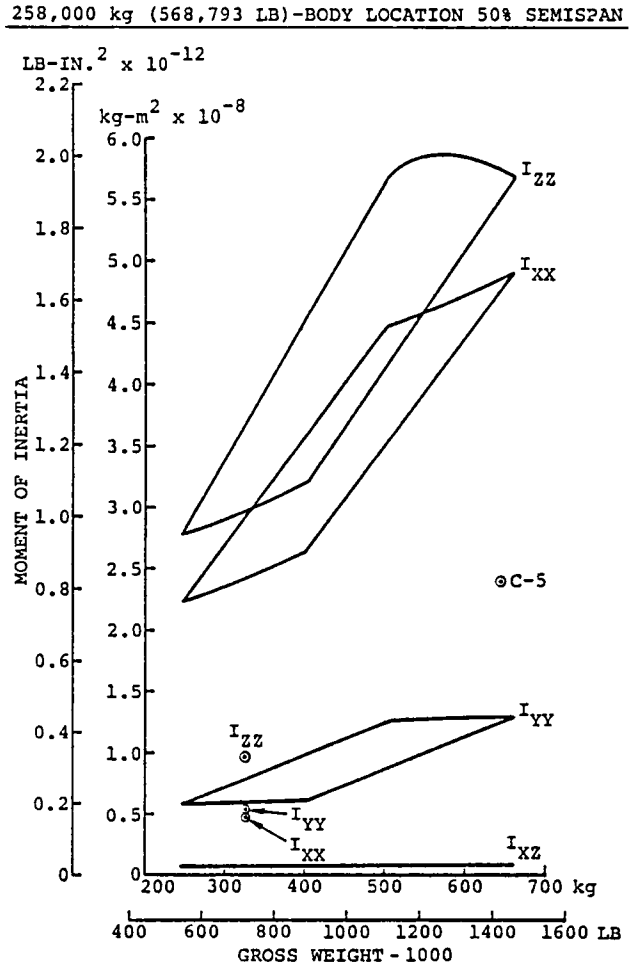

Figure C-8. Moment of Inertia Envelopes - Two-Body Aircraft Oval Fuselage

The seriousness of this is noted by the amount of rolling moment generated when using this entire area. With each tip panel operating differentially at a lift coefficient of 1.0, only 25 percent of the desired roll capability is achieved.

The feasibility of using direct force by deflecting engine thrust was checked. This was shown to be futile. The efficient way to generate large rolling moments is known to be by aerodynamically loading large areas with large moment arms.

Moving the fuselages inboard and increasing control area near the tips appears to be the only feasible way to alleviate control problems. A move of the fuselages from 50 to 40 percent semispan increases the roll capability by 30 percent due to inertia relief alone. Additional roll capability is also gained by the increase in wing outboard panel area.

C.1.4 Ride Quality Problems

Comparisons of C-5 roll capabilities to military specification requirements brought out some interesting aspects which are applicable to the two-body configuration. It is stated that increasing the C-5 present acceptable roll capabilities to meet more stringent requirements would further aggravate a potential "side-kick" problem. The C-5 flight control station is approximately 4.9m (16 ft) above the centerline of the fuselage. Abrupt rolls to demonstrate maximum capability produce a noticeable lateral force at the flight station since it is offset from the axis of rotation. This has not been a problem in service since the pilot does not normally use such violent maneuvers. The two-body configuration with the proposed roll capability equal to that of the present C-5 could, however, have serious problems.

Full roll control imposes a 0.6g vertical load to anyone at the flight station 30.8m (101 ft) out on the wing. If the roll rate then develops to 0.52 rad/sec (30 degrees/second), the flight station personnel will experience a very noticeable "side-kick" of approximately 0.9g laterally. These forces would probably be disconcerting to a pilot on final approach.

C.1.5 Landing Gear/Airframe Integration

The location of the landing gear is not directly related to the problems associated with the wing planform geometry; however, the wing structural requirements are impacted significantly by the location chosen. The aircraft defined by Figures C-1 and C-2 have both the nose and main landing gear bogie centerlines located on the two fuselage centerlines, providing minimum wing weight. The fuselage centerlines are located at 50 percent wing semispan; this equates to a fuselage separation distance of 61.6 and 58.8m (202 and 193 ft), respectively, for the two and three-body aircraft. For compatibility with a commercial runway width of 45.7m (150 ft), the maximum landing gear centerline separation distance is approximately 39.6m (130 ft). This maximum lateral separation of the main gear is based on the assumption that future improvements in airport performance systems technology would permit operation on a 45.7m (150 ft) wide runway. With this separation, the runway width is approximately 3.05m (10 ft) greater in width than the total gear treadwidth. If the fuselage locations remain at 50 percent semispan and the gear centerline separation is reduced to 39.6m (130 ft), the gear centerline to fuselage centerline displacement becomes 11.0 and 9.60m (36 and 31.5 ft), respectively, for the two and three-body aircraft. The down bending moment created by the landing gear being displaced inboard of the fuselage results in critical loads being input into the wing structure. Increased wing strength is required to react these loads thereby increasing wing weight. The two-body concept compatible with a 45.7m (150 ft) runway width is illustrated by the diagram shown in Figure C-9. In addition to the wing structural penalty, it is necessary to provide a housing/support of some type for the nose gear as shown on the diagram. This further increases the weight penalty for the minimum tread width gear concept. No weight difference is assumed for the wing relocation from the high to the low position. The increased aircraft weight resulting from these changes requires resizing of the air-

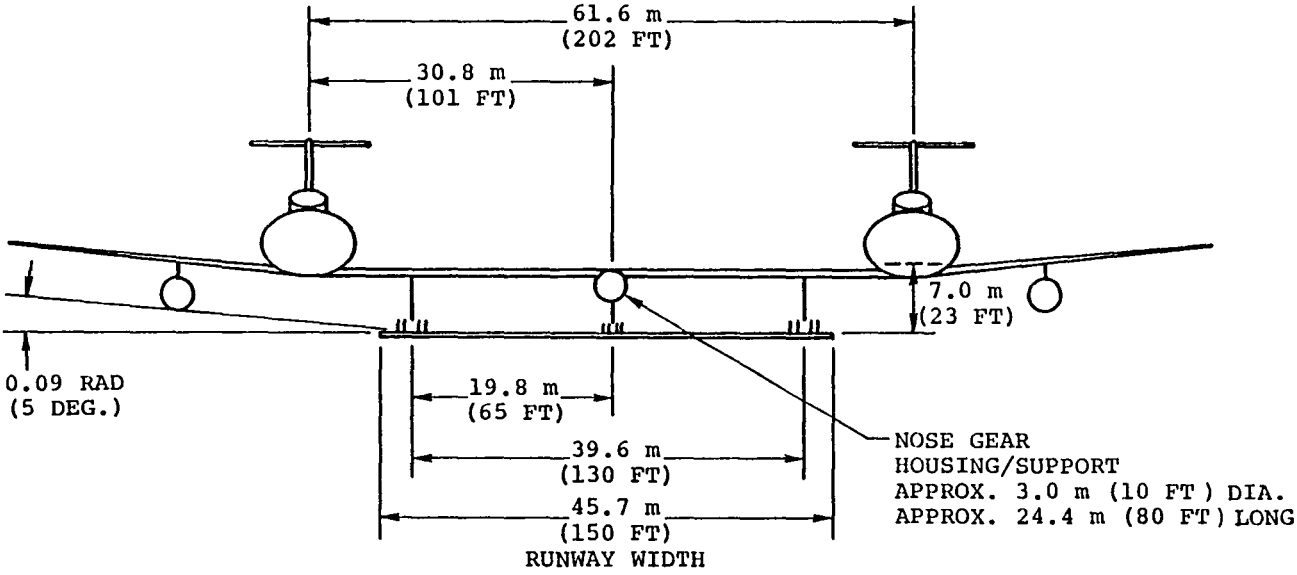

NOTE: BODY LOCATION AT 50% SEMISPAN

Figure C-9. Minimum Tread Width Gear Concept - Two-Body Aircraft

craft, thus escalating the weight penalty associated with the minimum tread width gear.

To provide a better understanding of the escalation effect resulting from aircraft resizing, the two-body aircraft is reconfigured with the 39.6m (130 ft) gear tread width change only. All other configuration characteristics remain unchanged. This change requires an increase in wing weight of approximately 32,568 kg (71,800 lb) which is assumed to be obtained by an equal reduction in payload as shown by configuration 1 in Figure C-10. Next, the aircraft is resized, configuration 2 in Figure C-10, to perform the same payload/range mission with this increased wing weight. Aircraft gross weight increases by 85,275 kg (188,000 lb) of which 16,329 kg (36,000 lb) is fuel and 68,946 kg (152,000 lb) is operating weight. To perform the required payload/range mission, the resizing results in an additional 52,707 kg (116,200 lb) as compared to configuration 1.

As previously stated, the minimum wing weight occurs for any give configuration where the landing gear centerline is located coincident with the fuselage centerline. Configuration 3 in Figure C-10 represents a configuration where both the landing gear and fuselage bodies have been moved inboard to the 39.6m (130 ft) separation distance. This configuration is obtained by the use of parametric output data given in Figure C-11. Using the upper plot of this figure it is determined

ITEM	BODY LOCATION (% SS)	BODY SEPARATION m (FT)	GEAR TREAD m (FT)	PAYLOAD -1000 kg (LB)	WING WT. -1000 kg (LB)	OPERATING WT. -1000 kg (LB)	FUEL WT. -1000 kg (LB)	GROSS WT. -1000 kg (LB)	DOC ¢/AMgkm (¢/ATNM)
B.L.	50	61.6 (202)	61.6 (202)	258.0 (568.8)	80.6 (177.8)	251.0 (553.3)	150.4 (331.5)	659.3 (1453.6)	3.77 (6.34)
1	50	61.6 (202)	39.6 (130)	225.4 (497.0)	113.2 (249.6)	283.5 (625.1)	150.4 (331.5)	659.3 (1453.6)	4.50 (7.56)
2	50	61.6 (202)	39.6 (130)	258.0 (568.8)	138.4 (305.1)	319.9 (705.3)	166.7 (367.6)	744.7 (1641.7)	4.33 (7.27)
3	35	39.6 (130)	39.6 (130)	258.0 (568.8)	91.0 (200.7)	271.4 (598.3)	165.7 (365.2)	695.0 (1532.3)	4.07 (6.83)

Figure C-10. Configuration Comparison - Minimum Width Gear Tread

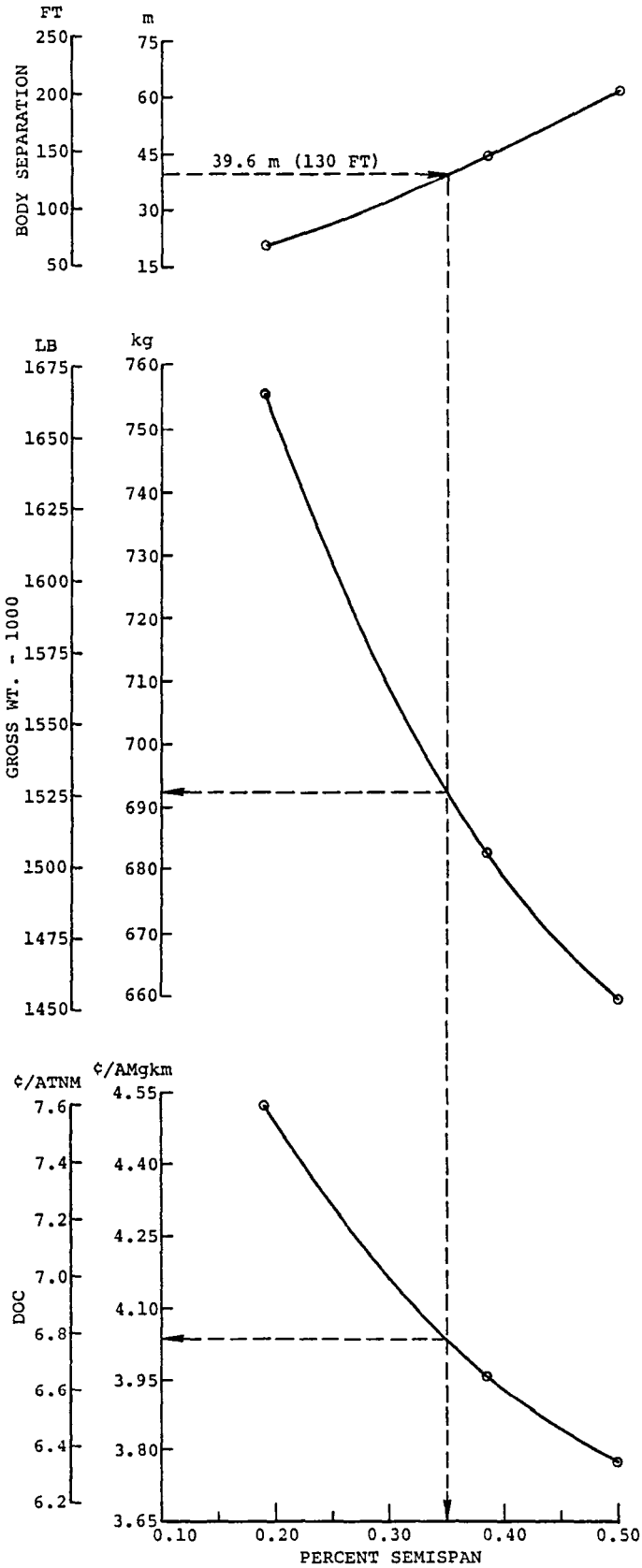

Figure C-11. Body Location Effects - 258,000 kg (568,793 lb) Two-Body Aircraft

that at a separation distance of 39.6m (130 ft), a body location of 35 percent semispan is required. Gross weight for this concept, as compared to the baseline (BL) 50 percent semispan aircraft, is increased by 35,698 kg (78,700 lb) of which 15,286 kg (33,700 lb) is fuel weight and 20,412 kg (45,000 lb) is operating weight. The slight difference found when these data are compared to the data given in Figure C-11 can be attributed to the inaccuracy of plotting three point data.

In summary, if the DOC values given in Figure C-10 are compared for the above configurations, it can be seen that the least penalty is incurred when the gear and body centerline locations coincide. It is noted that the weight and drag penalty associated with providing nose gear housing and support is not included in configurations 1 and 2 weight summaries. Hence, the true weight and DOC penalties for these configurations would be larger than indicated. The results of these data indicate that for runway compatibility, the fuselage separation should be no greater than 39.6m (130 ft) with a coincident landing gear location.

C.1.6 Conclusions

From the previous investigations it is shown that the basic problems associated with the aircraft result from large wing chord variations dictated by the wing planform concept used. It is apparent that structural improvements will result from planform concepts having reduced root chord lengths. Reducing the root chord length will redistribute the wing area and tend to increase the area of the outer panel. This will increase the chord length and the allowable thickness ratio of the wing outer panel. Aircraft control capability will also be improved with the increase in wing area outboard of the fuselage bodies.

C.2 WING PLANFORM SELECTION

Three wing planforms are investigated which have geometric characteristics selected on the basis of achieving a balance between the wing areas inboard and outboard of the fuselage bodies. These planforms are represented in Figure C-12 and are identified as planform numbers 2, 3, and 4. Planform number 1 retains the same geometric concept of the previous study and is used as a basis for comparison.

Two and three-body 350,000 kg (771,618 lb) payload aircraft are sized for each of the planforms given in Figure C-12 at three body locations. Both two and three-body aircraft are sized at body location of 50 percent semispan and at a fixed body separation distance of 39.6m (130 ft). The third

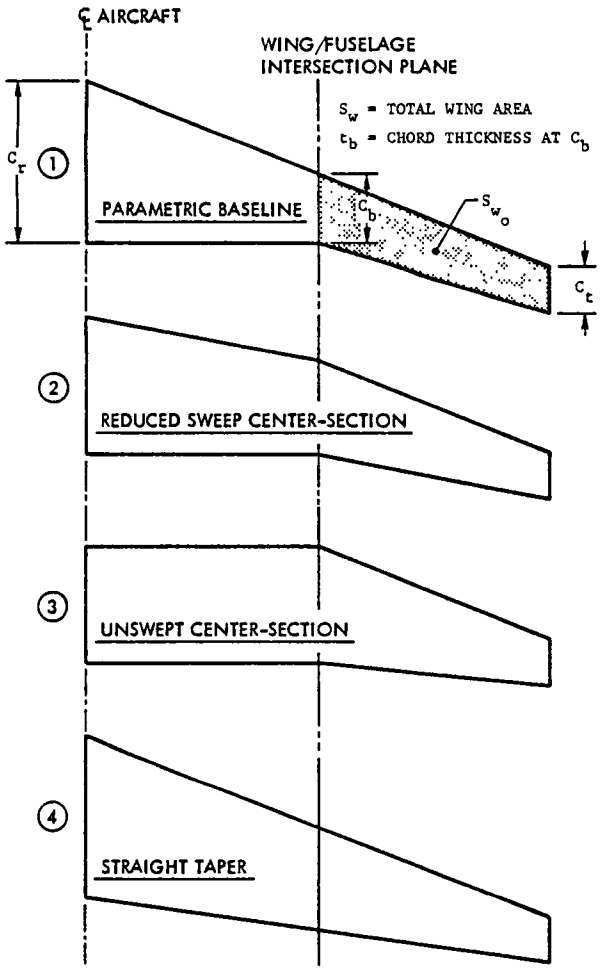

Figure C-12. Wing Planform Variations

location is 19 percent semispan for the two-body and 44.25 percent for the three-body.

A review of the two-body sizing data given in Figure C-13 indicates a selection of either planform number 3 or 4 is acceptable. Performance, structural, and control capability characteristics of these planforms are improved when compared to the baseline planform number 1 or to planform number 2. The ratio of the wing area outboard of the fuselage body to the total wing (S_{w_o}/S_w) is increased. This area relocation from the inboard panel to the outboard panel provides improved control capability and increases both chord length and thickness (C_b and t_b) at the outboard side of the fuselage where the wing maximum bending moment occurs. Wing chord variation is also reduced as indicated by the increase in taper ratio (C_t/C_r), thus improving section lift coefficient distribution and thereby improving thickness distribution.

The unswept center section planform number 3 and the straight taper planform number 4 also optimize at lower DOC values than do the other two planforms. Therefore, these planforms (3 and 4) are selected to be used on the two-body point design aircraft.

The three-body sizing data given in Figure C-14 show results very similar to those of the two-body aircraft sizing. However, as only one three-body aircraft is to be analyzed within the point design study, planform number 3 is selected. Although this planform does not have the minimum DOC it does have the best geometric characteristics. The ratio of outer wing area to total wing area, the ratio of tip chord to root chord, and wing break chord and thickness are maximized.

	COMPARISON DATA \ WING PLANFORM →	① PARAMETRIC BASELINE	② REDUCED SWEEP CENTER SECTION	③ UNSWEPT - CENTER SECTION	④ STRAIGHT TAPER
$\frac{\eta}{19\%}$	BODY SEPARATION - m	22.84	22.80	22.84	22.79
	WING AR	9.46	9.60	10.32	9.50
	S_w - m^2	1,529	1,499	1,399	1,515
	$S_{w_o} \div S_w$	0.58	0.60	0.67	0.65
	C_b - m	13.71	13.88	14.39	15.12
	t_b - m	2.01	2.05	2.17	2.32
	C_r - m	25.73	23.23	14.39	18.04
	$C_t \div C_r$	0.25	0.29	0.48	0.40
	WING WT - kg	134,122	134,008	131,899	126,876
	WING WT - kg/m^2	87.74	89.40	94.28	83.73
	OPER WT - kg	380,834	379,399	372,597	371,953
	BLOCK FUEL - kg	200,230	198,780	192,873	199,884
	GROSS WT - kg	970,051	966,923	953,177	960,748
	DOC - ¢/AMgkm ($.34/1)	4.45	4.42	4.33	4.40
$\frac{\eta}{39.62\ m}$	BODY SEPARATION - m	39.62	39.62	39.62	39.62
	WING AR	8.58	9.22	10.60	9.25
	S_w - m^2	1,606	1,510	1,382	1,429
	$S_{w_o} \div S_w$	0.37	0.40	0.53	0.47
	C_b - m	11.41	11.38	13.27	13.19
	t_b - m	1.64	1.64	2.05	2.02
	C_r - m	29.60	25.59	13.27	17.75
	$C_t \div C_r$	0.21	0.24	0.53	0.40
	WING WT - kg	96,377	105,210	116,048	93,563
	WING WT - kg/m^2	60.01	69.67	83.98	65.47
	OPER WT - kg	338,107	343,649	351,124	330,579
	BLOCK FUEL - kg	193,620	189,197	183,919	188,975
	GROSS WT - kg	919,348	919,741	921,057	906,371
	DOC - ¢/AMgkm ($.34/1)	4.20	4.17	4.14	4.11
$\frac{\eta}{50\%}$	BODY SEPARATION - m	67.37	59.49	59.27	61.97
	WING AR	8.34	8.13	10.41	10.85
	S_w - m^2	2,177	1,742	1,350	1,416
	$S_{w_o} \div S_w$	0.19	0.22	0.37	0.32
	C_b - m	8.88	9.63	12.39	10.66
	t_b - m	1.29	1.39	1.98	1.66
	C_r - m	36.98	29.57	12.39	16.32
	$C_t \div C_r$	0.15	0.20	0.61	0.40
	WING WT - kg	92,316	82,899	99,746	82,716
	WING WT - kg/m^2	42.38	47.60	73.87	58.44
	OPER WT - kg	343,172	323,847	331,656	312,194
	BLOCK FUEL - kg	203,966	192,647	180,217	174.401
	GROSS WT - kg	936,490	903,877	897,150	870,654
	DOC - ¢/AMgkm ($.34/1)	4.35	4.14	4.02	3.88

Figure C-13. Wing Planform Comparison - Two-Body Aircraft (Metric Units) (Sheet 1 of 2)

	COMPARISON DATA \ WING PLANFORM →	① BASELINE	② REDUCED SWEEP CENTER SECTION	③ UNSWEPT - CENTER SECTION	④ STRAIGHT TAPER
$\frac{\eta}{19\%}$	BODY SEPARATION -FT	74.95	74.80	74.92	74.78
	WING AR	9.46	9.60	10.32	9.50
	S_w -SQ.FT.	16,457	16,139	15,063	16,307
	$S_{w_o} - S_w$	0.58	0.60	0.67	0.65
	C_b - FT	44.98	45.54	47.21	49.60
	t_b - FT	6.59	6.71	7.12	7.60
	C_r - FT	84.42	76.22	47.21	59.19
	$C_t - C_r$	0.25	0.29	0.48	0.40
	WING WT - LB	295,689	295,437	290,788	279,714
	WING WT - LB/SQ FT	17.97	18.31	19.31	17.15
	OPER WT - LB	839,596	836,431	821,436	820,016
	BLOCK FUEL - LB	441,432	438,235	425,212	440,669
	GROSS WT - LB	2,138,597	2,131,700	2,101,395	2,118,087
	DOC - ¢/ATNM (1.30/GAL)	7.47	7.43	7.27	7.40
$\frac{\eta}{130\ FT}$	BODY SEPARATION -FT	130	130	130	130
	WING AR	8.58	9.22	10.60	9.25
	S_w -SQ.FT.	17,288	16,249	14,874	15,380
	$S_{w_o} - S_w$	0.37	0.40	0.53	0.47
	C_b - FT	37.43	37.33	43.54	43.29
	t_b - FT	5.38	5.37	6.74	6.62
	C_r - FT	97.12	83.96	43.54	58.25
	$C_t - C_r$	0.21	0.24	0.53	0.40
	WING WT - LB	212,474	231,949	255,842	206,270
	WING WT - LB/SQ FT	12.29	14.27	17.20	13.41
	OPER WT - LB	745,399	757,617	774,096	728,803
	BLOCK FUEL - LB	426,859	417,109	405,473	416,619
	GROSS WT - LB	2,026,816	2,027,681	2,030,583	1,998,206
	DOC - ¢/ATNM (1.30/GAL)	7.06	7.01	6.96	6.91
$\frac{\eta}{50\%}$	BODY SEPARATION -FT	221.02	195.18	194.45	203.31
	WING AR	8.34	8.13	10.41	10.85
	S_w -SQ.FT.	23,437	18,752	14,535	15,238
	$S_{w_o} - S_w$	0.19	0.22	0.37	0.32
	C_b - FT	29.13	31.60	40.66	34.99
	t_b - FT	4.22	4.55	6.49	5.46
	C_r - FT	121.33	97.03	40.66	53.54
	$C_t - C_r$	0.15	0.20	0.61	0.40
	WING WT - LB	203,521	182,760	219,903	182,358
	WING WT - LB/SQ FT	8.68	9.75	15.13	11.97
	OPER WT - LB	756,565	713,960	731,177	688,269
	BLOCK FUEL - LB	449,669	424,714	397,310	384,489
	GROSS WT - LB	2,064,606	1,992,708	1,977,876	1,919,464
	DOC - ¢/ATNM (1.30/GAL)	7.31	6.95	6.75	6.52

Figure C-13. Wing Planform Comparison - Two-Body Aircraft (Customary Units) (Sheet 2 of 2)

	COMPARISON DATA \ WING PLANFORM →	① PARAMETRIC BASELINE	② REDUCED SWEEP CENTER SECTION	③ UNSWEPT - CENTER SECTION	④ STRAIGHT TAPER
$\underline{\eta}$ 39.62 m	BODY SEPARATION - m	39.62	39.62	39.62	39.62
	WING AR	8.96	9.23	10.30	9.00
	S_w - m^2	1,541	1,523	1,488	1,503
	$S_{w_o} \div S_w$	0.41	0.44	0.54	0.47
	C_b - m	12.14	12.72	14.03	13.77
	t_b - m	1.31	1.41	1.65	1.60
	C_r - m	24.64	21.68	14.03	18.46
	$C_t \div C_r$	0.26	0.31	0.53	0.40
	WING WT - kg	147,106	149,403	159,258	130,607
	WING WT - kg/m^2	95.45	98.14	107.02	86.91
	OPER WT - kg	403,606	403,530	419,577	382,621
	BLOCK FUEL - kg	207,779	205,200	210,415	204,821
	GROSS WT - kg	1,002,070	998,954	1,021,201	977,564
	DOC - ¢/AMgkm ($0.34/1)	4.64	4.61	4.74	4.52
$\underline{\eta}$ 44.25%	BODY SEPARATION - m	57.10	57.77	59.47	57.12
	WING AR	9.64	10.80	12.29	11.10
	S_w - m^2	1,727	1,579	1,469	1,501
	$S_{w_o} \div S_w$	0.29	0.31	0.43	0.38
	C_b - m	10.09	9.94	12.18	11.46
	t_b - m	1.12	1.10	1.51	1.37
	C_r - m	26.78	22.20	12.18	16.61
	$C_t - C_r$	0.22	0.26	0.58	0.40
	WING WT - kg	127,950	138,005	139,898	122,674
	WING WT - kg/m^2	74.12	87.40	95.21	81.73
	OPER WT - kg	382,798	387,658	387,972	366,592
	BLOCK FUEL - kg	198,459	190,894	191,010	186,271
	GROSS WT - kg	970,097	966,054	966,504	939,451
	DOC - ¢/AMgkm ($0.34/1)	4.48	4.40	4.40	4.26
$\underline{\eta}$ 50.0%	BODY SEPARATION - m	64.62	65.81	66.12	66.39
	WING AR	9.23	10.64	12.22	11.90
	S_w - m^2	1,809	1,628	1,431	1,482
	$S_{w_o} \div S_w$	0.23	0.26	0.38	0.32
	C_b - m	9.45	9.21	11.81	10.47
	t_b - m	1.05	1.02	1.48	1.26
	C_r - m	28.00	22.93	11.81	15.94
	$C_t \div C_r$	0.21	0.24	0.61	0.40
	WING WT - kg	114,193	124,281	124,272	116,855
	WING WT - kg/m^2	63.13	76.31	86.81	78.90
	OPER WT - kg	369,677	372,822	369,328	358,249
	BLOCK FUEL - kg	199,608	189,320	186,978	181,278
	GROSS WT - kg	958,257	949,275	943,024	925,153
	DOC - ¢/AMgkm ($0.34/1)	4.44	4.33	4.29	4.18

Figure C-14. Wing Planform Comparison - Three-Body Aircraft (Metric Units) (Sheet 1 of 2)

	COMPARISON DATA \ WING PLANFORM →	① BASELINE	② REDUCED SWEEP CENTER SECTION	③ UNSWEPT - CENTER SECTION	④ STRAIGHT TAPER
$\underline{\eta}$ 130 FT	BODY SEPARATION -FT	130	130	130	130
	WING AR	8.96	9.23	10.30	9.00
	S_w -SQ.FT.	16,589	16,391	16,022	16,174
	$S_{w_o} \div S_w$	0.41	0.44	0.54	0.47
	C_b - FT	39.84	41.74	46.03	45.18
	t_b - FT	4.29	4.64	5.41	5.24
	C_r - FT	80.83	71.13	46.03	60.56
	$C_t - C_r$	0.26	0.31	0.53	0.40
	WING WT - LB	324,314	329,378	351,191	287,940
	WING WT - LB/SQ FT	19.55	20.10	21.92	17.80
	OPER WT - LB	889,798	889,632	925,008	843,534
	BLOCK FUEL - LB	458,072	452,388	463,886	451,553
	GROSS WT - LB	2,209,187	2,202,317	2,251,364	2,155,160
	DOC - ¢/ATNM (1.30/GAL)	7.80	7.75	7.97	7.59
$\underline{\eta}$ 44.25%	BODY SEPARATION -FT	187.33	189.53	195.10	187.41
	WING AR	9.64	10.80	12.29	11.10
	S_w -SQ.FT.	18,585	16,995	15,816	16,160
	$S_{w_o} \div S_w$	0.29	0.31	0.43	0.38
	C_b - FT	33.11	32.62	39.97	37.60
	t_b - FT	3.66	3.61	4.94	4.50
	C_r - FT	87.86	72.84	39.97	54.51
	$C_t - C_r$	0.22	0.26	0.58	0.40
	WING WT - LB	282,081	304,249	308,422	270,450
	WING WT - LB/SQ FT	15.18	17.90	19.50	16.74
	OPER WT - LB	843,926	854,639	855,332	808,197
	BLOCK FUEL - LB	437,527	420,849	421,104	410,657
	GROSS WT - LB	2,138,697	2,129,785	2,130,777	2,071,135
	DOC - ¢/ATNM (1.30/GAL)	7.52	7.40	7.40	7.16
$\underline{\eta}$ 50.0%	BODY SEPARATION -FT	212.02	215.92	216.92	217.81
	WING AR	9.23	10.64	12.22	11.90
	S_w -SQ.FT.	19,471	17,529	15,407	15,947
	$S_{w_o} - S_w$	0.23	0.26	0.38	0.32
	C_b - FT	31.02	30.21	38.75	34.34
	t_b - FT	3.43	3.35	4.84	4.13
	C_r - FT	91.87	75.24	38.75	52.30
	$C_t - C_r$	0.21	0.24	0.61	0.40
	WING WT - LB	251,752	273,993	273,972	257,621
	WING WT - LB/SQ FT	12.93	15.63	17.78	16.16
	OPER WT - LB	814,998	821,931	814,228	789,803
	BLOCK FUEL - LB	440,061	417,379	412,215	399,650
	GROSS WT - LB	2,112,595	2,092,794	2,079,013	2,039,613
	DOC - ¢/ATNM (1.30/GAL)	7.46	7.28	7.20	7.02

Figure C-14. Wing Planform Comparison - Three-Body Aircraft (Customary Units) (Sheet 2 of 2)

C.3 BODY SPANWISE LOCATION SELECTION

Lateral control capability requirements impose a limit on the spanwise location of the fuselage bodies. As body locations are moved outboard, aircraft roll inertia increases and lateral control effectiveness decreases (wing area available to provide capability decreases). To define a reasonable body spanwise location limit, the lateral control capability is analyzed for four body locations, 19, 34.9, 38, and 50 percent semispan. The two-body unswept wing planform number 3 aircraft of the previous wing planform selection study is used for this analysis. The lateral control task for establishing the requirement shown in Figure C-15 and discussed in paragraph C.1.3 is used as the criterion to evaluate the aircraft configured for the various body locations.

Wing characteristics of the evaluated aircraft are a 0.4 rad (25 degree) quarter chord sweep angle and aspect ratios between 10.32 and 10.6. Aileron chord is 25 percent of the local wing chord and aileron span is from 70 percent semispan to just short of the tip. Spoiler chord is 15 percent of the local wing chord with the hinge line at 60 percent of the local wing chord. Spoiler span is from the inboard tip of the aileron (70 percent semispan) to the outer side of the fuselage. No spoilers are used inboard of the bodies. Maximum spoiler deflection is 1.05 rad (60 degrees), and maximum aileron deflection is 0.44 rad (25 degrees) trailing edge up and 0.26 rad (15 degrees) trailing edge down, giving 0.70 rad (40 degrees) total deflection. These specifications for the ailerons and spoilers are the same as defined for the point design aircraft.

Datcom methods are used to estimate the lateral control effectiveness. Adjustment factors based on C-5 flight test data are appplied to the lateral control effectiveness values. C-5 aeroelastic characteristics are used as being representative of multibody flexibility characteristics. Flight conditions are at sea level and 67.9 m/sec (132 knots) with flaps extended.

Figure C-16 is a summary of the two-body aircraft lateral control effectivness and inertias. C-5 data are also shown in this figure for comparison. Full lateral control roll acceleration calculated from these data are shown in Figure C-17. All of the two-body aircraft have less than half of the C-5 roll acceleration capability. Figure C-18 shows estimated time histories of step input full lateral control roll maneuvers for these aircraft. The military specification requirement from Reference 5 for Class III, Category C, Level 1, flight is also shown. The two-body aircraft do not meet this requirement.

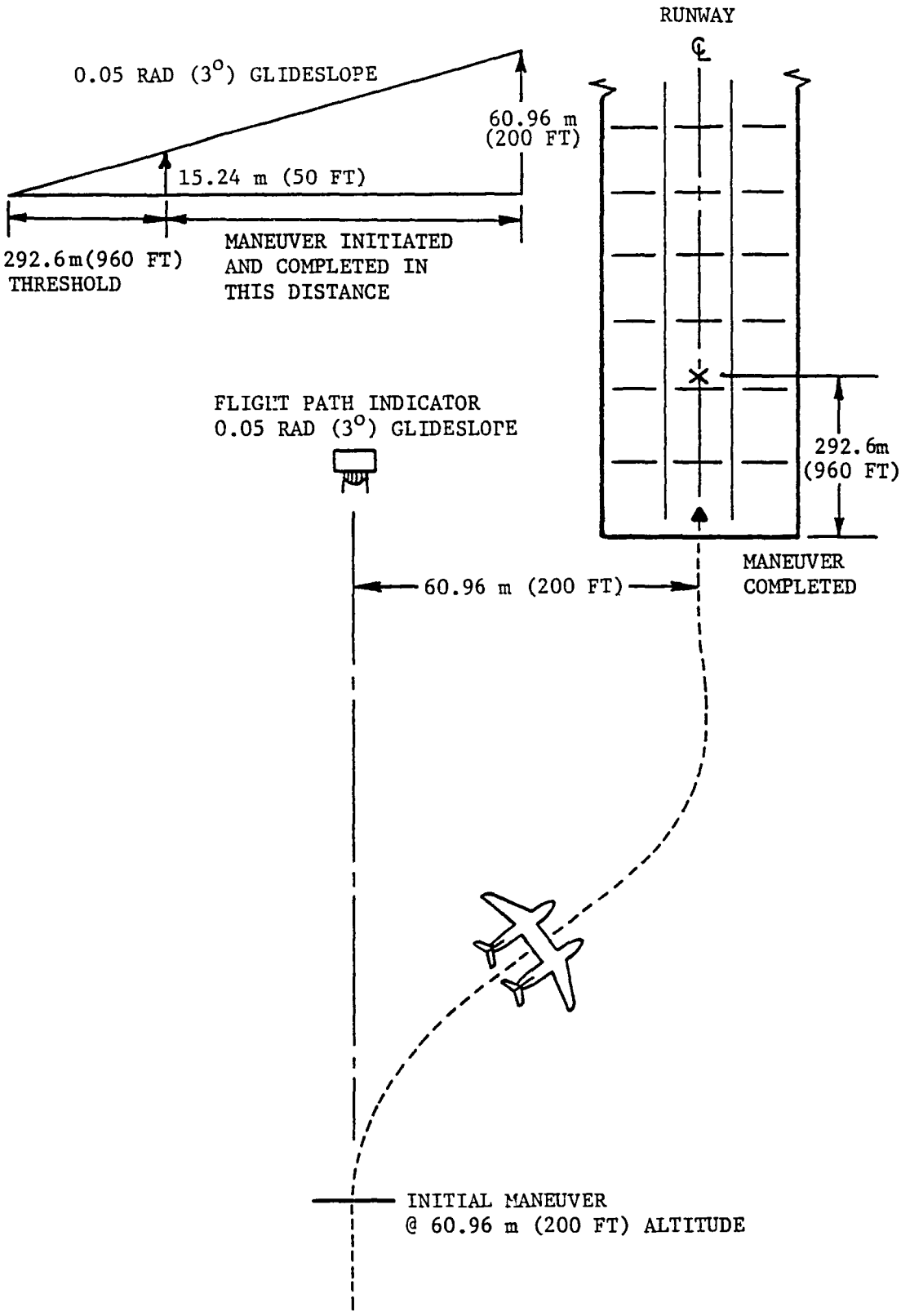

Figure C-15. Typical Runway Offset Maneuver - Pure Bank for Turn and Displacement

BODY POSITIONS (% SEMISPAN)	C_{l_δ} (FULL LATERAL CONTROL -SPOILERS & AILERONS)	I_{xx} MAXIMUM $kg\ m^2 \times 10^{-8}$ (LB IN $^2 \times 10^{-12}$)
19	0 1196	5 73 (1 96)
38	0 0872	7 31 (2 50)
50	0 0662	8 72 (2.98)
34 8	0 0909	7 02 (2 4)
(C-5)	0 0983	0 524 (0 179)

Figure C-16. Lateral Control Effectiveness and Inertias - Two-Body Aircraft

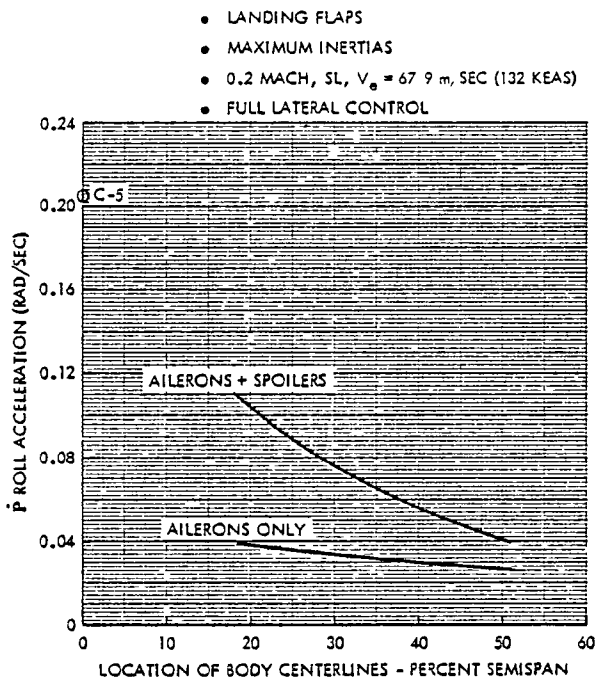

Figure C-17. Roll Acceleration - Two-Body Aircraft

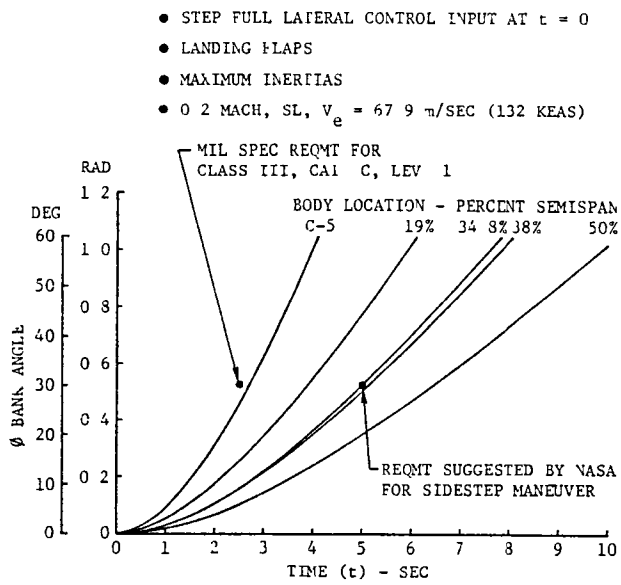

Figure C-18. Roll Time Histories - Two-Body Aircraft

Bank angle time histories for maximum lateral displacement are estimated from data in Figure C-18. These data are used to generate a lateral displacement time history during the final approach sidestep maneuver. The lateral displacements achieved are plotted in Figure C-19. Maximum bank angle is limited to 0.26 rad (15 degrees), and data are calculated for 50, 75, and 100 percent maximum lateral control. Figure C-20 shows maximum roll rate and bank angles, minimum wing tip clearances, and maximum lift losses due to

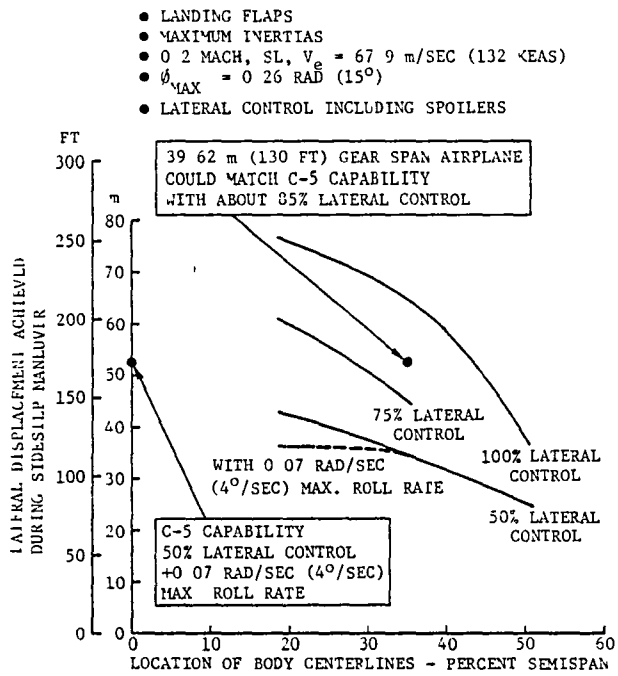

Figure C-19. Sidestep Maneuver Capability - Two-Body Aircraft

BODY POSITION - % SEMISPAN	LATERAL CONTROL -PERCENT MAXIMUM	MAXIMUM ROLL RATE -RAD/SEC (DEG/SEC)	MAXIMUM BANK ANGLE -RAD (DEG)	MINIMUM WING TIP CLEARANCE -m (FT)	MAX. ΔC_L DUE TO LAT. CONTROL
19.0	50	0.12 (6.6)	0.19 (11.0)	16 (52)	0.25
19.0	75	0.17 (9.6)	0.25 (14.5)	12 (40)	0.41
19.0	100	0.20 (11.2)	*0.26 (15.0)	8 (25)	0.57
34.8	50	0.09 (5.0)	0.15 (8.5)	18 (60)	0.14
34.8	75	0.12 (6.9)	0.21 (12.1)	15 (48)	0.23
34.8	100	0.15 (8.8)	0.26 (15.0)	11 (37)	0.32
50.0	50	0.06 (3.2)	0.10 (5.8)	20 (65)	0.06
50.0	100	0.11 (6.4)	0.17 (10.0)	17 (56)	0.13
(C-5)	50	*0.07 (4.0)	0.21 (12.0)	16 (54)	0.15

*CONSTRAINED TO THIS MAXIMUM VALUE

Figure C-20. Sidestep Maneuver Characteristics - Two-Body Aircraft

lateral control for the data points in Figure C-19. Note that during the C-5 sidestep maneuver used for the comparison, the roll rate is not allowed to exceed 0.07 rad/sec (4 degrees/sec) and only 50 percent lateral control is used. These conditions correspond to a flight test point that is rated satisfactory in the sidestep maneuver.

None of the two-body aircraft matches the C-5, 50 percent lateral control sidestep maneuver capability. However, Figure C-19 shows that the 34.8 percent semispan two-body aircraft with spoilers and ailerons can match the C-5 capability in the sidestep maneuver at conditions of approximately 85 percent lateral control with no limit on maximum roll rate. The maximum two-body aircraft roll rate during this maneuver is about 0.134 rad/sec (7.7 degrees/sec) and the wing tip minimum ground clearance is about 13.4m (44 ft). This contrasts to the C-5 conditions during this maneuver of .07 rad/sec (4 degrees/sec) maximum roll rate and wing tip minimum ground clearance of 16.5m (54 ft).

As previously stated, this preliminary analysis shows that the 34.8 percent semispan body location aircraft can execute the sidestep maneuver, but only with no roll rate restrictions and using approximately 85 percent lateral control. Preliminary results from the NASA flight simulation confirmed that this maneuver is a reasonable test of lateral control capability. It appears that if an aircraft can achieve 0.52 rad (30 degrees) of bank angle in 5.0 seconds or less, the performance in the sidestep maneuver is adequate. This bank angle capability is achieved with a 34.8 percent semispan body location (39.6m (130 ft) landing gear separation) or less, as shown in Figure C-16 and explained above. Therefore, a maximum body separation distance of 39.6m (130 ft) is selected for the point design aircraft.

This Page Intentionally Left Blank

APPENDIX D

FLUTTER ANALYSIS METHODS AND PROCEDURES

Flutter boundaries for the point design aircraft are computed using a flutter determinate solution with doublet lattice aerodynamics and coupled wing modes and presented at matched Mach numbers, velocities, and altitudes. Whenever flutter instabilities exist inside the required 20 percent margin, optimum stiffness curves are defined by adding wing stiffness where a maximum increase in flutter speed is obtained for the least weight penalty. After the new optimum stiffness distributions are recycled through weight estimation and aircraft sizing programs, a new set of flutter boundaries are computed.

Two separate computer programs are used for flutter calculations: one for flutter boundaries and the other for optimum stiffness distributions. Both programs use symmetric or antisymmetric vibration modes derived from a wing beam model with rigid fuselage, empennage, engines and pylon, and a k-type determinate solution to evaluate the flutter velocities. The program that calculates flutter boundaries uses unsteady doublet lattice aerodynamics applied to all surfaces, coupled wing modes, and computes the flutter velocities for 10 altitudes and 8 combinations of fuel, cargo, and symmetries. Optimum stiffness distributions are computed at one altitude, symmetry, fuel, and cargo condition (generally, the most critical) using modified unsteady strip theory aerodynamics, applied only to the wing, and a set of uncoupled cantilevered wing bending and torsion modes. Flutter derivatives (the change in flutter velocity divided by the weight penalty) are derived for each wing panel. Stiffness is increased where the flutter derivatives are the largest and whenever possible is decreased for the smallest derivative values. Total stiffness changes are limited to effect an overall change in flutter velocity increment (the difference between required and actual) of 15 percent, which requires at least 7 resizing steps to change the initial flutter velocity to the required flutter velocity. Incrementing the wing stiffness values in this manner is intended to accomplish (1) more uniformity of the flutter derivatives along the wing span, (2) accountability of changes in critical flutter mode characteristics, (3) define lowest stiffness boundaries for all flutter modes

encountered and (4) determine the least weight penalty required to achieve the 20 percent flutter margin.

Flutter boundaries are computed using a detailed representation of the configuration under consideration. Three-dimensional unsteady aerodynamic influence coefficients are calculated for the wing, empennage, fuselage, engines, and pylons using a reasonable panel description for all components based on their expected effects on the flutter results. For instance, the wing panel description is more detailed than the fuselage since the wing is flexible and the fuselage is considered rigid. Similar statements exist for the panel arrangements of the other components compared to the wing. Illustrations of the doublet lattice panel descriptions appear in Figures D-1, D-2, D-3, and D-4. Flutter results were verified by using modified strip theory and a larger number of streamwise doublet lattice panel arrangements. All analyses gave the same or very close to the same results. Coupled vibration modes are computed for the flexible wing with all other components rigid. Eighteen (18) coupled aircraft elastic, plus 3 rigid body modes were used in the flutter analysis for all configurations. These modes are based on weight and stiffness data provided by an analytical structural weight estimation routine (Section 2.7.3). Coupled mode displacements are computed for all flexible and rigid components for zero and mission fuel and zero and full cargo. Results of the vibration solution are illustrated as vector plots of the displacements at the leading and trailing edges of the lifting surfaces and at the elastic axis for other components, as shown in Figures D-5 through D-64 for the two-body MB2 aircraft with the unswept center section wing and the optimum stiffness distribution. Additional plots were completed for the other point design aircraft as an aid to understanding the flutter mechanism; however, only the two-body data are given as a typical example of the analysis. Fifteen (15) elastic modes were plotted for the vibration mode plots because flutter involved only the first several elastic modes, and these plots were included to show that all of the low frequency vibration modes were included in this analysis. These modal data are used to compute the generalized mass (weight times the square of the modal displacement), stiffness (generalized mass times the frequency squared), and aerodynamics (product of the complex panel lift, its respective modal displacement, complex downwash, and dynamic pressure). These generalized matrices

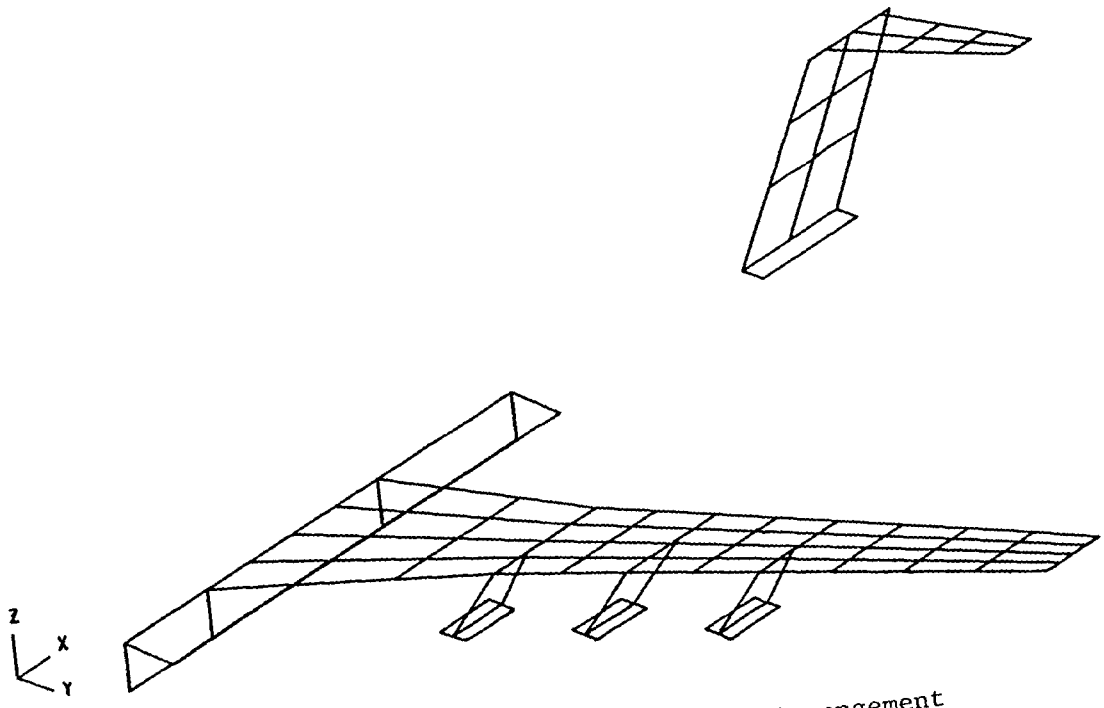

Figure D-1. Doublet Lattice Panel Arrangement Single Body Reference SBR Aircraft

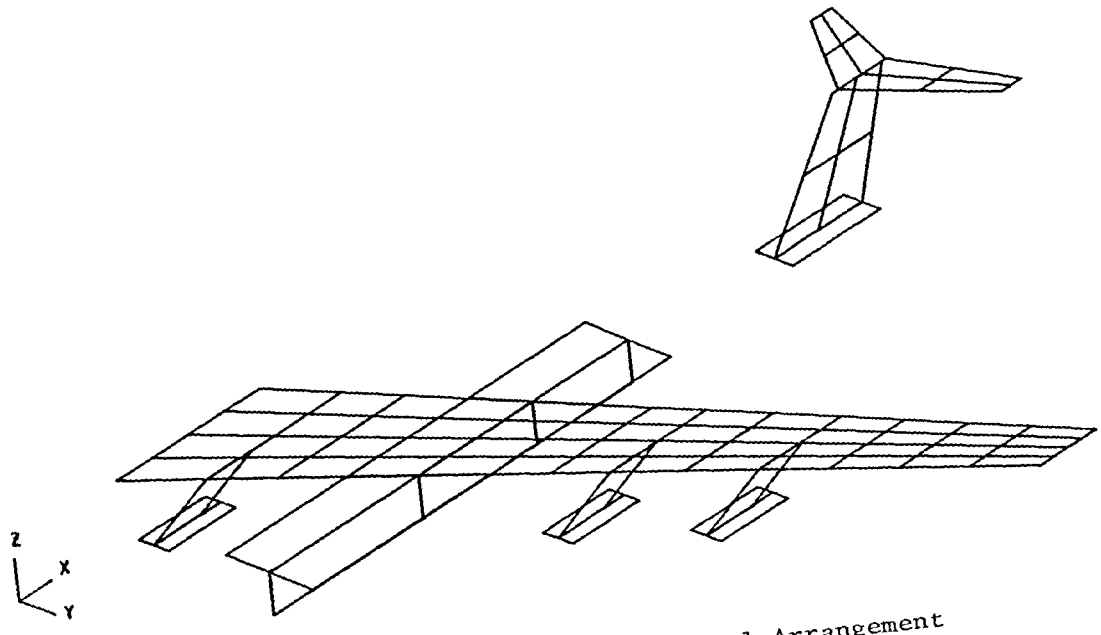

Figure D-2. Doublet Lattice Panel Arrangement Two-Body MB1 Aircraft

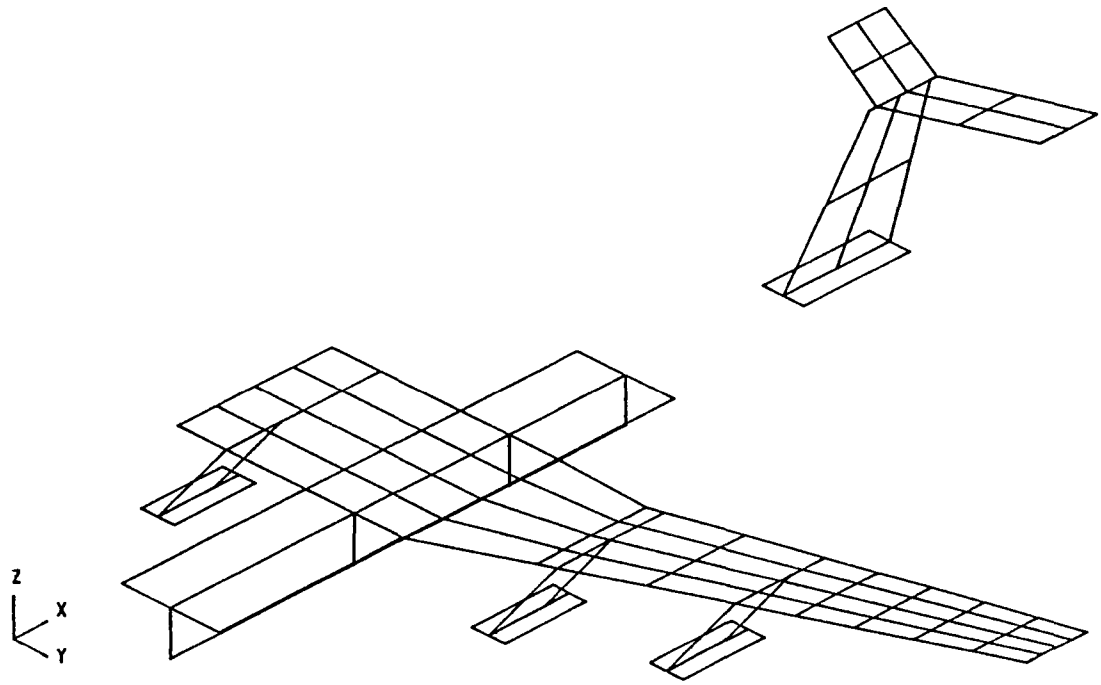

Figure D-3. Doublet Lattice Panel Arrangement
Two-Body MB2 Aircraft

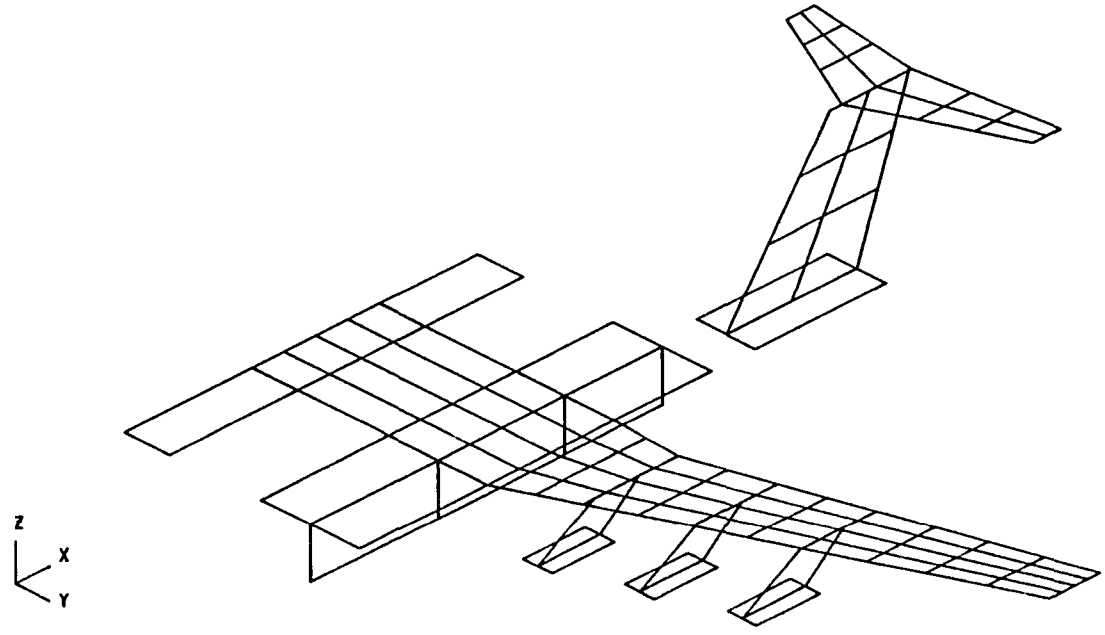

Figure D-4. Doublet Lattice Panel Arrangement
Three-Body MB3 Aircraft

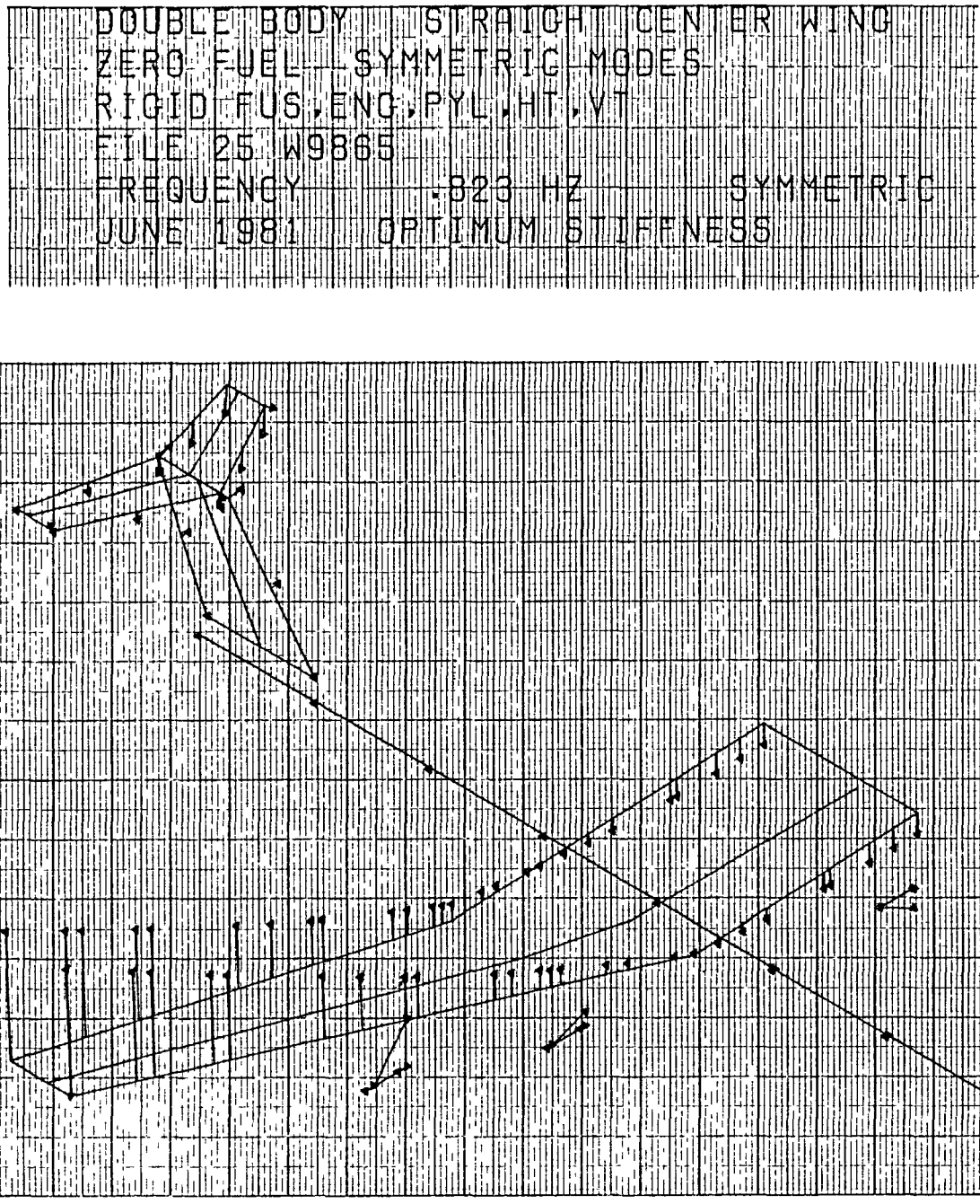

Figure D-5. Displacement Vectors - Symmetric Mode No. 1 - Two-Body MB2 Aircraft

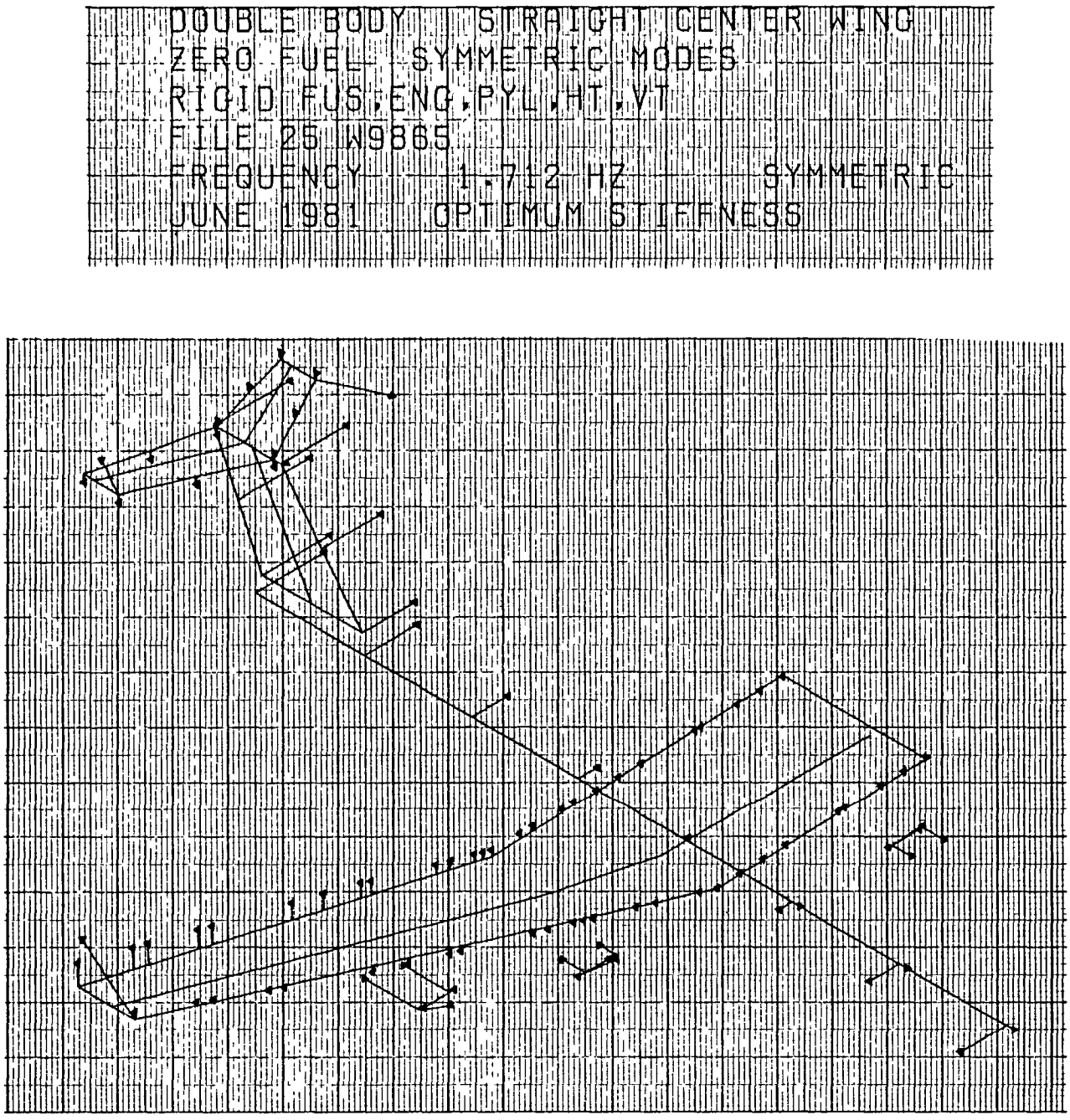

Figure D-6. Displacement Vectors - Symmetric Mode No. 2 - Two-Body MB2 Aircraft

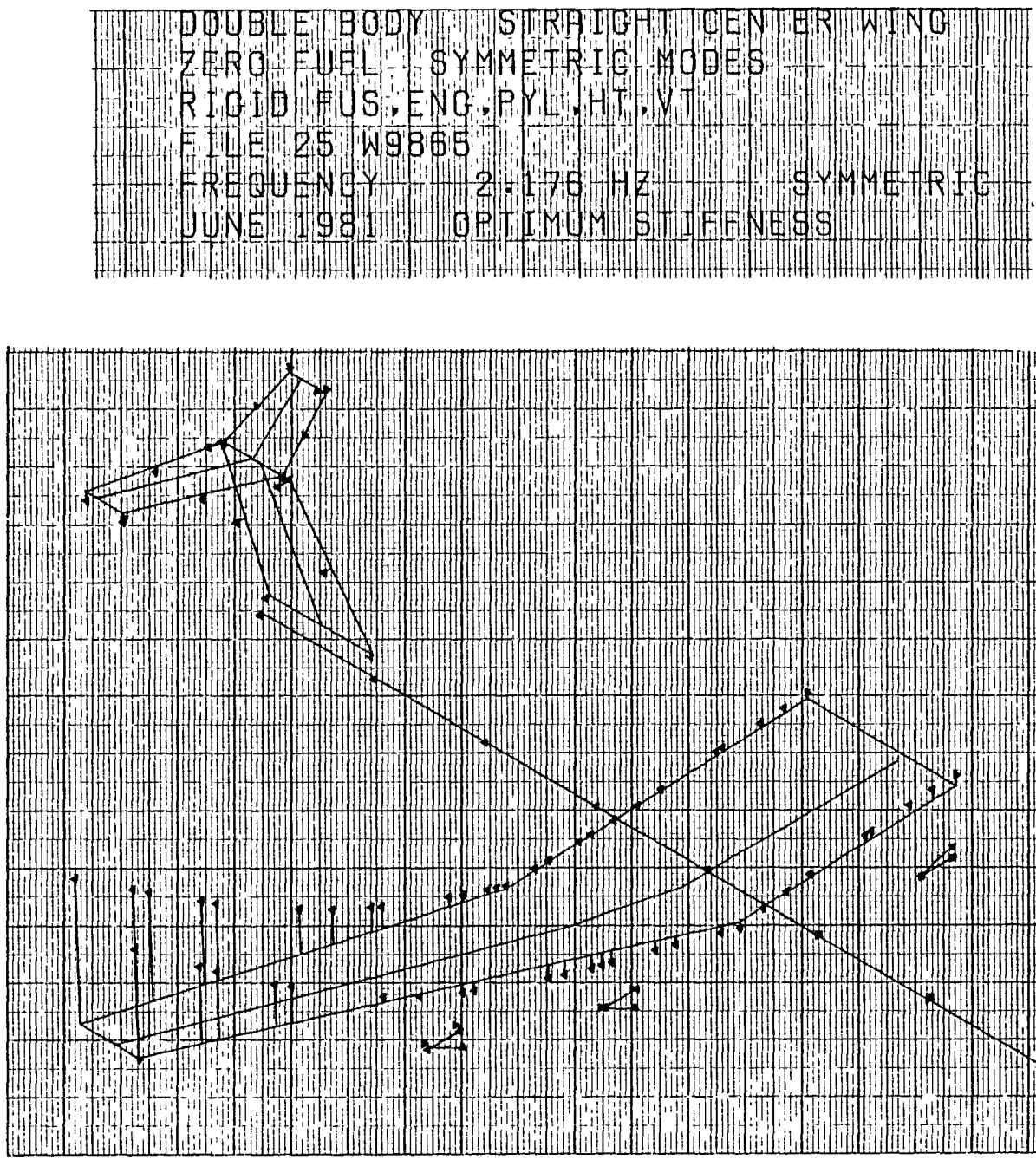

Figure D-7. Displacement Vectors - Symmetric Mode No. 3 - Two-Body MB2 Aircraft

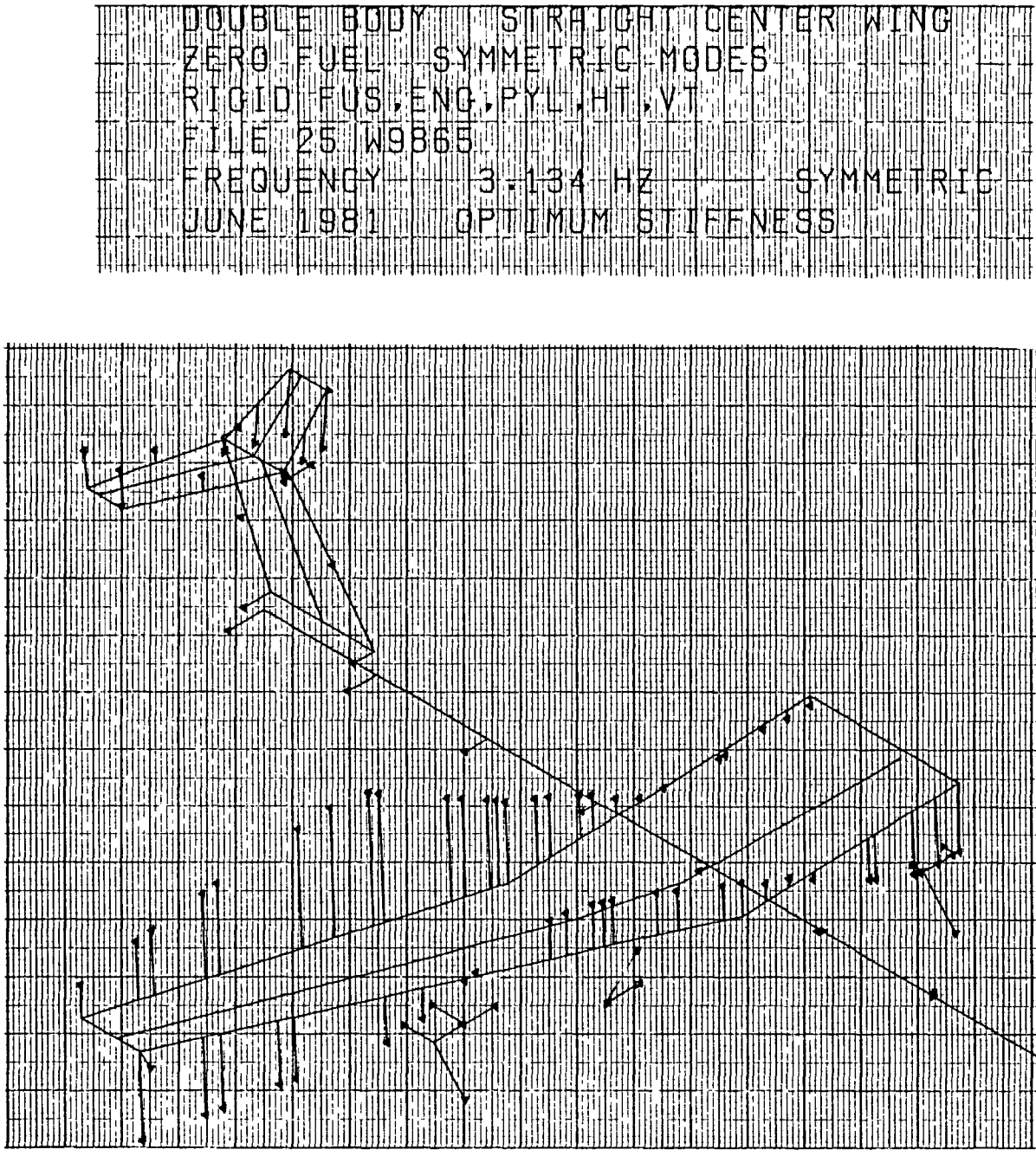

Figure D-8. Displacement Vectors - Symmetric Mode No. 4 - Two-Body MB2 Aircraft

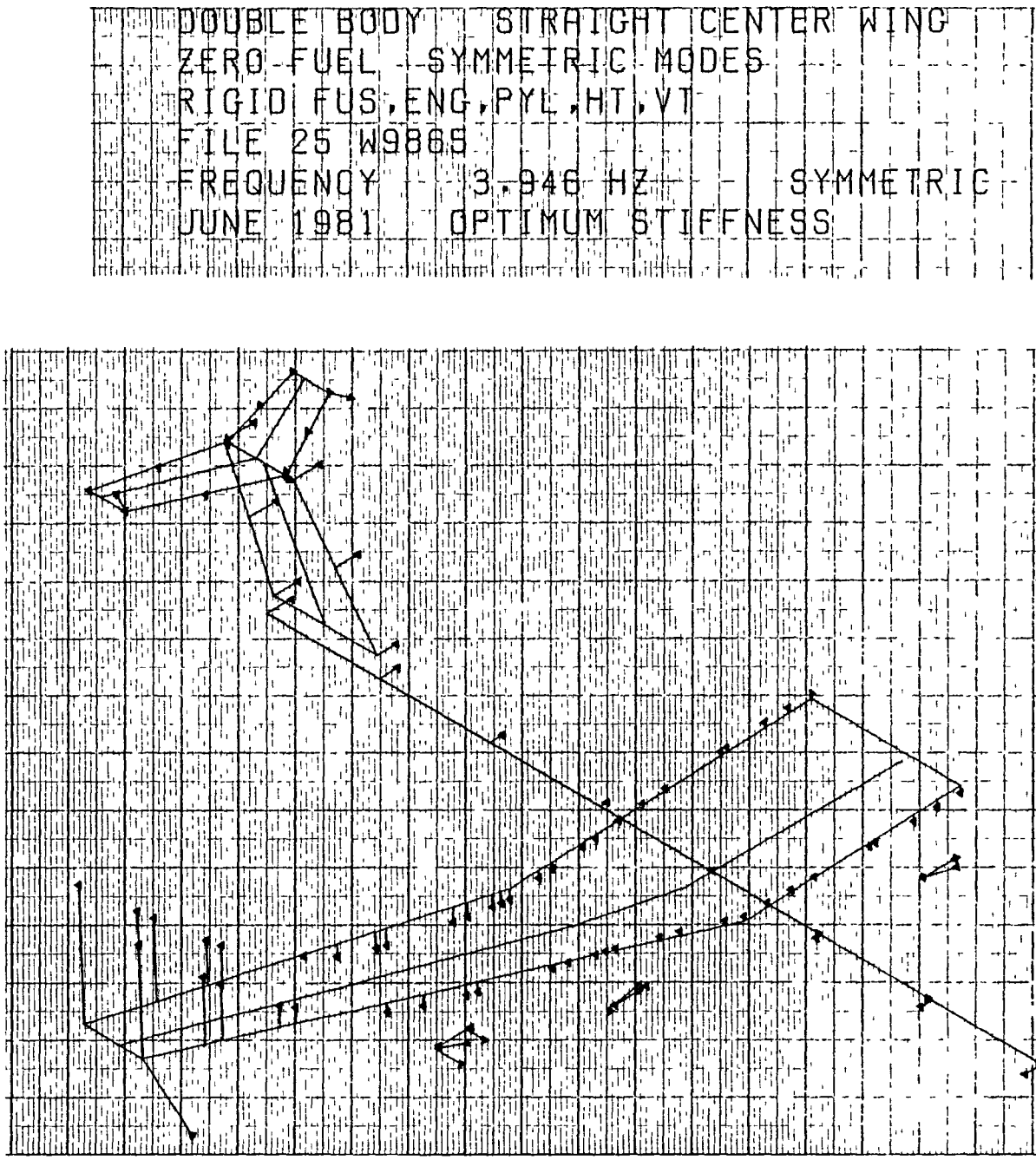

Figure D-9. Displacement Vectors - Symmetric Mode No. 5 - Two-Body MB2 Aircraft

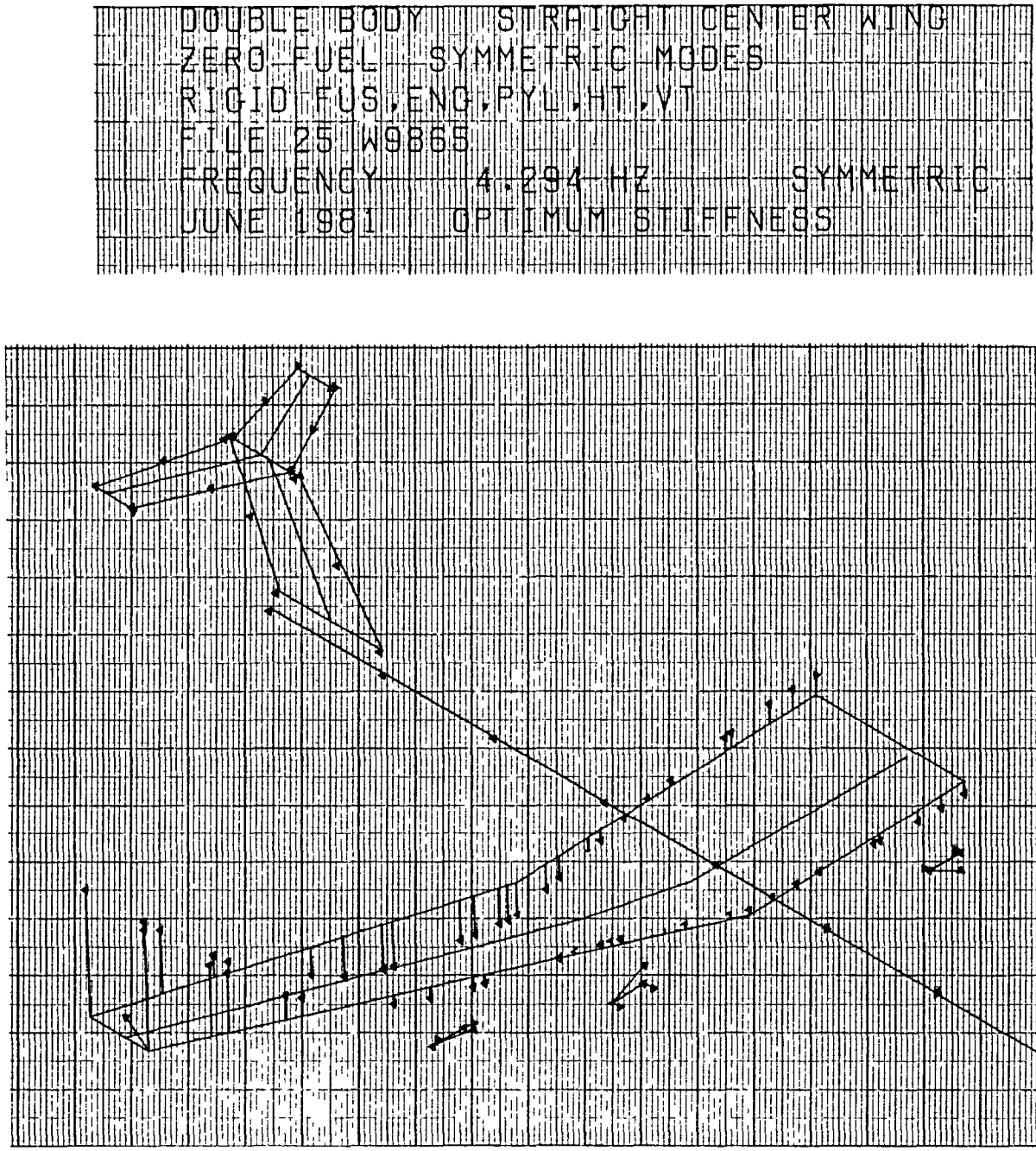

Figure D-10. Displacement Vectors - Symmetric Mode No. 6 - Two-Body MB2 Aircraft

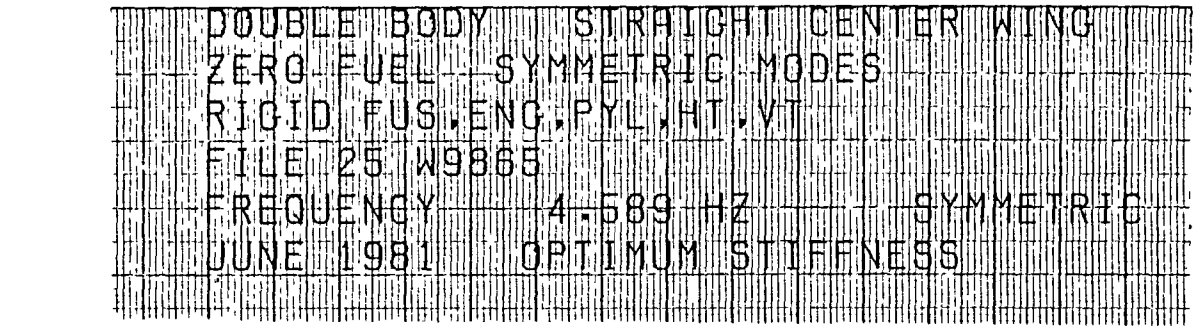

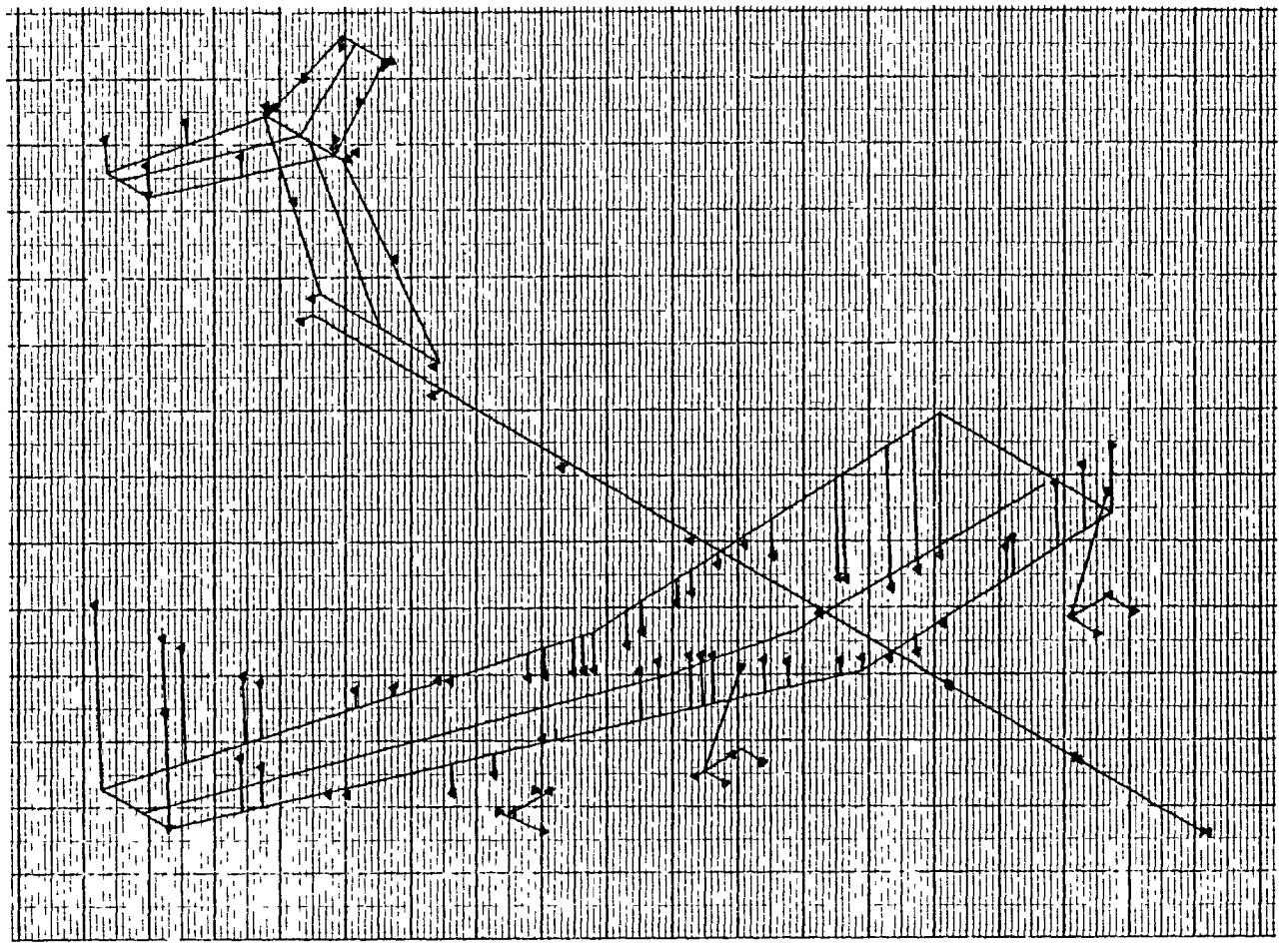

Figure D-11. Displacement Vectors - Symmetric Mode No. 7 - Two-Body MB2 Aircraft

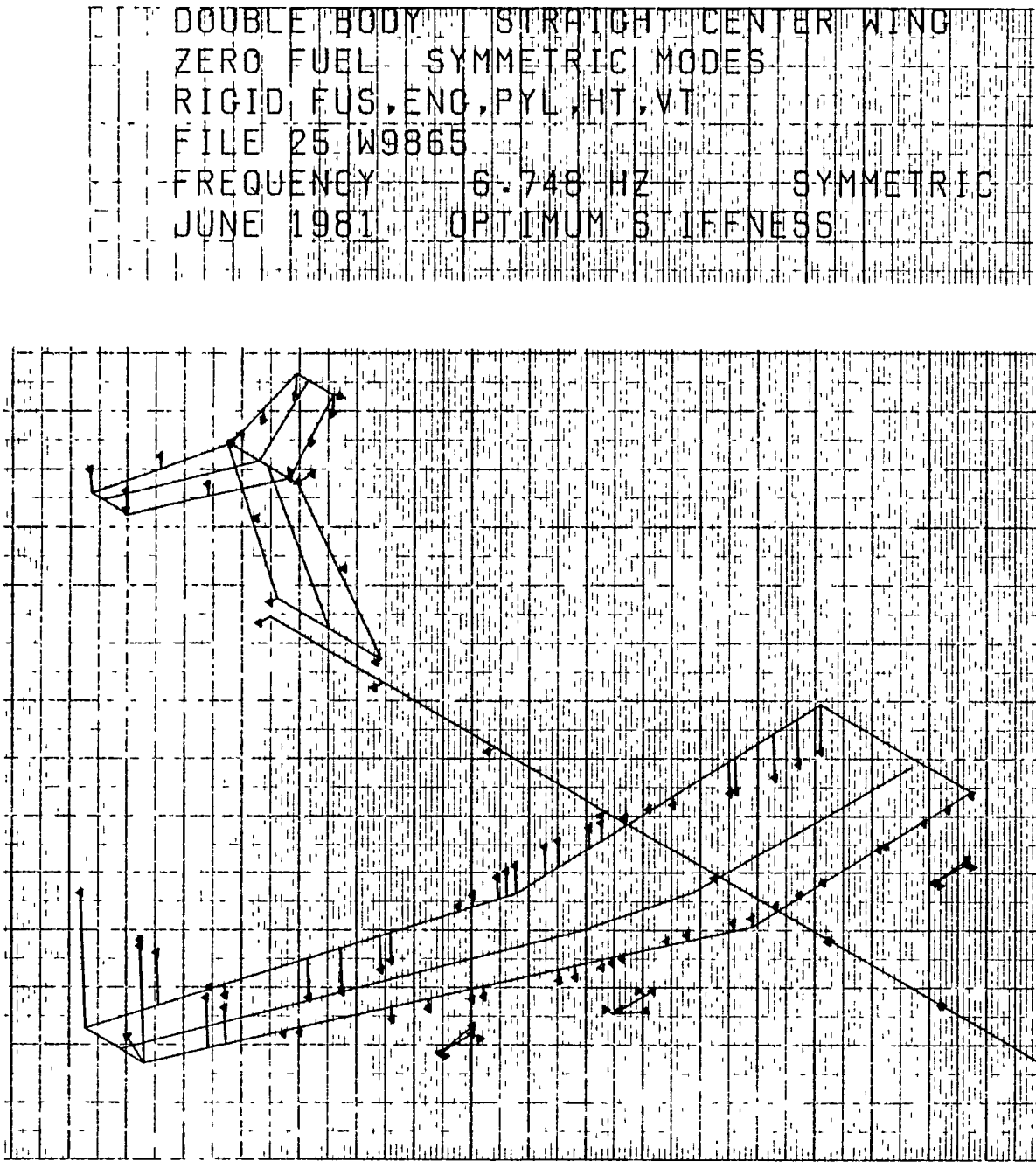

Figure D-12. Displacement Vectors - Symmetric Mode No. 8 - Two-Body MB2 Aircraft

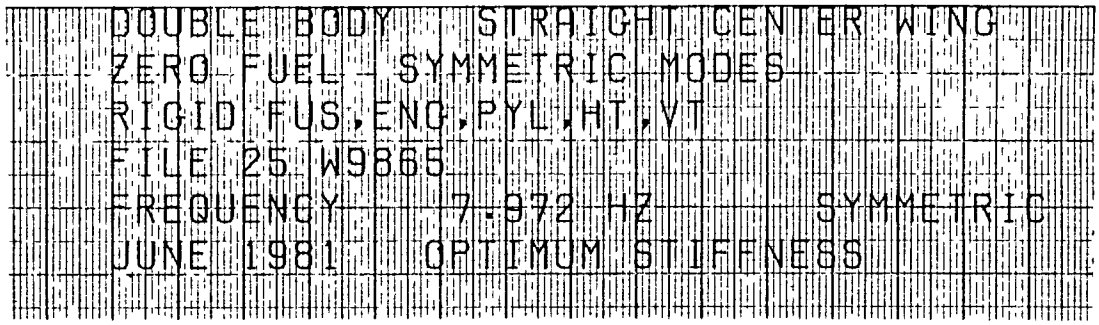

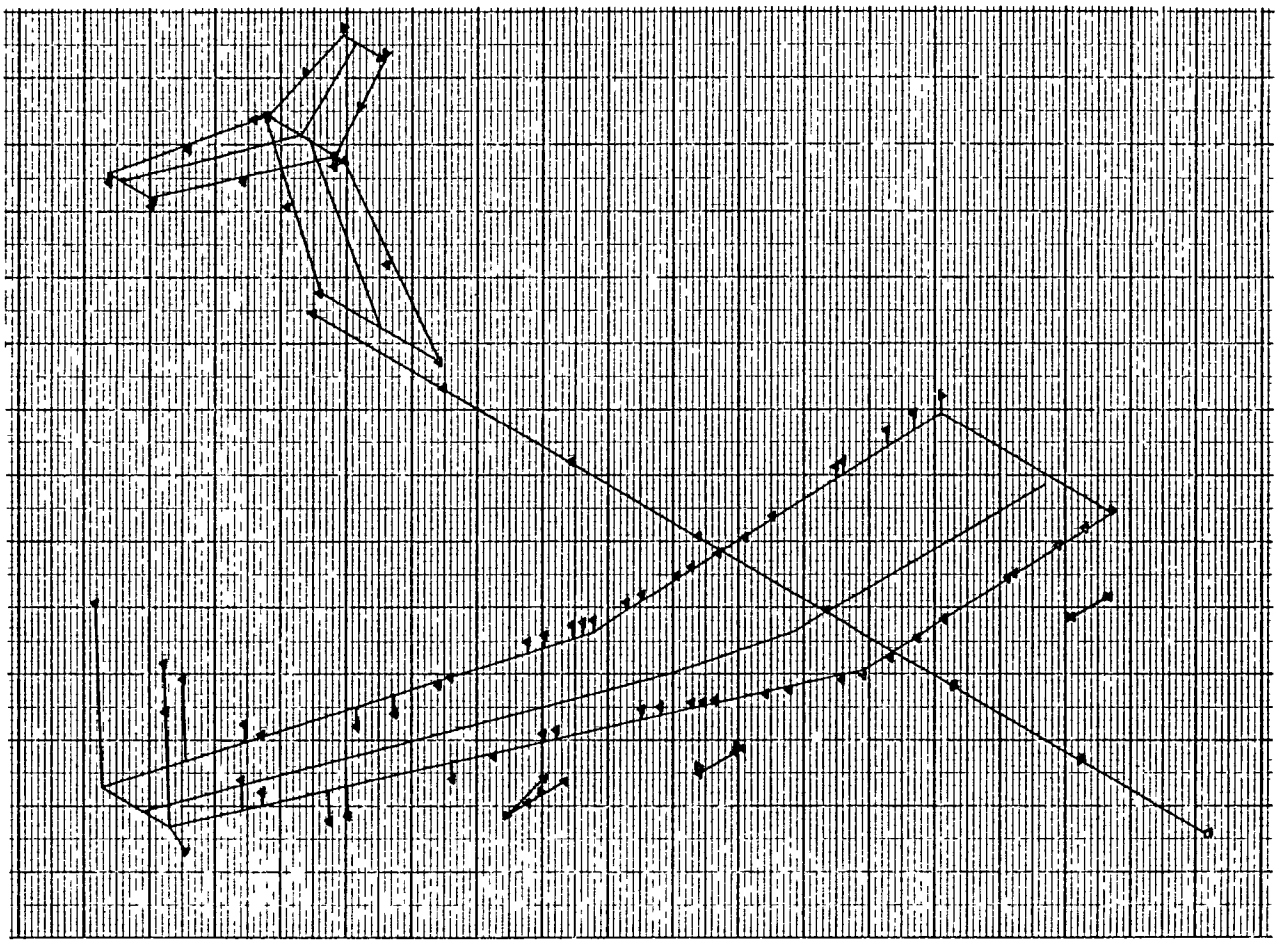

Figure D-13. Displacement Vectors - Symmetric Mode No. 9 - Two-Body MB2 Aircraft

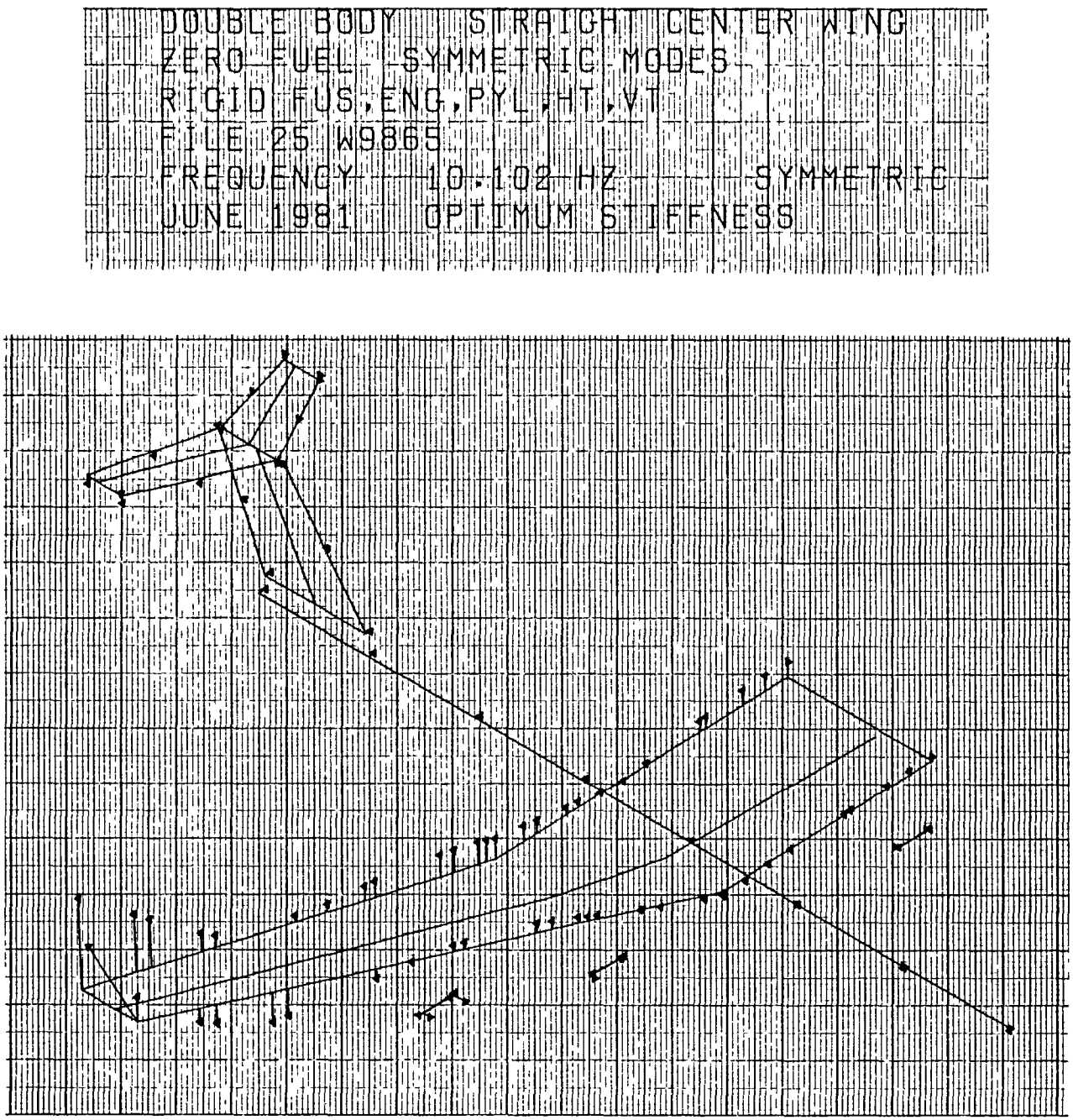

Figure D-14. Displacement Vectors - Symmetric Mode No. 10 - Two-Body MB2 Aircraft

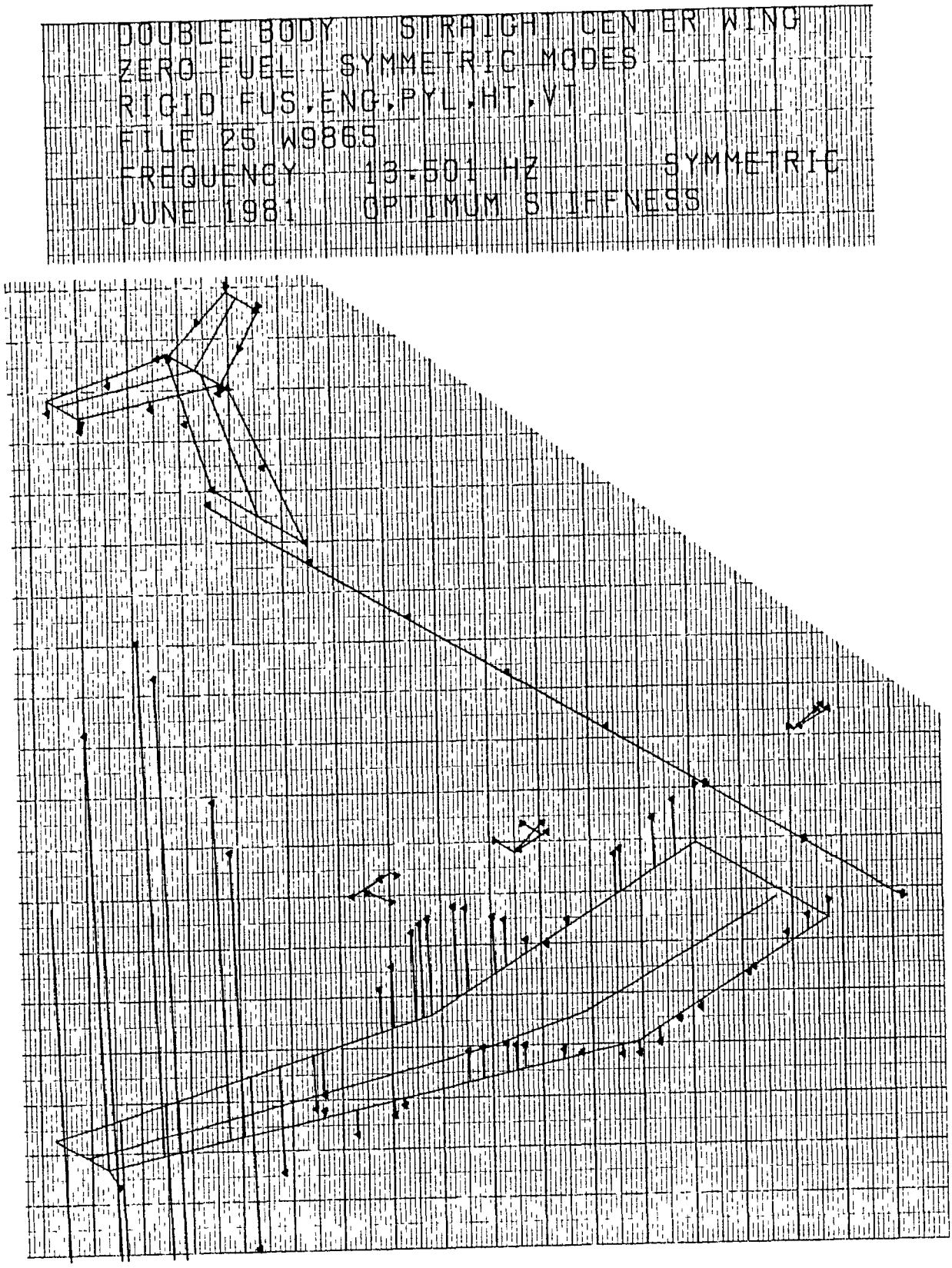

Figure D-15. Displacement Vectors - Symmetric Mode No. 11 - Two-Body MB2 Aircraft

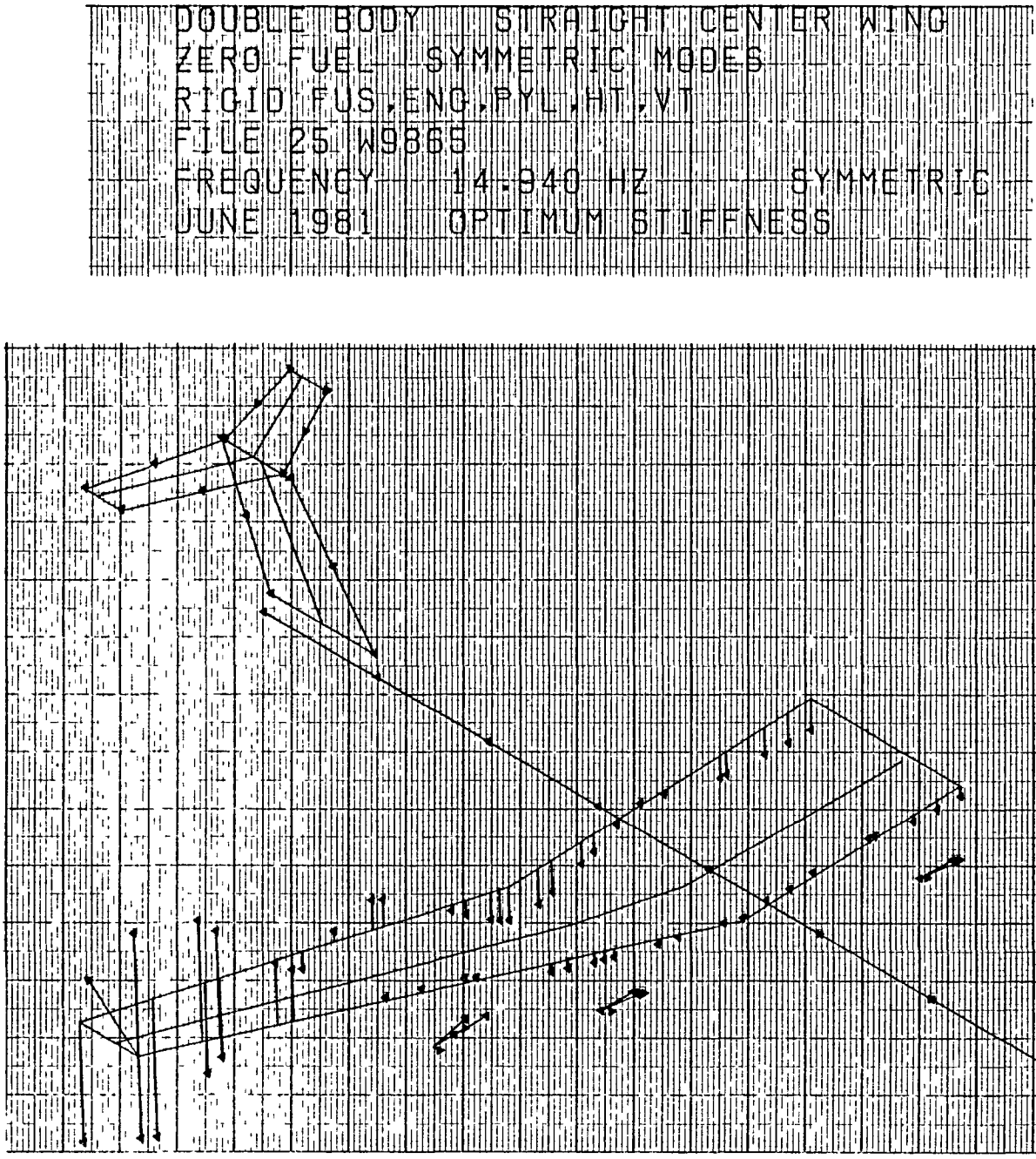

Figure D-16. Displacement Vectors - Symmetric
Mode No. 12 - Two-Body MB2 Aircraft

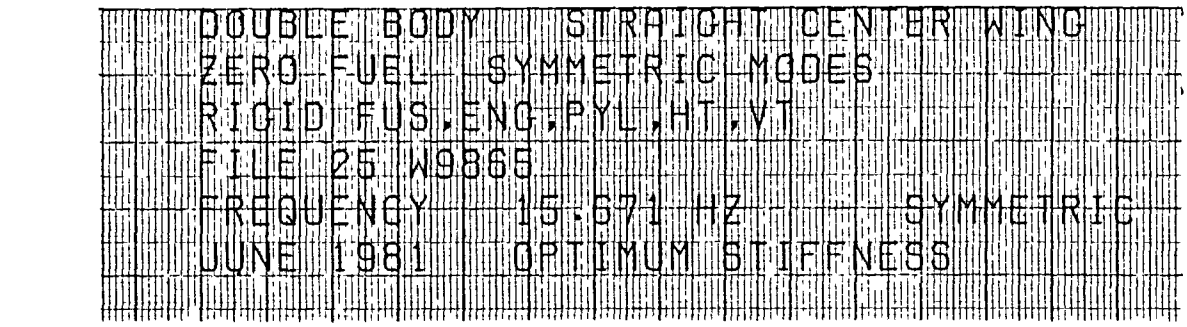

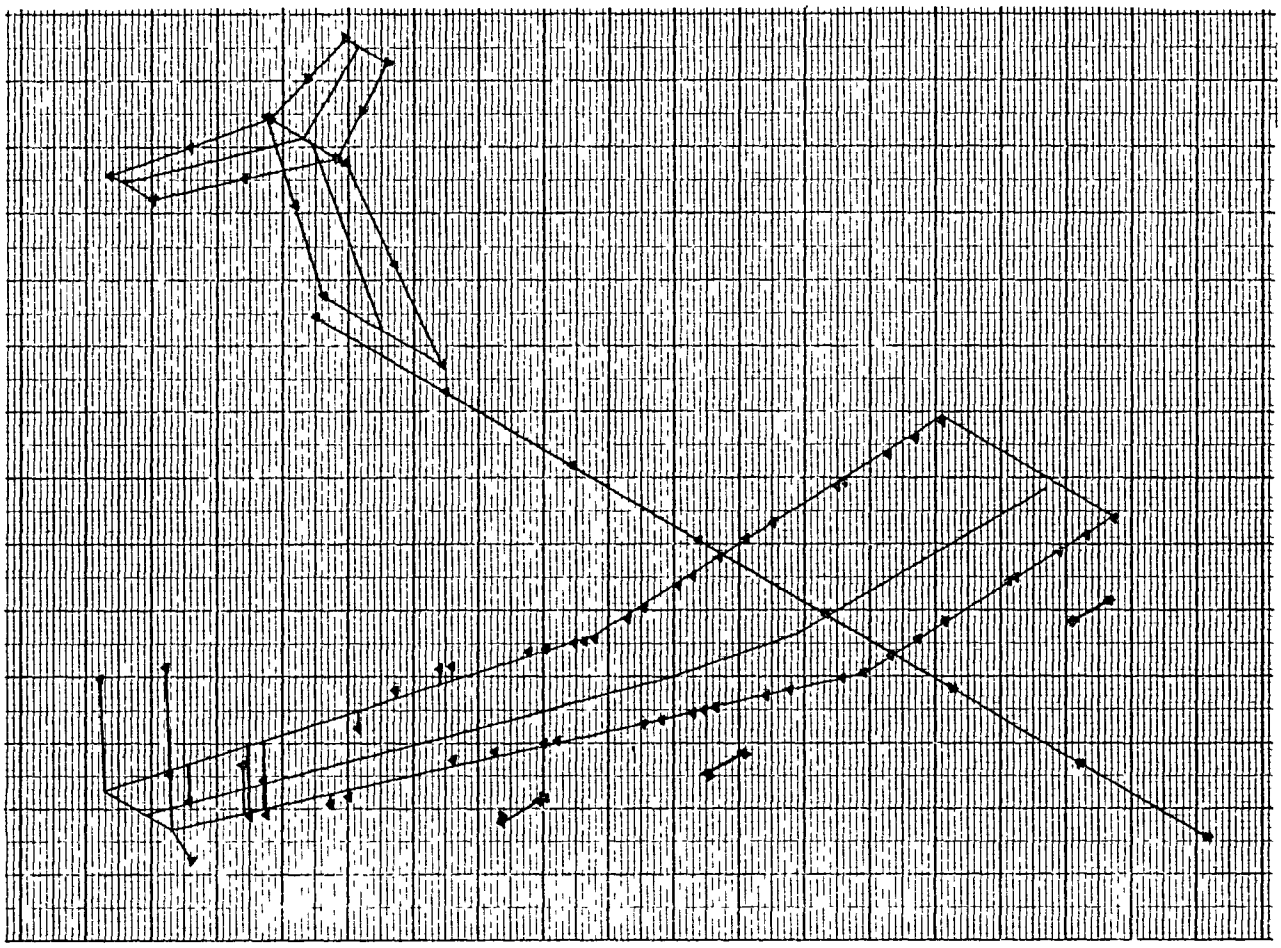

Figure D-17. Displacement Vectors - Symmetric Mode No. 13 - Two-Body MB2 Aircraft

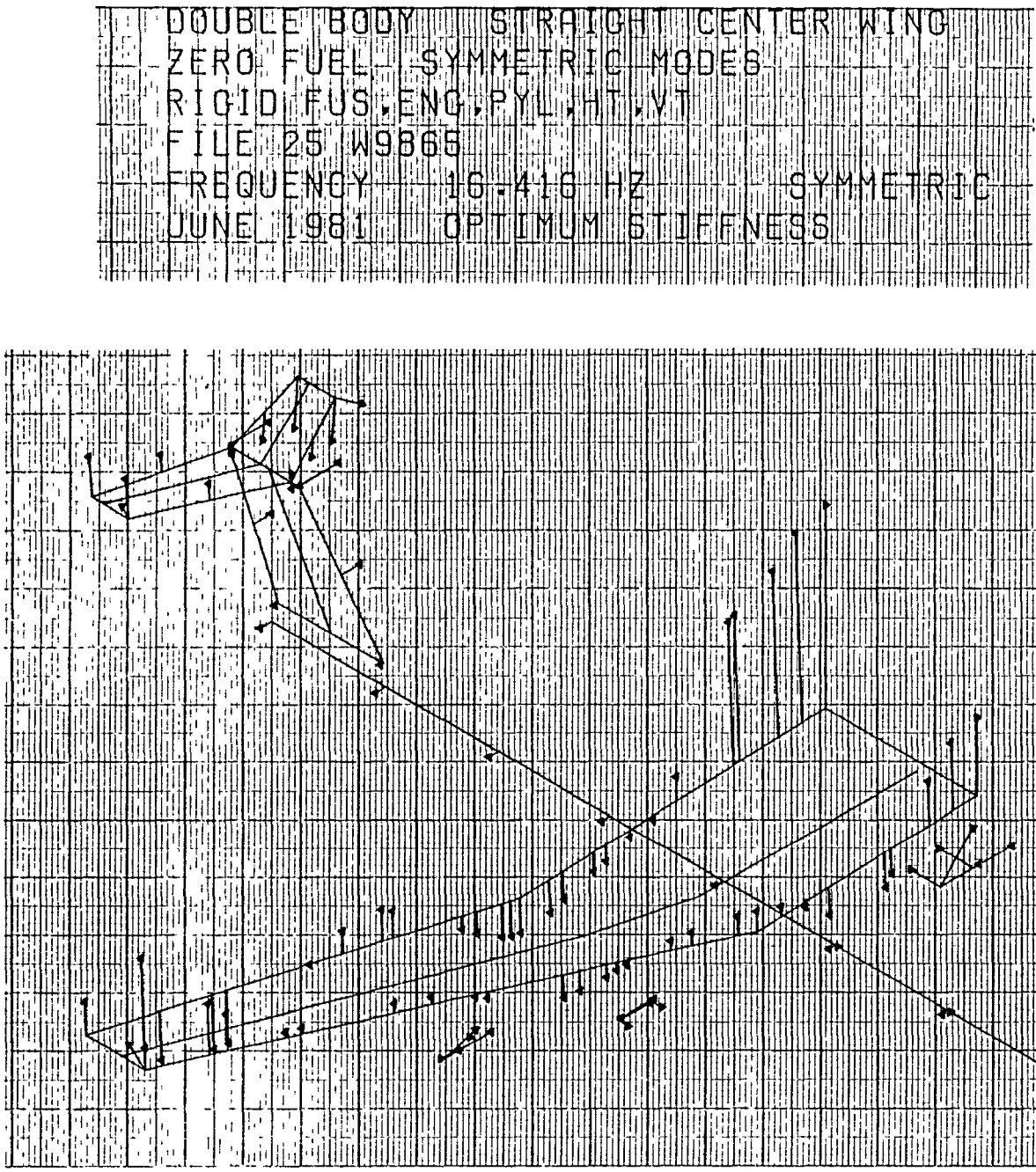

Figure D-18. Displacement Vectors - Symmetric Mode No. 14 - Two-Body MB2 Aircraft

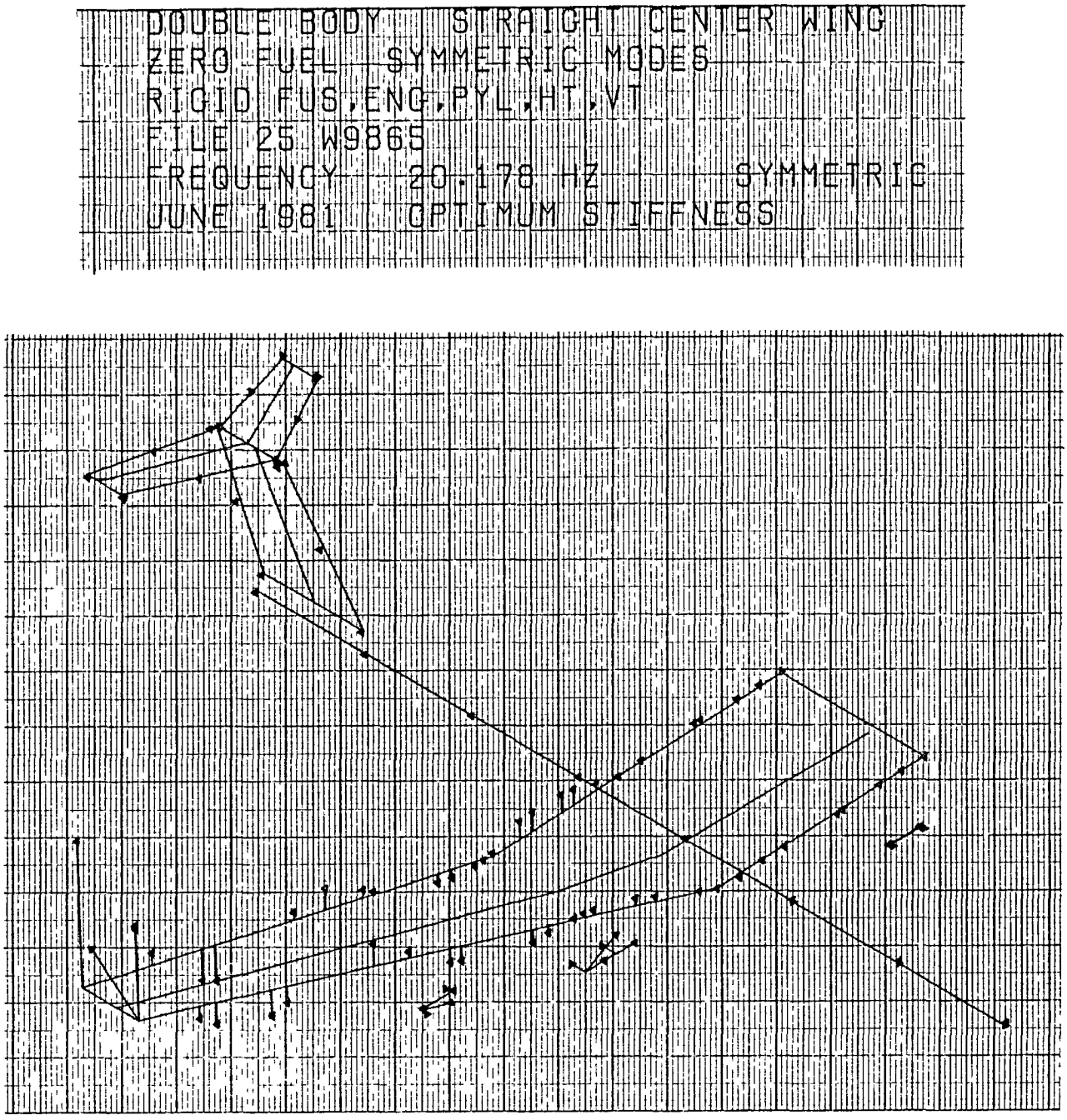

Figure D-19. Displacement Vectors - Symmetric Mode No. 15 - Two-Body MB2 Aircraft

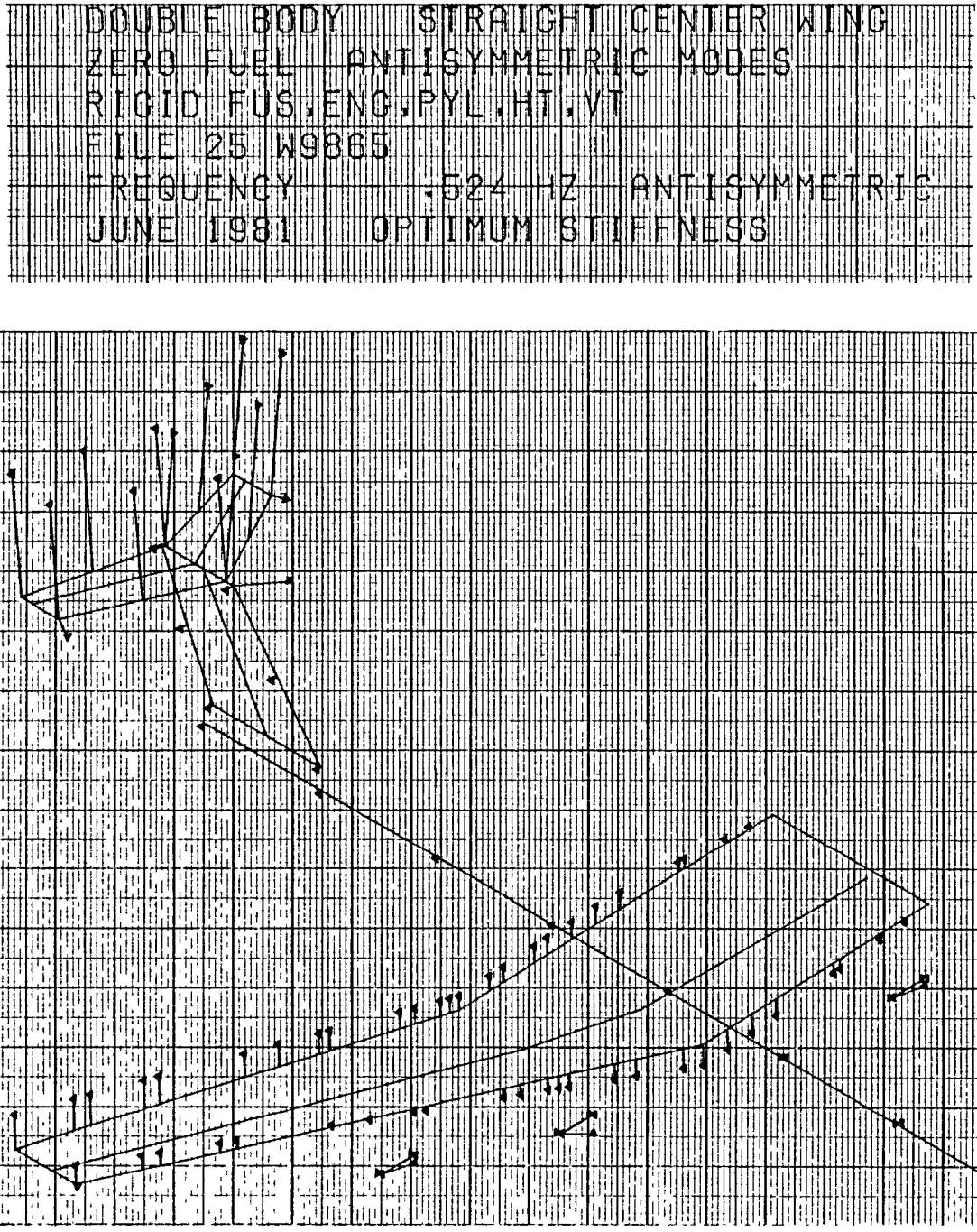

Figure D-20. Displacement Vectors - Antisymmetric Mode No. 1 - Two-Body MB2 Aircraft

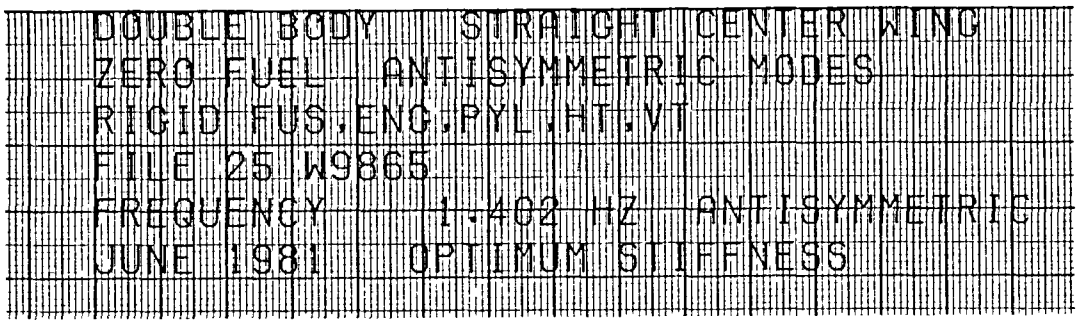

Figure D-21. Displacement Vectors - Antisymmetric Mode No. 2 - Two-Body MB2 Aircraft

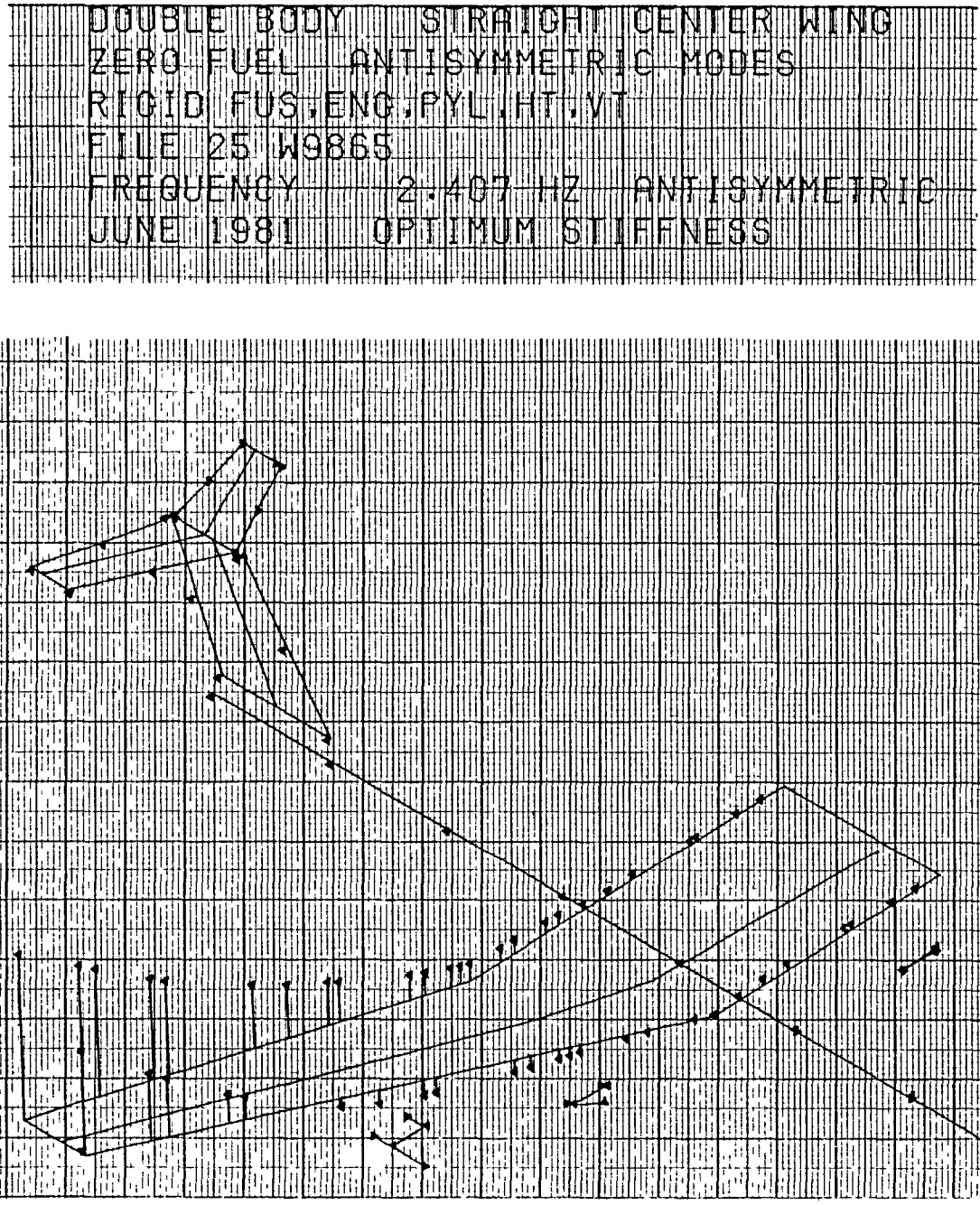

Figure D-22. Displacement Vectors - Antisymmetric Mode No. 3 - Two-Body MB2 Aircraft

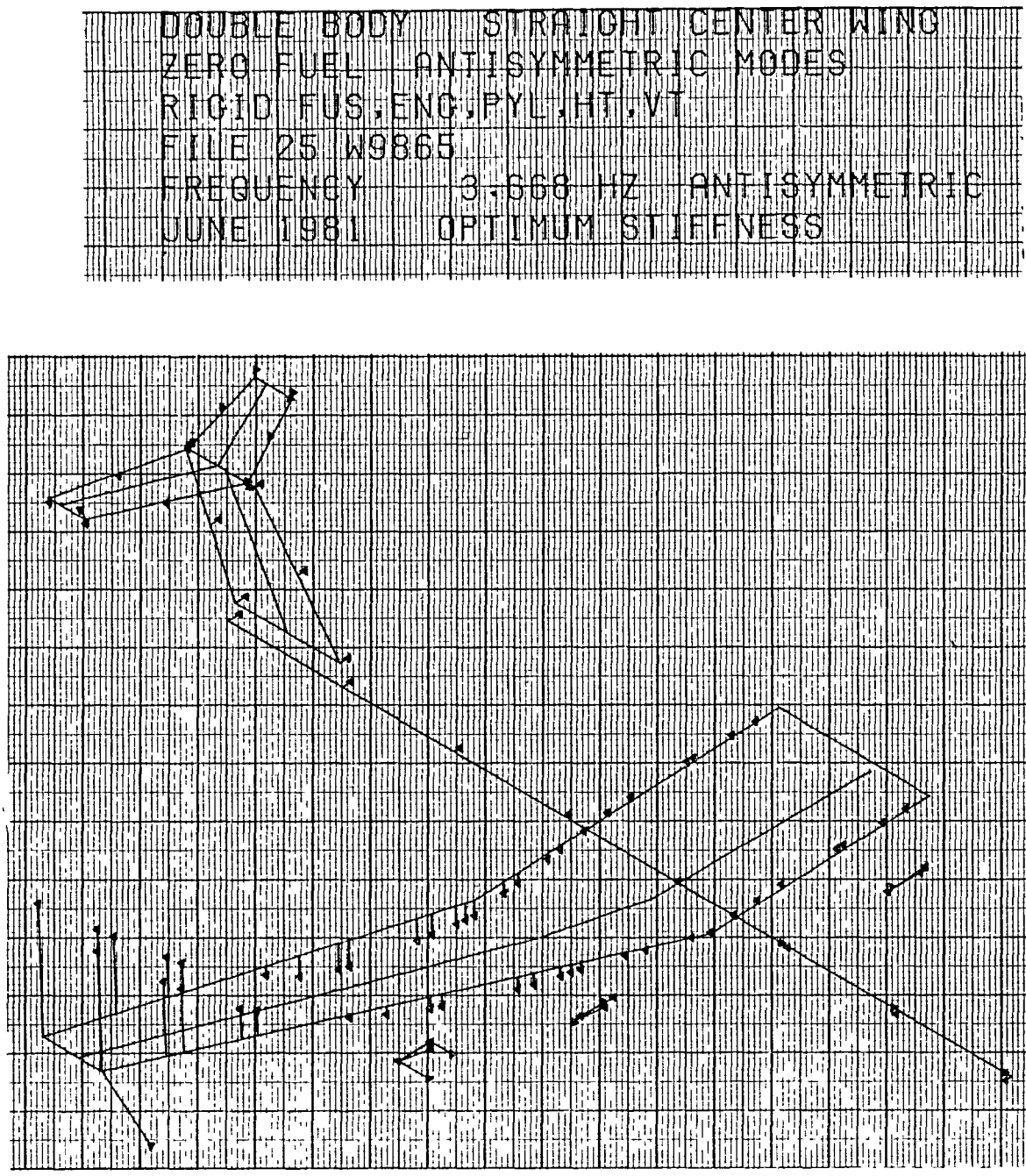

Figure D-23. Displacement Vectors - Antisymmetric Mode No. 4 - Two-Body MB2 Aircraft

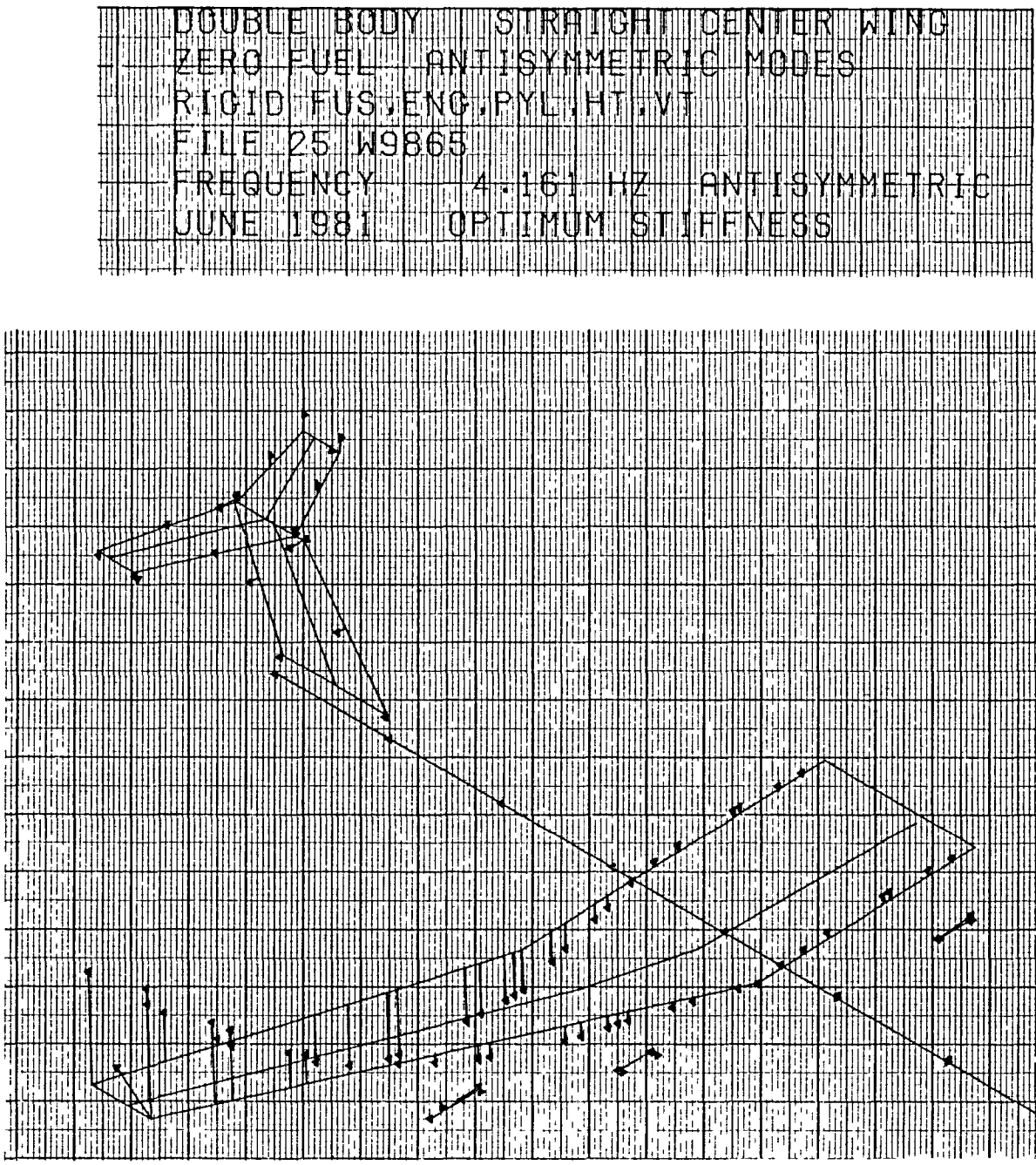

Figure D-24. Displacement Vectors - Antisymmetric Mode No. 5 - Two-Body MB2 Aircraft

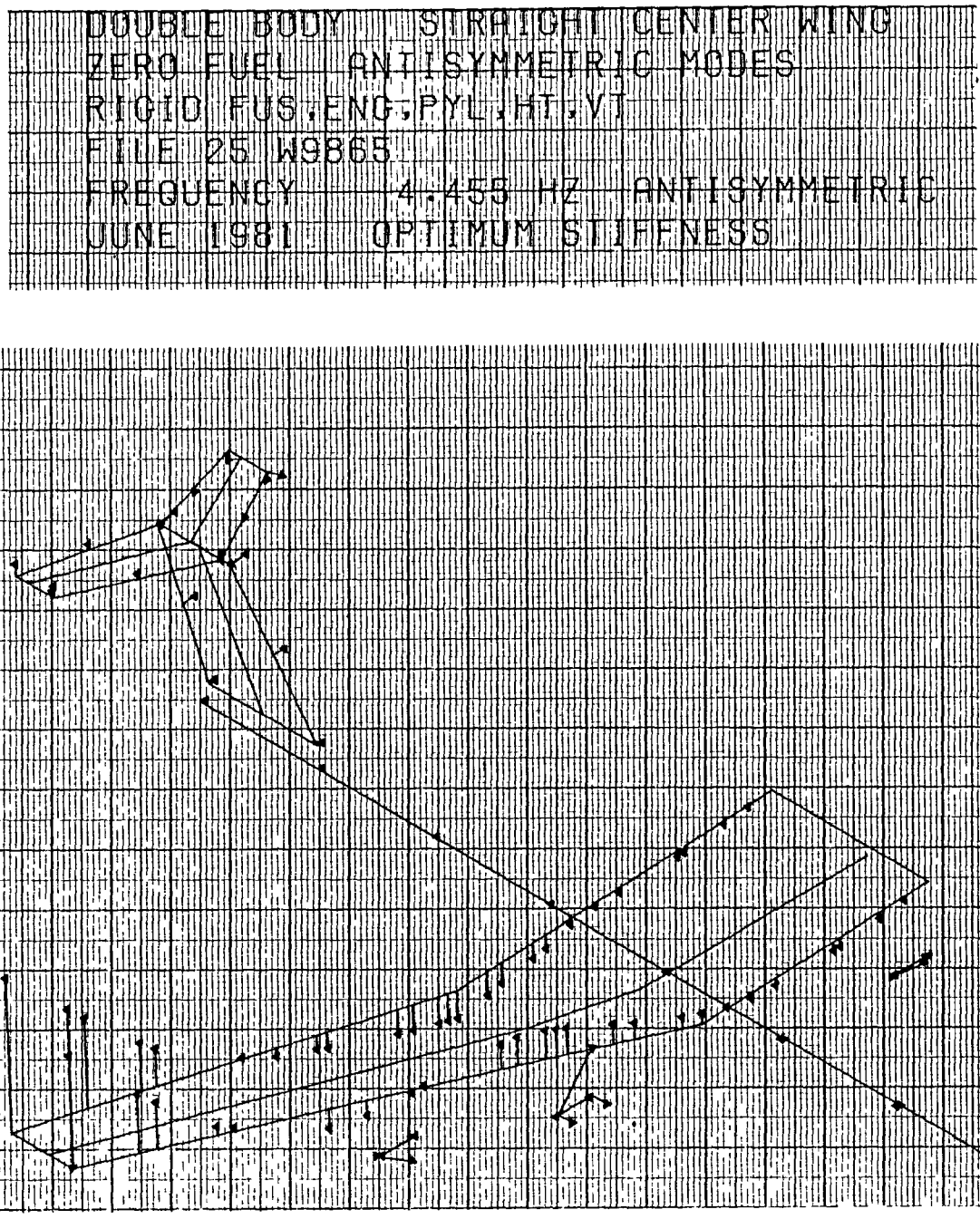

Figure D-25. Displacement Vectors - Antisymmetric Mode No. 6 - Two-Body MB2 Aircraft

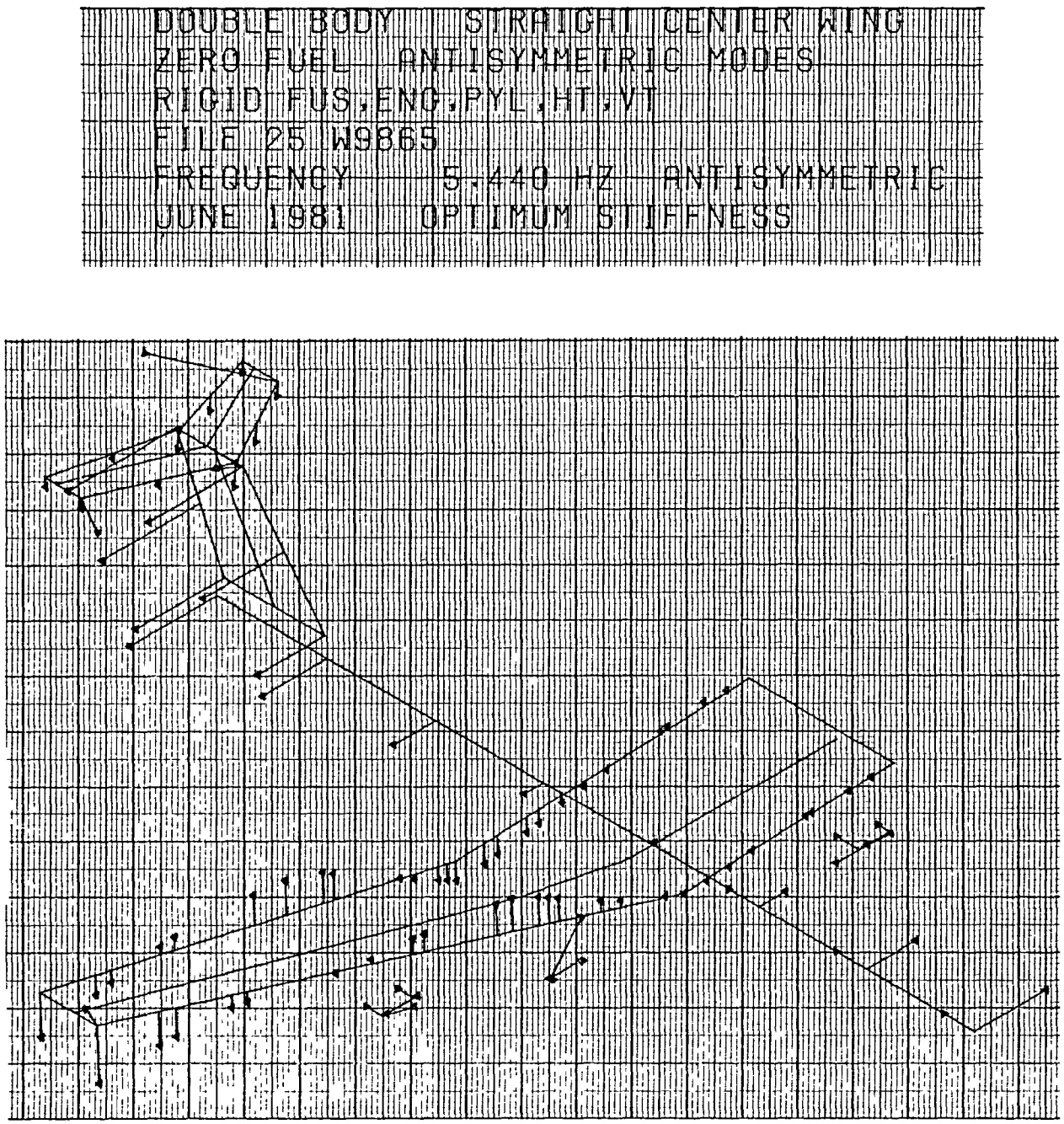

Figure D-26. Displacement Vectors - Antisymmetric Mode No. 7 - Two-Body MB2 Aircraft

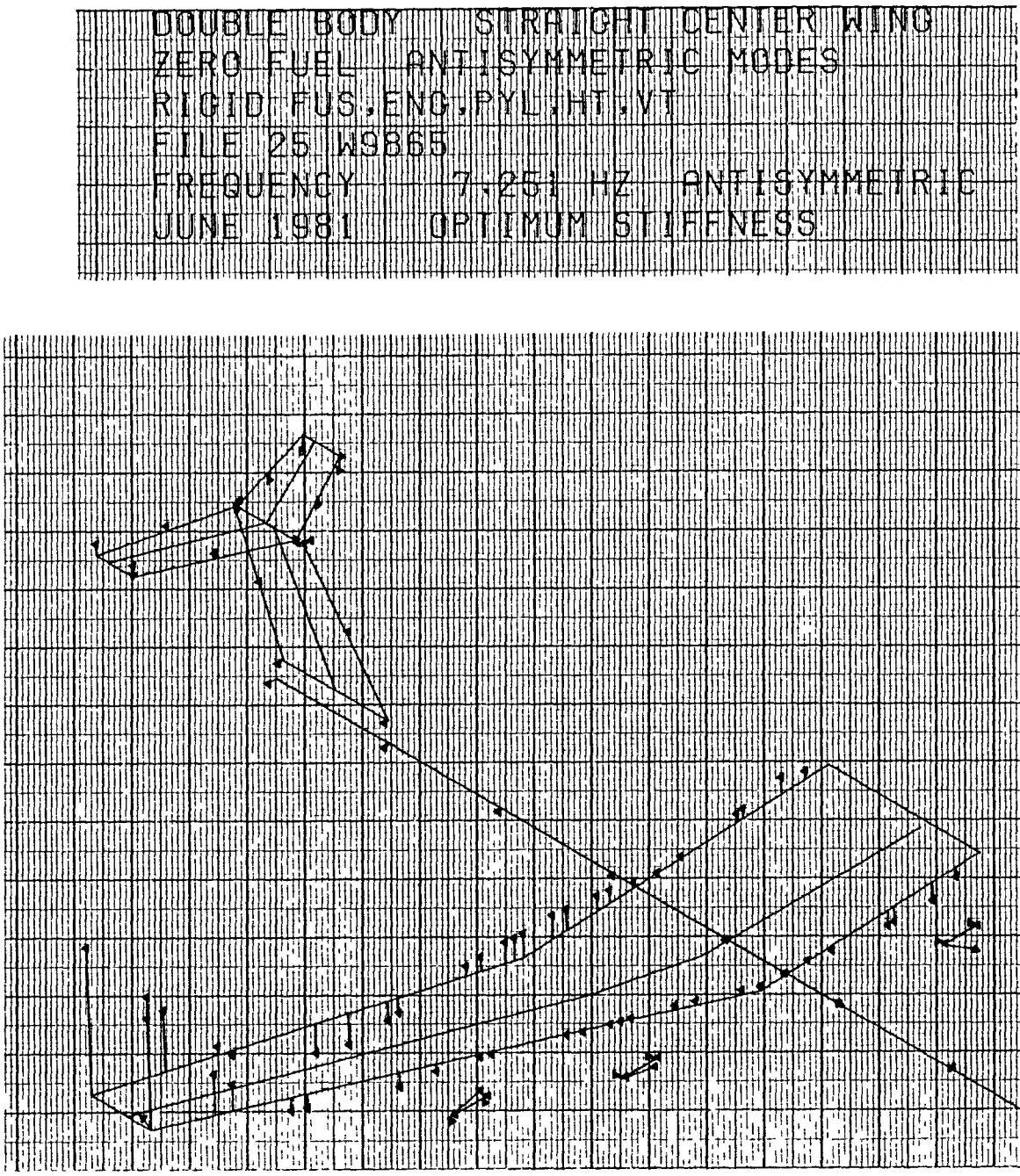

Figure D-27. Displacement Vectors - Antisymmetric Mode No. 8 - Two-Body MB2 Aircraft

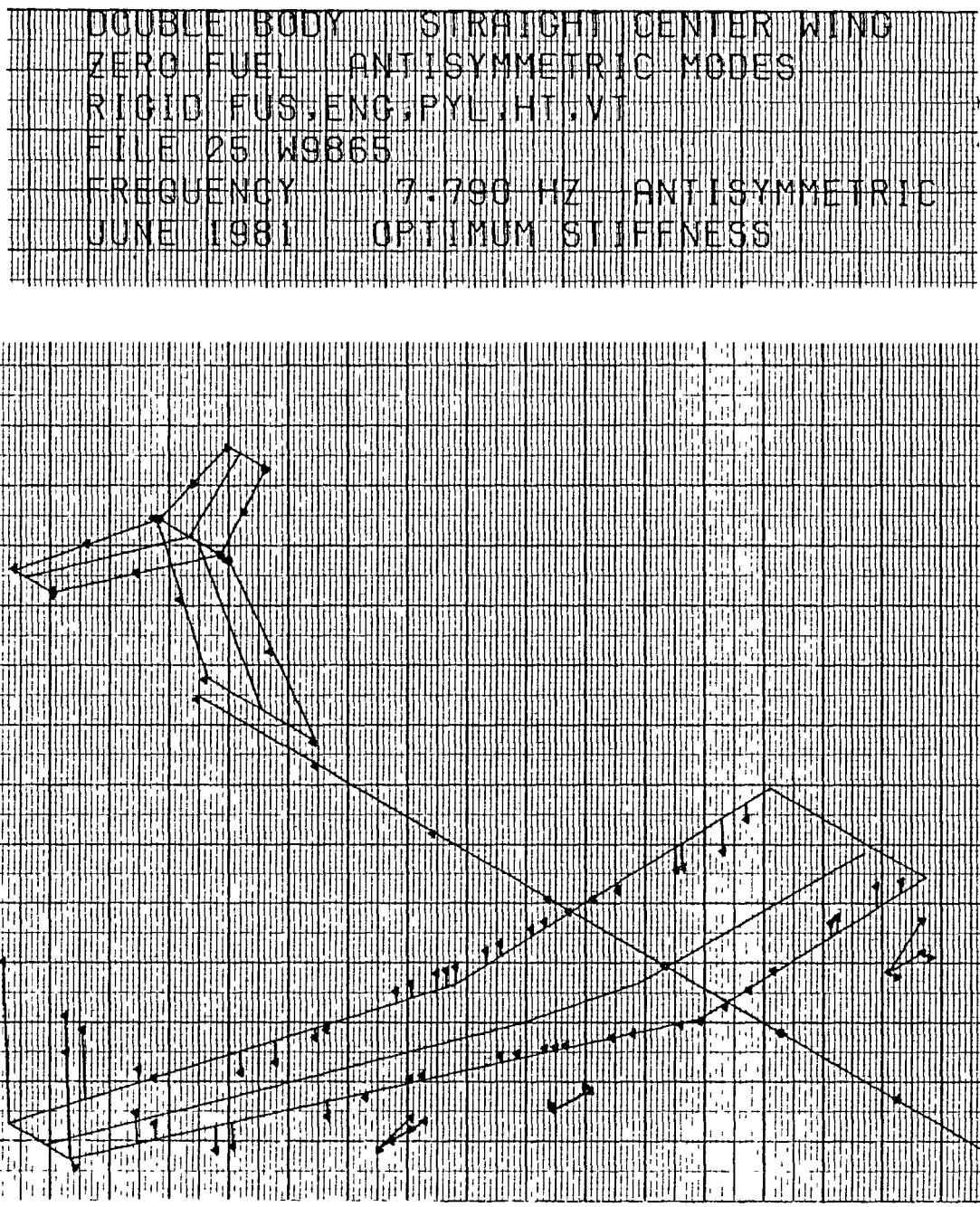

Figure D-28. Displacement Vectors - Antisymmetric Mode No. 9 - Two-Body MB2 Aircraft

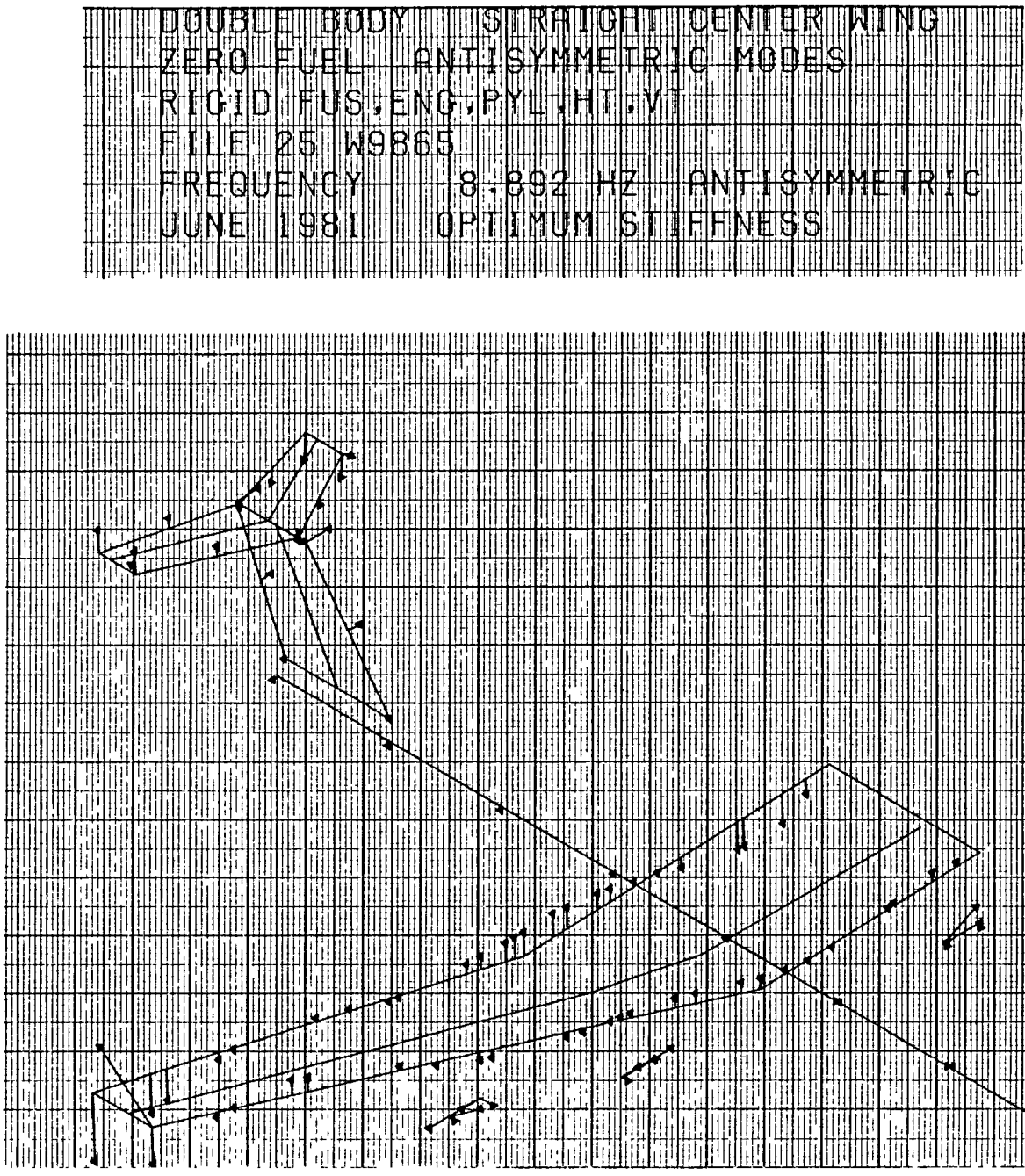

Figure D-29. Displacement Vectors - Antisymmetric Mode No. 10 - Two-Body MB2 Aircraft

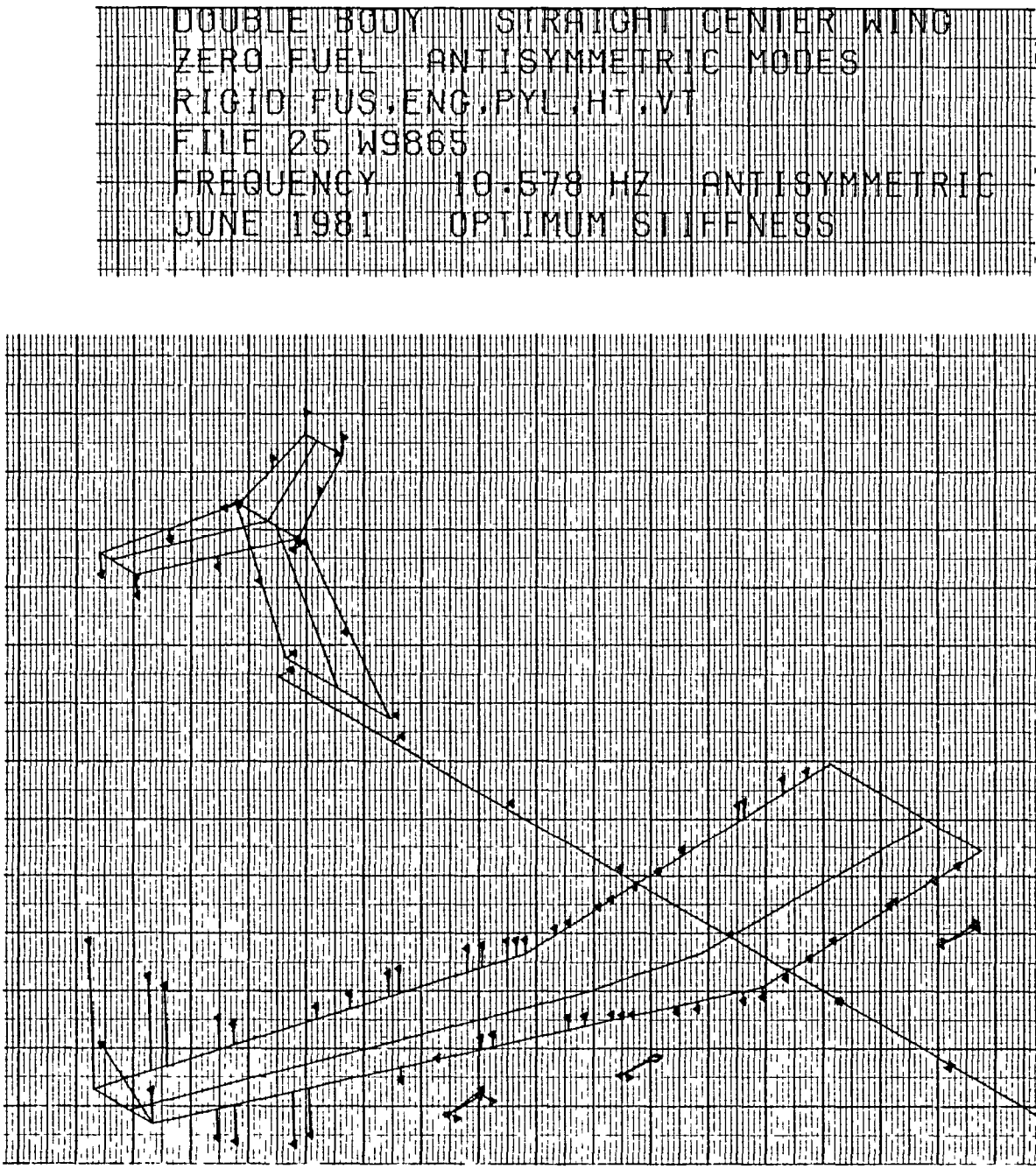

Figure D-30. Displacement Vectors - Antisymmetric Mode No. 11 - Two-Body MB2 Aircraft

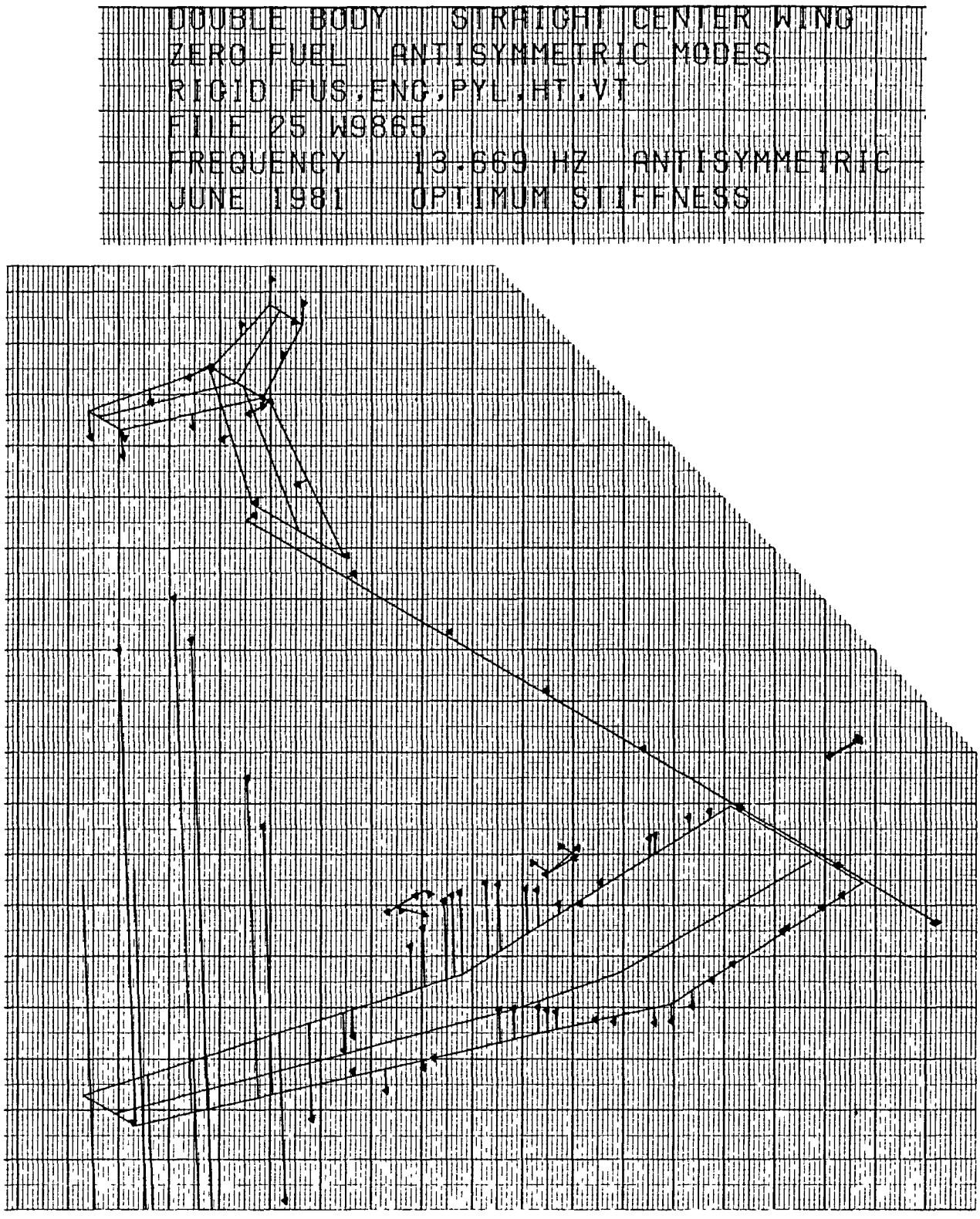

Figure D-31. Displacement Vectors - Antisymmetric Mode No. 12 - Two-Body MB2 Aircraft

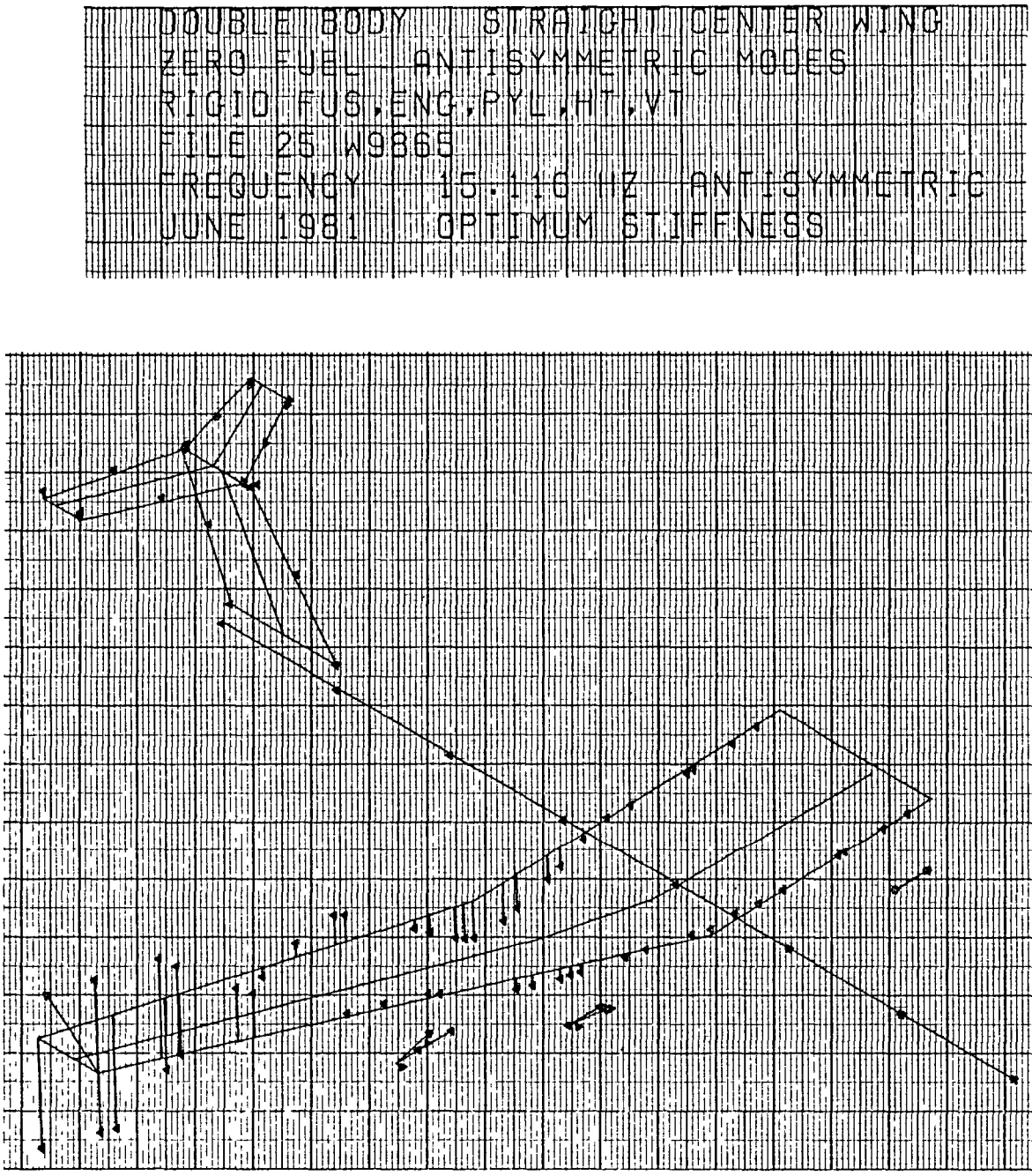

Figure D-32. Displacement Vectors - Antisymmetric Mode No. 13 - Two-Body MB2 Aircraft

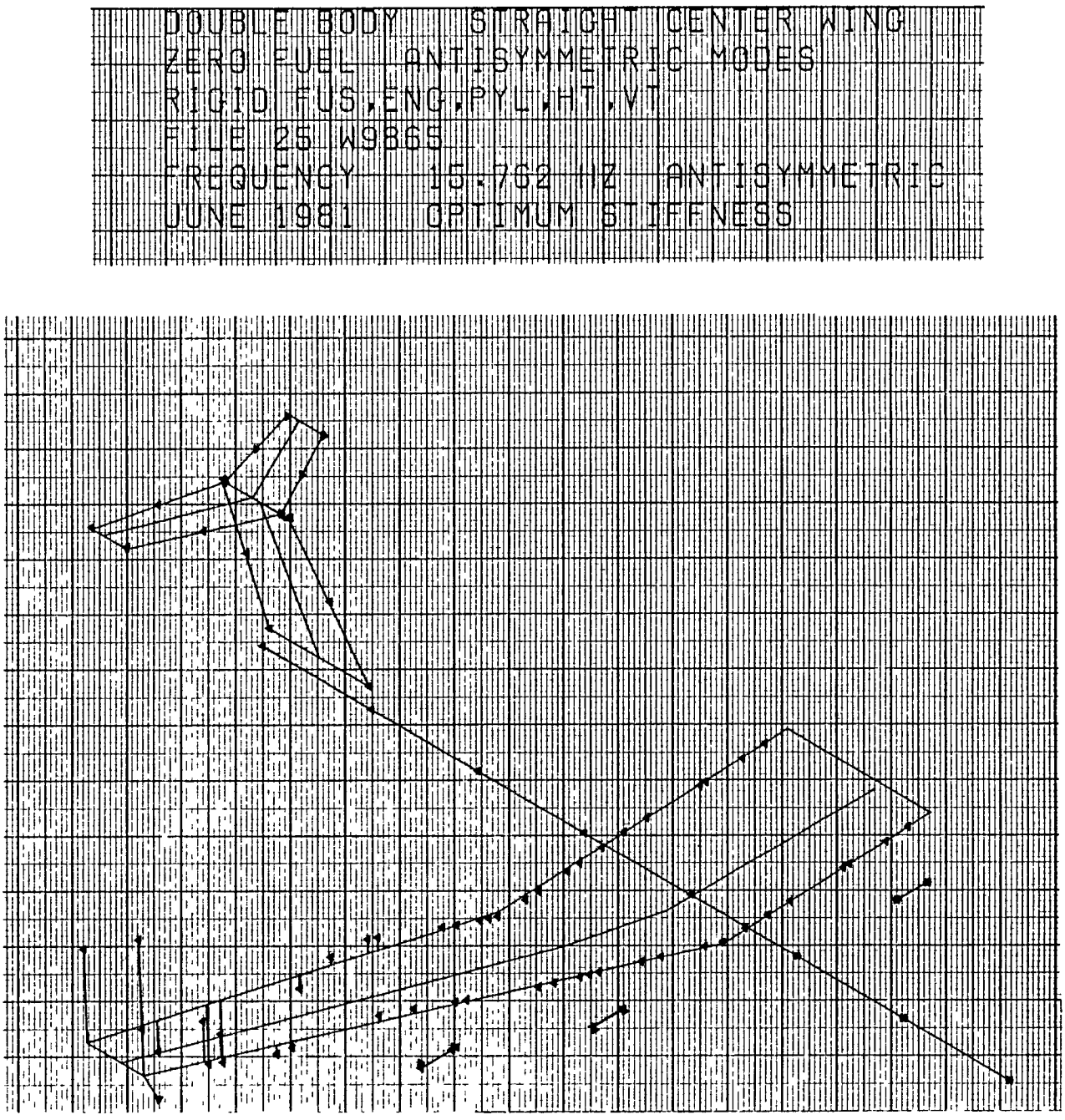

Figure D-33. Displacement Vectors - Antisymmetric Mode No. 14 - Two-Body MB2 Aircraft

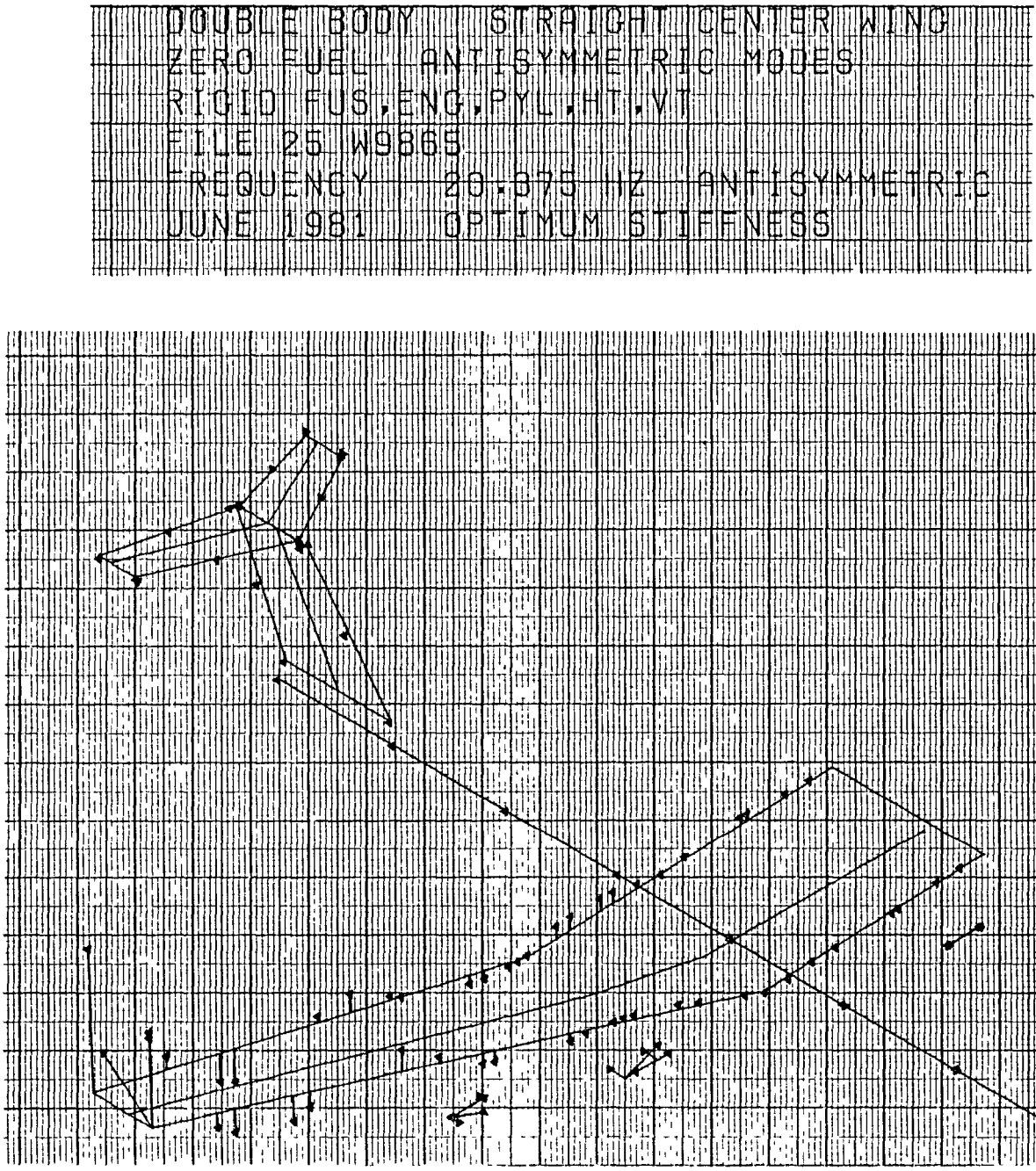

Figure D-34. Displacement Vectors - Antisymmetric Mode No. 15 - Two-Body MB2 Aircraft

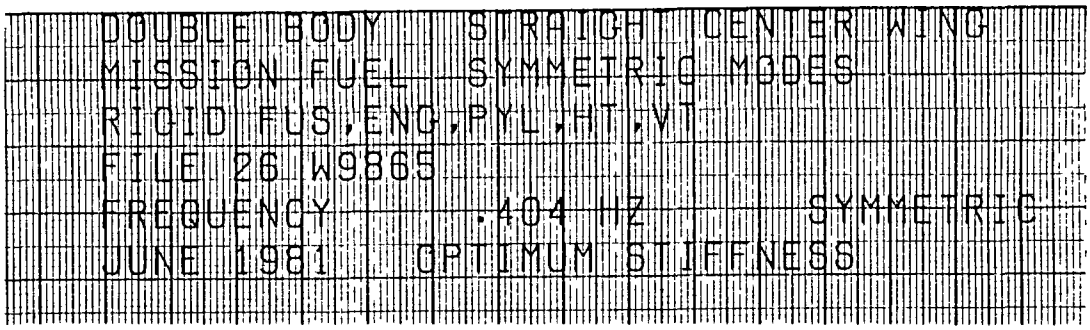

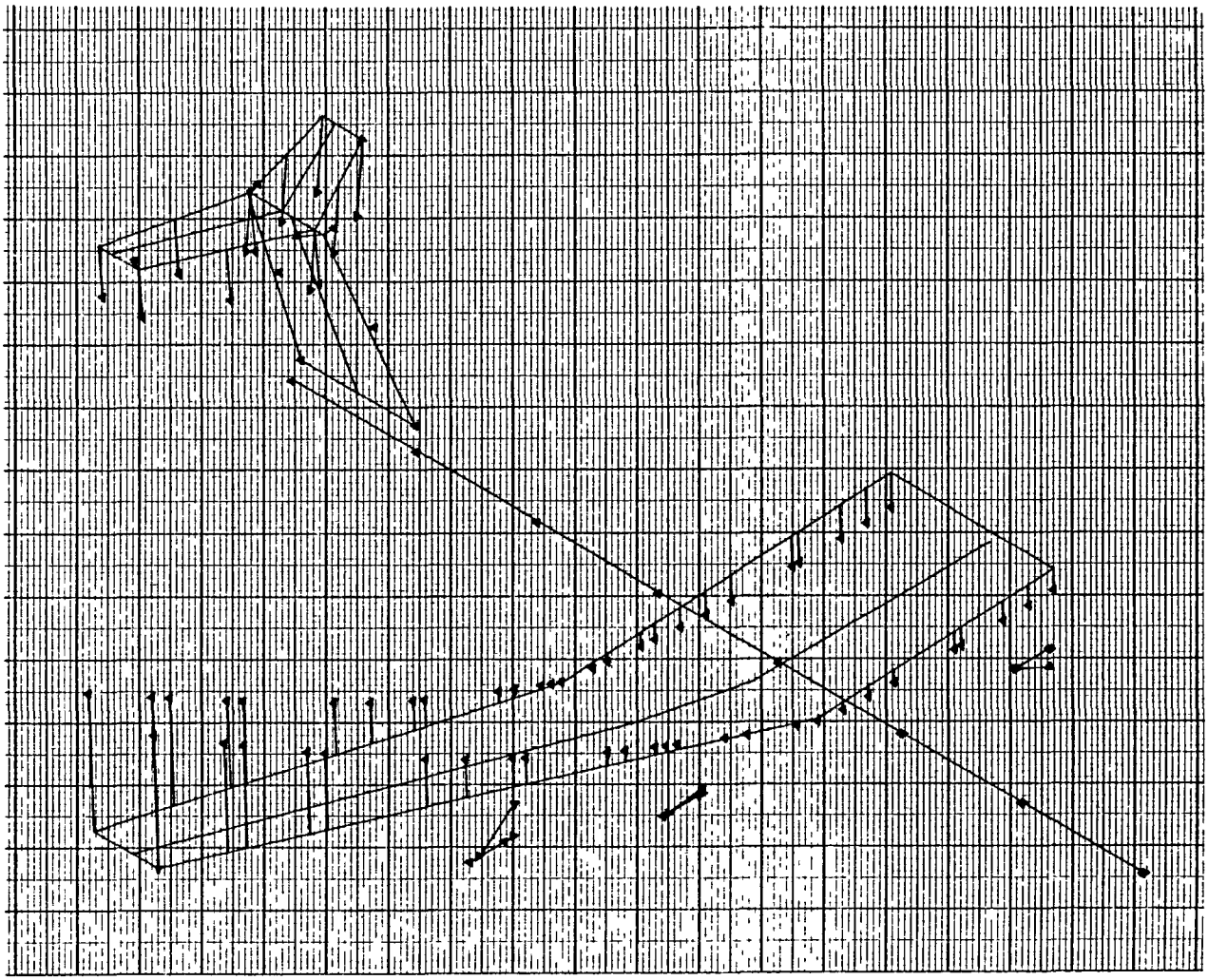

Figure D-35. Displacement Vectors - Symmetric Mode No. 1 - Two-Body MB2 Aircraft

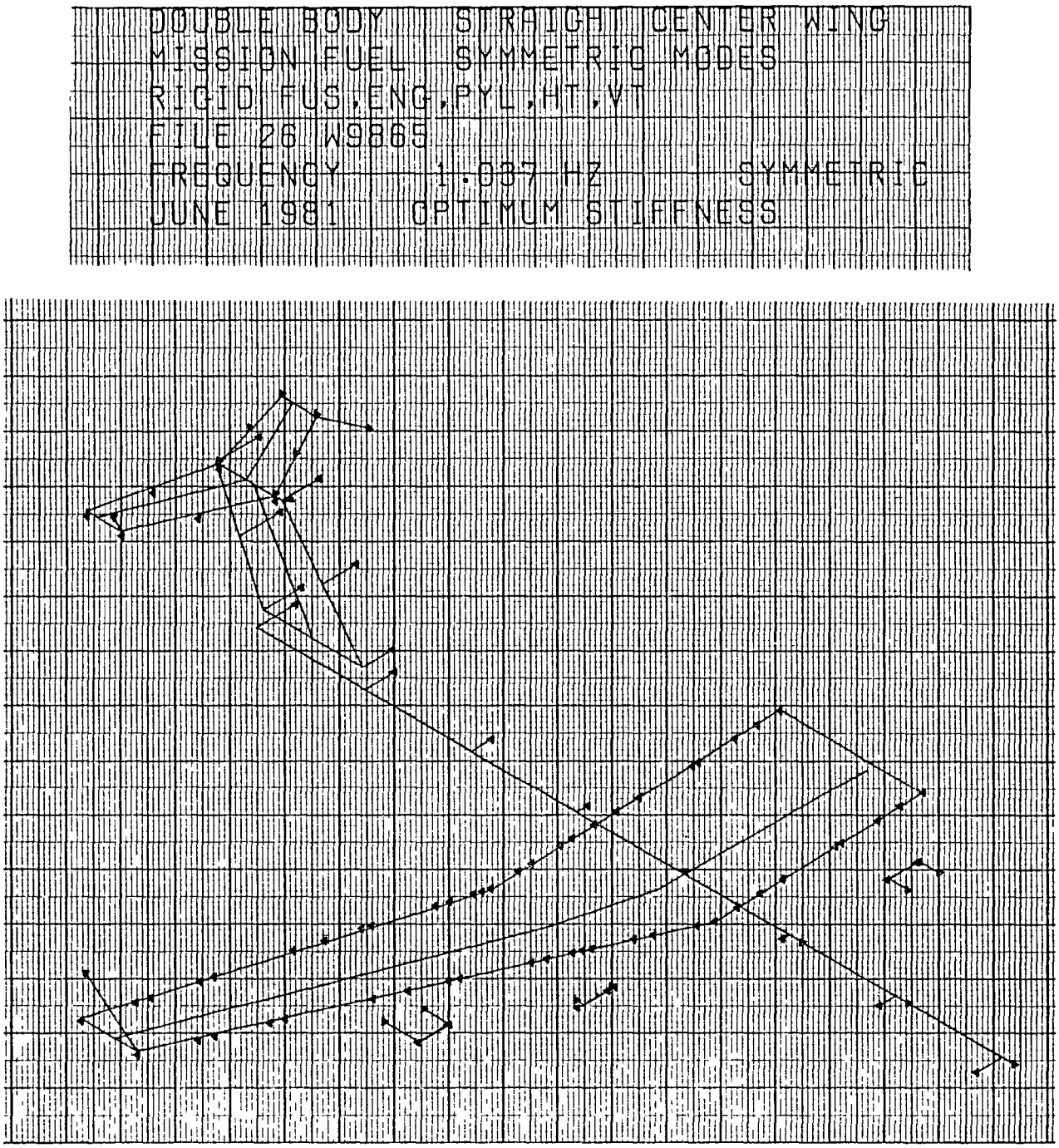

Figure D-36. Displacement Vectors - Symmetric Mode No. 2 - Two-Body MB2 Aircraft

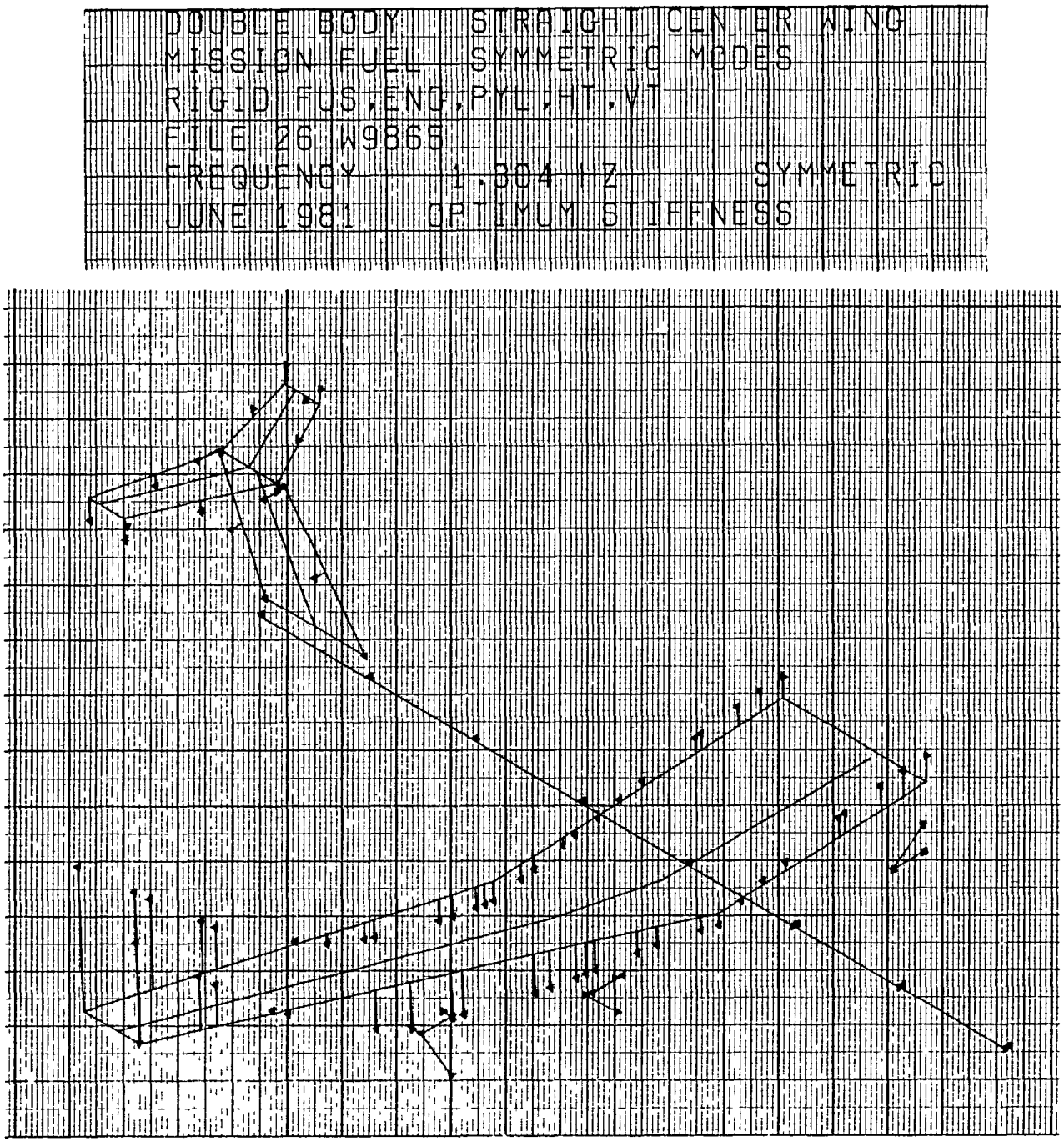

Figure D-37. Displacement Vectors - Symmetric Mode No. 3 - Two-Body MB2 Aircraft

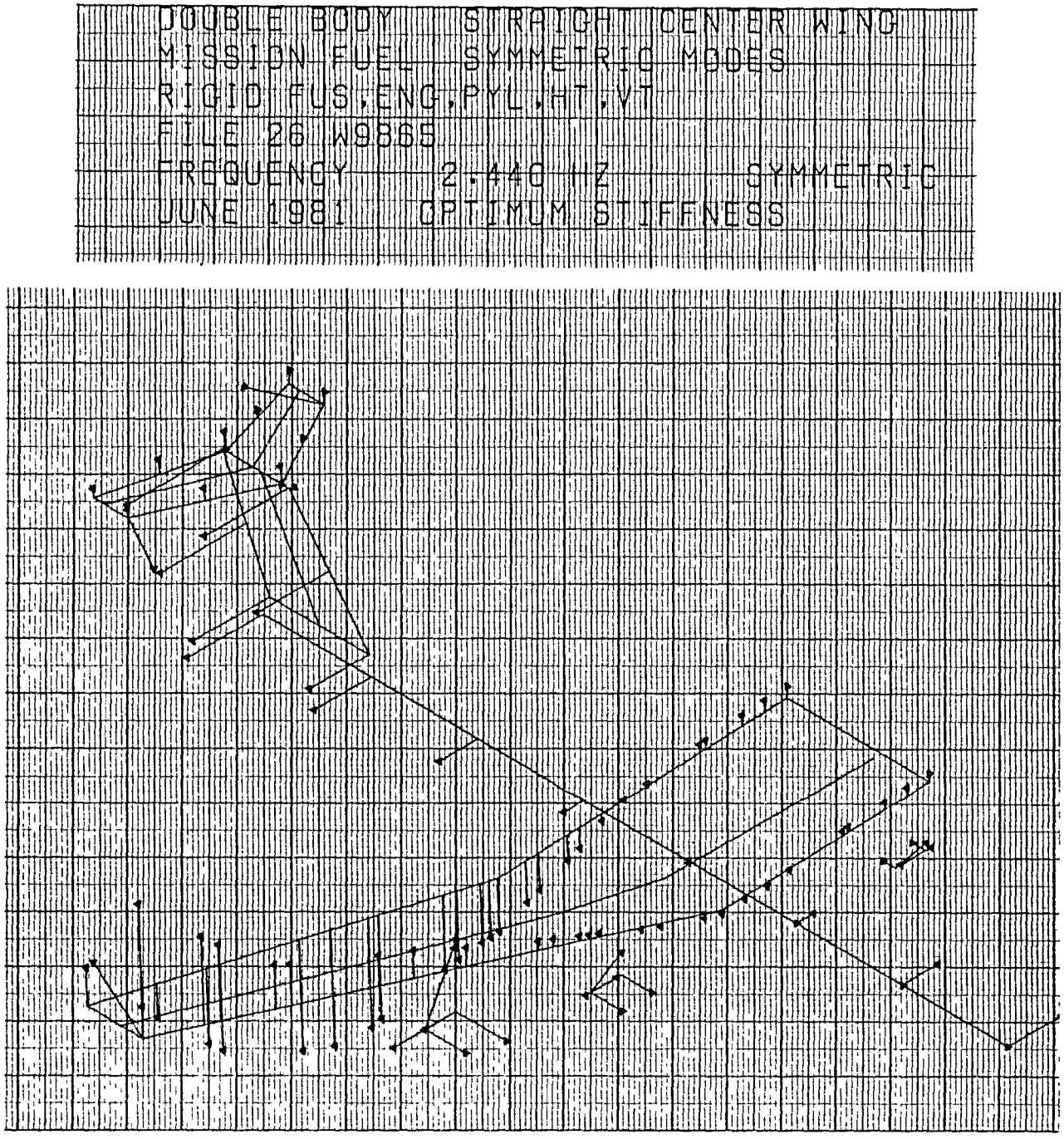

Figure D-38. Displacement Vectors - Symmetric Mode No. 4 - Two-Body MB2 Aircraft

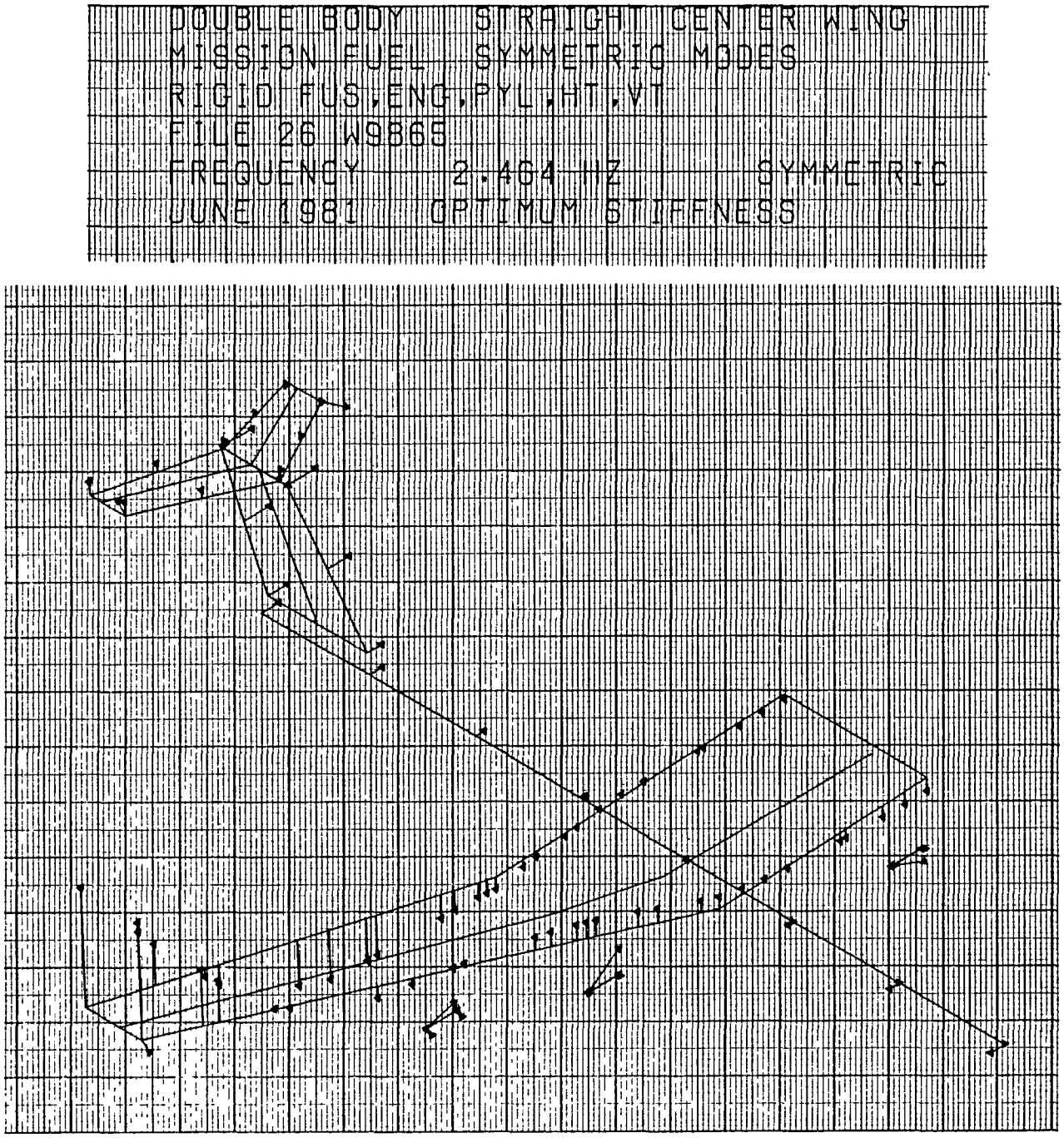

Figure D-39. Displacement Vectors - Symmetric Mode No. 5 - Two-Body MB2 Aircraft

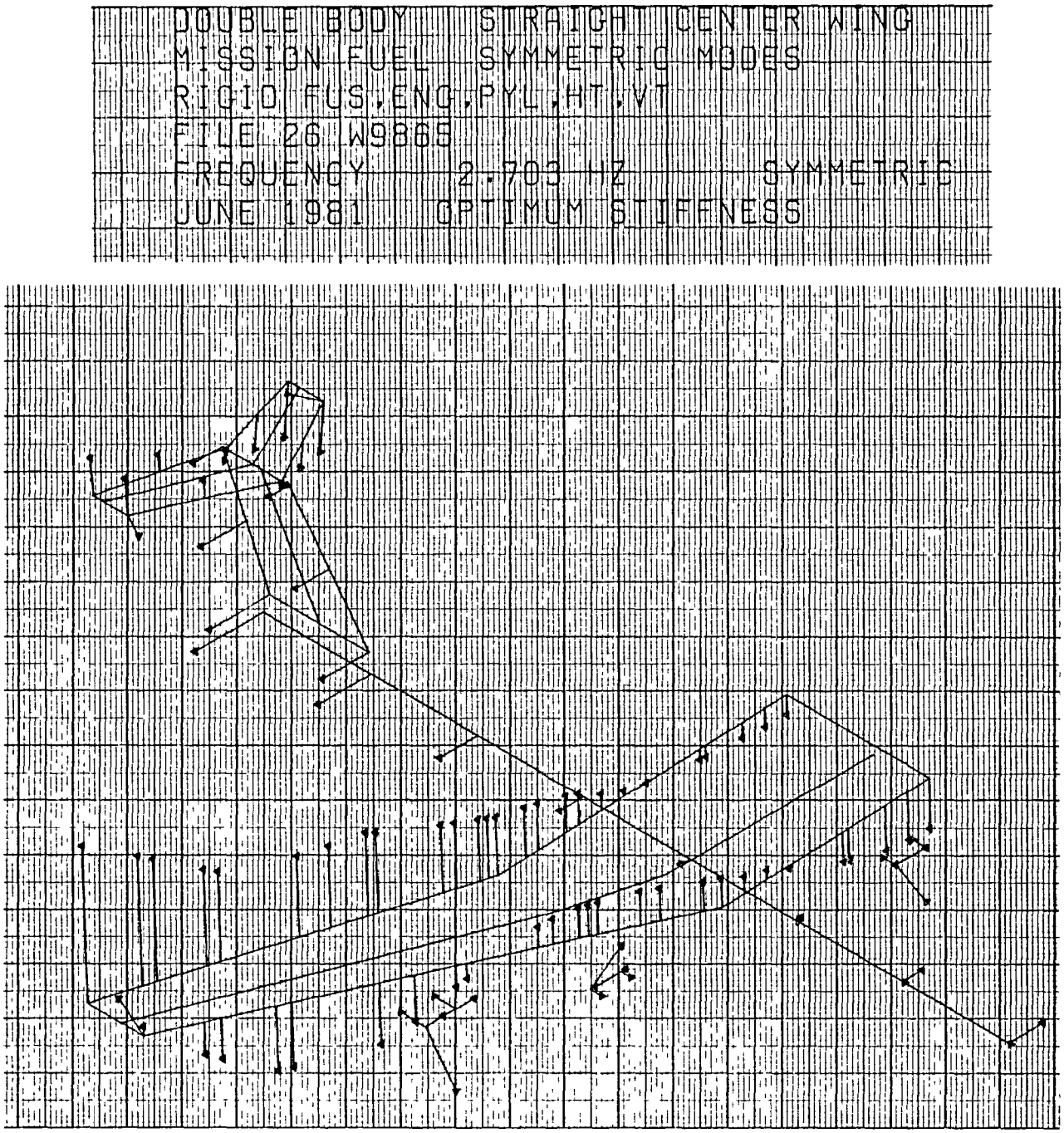

Figure D-40. Displacement Vectors - Symmetric Mode No. 6 - Two-Body MB2 Aircraft

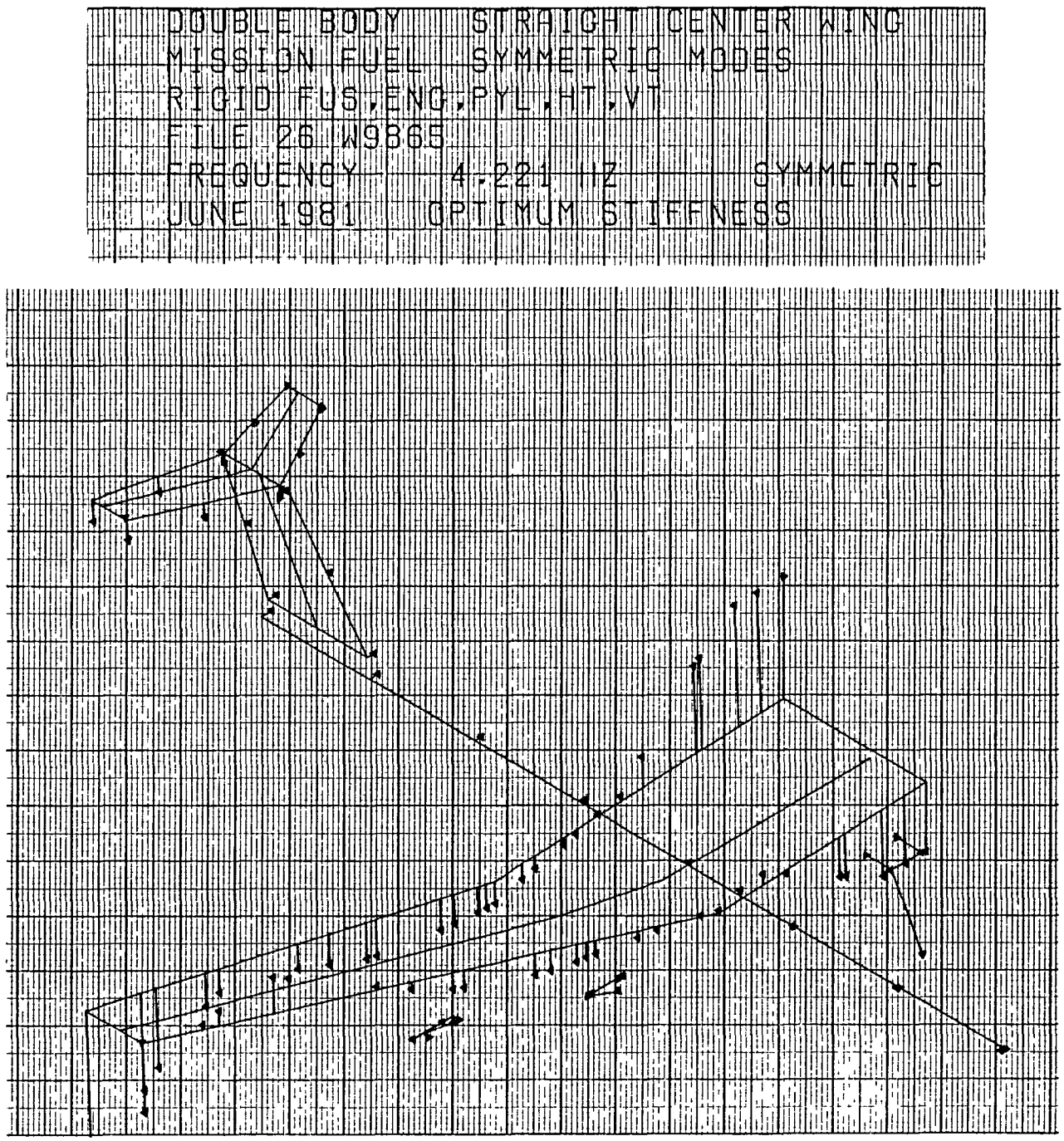

Figure D-41. Displacement Vectors - Symmetric Mode No. 7 - Two-Body MB2 Aircraft

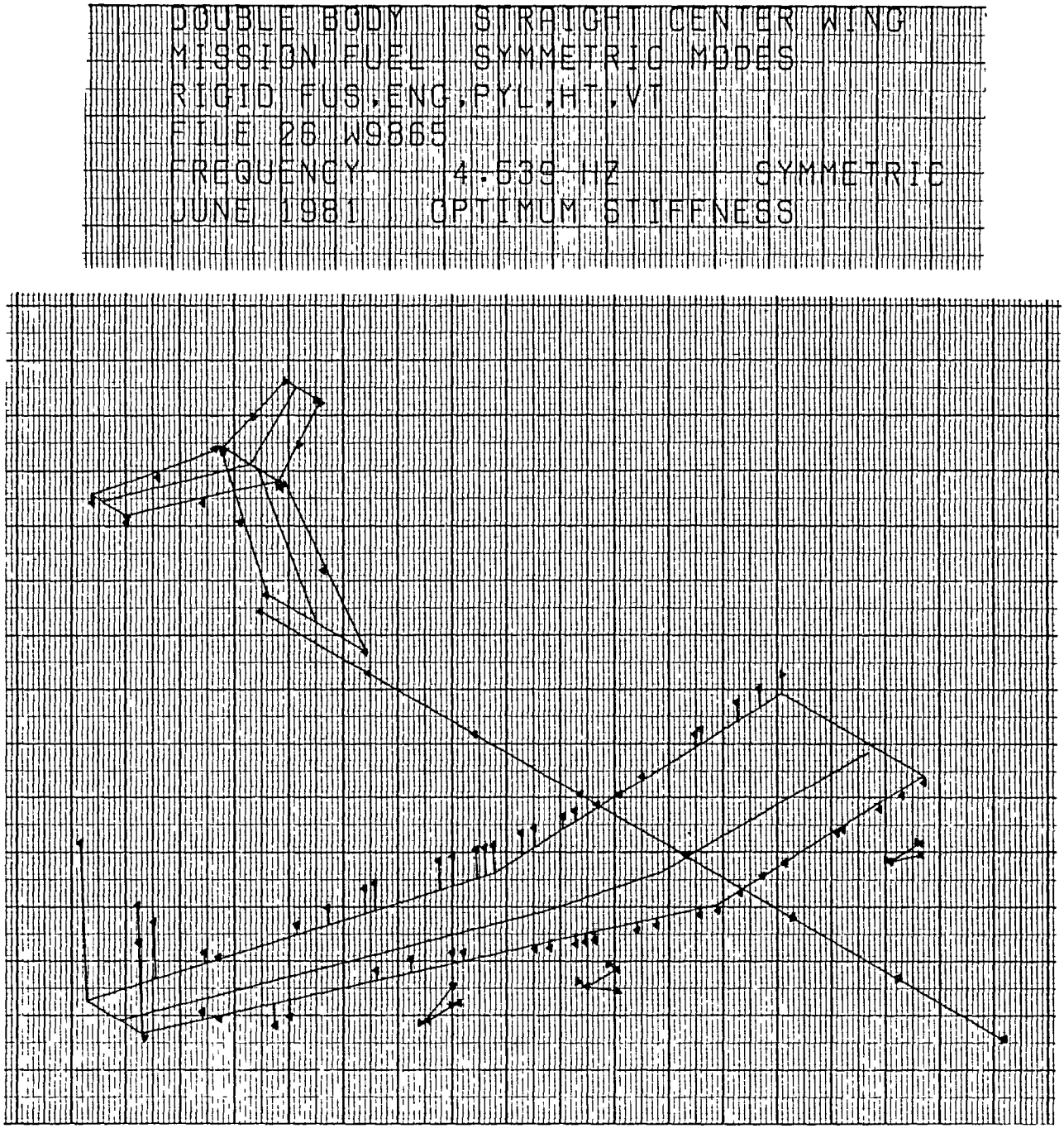

Figure D-42. Displacement Vectors - Symmetric Mode No. 8 - Two-Body MB2 Aircraft

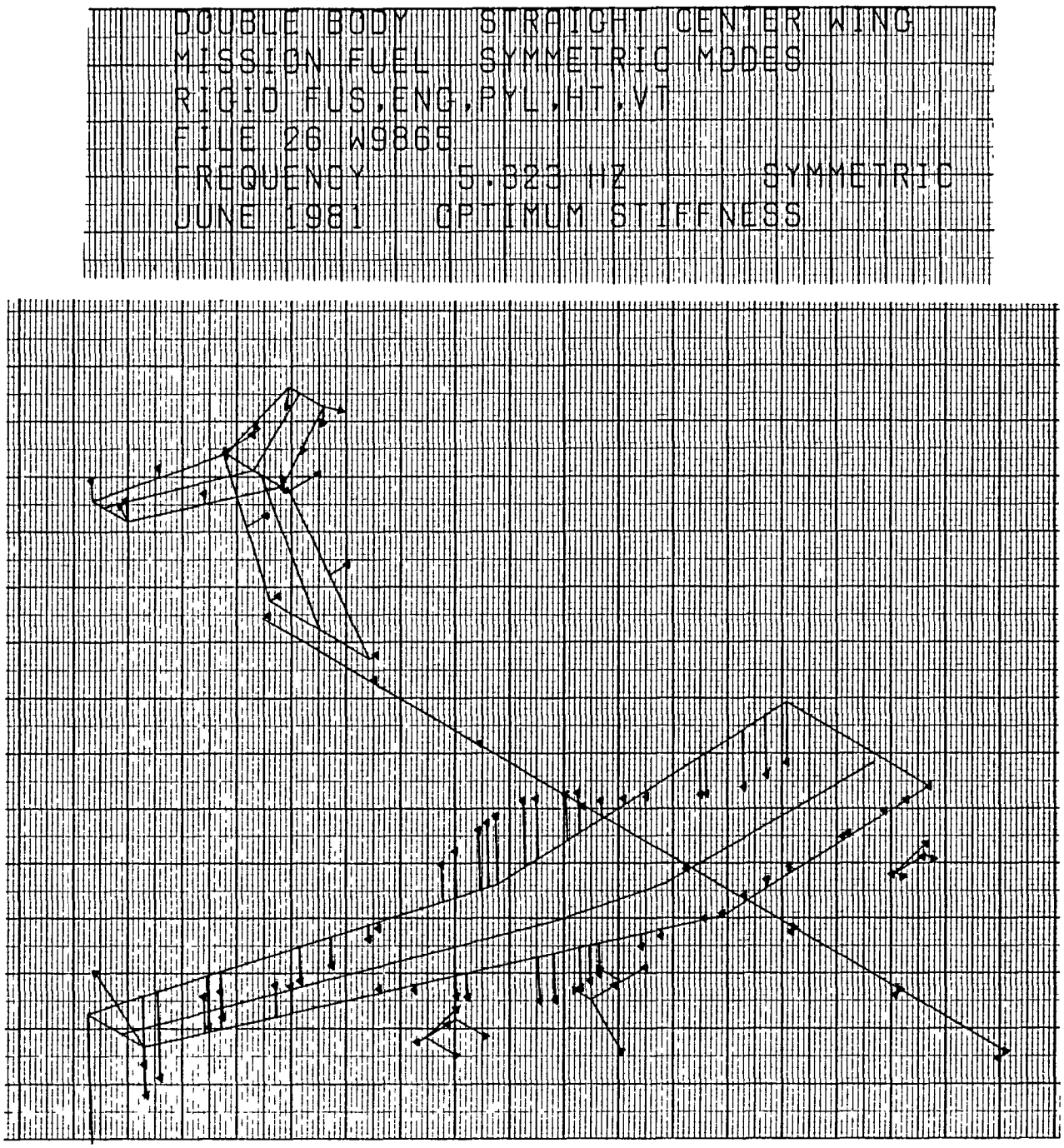

Figure D-43. Displacement Vectors - Symmetric Mode No. 9 - Two-Body MB2 Aircraft

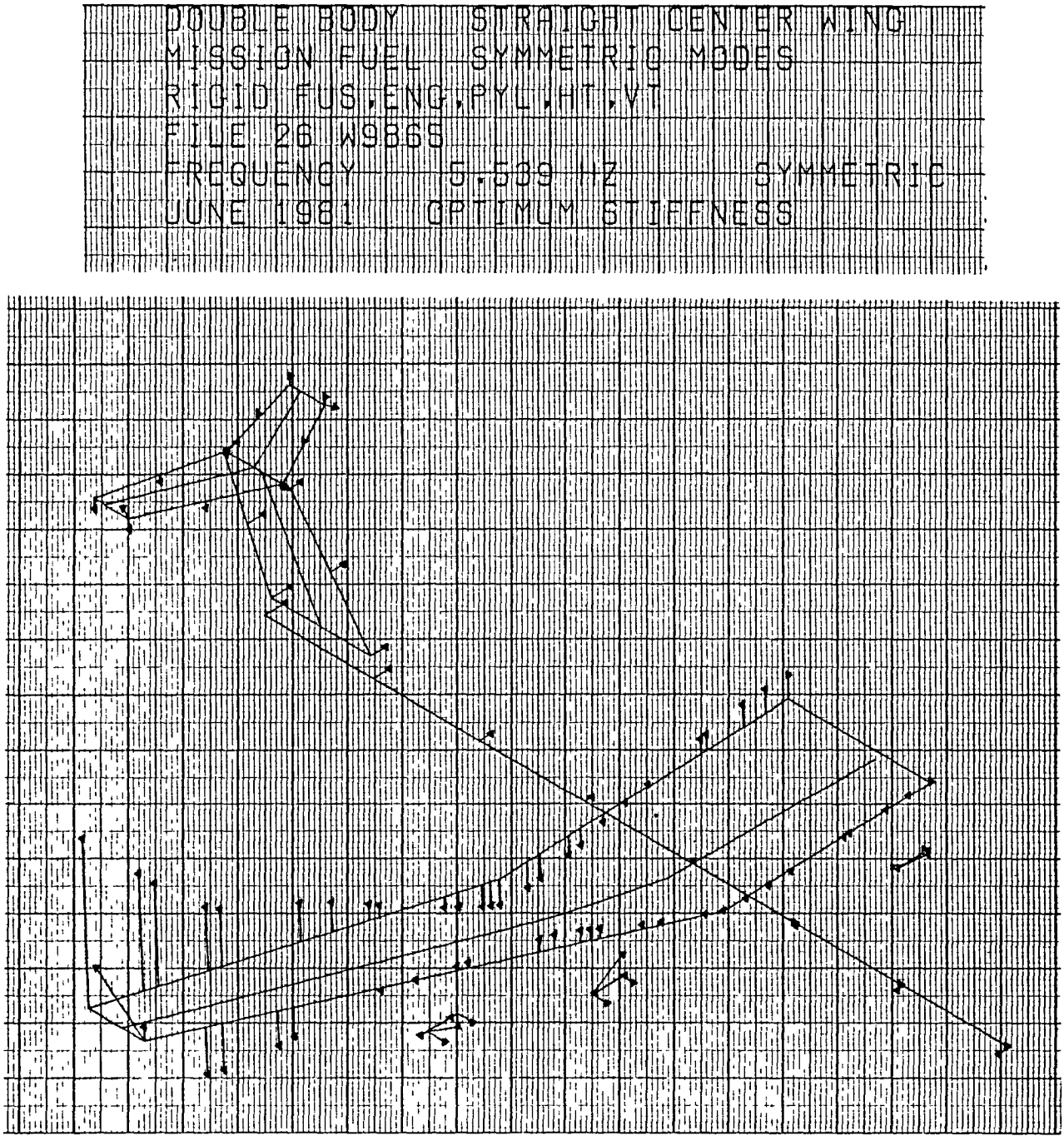

Figure D-44. Displacement Vectors - Symmetric Mode No. 10 - Two-Body MB2 Aircraft

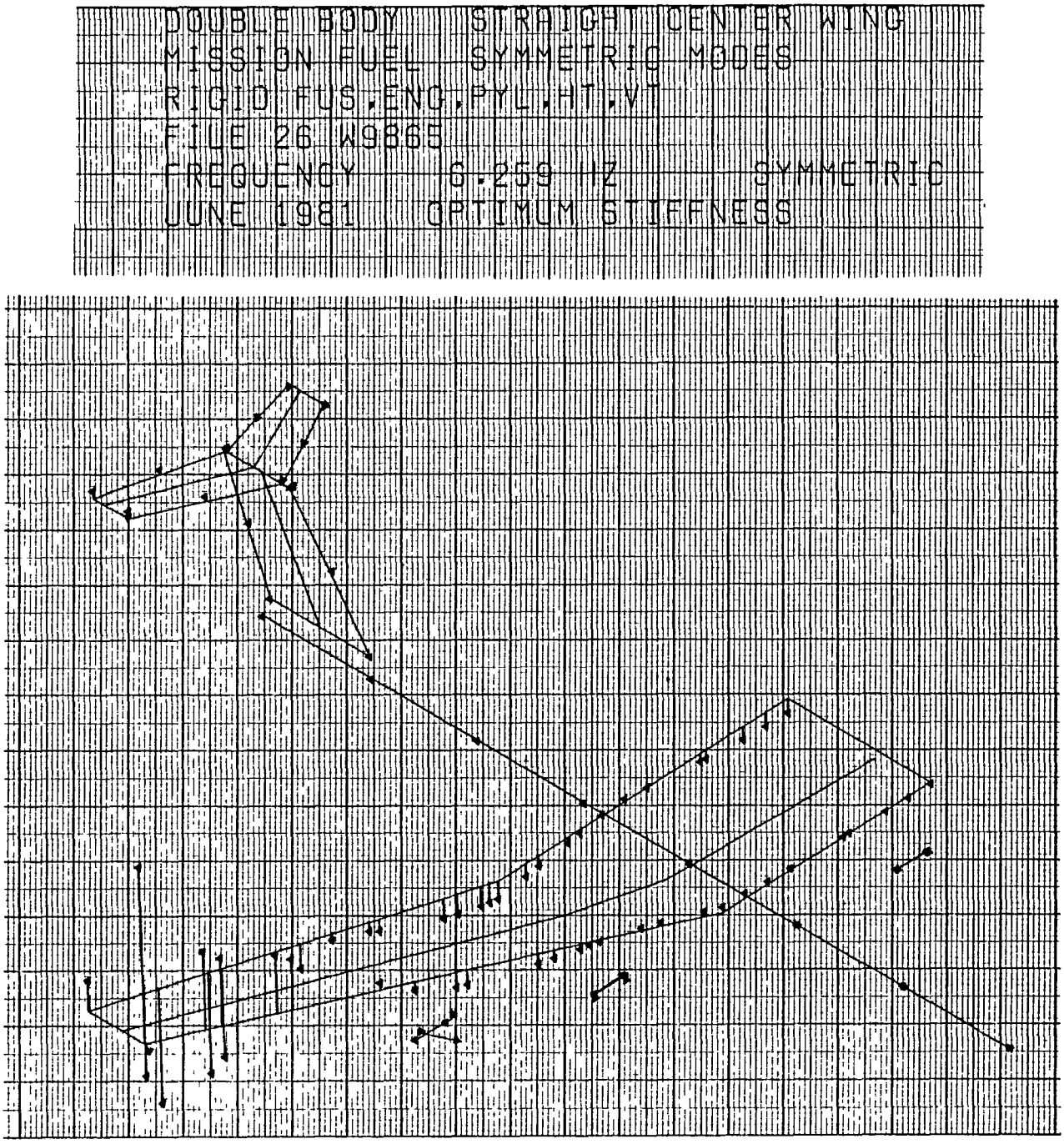

Figure D-45. Displacement Vectors - Symmetric Mode No. 11 - Two-Body MB2 Aircraft

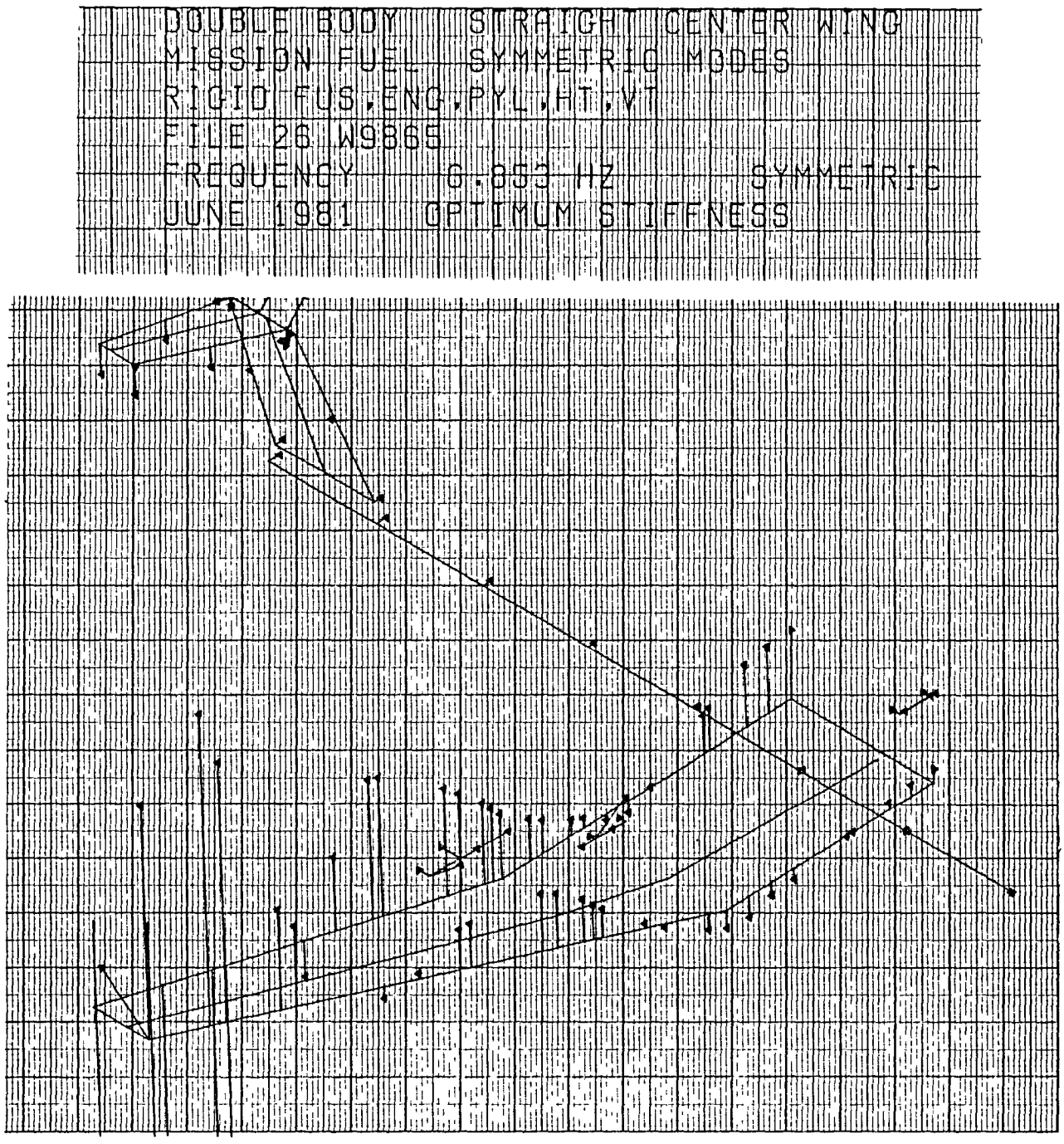

Figure D-46. Displacement Vectors - Symmetric Mode No. 12 - Two-Body MB2 Aircraft

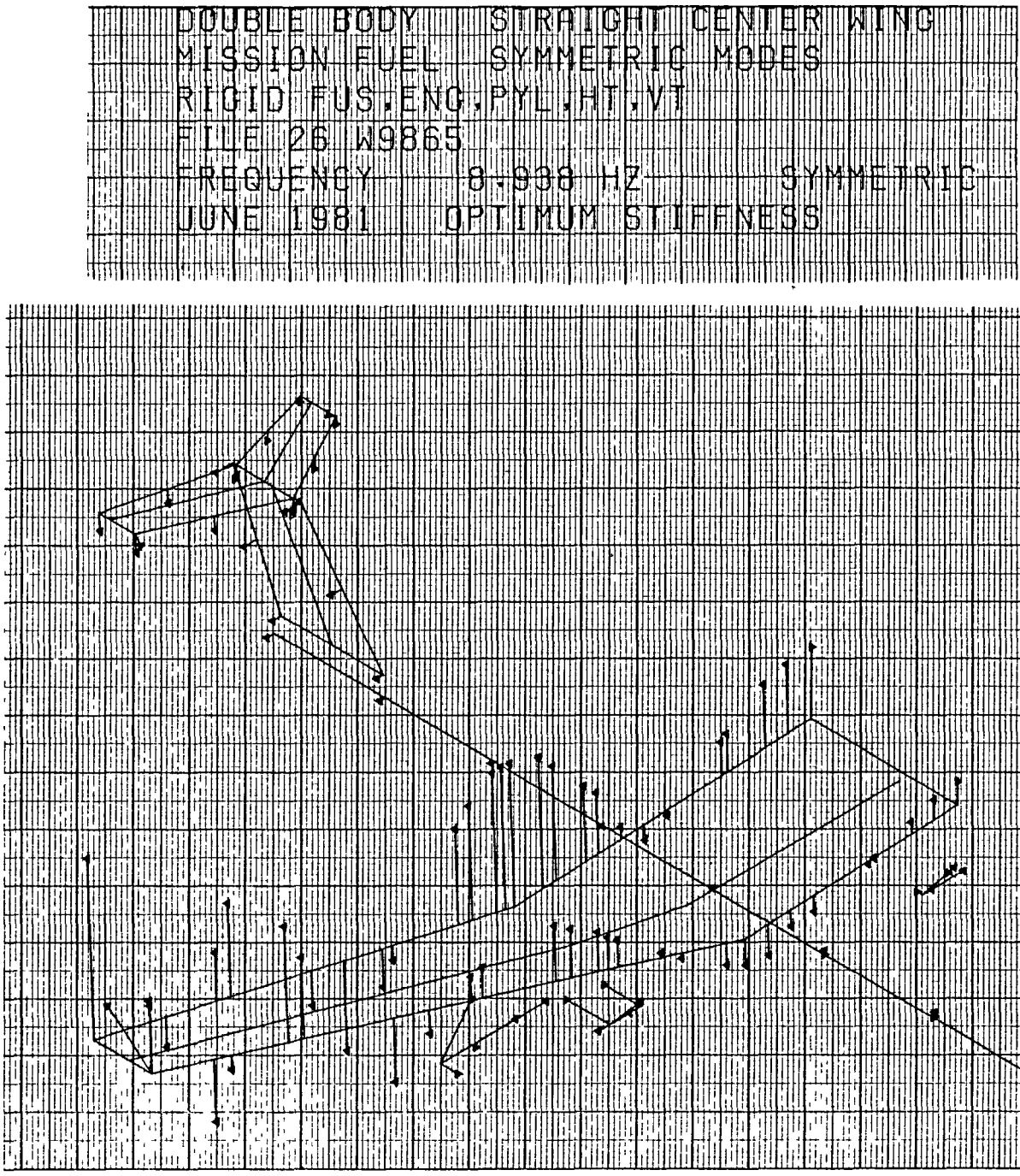

Figure D-47. Displacement Vectors - Symmetric Mode No. 13 - Two-Body MB2 Aircraft

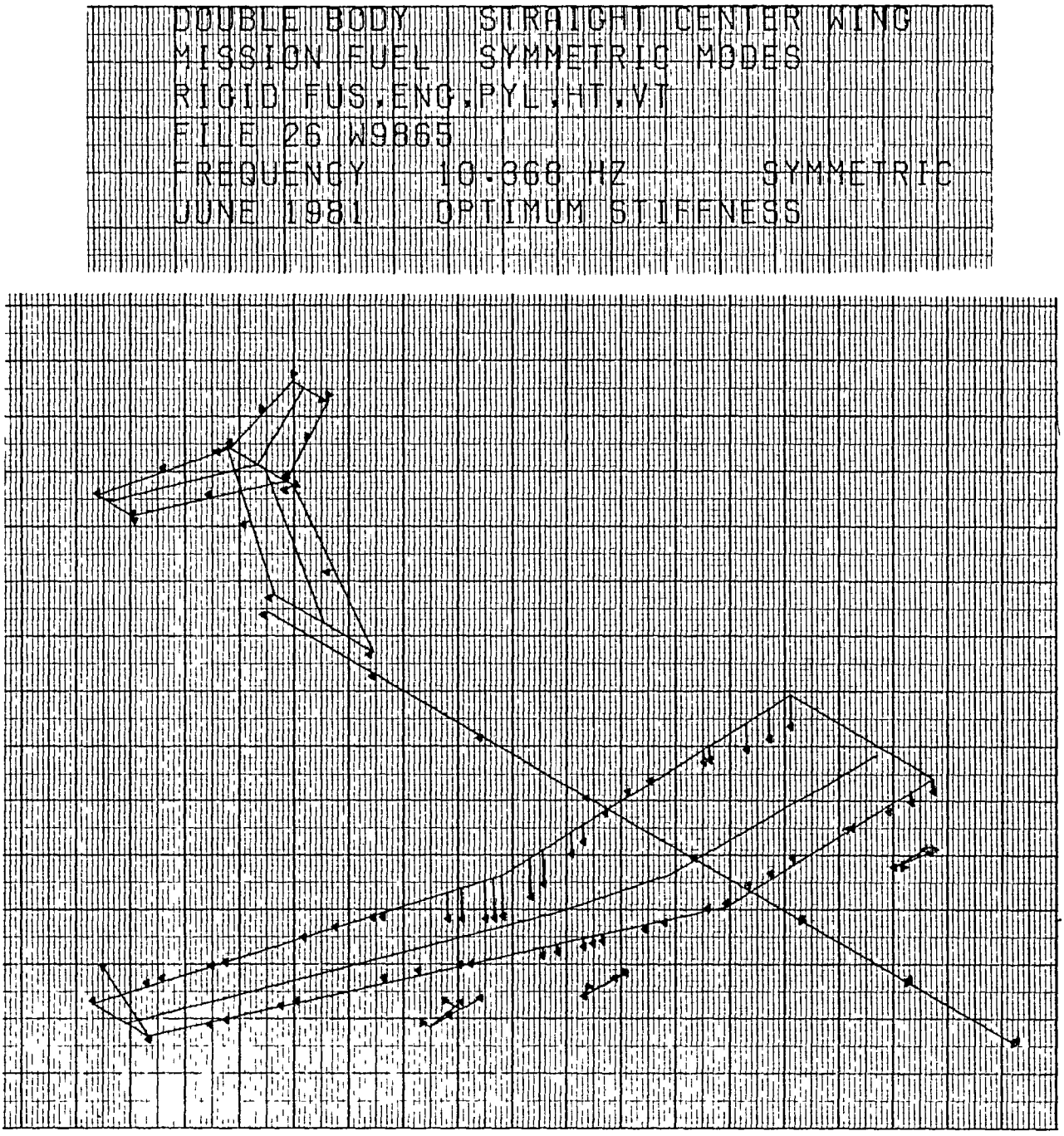

Figure D-48. Displacement Vectors - Symmetric Mode No. 14 - Two-Body MB2 Aircraft

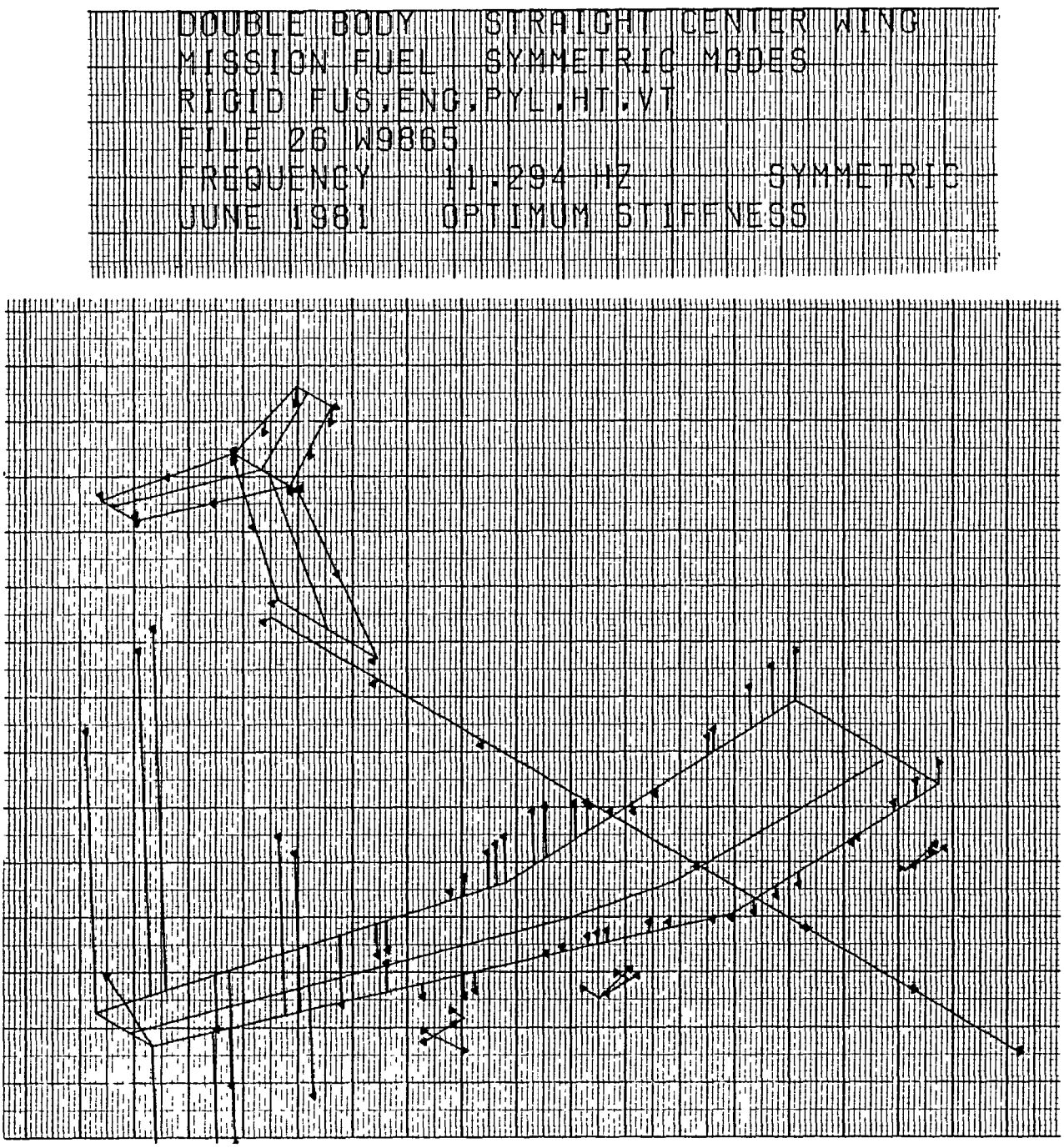

Figure D-49. Displacement Vectors - Symmetric Mode No. 15 - Two-Body MB2 Aircraft

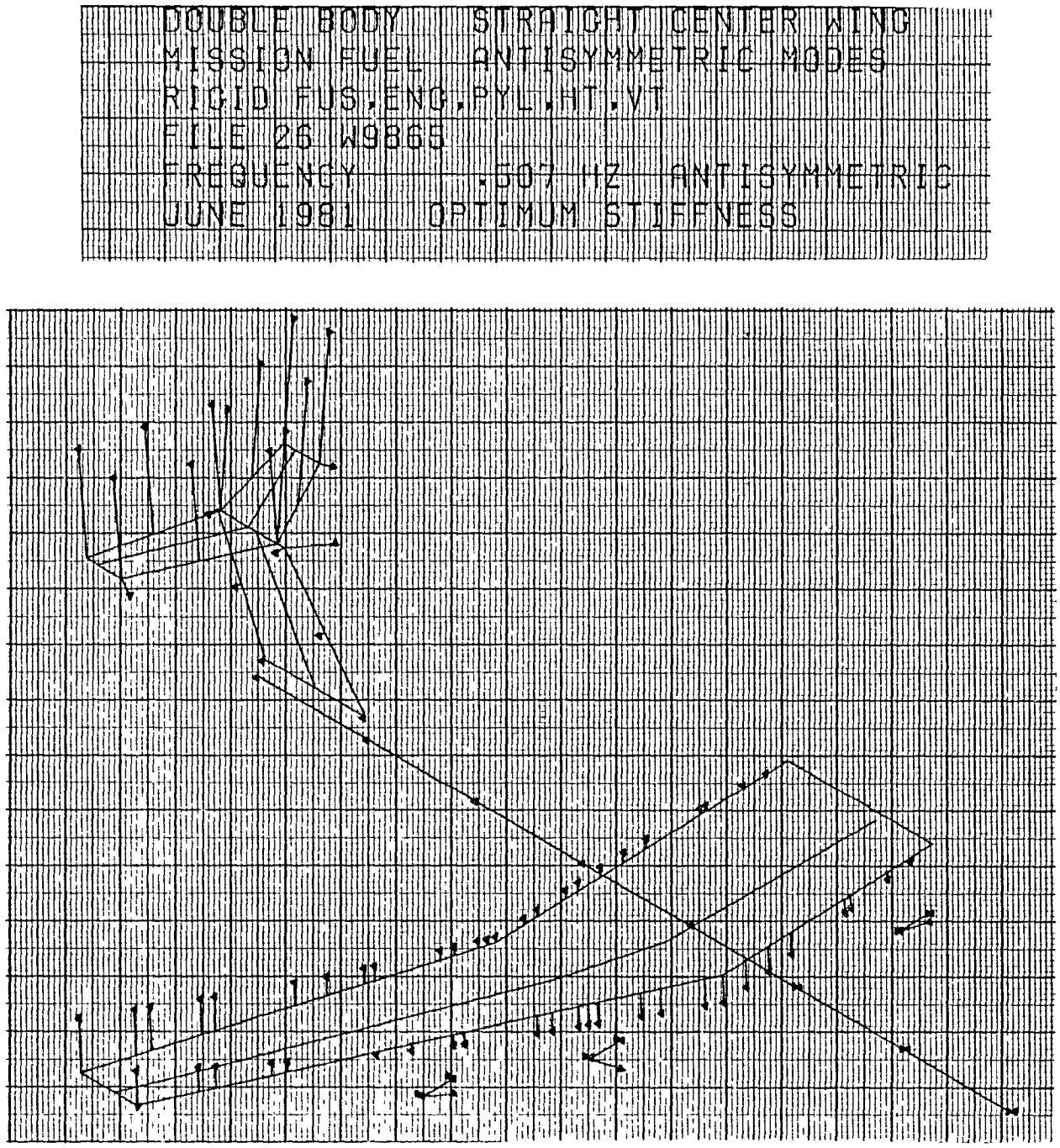

Figure D-50. Displacement Vectors - Antisymmetric Mode No. 1 - Two-Body MB2 Aircraft

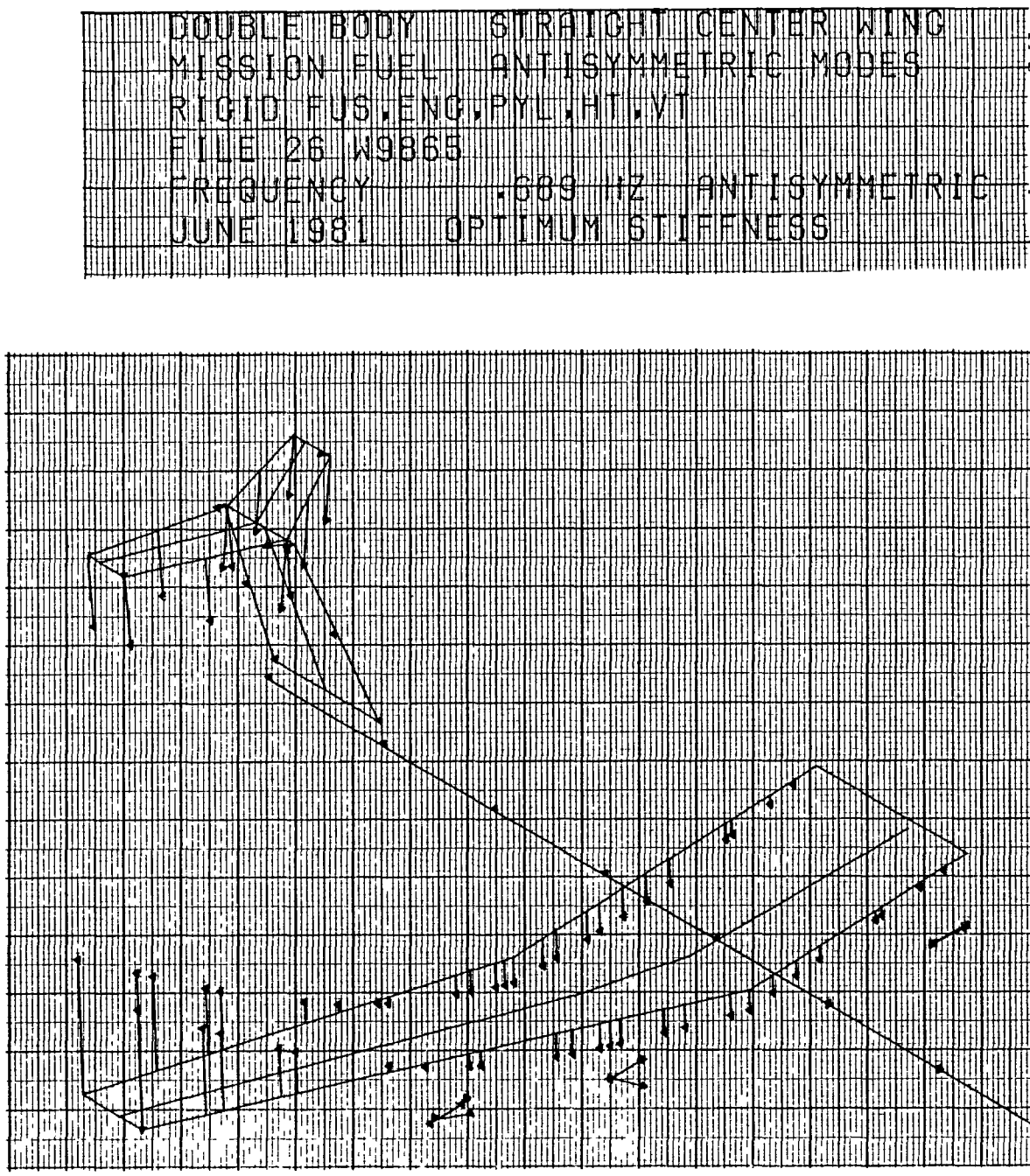

Figure D-51. Displacement Vectors - Antisymmetric Mode No. 2 - Two-Body TE2 Aircraft

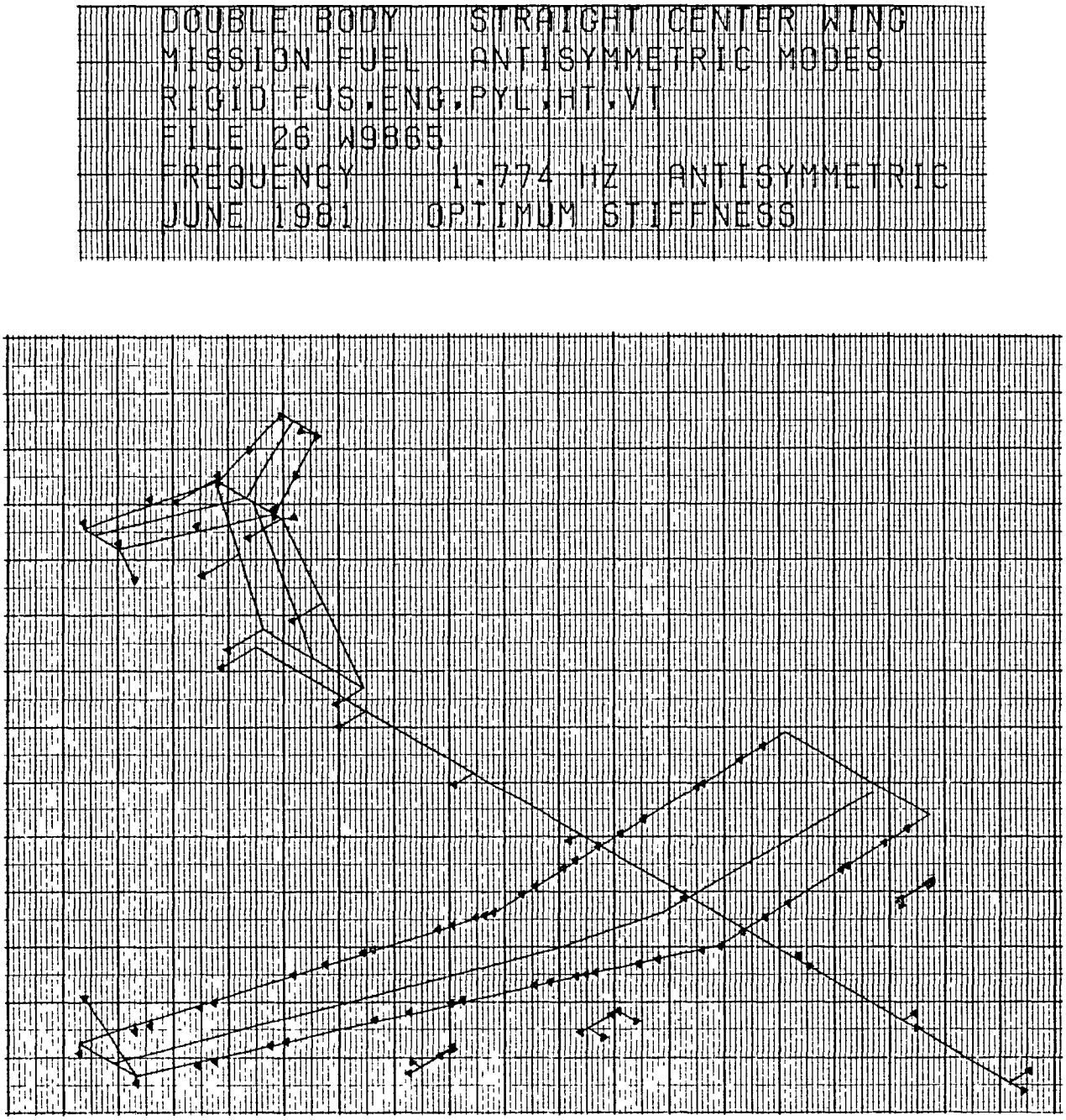

Figure D-52. Displacement Vectors - Antisymmetric Mode No. 3 - Two-Body MB2 Aircraft

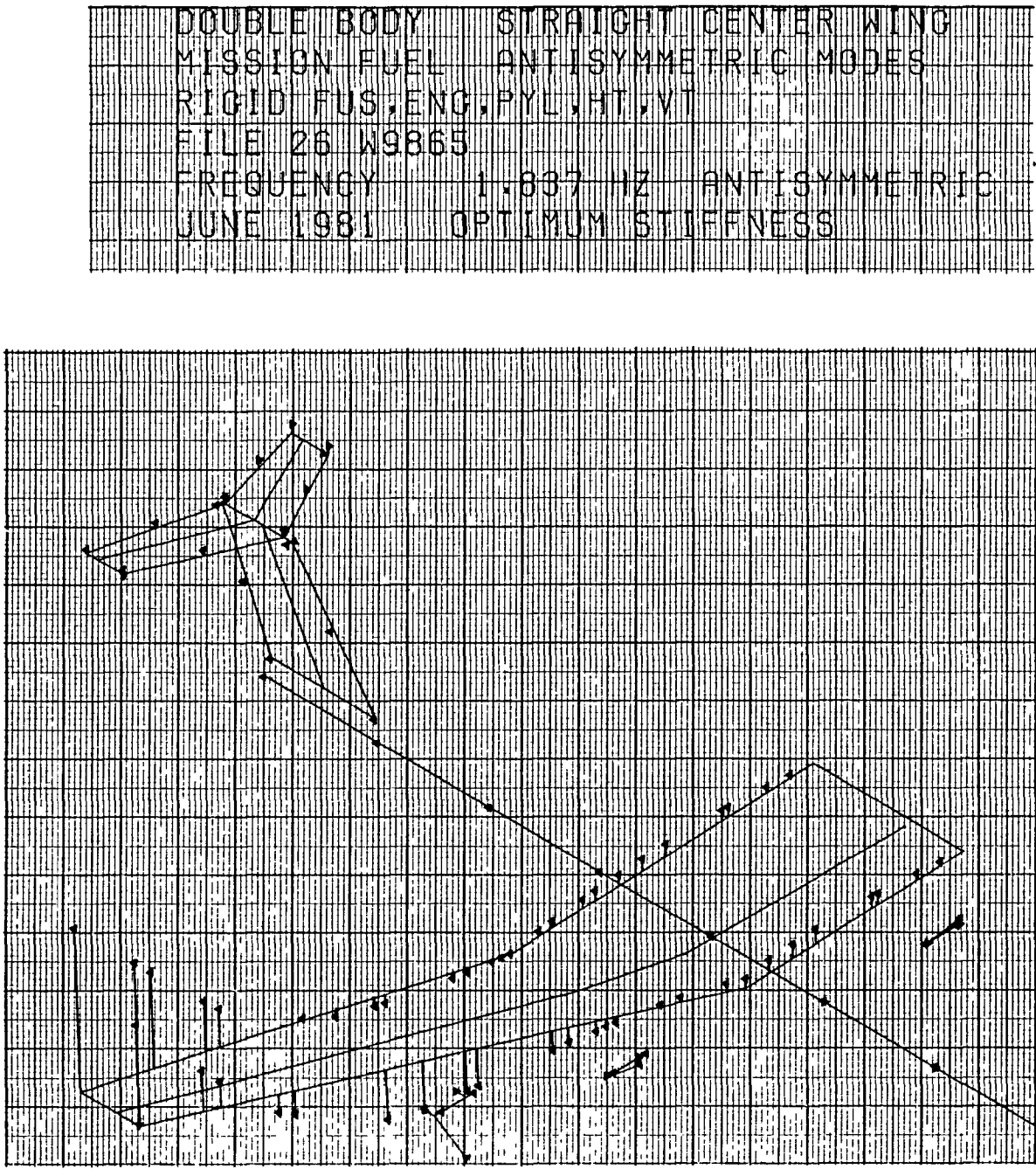

Figure D-53. Displacement Vectors - Antisymmetric Mode No. 4 - Two-Body MB2 Aircraft

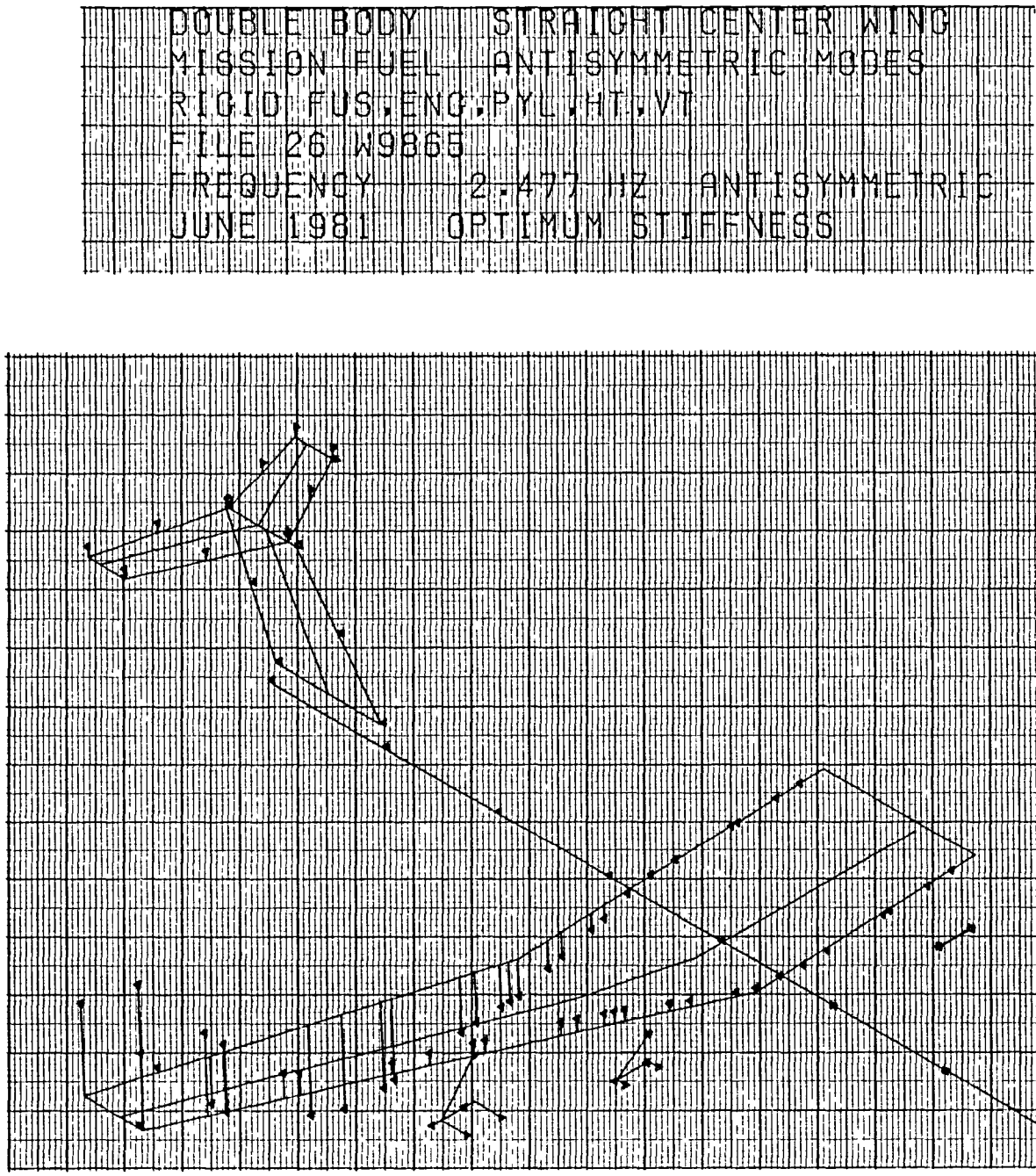

Figure D-54. Displacement Vectors - Antisymmetric Mode No. 5 - Two-Body MB2 Aircraft

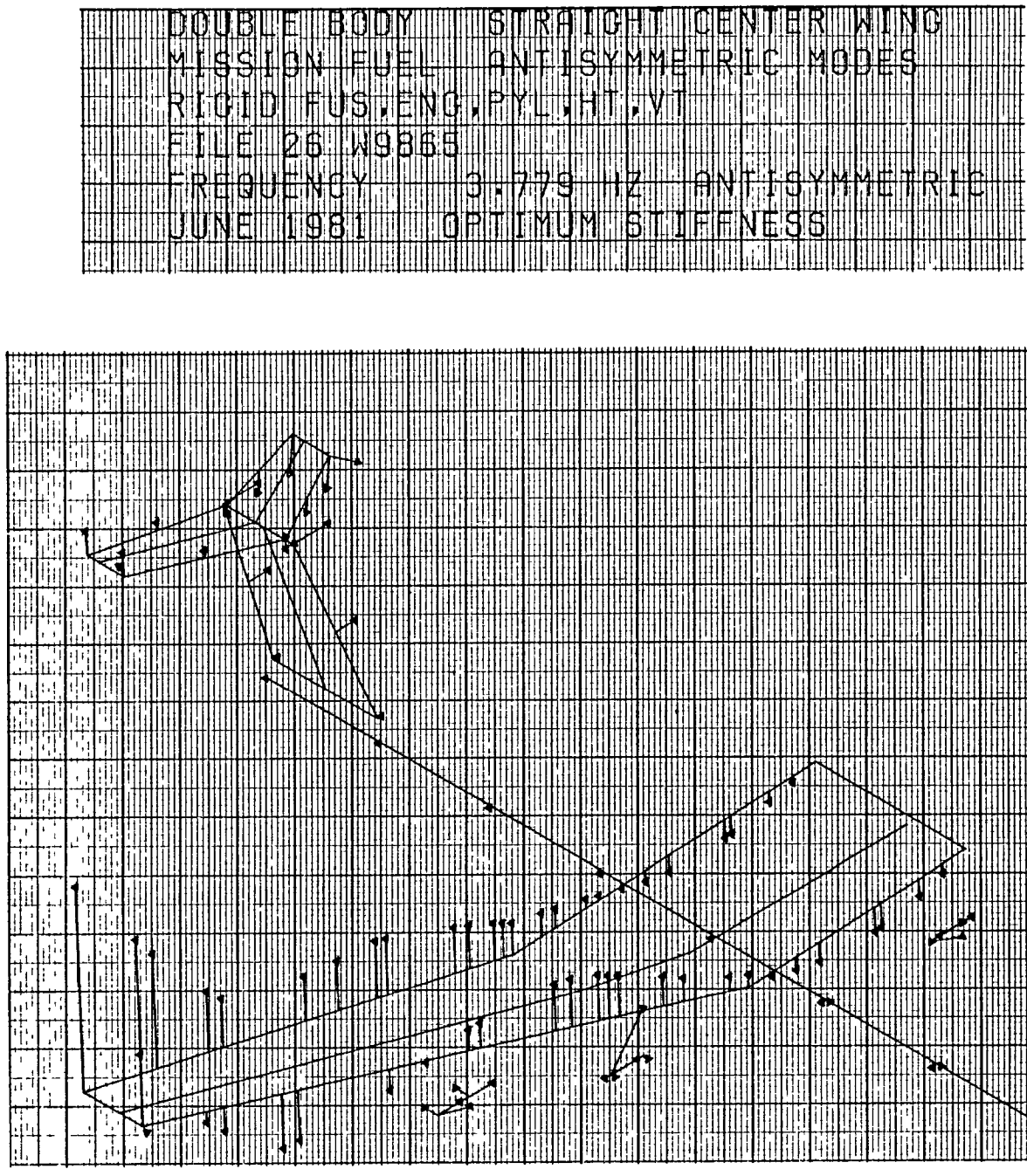

Figure D-55. Displacement Vectors - Antisymmetric Mode No. 6 - Two-Body MB2 Aircraft

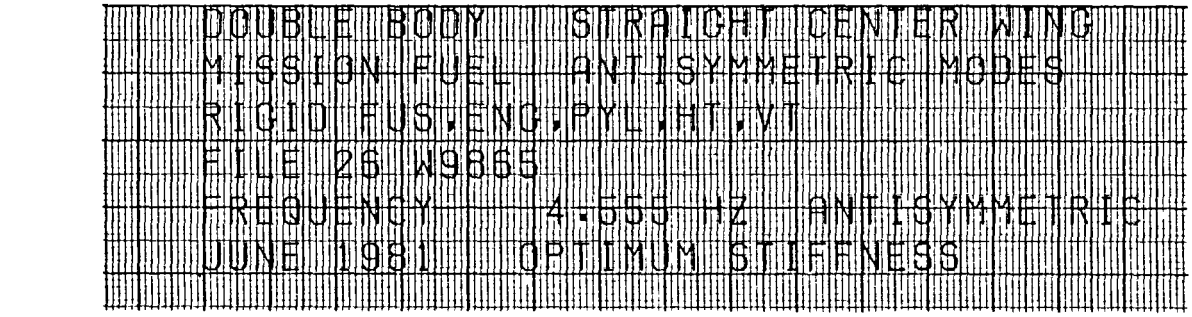

Figure D-56. Displacement Vectors - Antisymmetric Mode No. 7 - Two-Body MB2 Aircraft

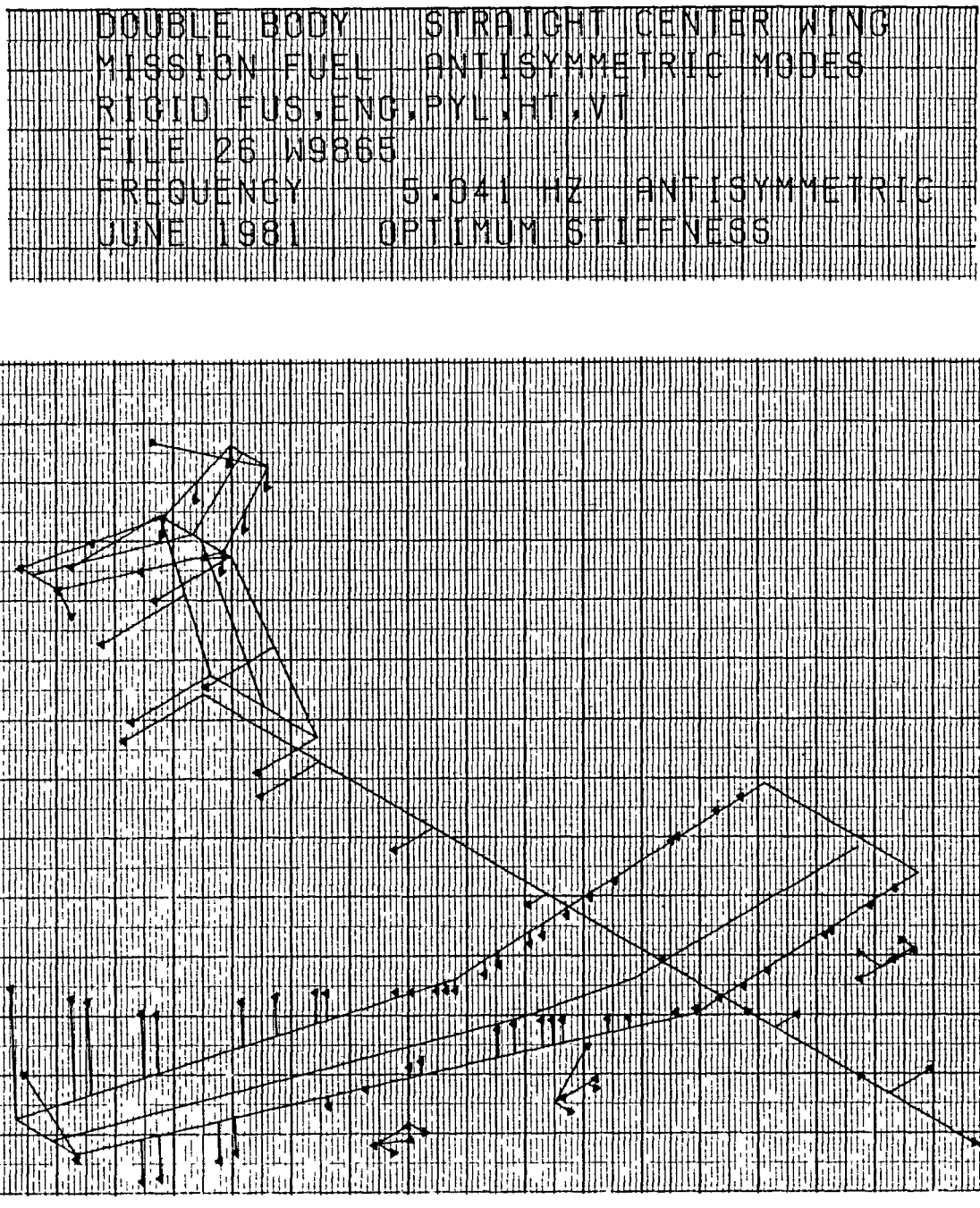

Figure D-57. Displacement Vectors - Antisymmetric Mode No. 8 - Two-Body MB2 Aircraft

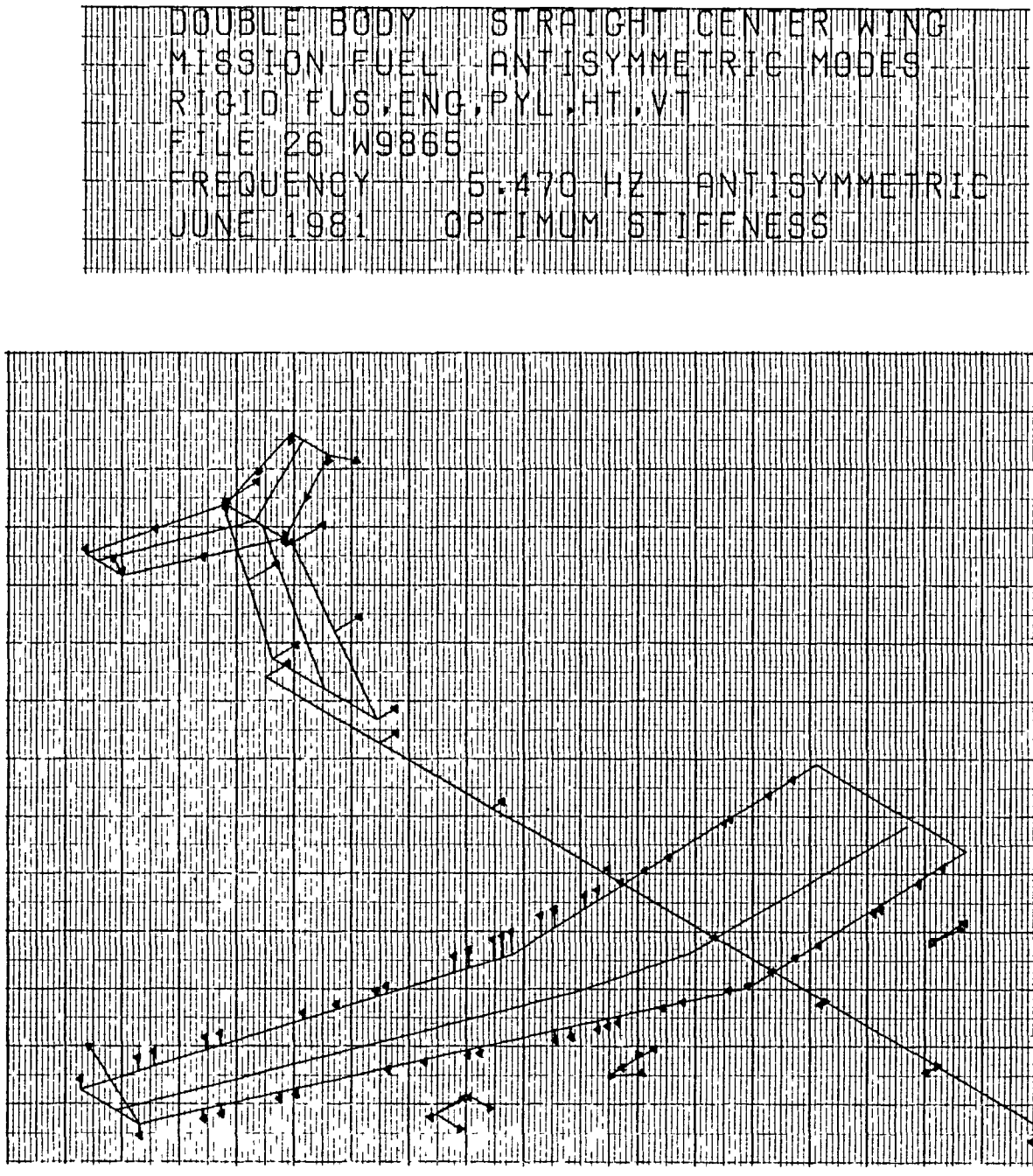

Figure D-58. Displacement Vectors - Antisymmetric Mode No. 9 - Two-Body MB2 Aircraft

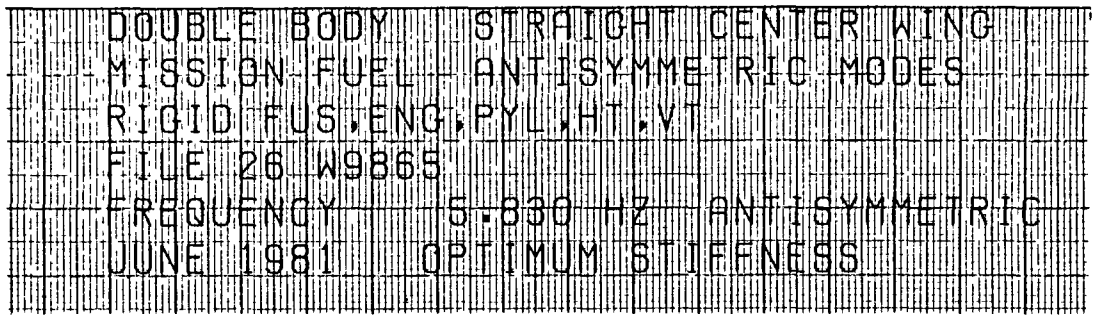

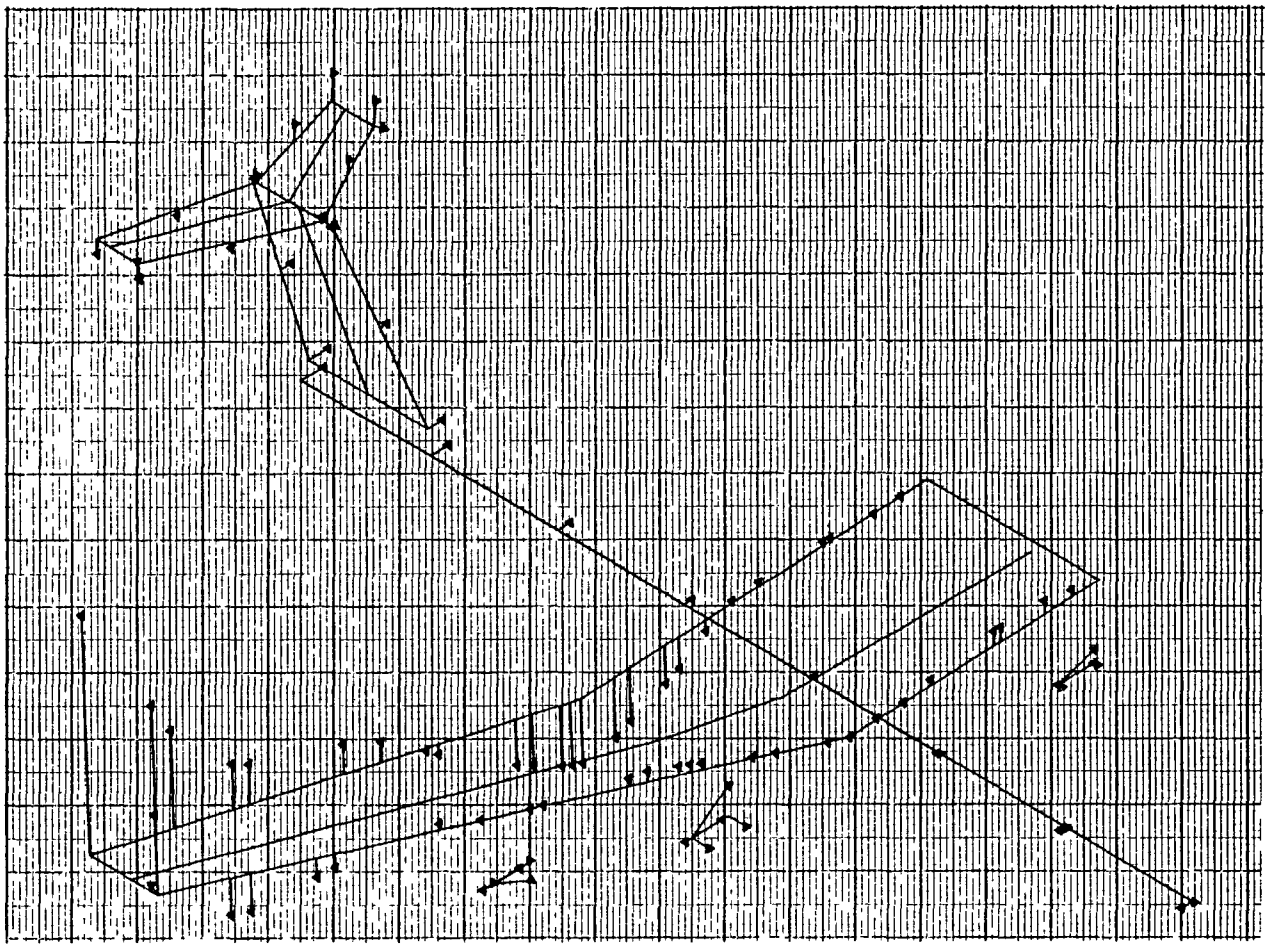

Figure D-59. Displacement Vectors - Antisymmetric Mode No. 10 - Two-Body MB2 Aircraft

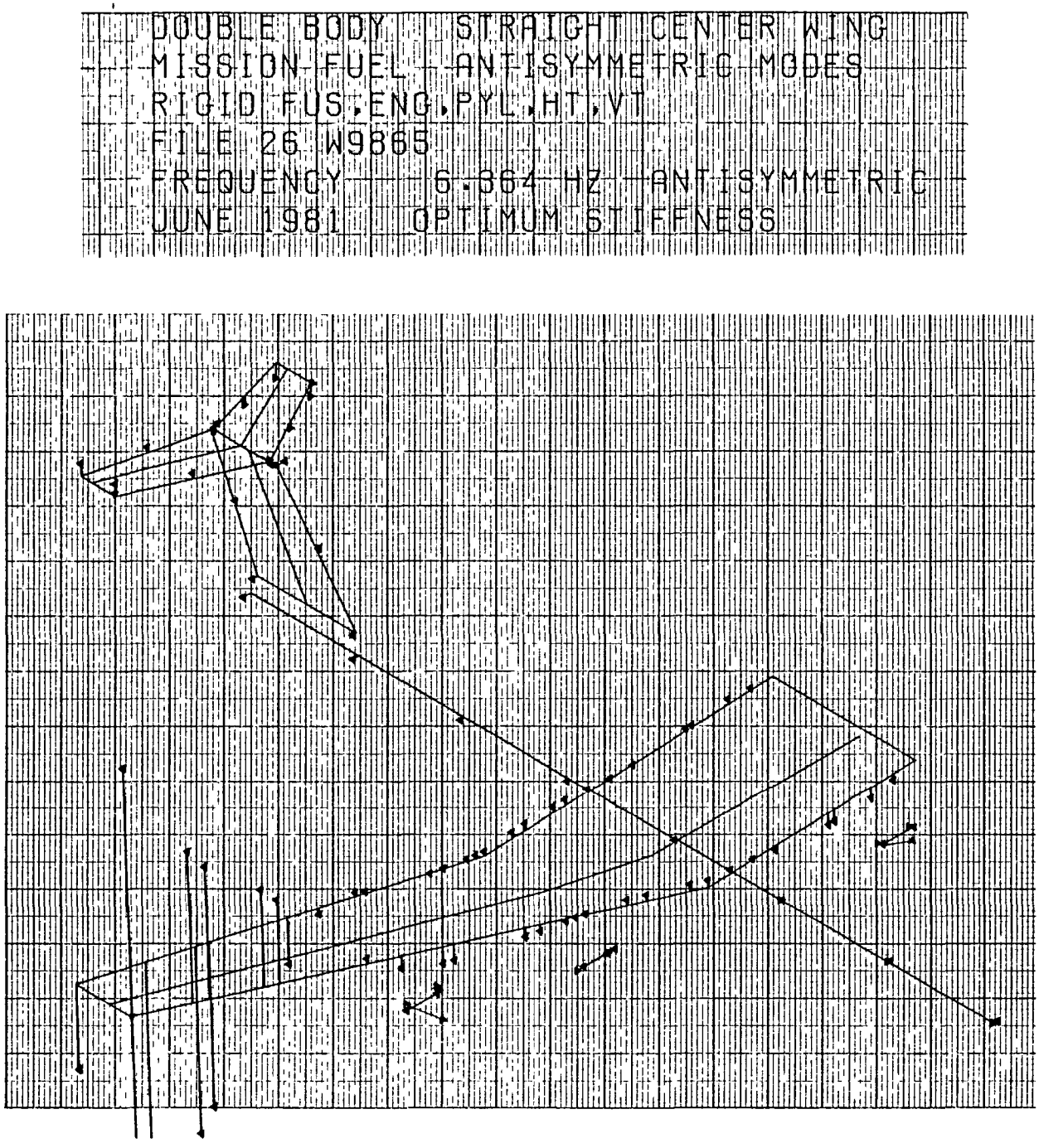

Figure D-60. Displacement Vectors - Antisymmetric Mode No. 11 - Two-Body MB2 Aircraft

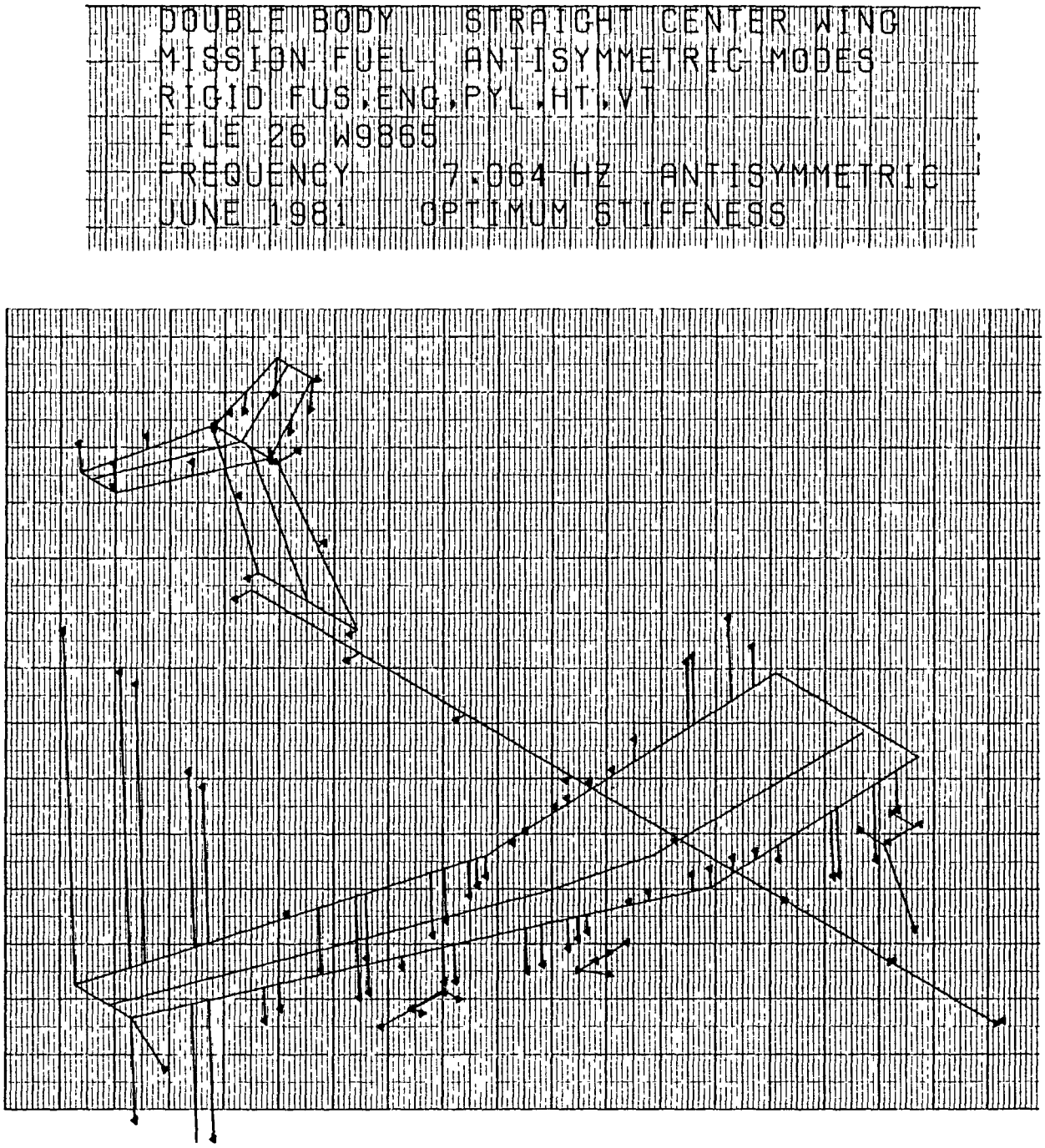

Figure D-61. Displacement Vectors - Antisymmetric Mode No. 12 - Two-Body MB2 Aircraft

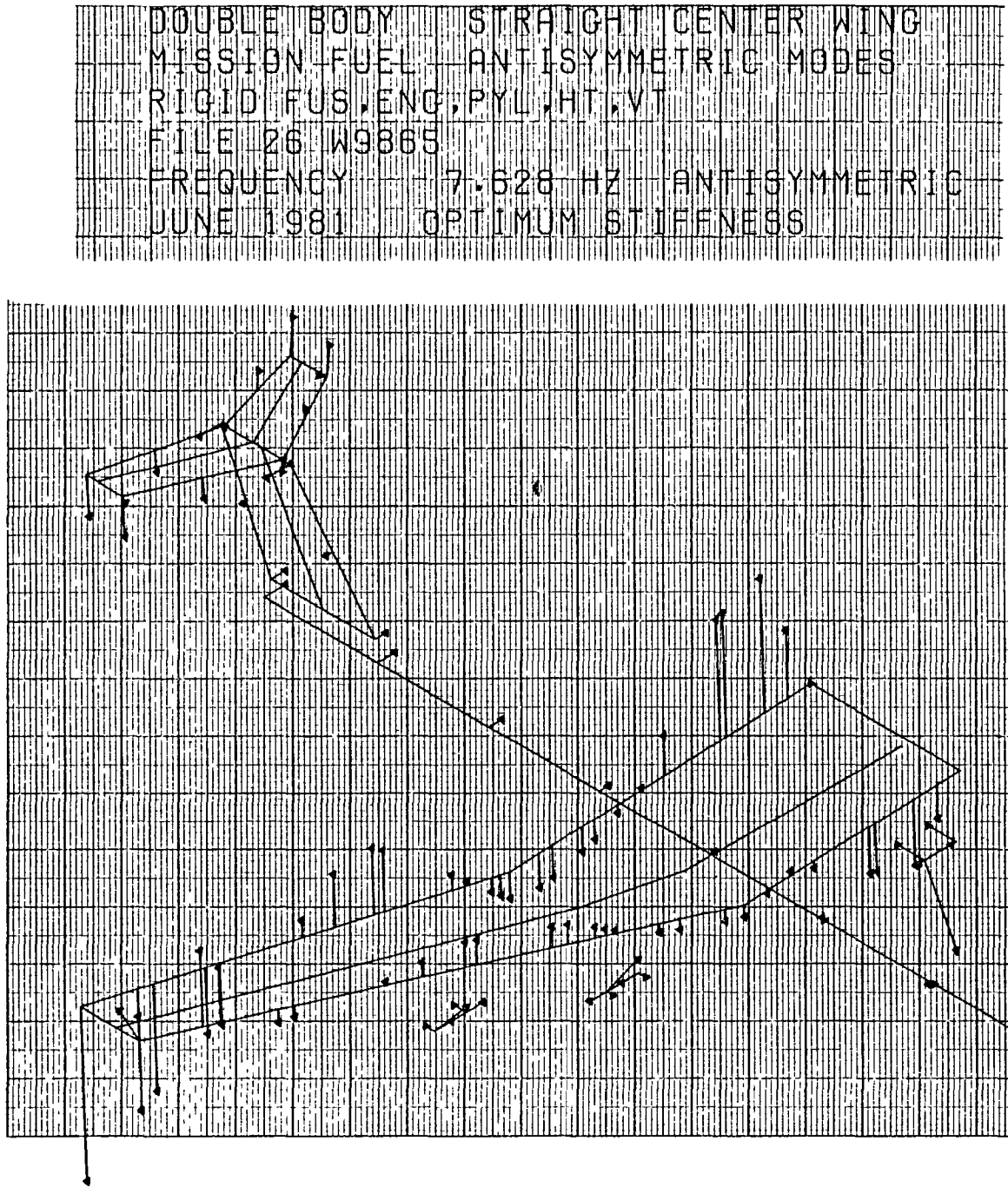

Figure D-62. Displacement Vectors - Antisymmetric Mode No. 13 - Two-Body MB2 Aircraft

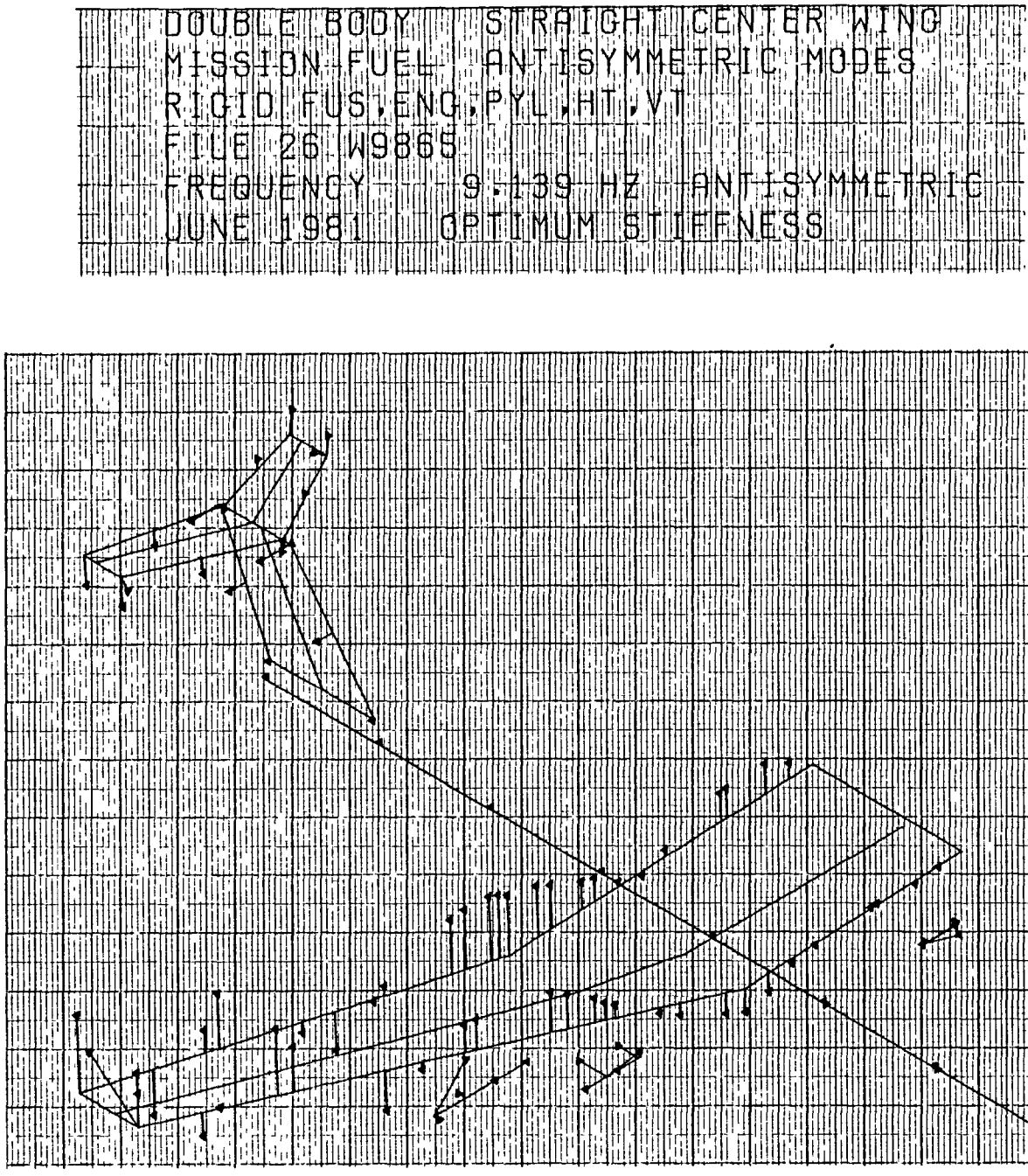

Figure D-63. Displacement Vectors - Antisymmetric Mode No. 14 - Two-Body MB2 Aircraft

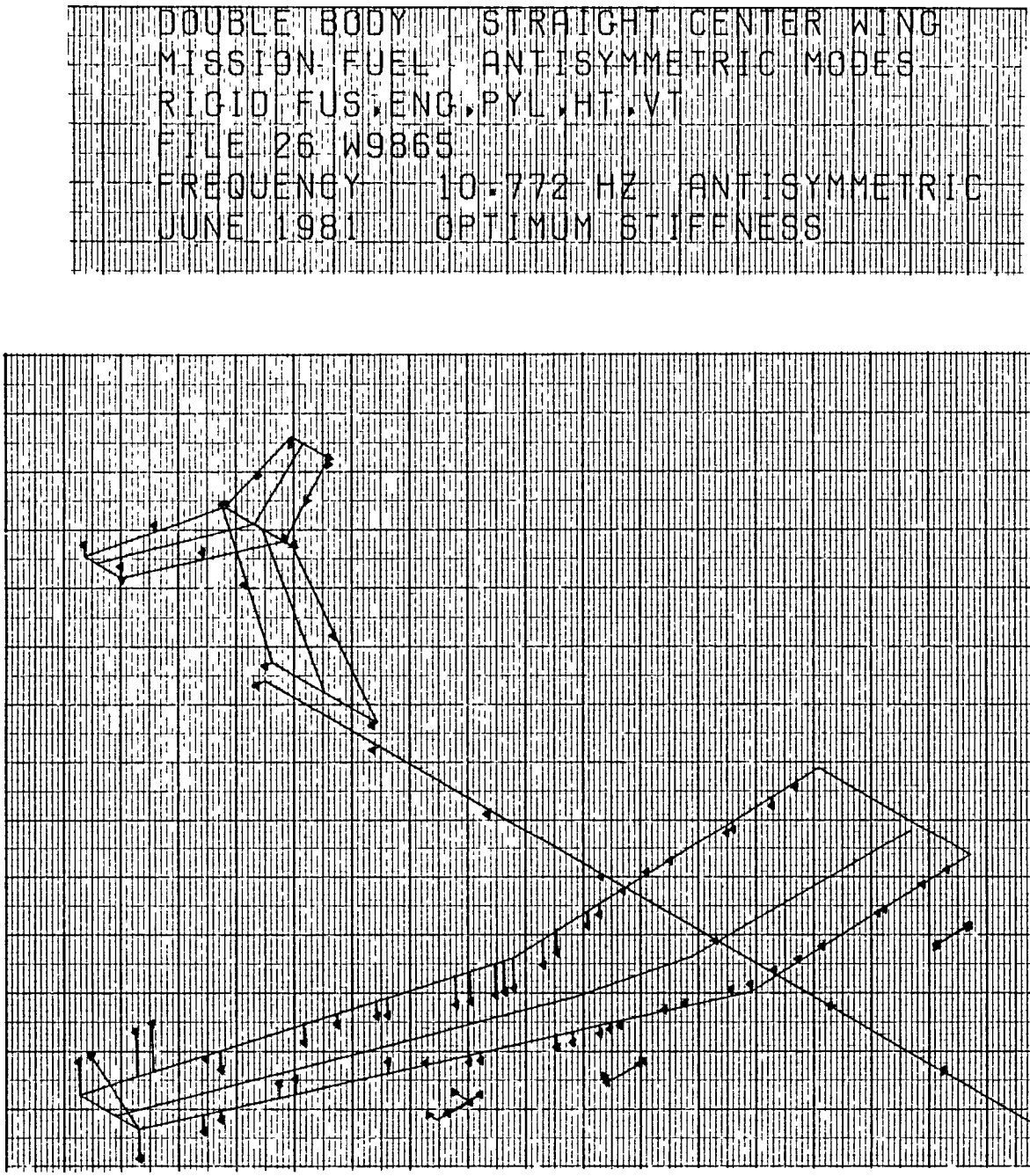

Figure D-64. Displacement Vectors - Antisymmetric Mode No. 15 - Two-Body MB2 Aircraft

are cast into the conventional flutter determinate solution and solved for a complete set of eigen values at each reduced frequency (semichord times frequency divided by velocity) value selected for this analysis. The real part of each eigen value is used to determine the frequency and velocity, and the ratio of the imaginary to real part is interpreted as the required structural damping to maintain harmonic motion. Results of these eigen value calculations are presented as velocity-frequency plots, e.g., Figure D-65, and velocity-damping plots, e.g., Figure D-66. Constant values of reduced frequency emanate radially from the origin, e.g., Figure D-65. The flutter point for each model is determined when the velocity-damping curve crosses the positive three percent damping value. A set of curves, i.e., velocity-frequency and velocity-damping, are for each combination of fuel, cargo, altitude, Mach number, and configuration studies. Figures D-65 through D-112 are velocity-frequency and velocity damping curves for the two-body MB2 aircraft for selected altitudes at Mach numbers of 0.50 and 0.80. Similar curves exist for the other altitudes. Cargo condition are not included for conciseness. Flutter velocities from each set of curves representing one Mach number and altitude for a given structural configuration are cross plotted on an intermediate summary curve of altitude versus flutter velocity in Figures D-113 through D-130, for a specific Mach number. When the flutter boundary is to the right of the constant Mach line the system is stable, to the left unstable. When the flutter points cross the constant Mach line then a matched point is determined and this point entered on the final summary plot of velocity, in equivalent airspeed, versus Mach number, e.g., Figure D-114. Although only two Mach numbers are used in this analysis, i.e., 0.50 and 0.80, sufficient information can be obtained to clearly establish trends for the flutter boundaries above, below, and in between the Mach numbers computed. For example, the most critical flutter mode in Figures D-117 and D-119 decreased by 19.0 m/sec (37 knots) equivalent airspeed at 12,192.0 m (40,000 ft) and 10.8 m/sec (21 knots) equivalent airspeed at minus 6,096.0 m (20,000 ft) when changing from Mach 0.50 to Mach 0.80. Using these changes in flutter velocity, the Prandtl-Glauert relationship for other Mach numbers, changes in mass ratio, and the constant Mach lines drawn on the altitude-velocity plots, flutter velocities for other Mach numbers can be inferred with reasonable accuracy.

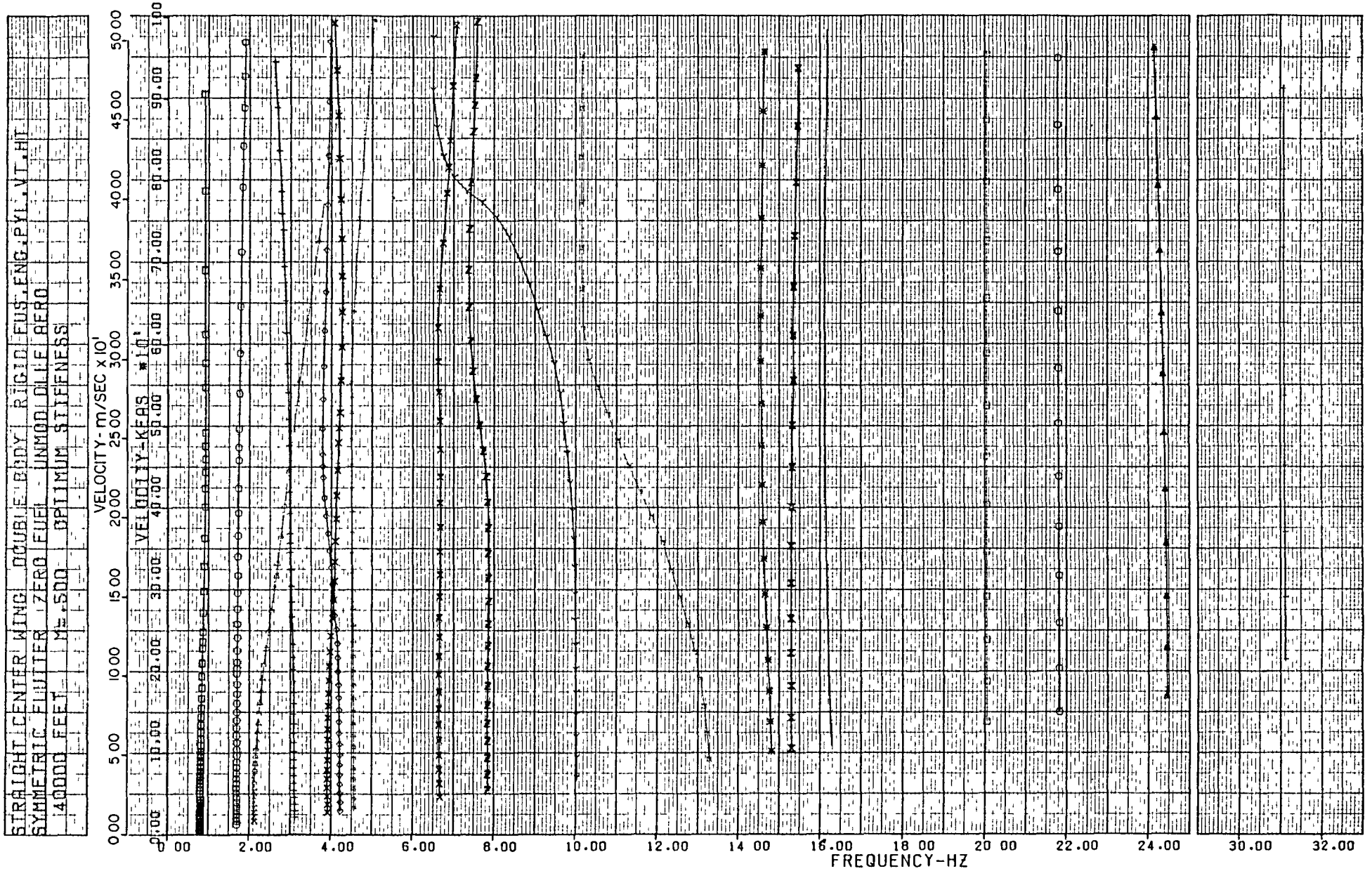

Figure D-65. Symmetric Velocity - Frequency, Stiffness at 40,000 Ft 0.50 Mach, Zero Fuel - Two-Body MB2 Aircraft

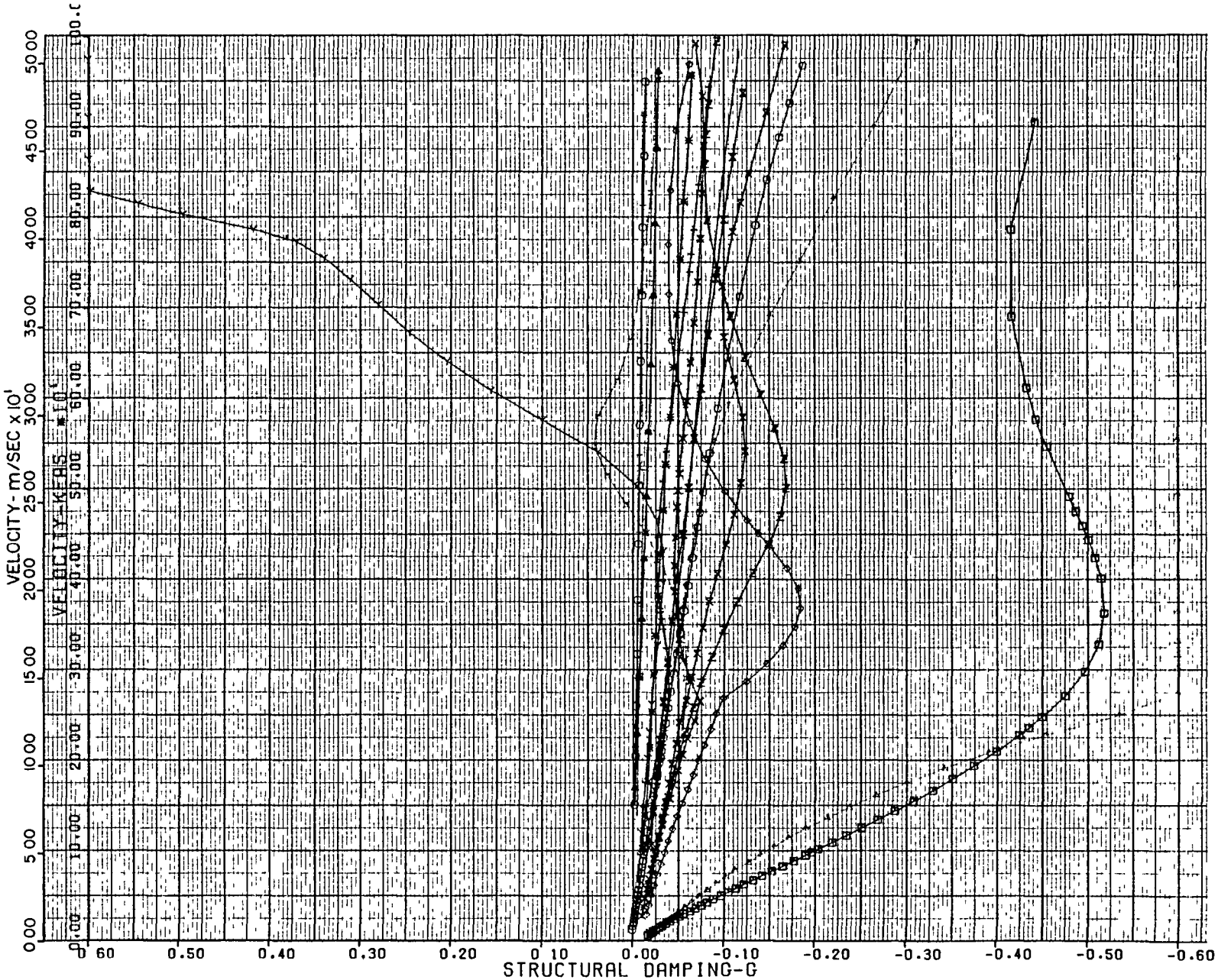

Figure D-66. Symmetric Velocity - Damping, Stiffness at 40,000 Ft 0.50 Mach, Zero Fuel - Two-Body MB2 Aircraft

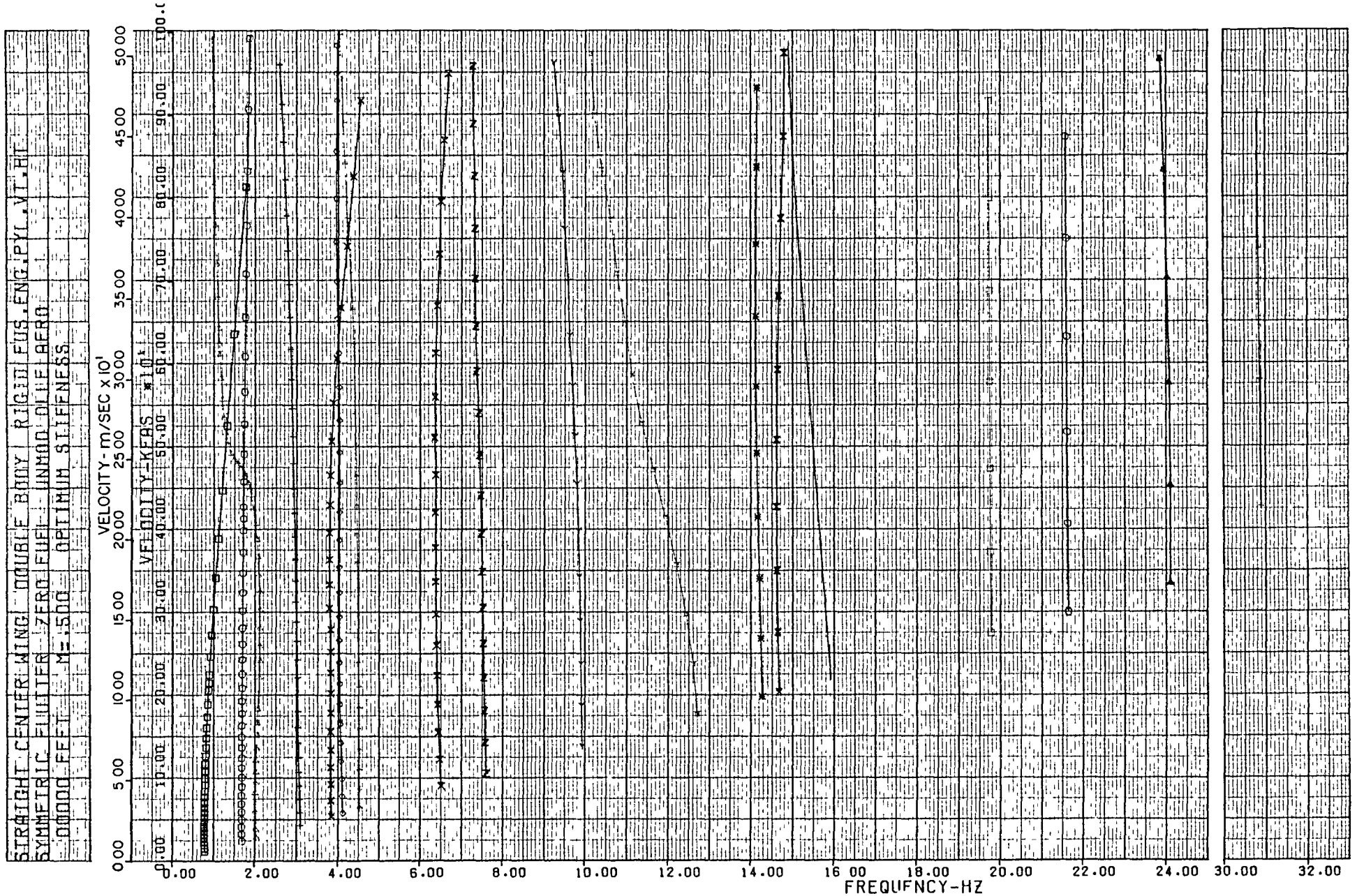

Figure D-67. Symmetric Velocity - Frequency, Stiffness at 0 Ft 0.50 Mach, Zero Fuel - Two-Body MB2 Aircraft

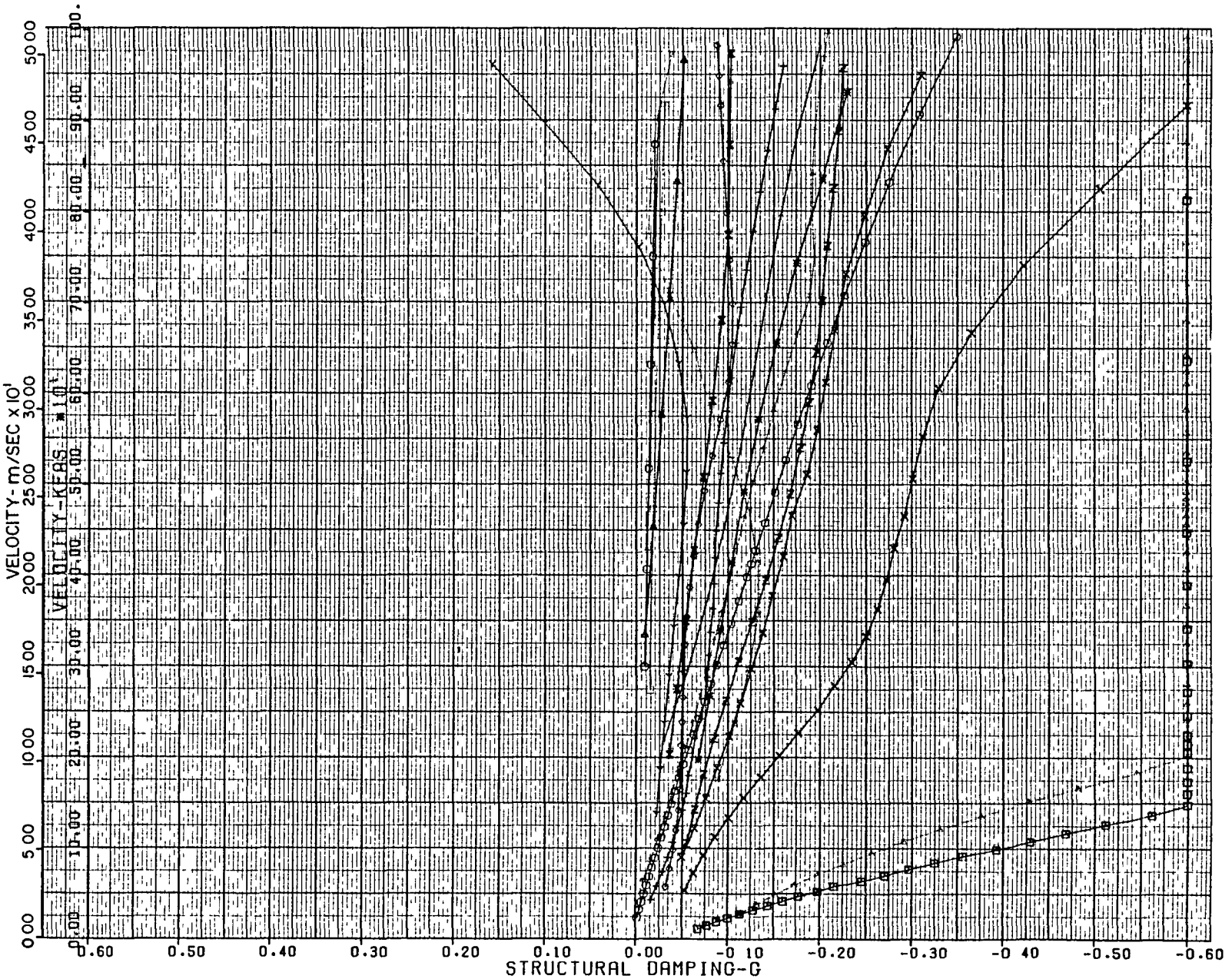

Figure D-68. Symmetric Velocity - Damping, Stiffness at 0 Ft 0.50 Mach, Zero Fuel - Two-Body MB2 Aircraft

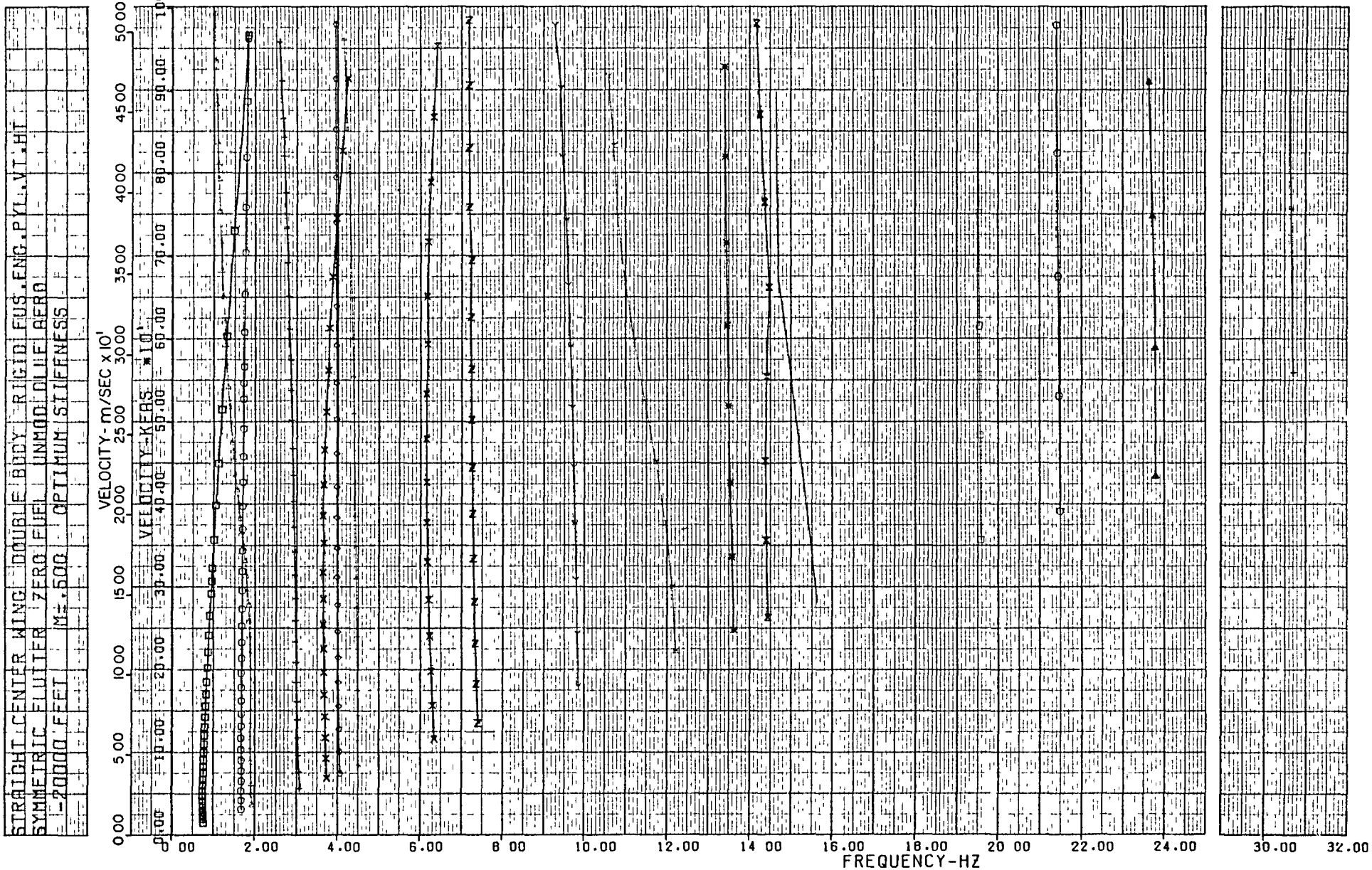

Figure D-69. Symmetric Velocity - Frequency, Stiffness at -20,000 Ft
0.50 Mach, Zero Fuel - Two-Body MB2 Aircraft

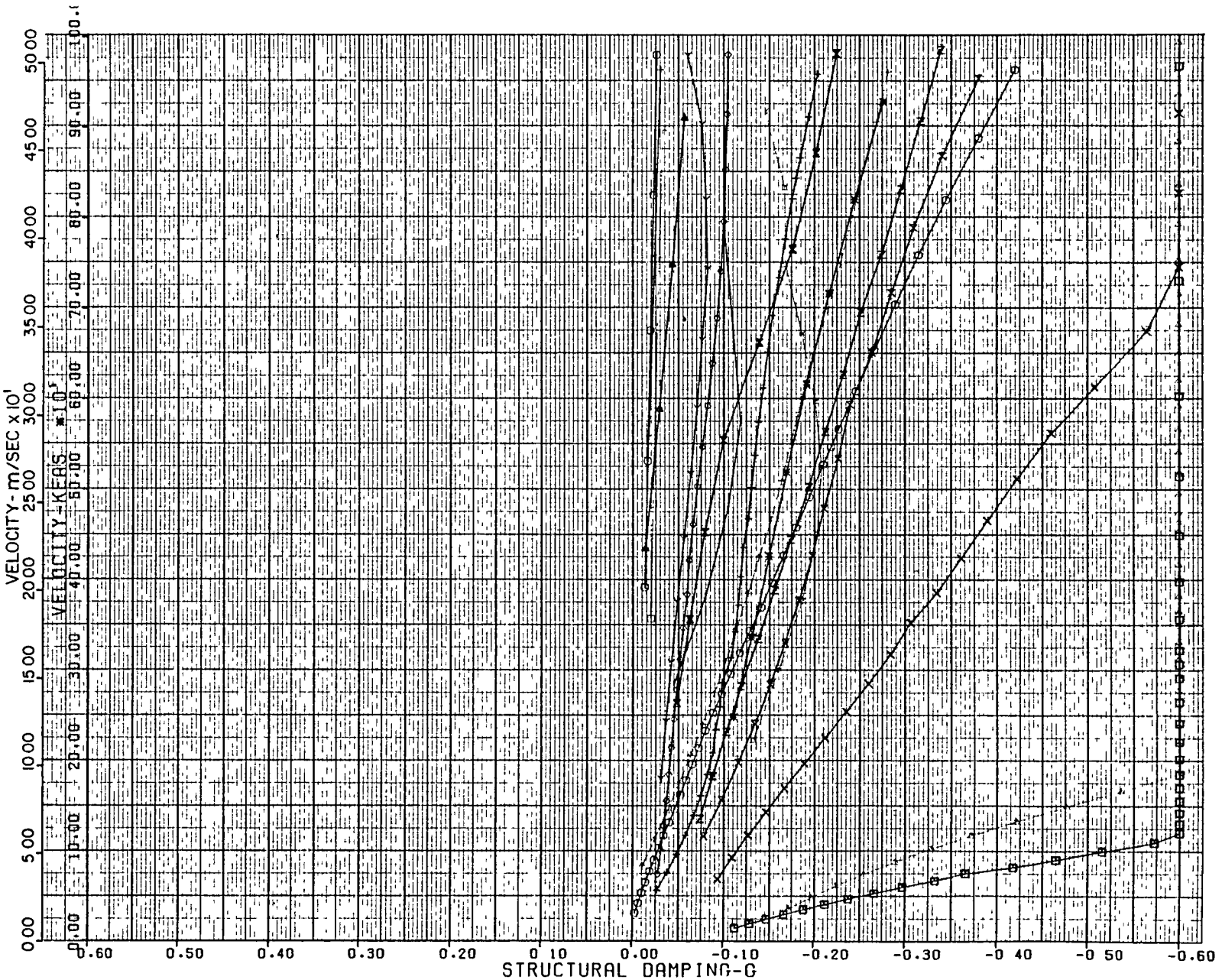

Figure D-70. Symmetric Velocity - Damping, Stiffness at -20,000 Ft 0.50 Mach, Zero Fuel - Two-Body MB2 Aircraft

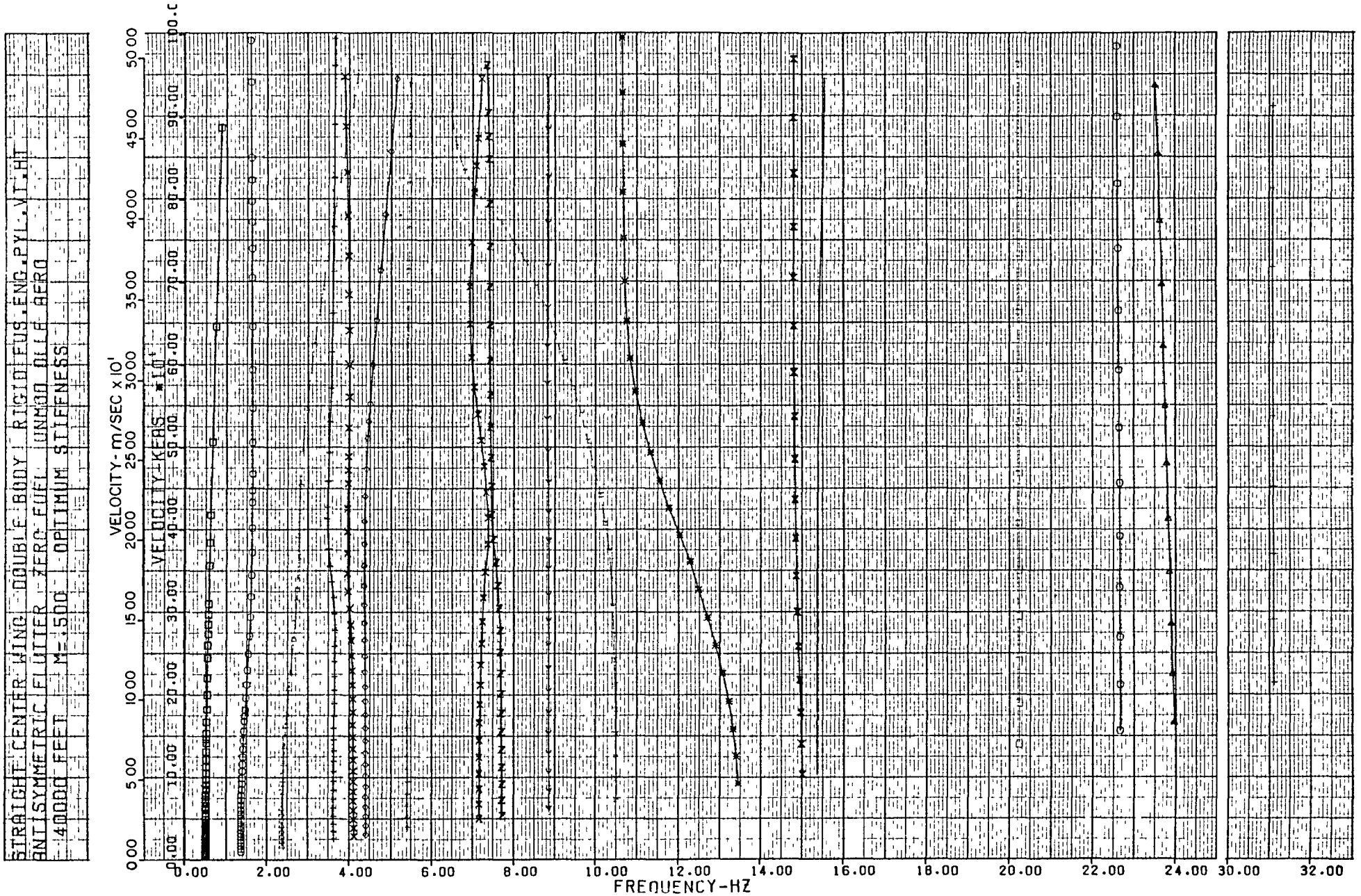

Figure D-71. Antisymmetric Velocity - Frequency, Stiffness at 40,000 Ft 0.50 Mach, Zero Fuel - Two-Body MB2 Aircraft

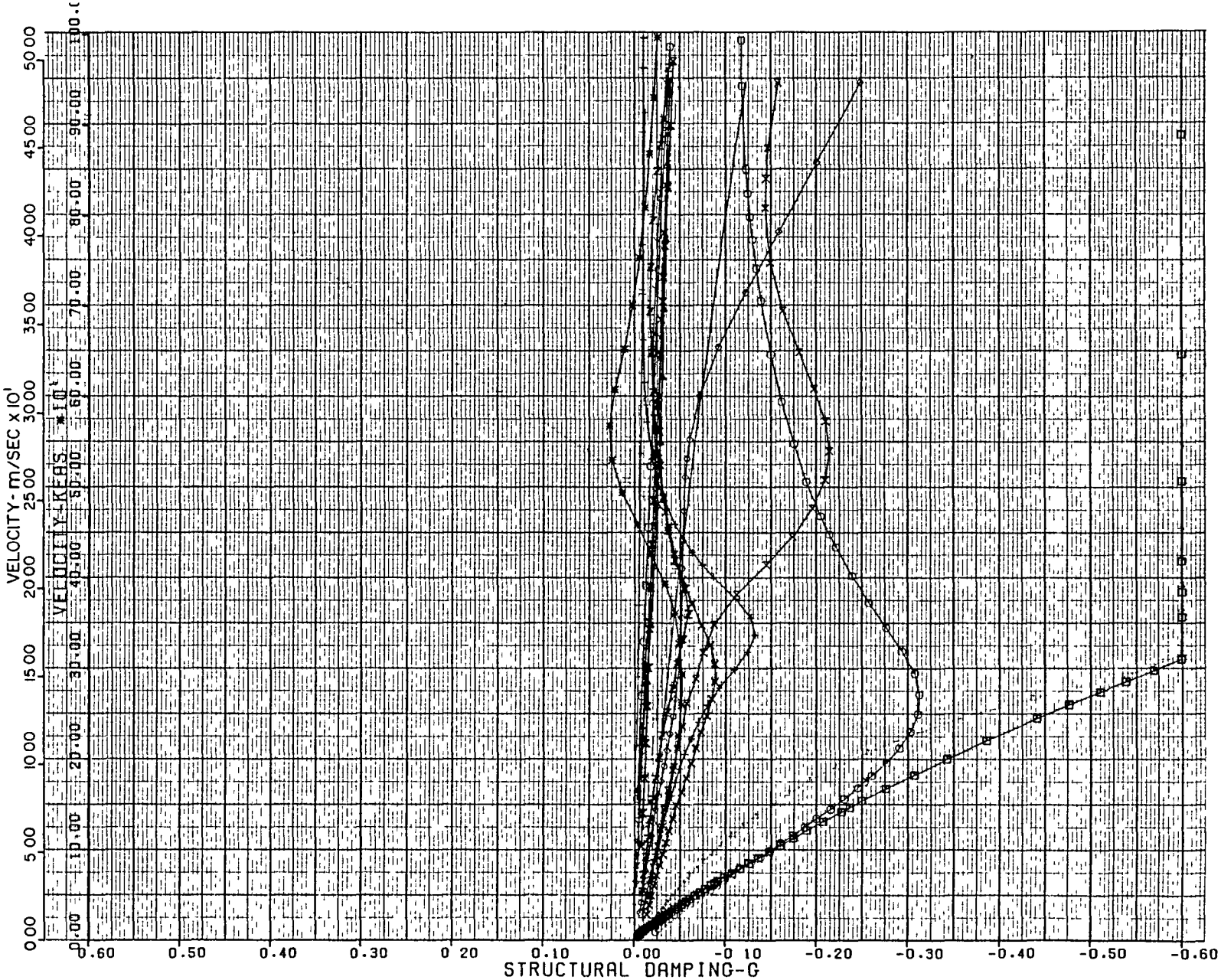

Figure D-72. Antisymmetric Velocity - Damping, Stiffness at 40,000 Ft 0.50 Mach, Zero Fuel - Two-Body MB2 Aircraft

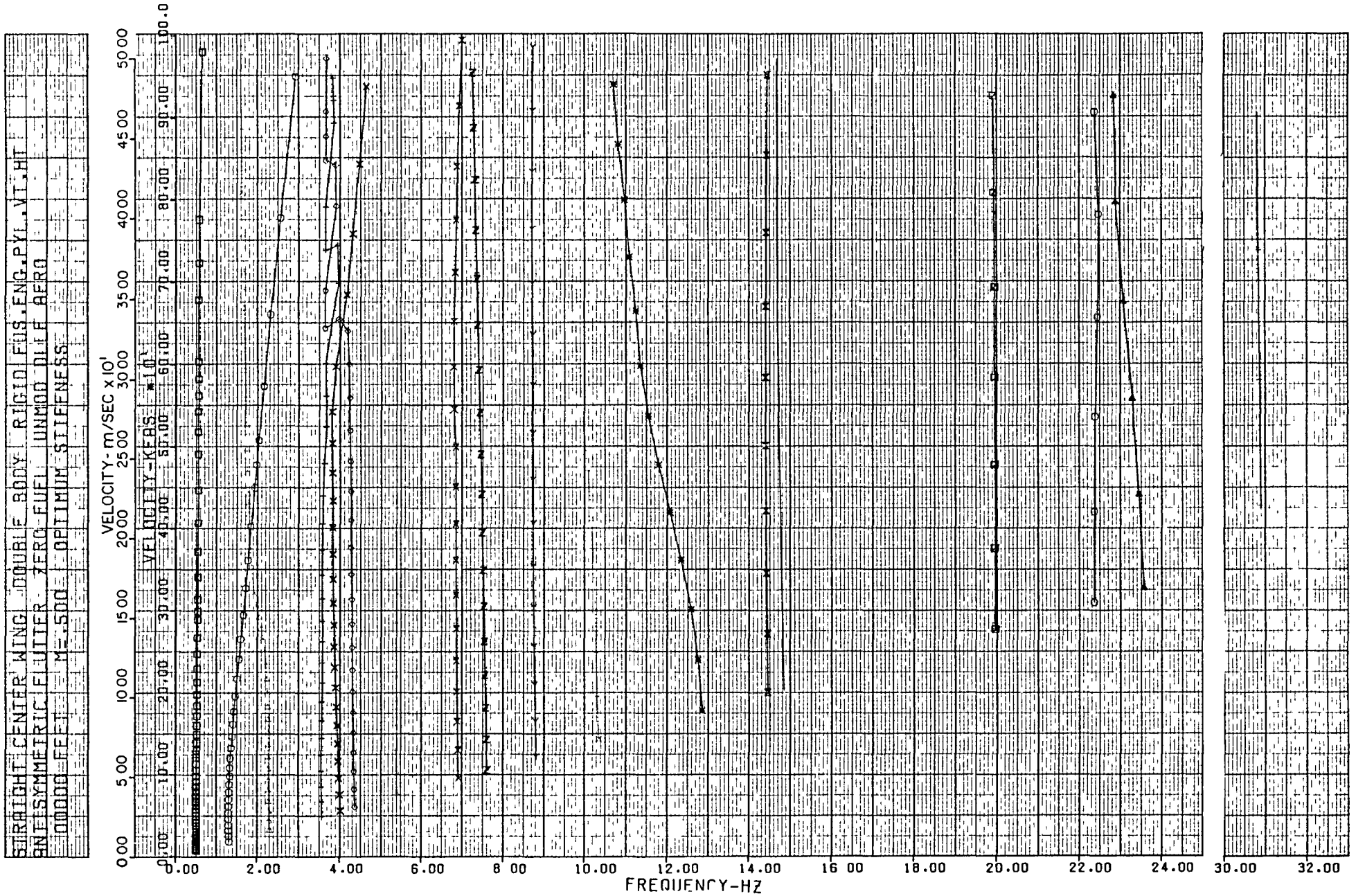

Figure D-73. Antisymmetric Velocity - Frequency, Stiffness at 0 Ft 0.50 Mach, Zero Fuel - Two-Body MB2 Aircraft

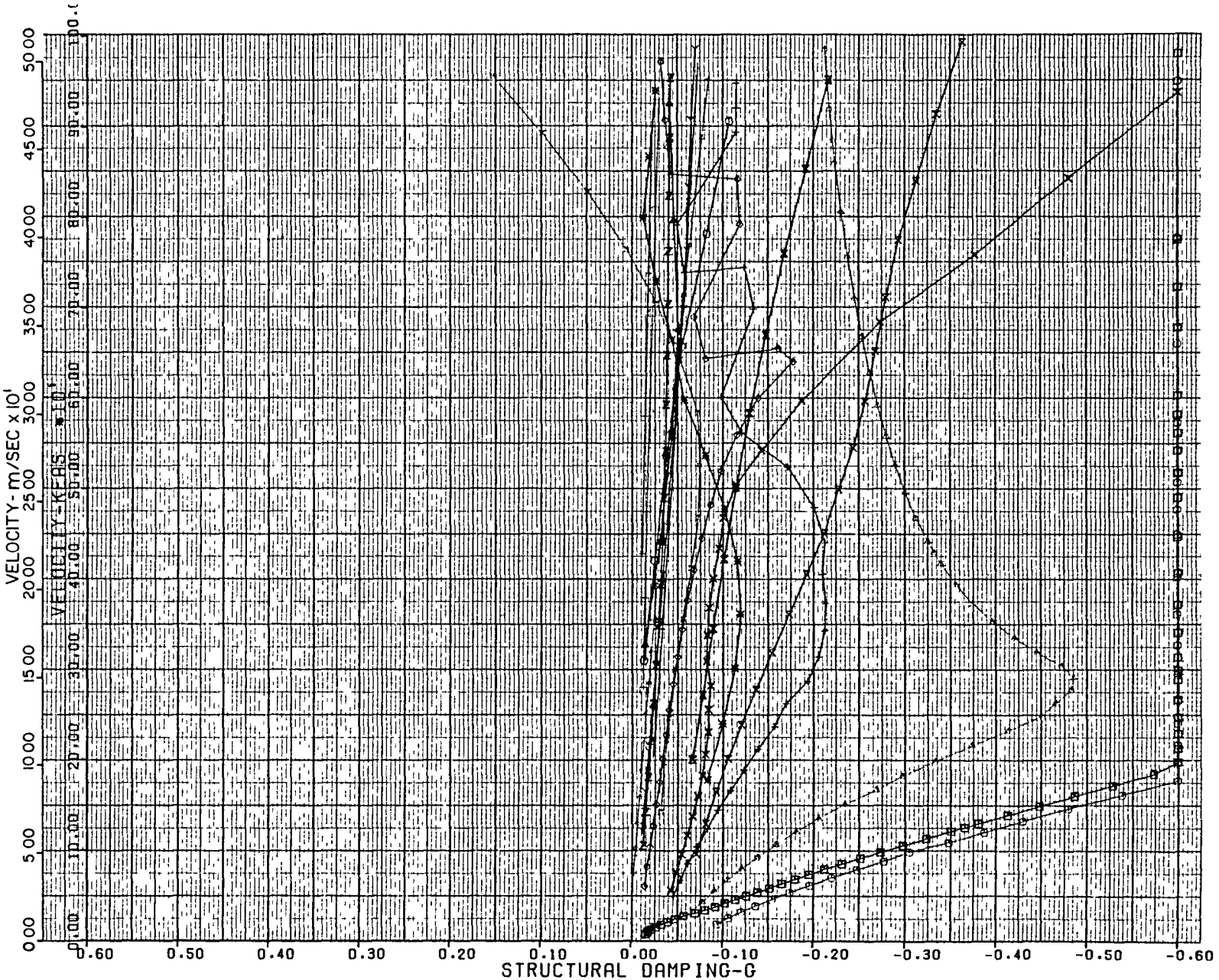

Figure D-74. Antisymmetric Velocity - Damping, Stiffness at 0 Ft 0.50 Mach, Zero Fuel - Two-Body MB2 Aircraft

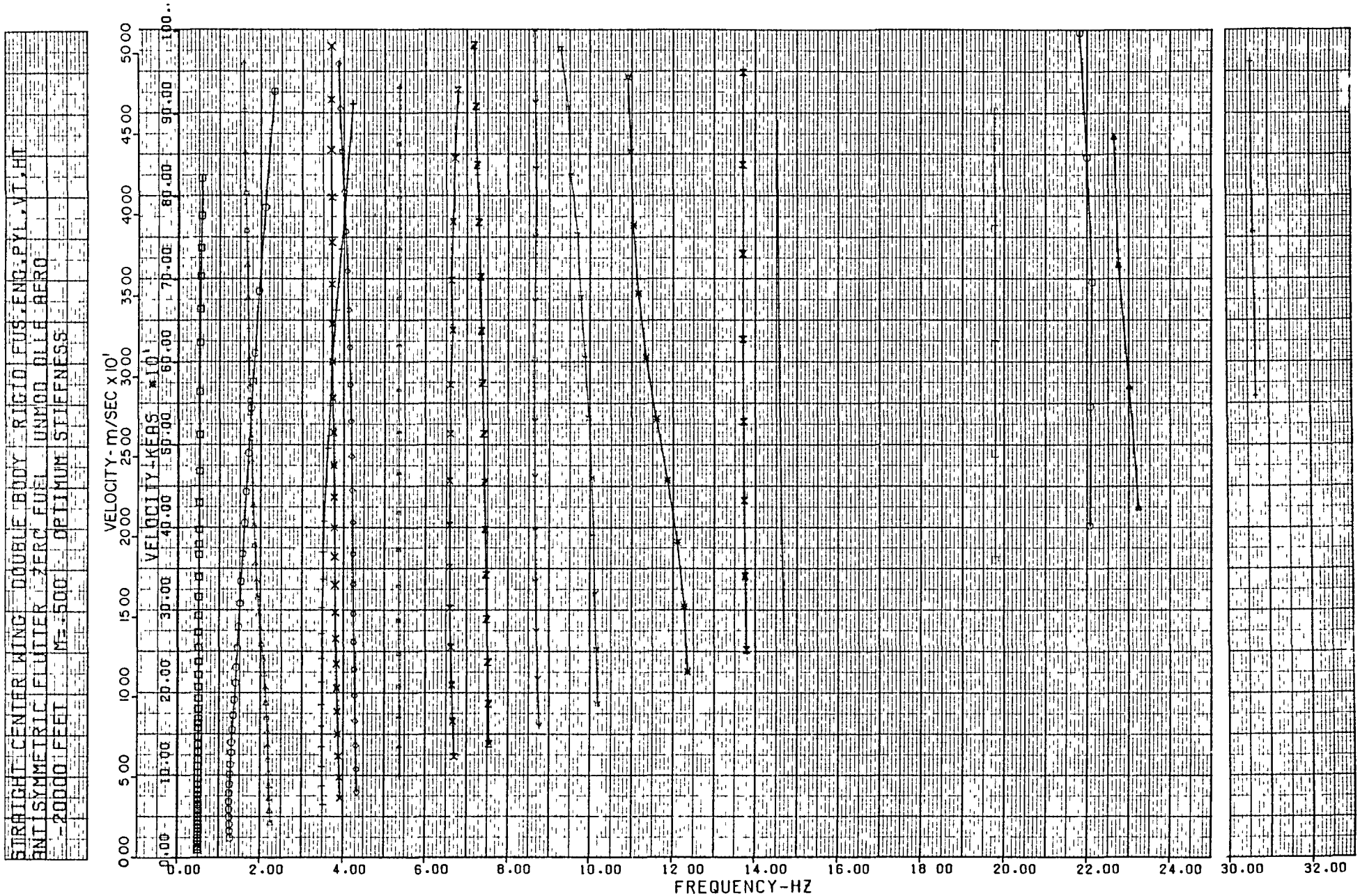

Figure D-75. Antisymmetric Velocity - Frequency, Stiffness at -20,000 Ft 0.50 Mach, Zero Fuel - Two-Body MB2 Aircraft

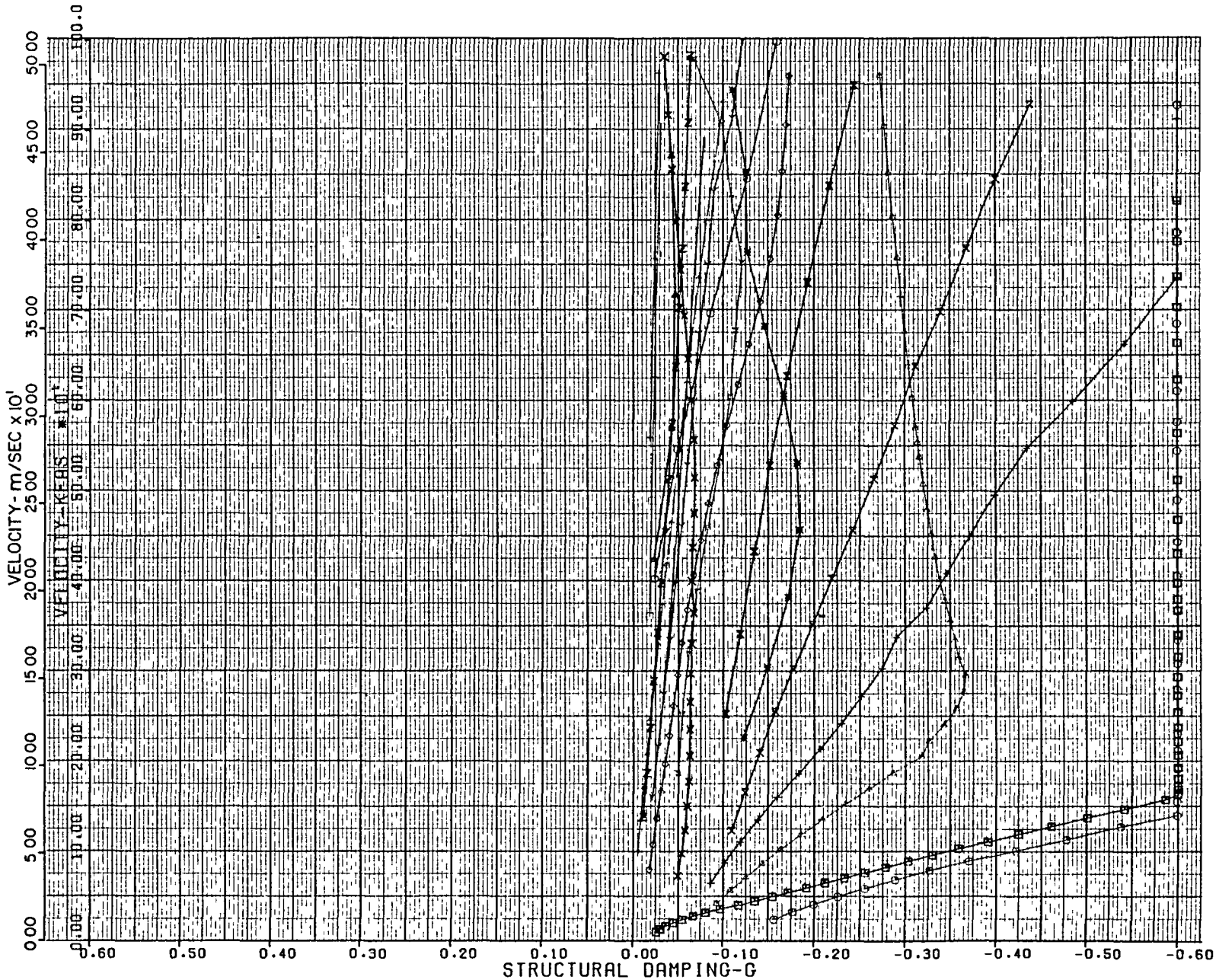

Figure D-76. Antisymmetric Velocity - Damping, Stiffness at -20,000 Ft 0.50 Mach, Zero Fuel - Two-Body MB2 Aircraft

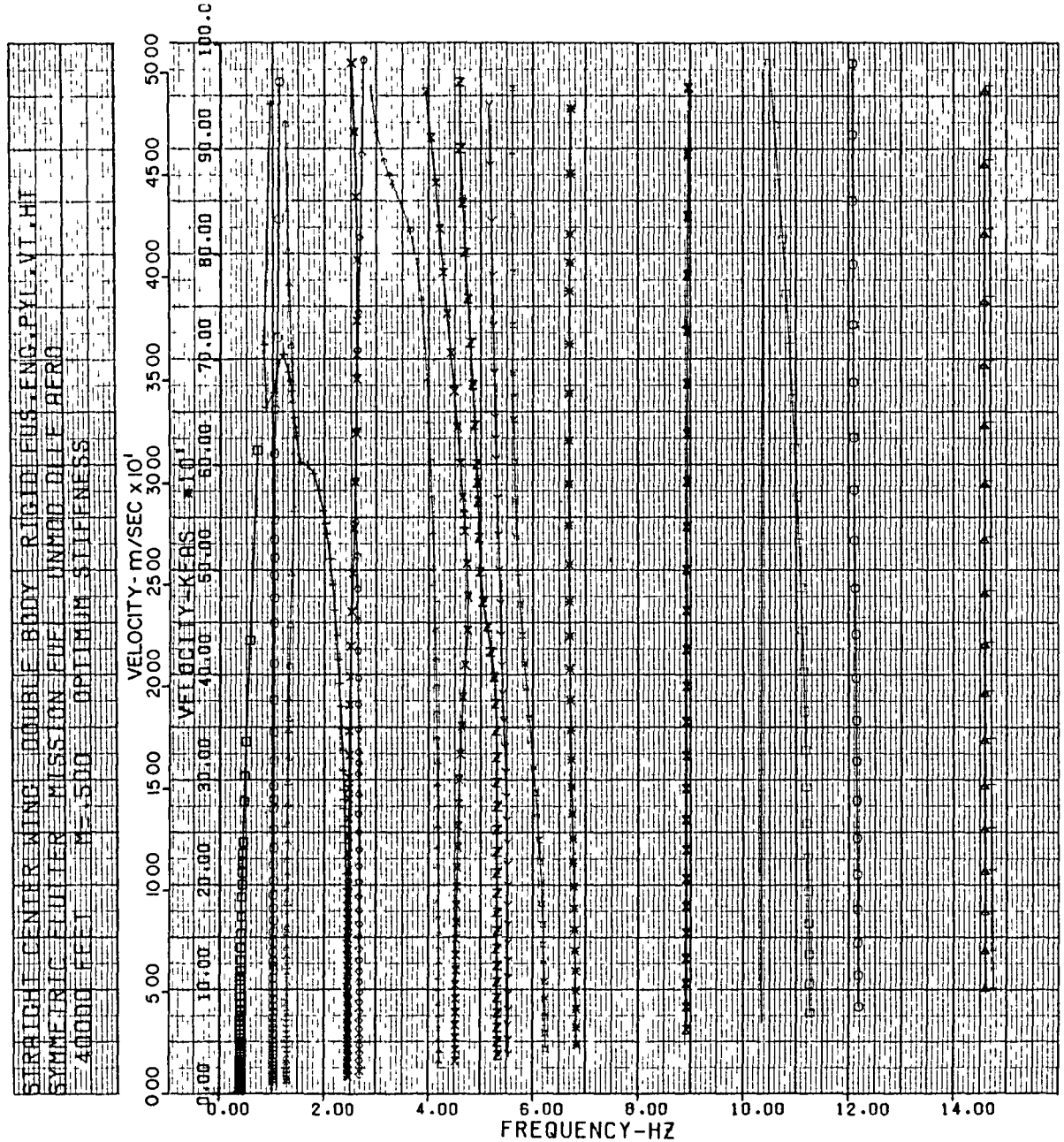

Figure D-77. Symmetric Velocity - Frequency, Stiffness at 40,000 Ft 0.50 Mach, Mission Fuel - Two-Body MB2 Aircraft

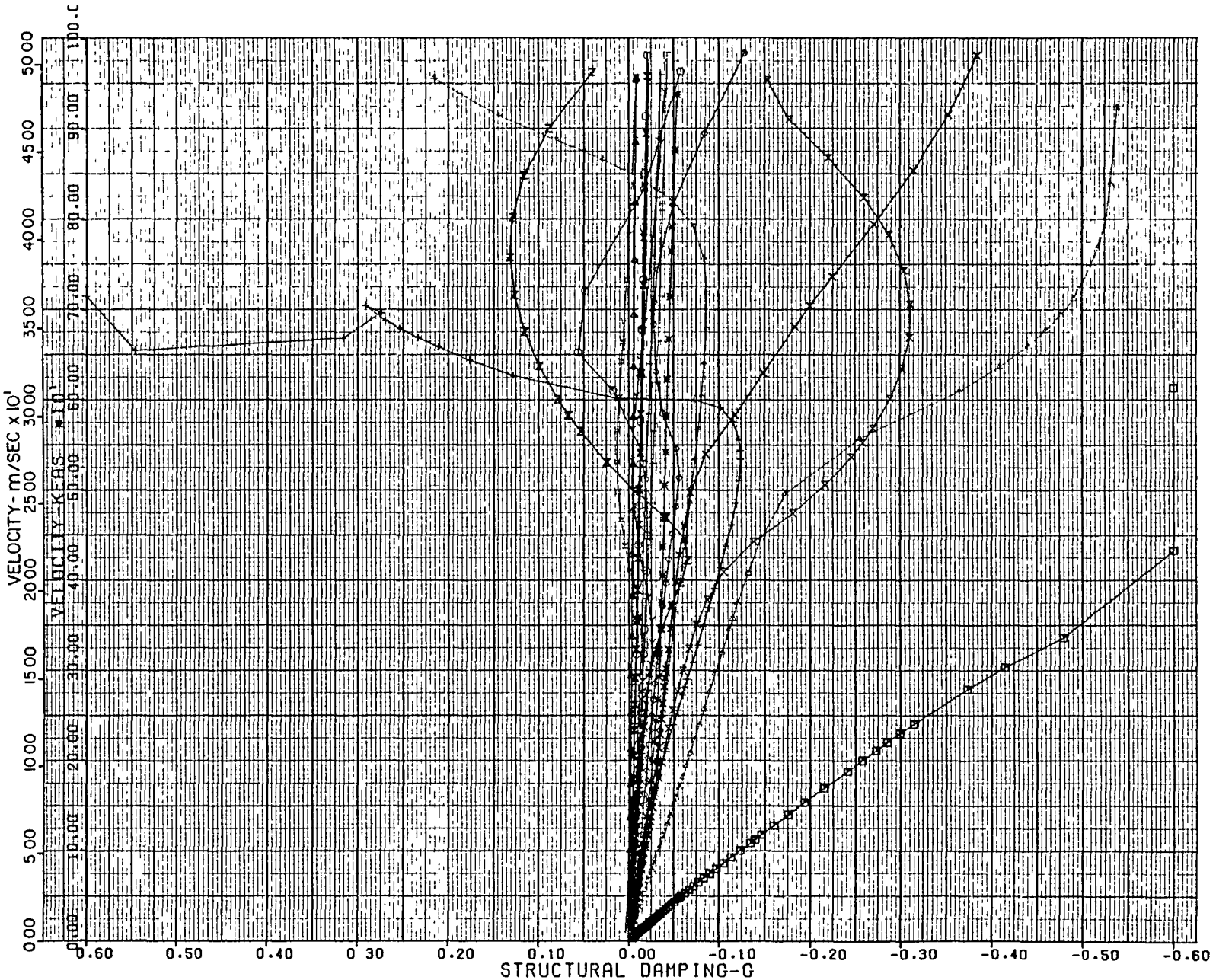

Figure D-78. Symmetric Velocity - Damping, Stiffness at 40,000 Ft 0.50 Mach, Mission Fuel - Two-Body MB2 Aircraft

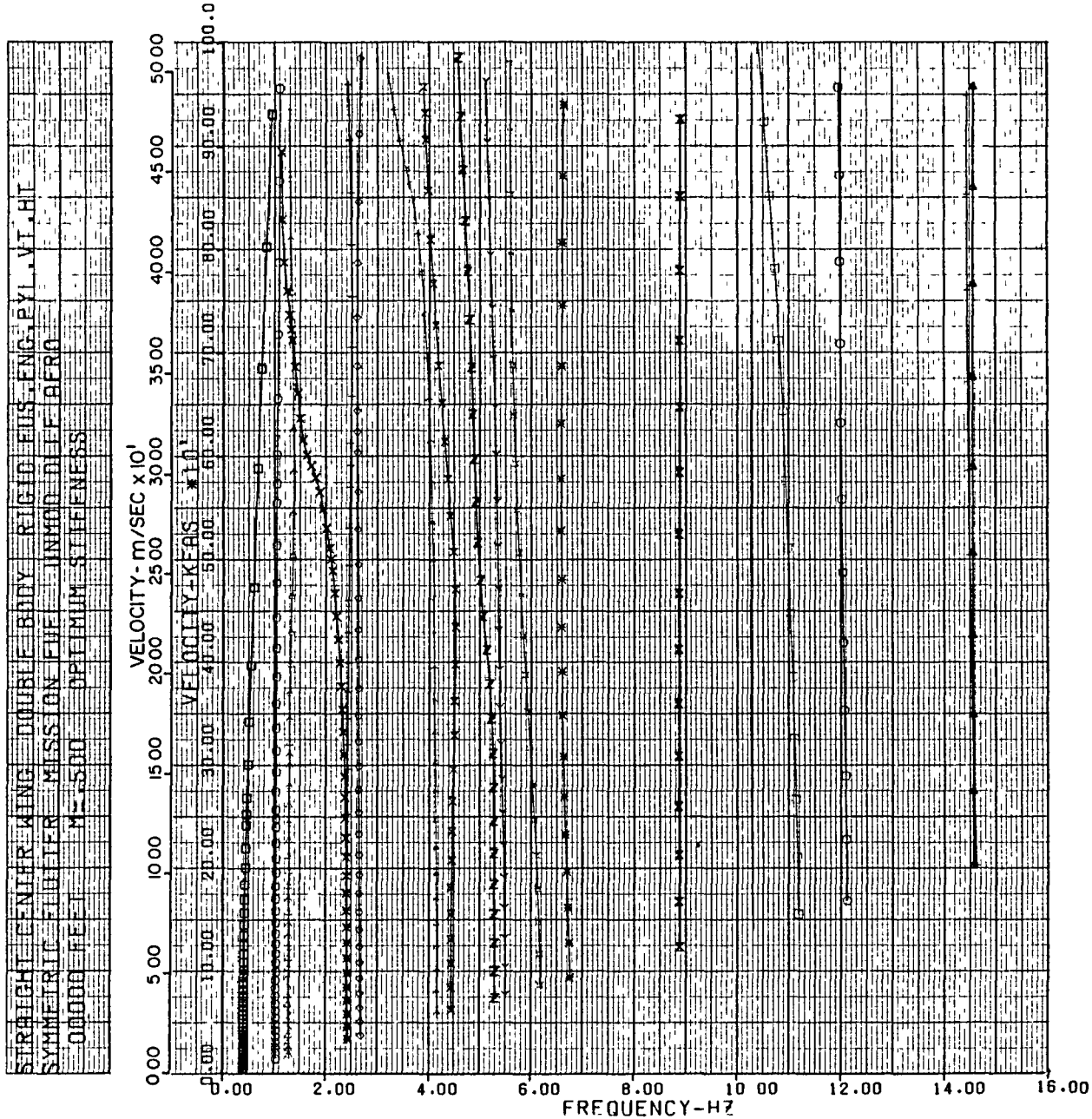

Figure D-79. Symmetric Velocity - Frequency, Stiffness at 0 Ft 0.50 Mach, Mission Fuel - Two-Body MB2 Aircraft

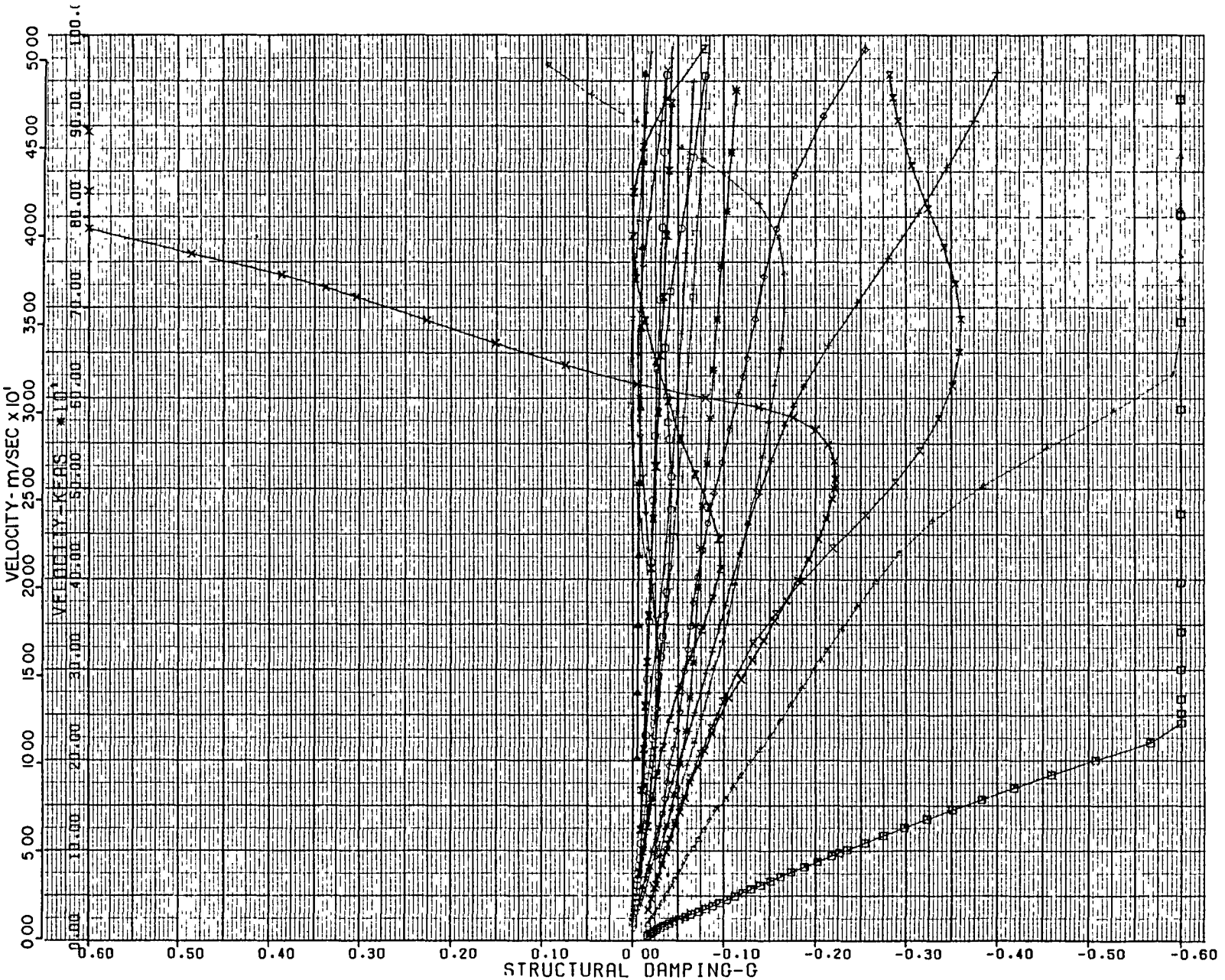

Figure D-80. Symmetric Velocity - Damping, Stiffness at 0 Ft 0.50 Mach, Mission Fuel - Two-Body MB2 Aircraft

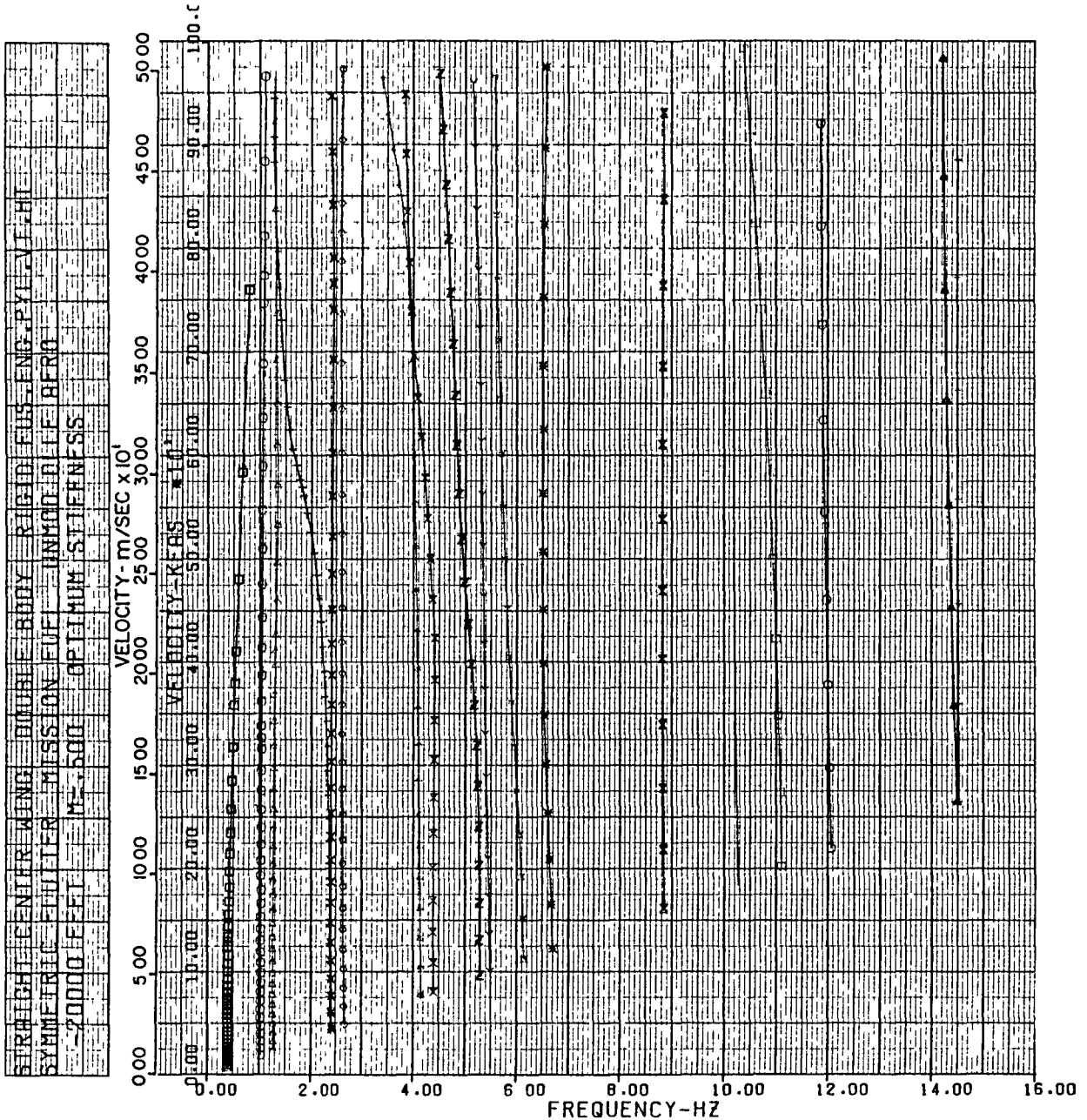

Figure D-81. Symmetric Velocity - Frequency, Stiffness at -20,000 Ft 0.50 Mach, Mission Fuel - Two-Body MB2 Aircraft

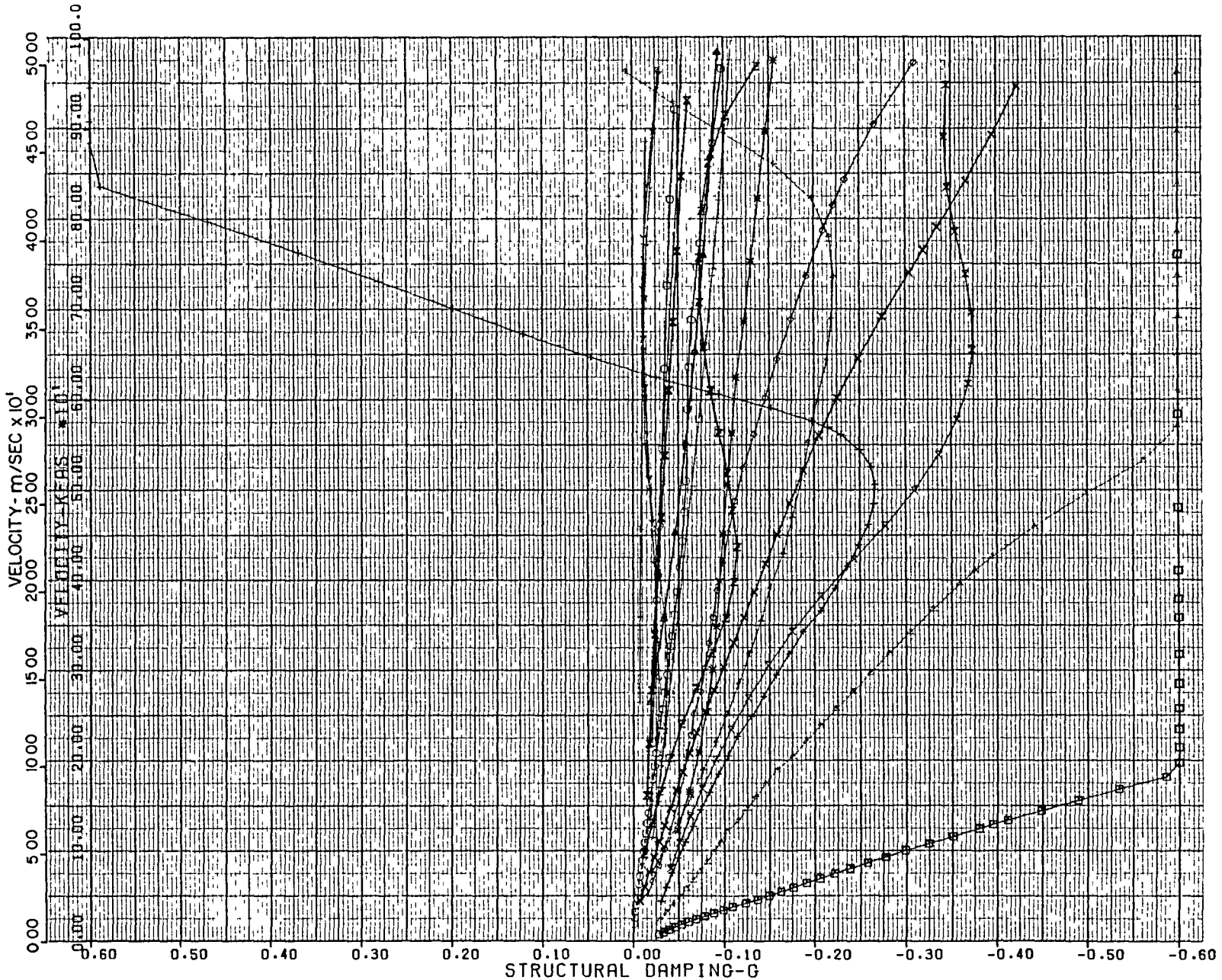

Figure D-82. Symmetric Velocity - Damping, Stiffness at -20,000 Ft 0.50 Mach, Mission Fuel - Two-Body MB2 Aircraft

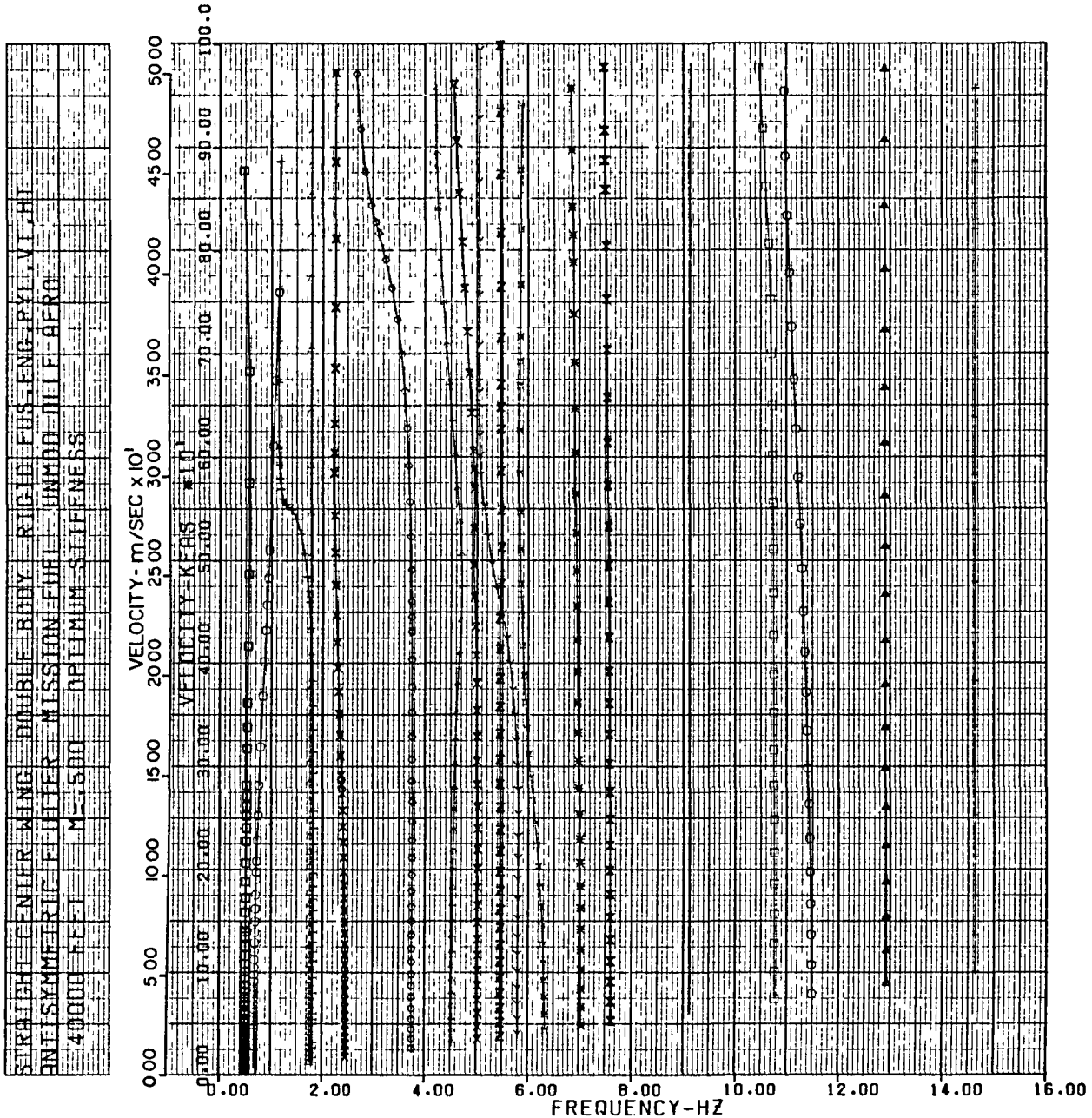

Figure D-83. Antisymmetric Velocity - Frequency, Stiffness at 40,000 Ft 0.50 Mach, Mission Fuel - Two-Body MB2 Aircraft

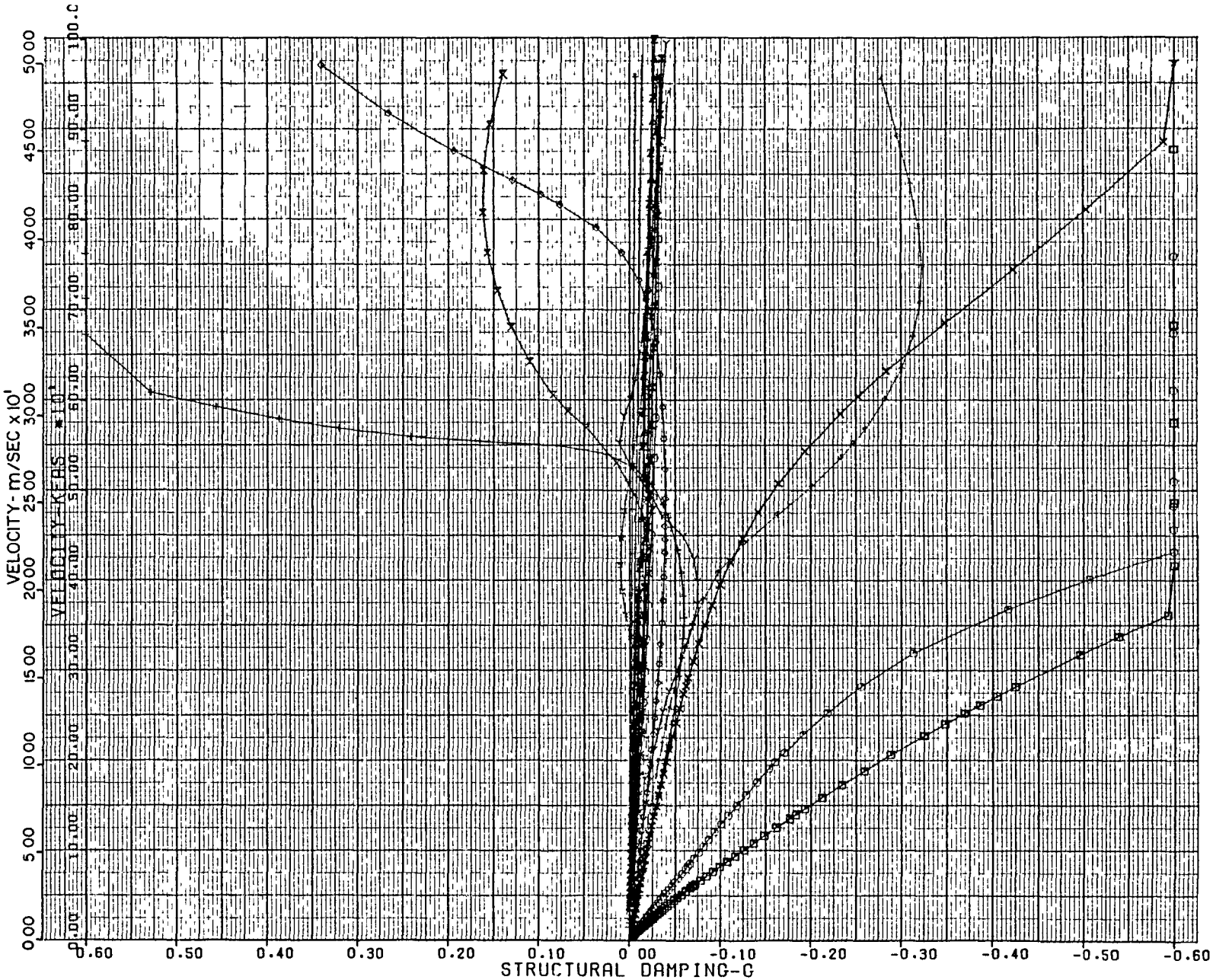

Figure D-84. Antisymmetric Velocity - Damping, Stiffness at 40,000 Ft 0.50 Mach, Mission Fuel - Two-Body MB2 Aircraft

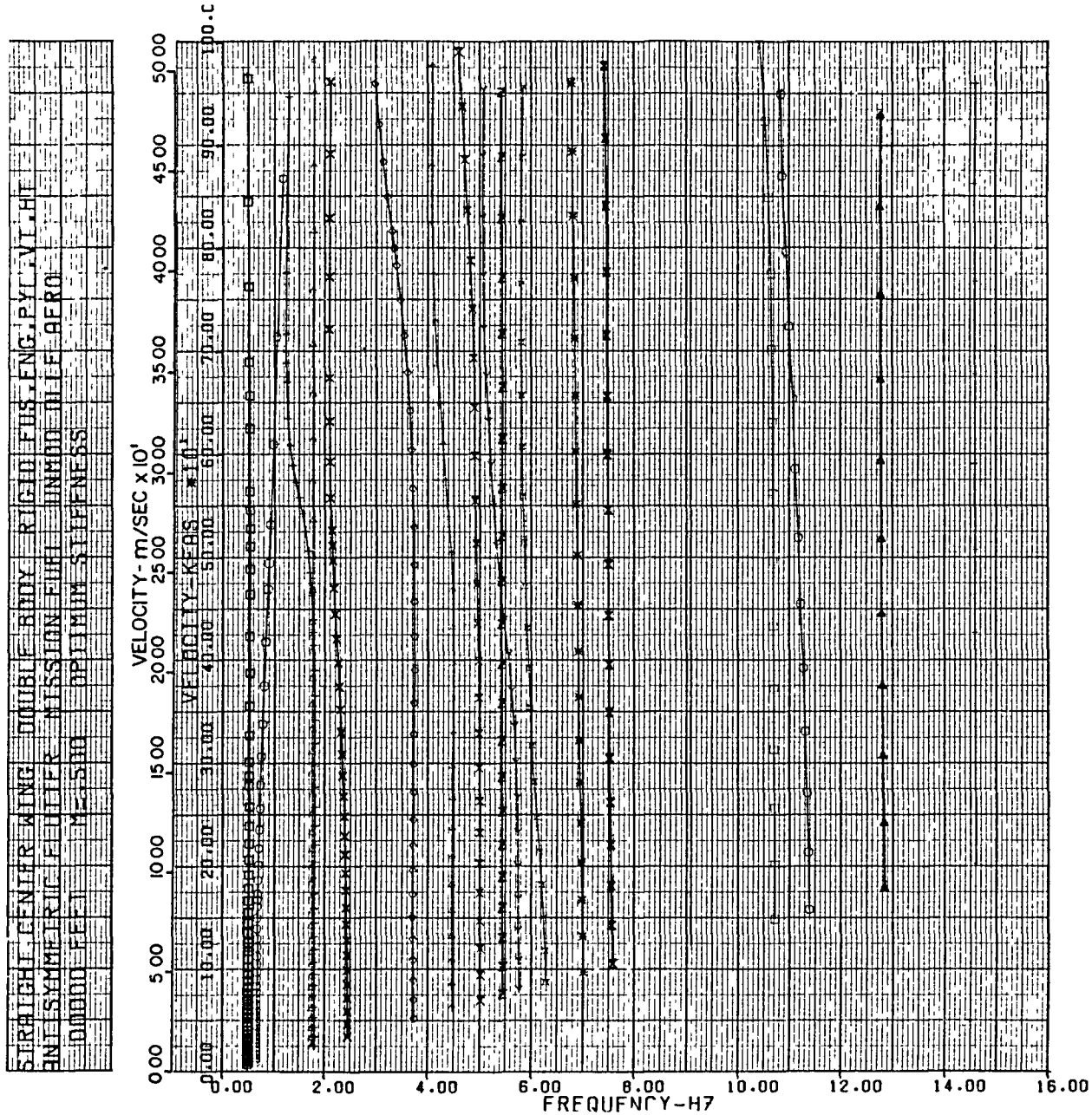

Figure D-85. Antisymmetric Velocity - Frequency, Stiffness at 0 Ft 0.50 Mach, Mission Fuel - Two-Body MB2 Aircraft

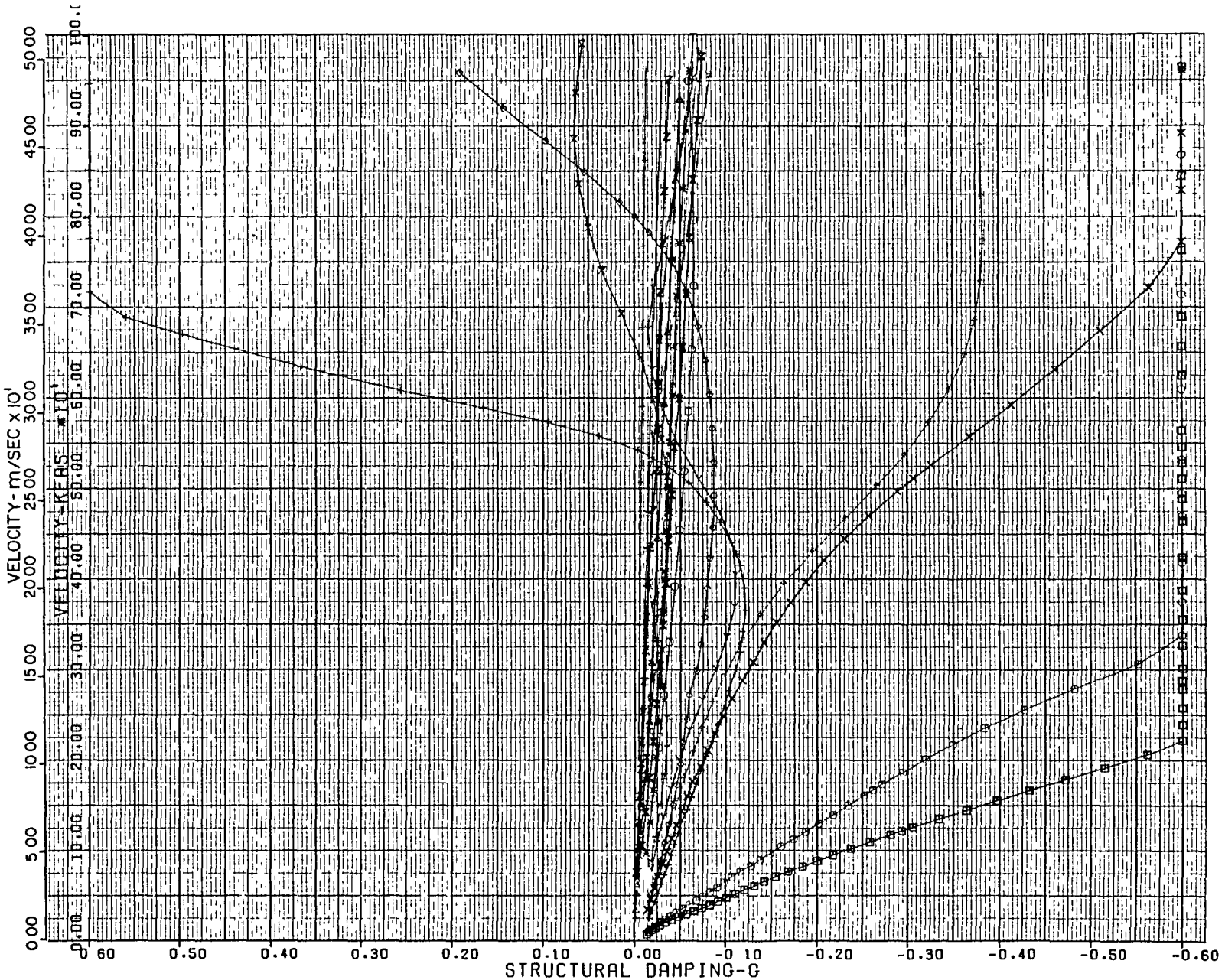

Figure D-86. Antisymmetric Velocity - Damping, Stiffness at 0 Ft 0.50 Mach, Mission Fuel - Two-Body MB2 Aircraft

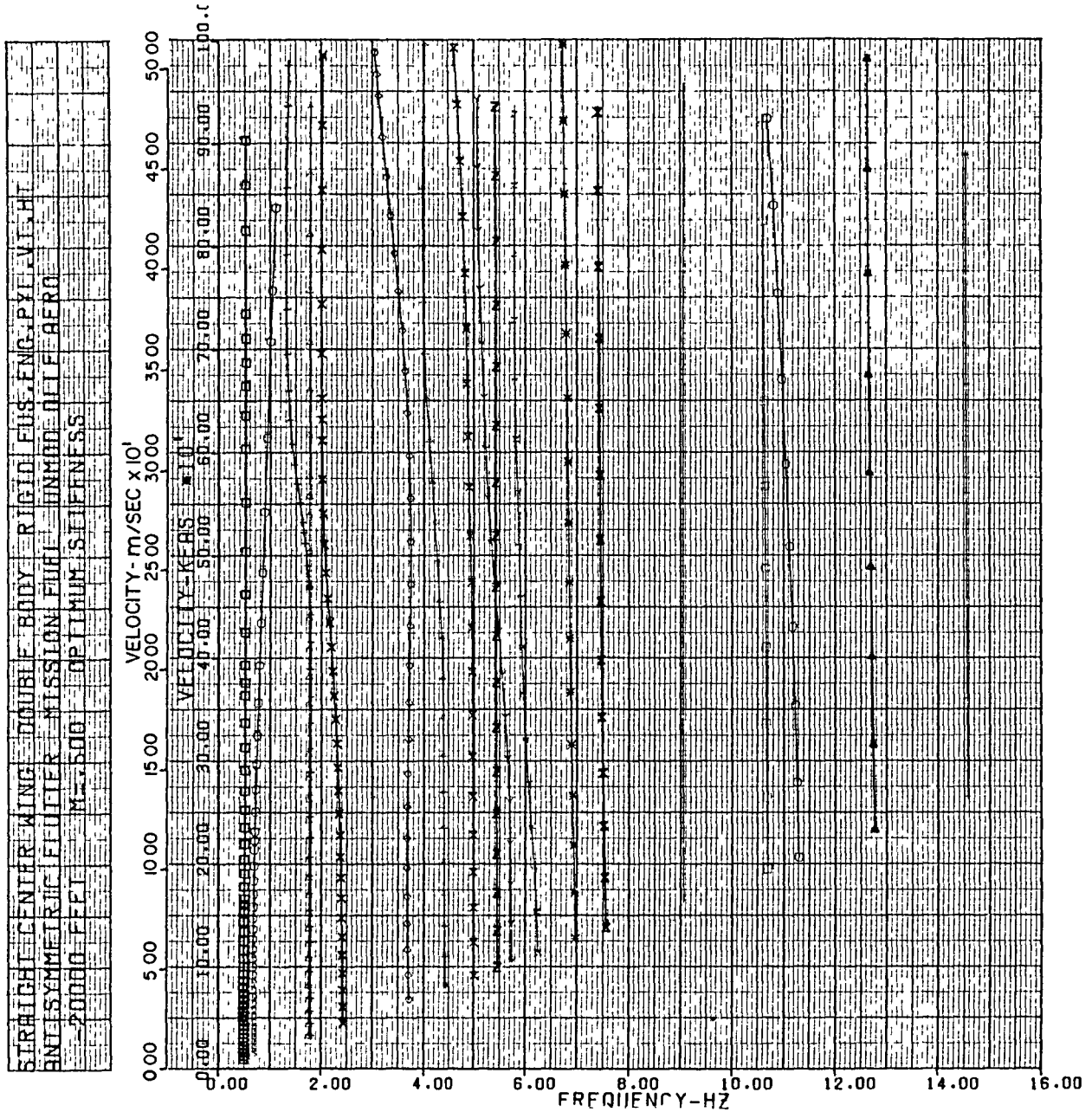

Figure D-87. Antisymmetric Velocity - Frequency, Stiffness at -20,000 Ft 0.50 Mach, Mission Fuel - Two-Body MB2 Aircraft

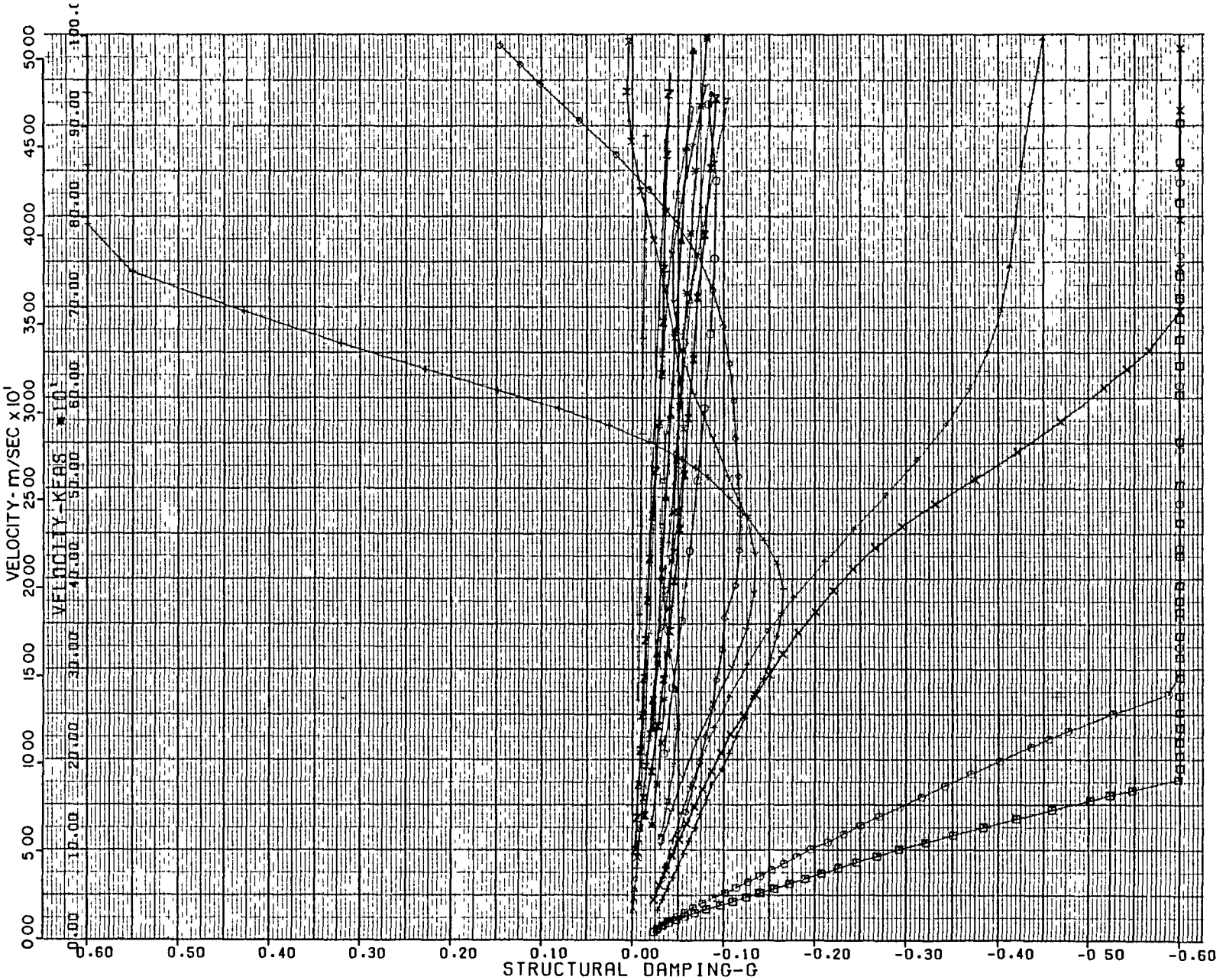

Figure D-88. Antisymmetric Velocity - Damping, Stiffness at -20,000 Ft 0.50 Mach, Mission Fuel - Two-Body MB2 Aircraft

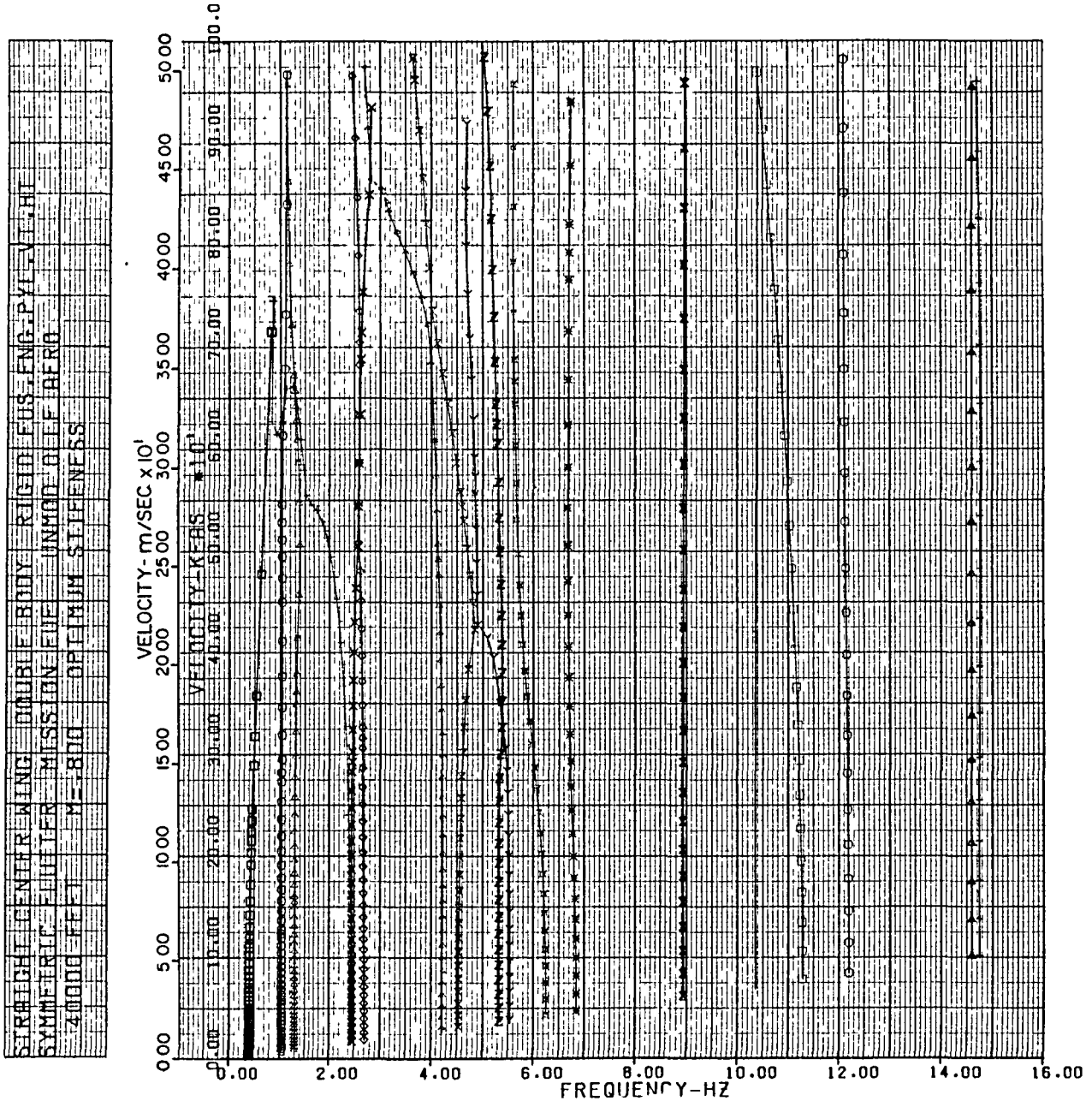

Figure D-89. Symmetric Velocity - Frequency, Stiffness at 40,000 Ft 0.80 Mach, Zero Fuel - Two-Body MB2 Aircraft

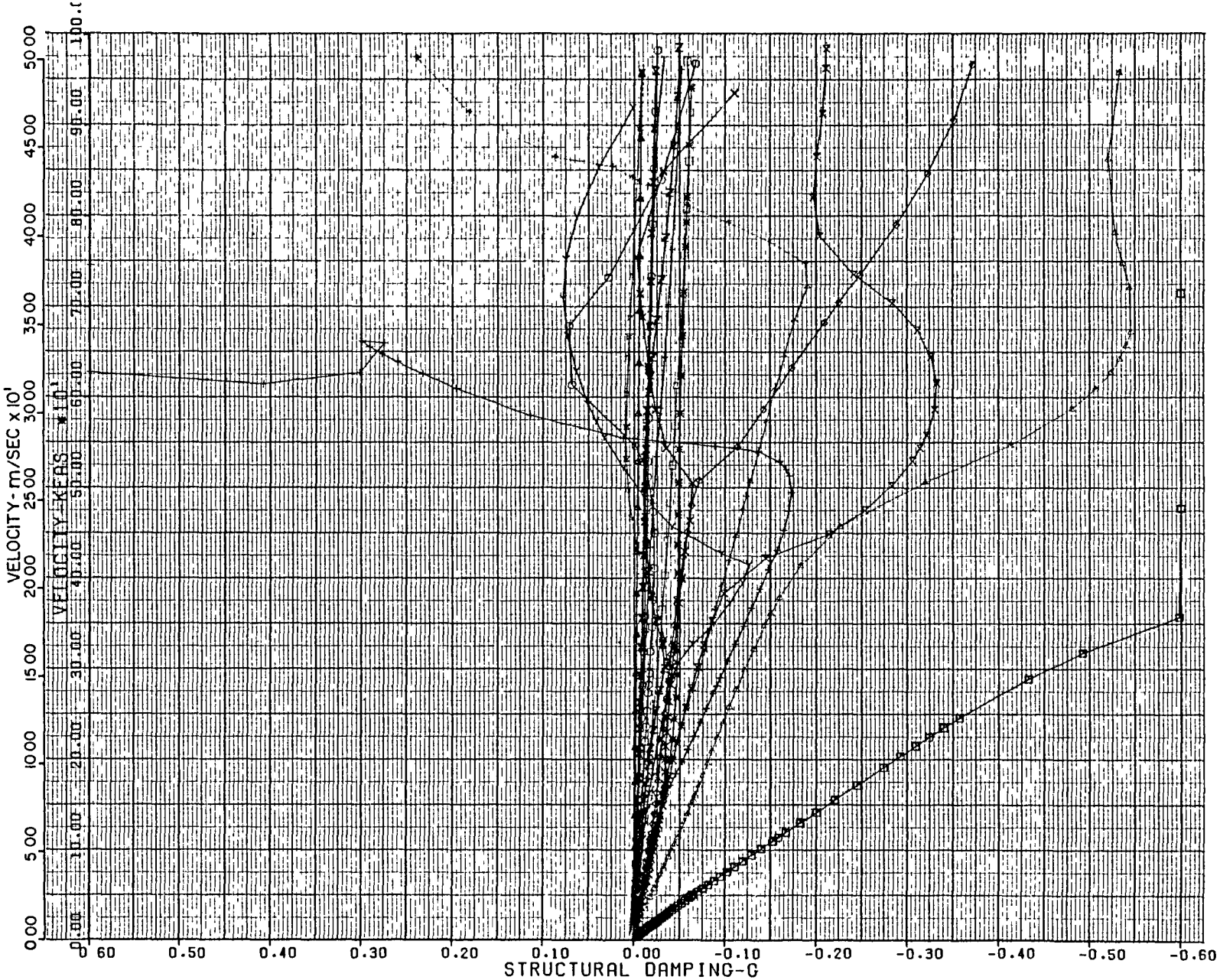

Figure D-90. Symmetric Velocity - Damping, Stiffness at 40,000 Ft 0.80 Mach, Zero Fuel - Two-Body MB2 Aircraft

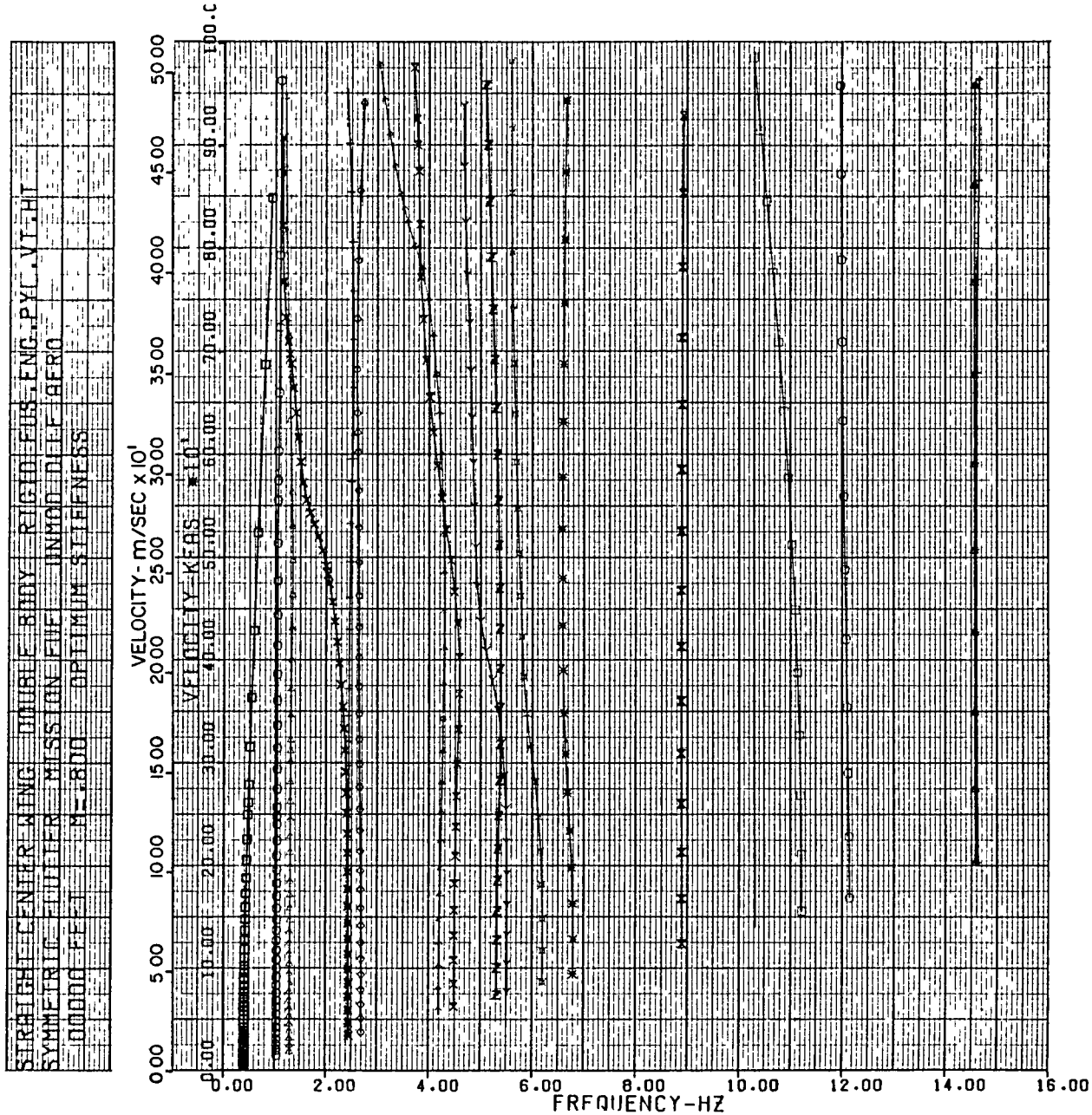

Figure D-91. Symmetric Velocity - Frequency, Stiffness at 0 Ft 0.80 Mach, Zero Fuel - Two-Body MB2 Aircraft

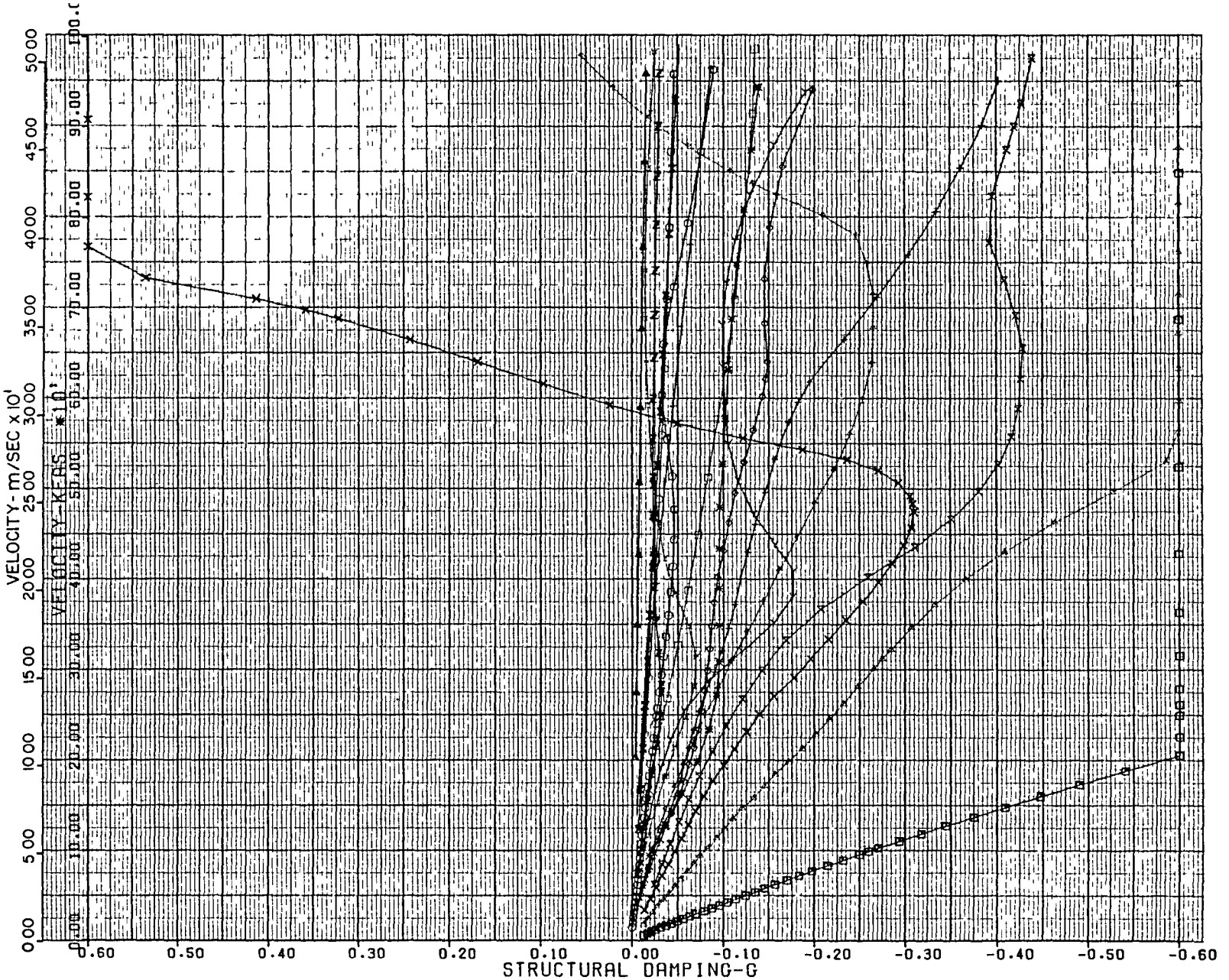

Figure D-92. Symmetric Velocity - Damping, Stiffness at 0 Ft 0.80 Mach, Zero Fuel - Two-Body MB2 Aircraft

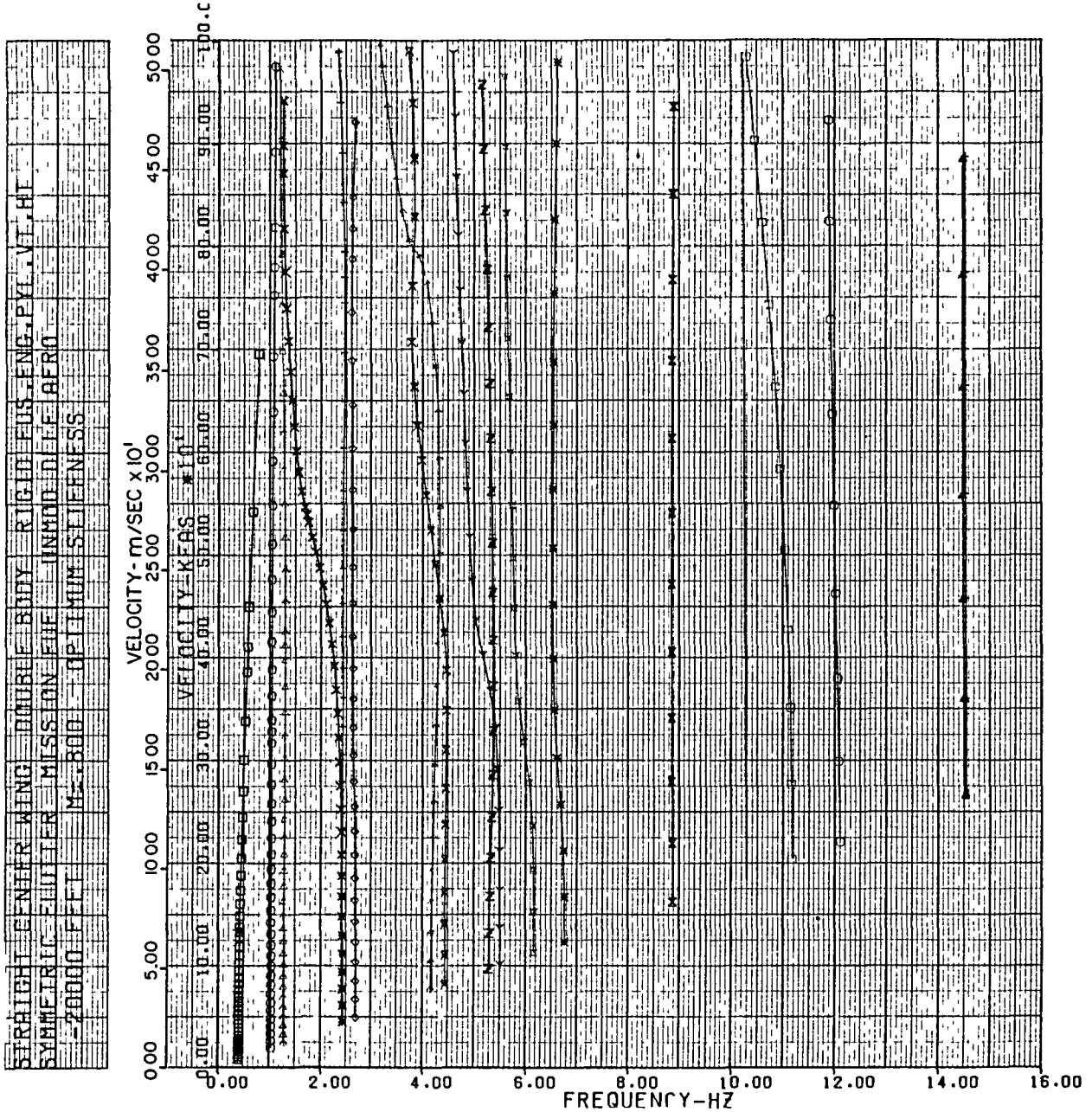

Figure D-93. Symmetric Velocity - Frequency, Stiffness at -20,000 Ft 0.80 Mach, Zero Fuel - Two-Body MB2 Aircraft

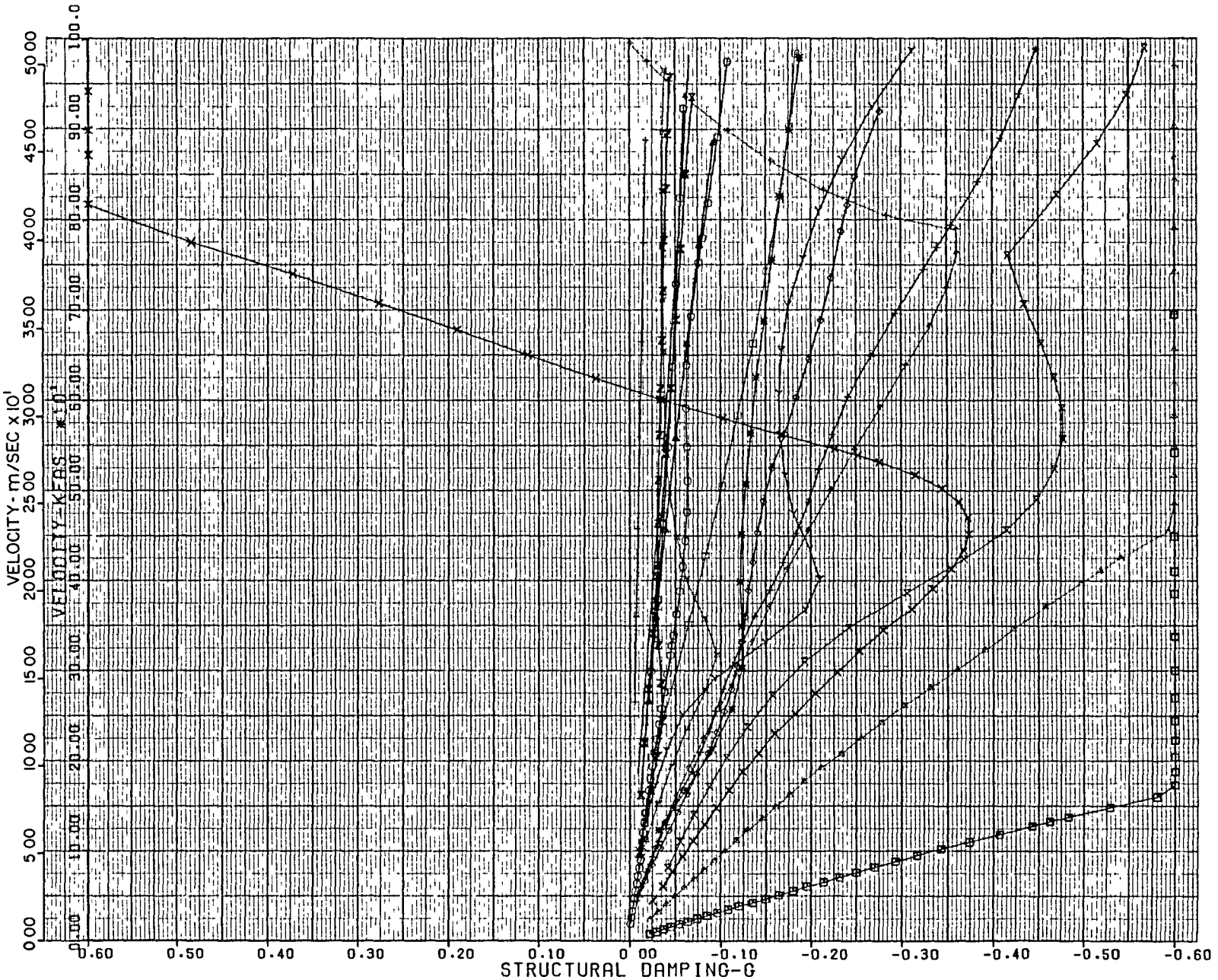

Figure D-94. Symmetric Velocity - Damping, Stiffness at -20,000 Ft 0.80 Mach, Zero Fuel - Two-Body MB2 Aircraft

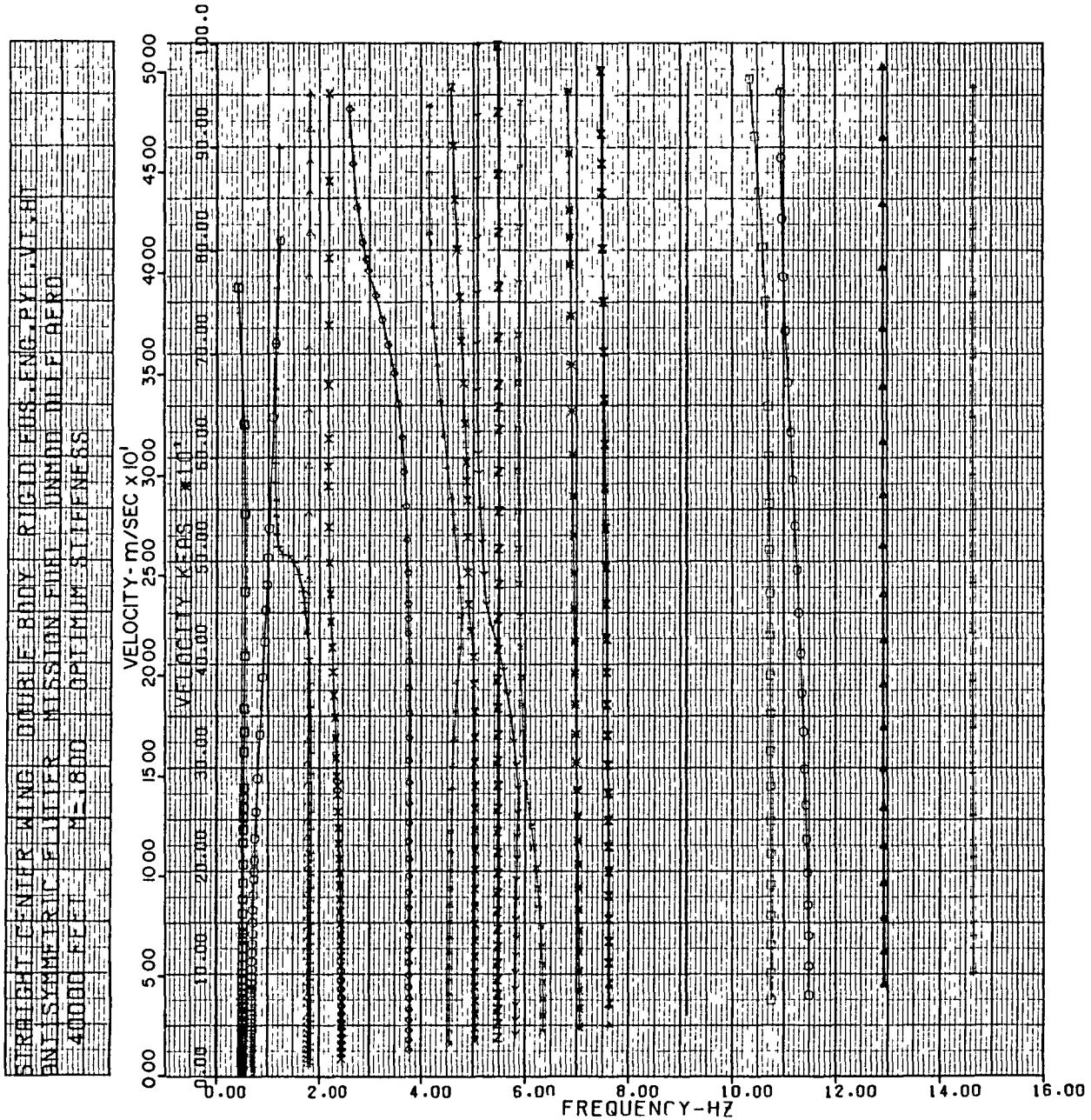

Figure D-95. Antisymmetric Velocity - Frequency, Stiffness at 40,000 Ft 0.80 Mach, Zero Fuel - Two-Body MB2 Aircraft

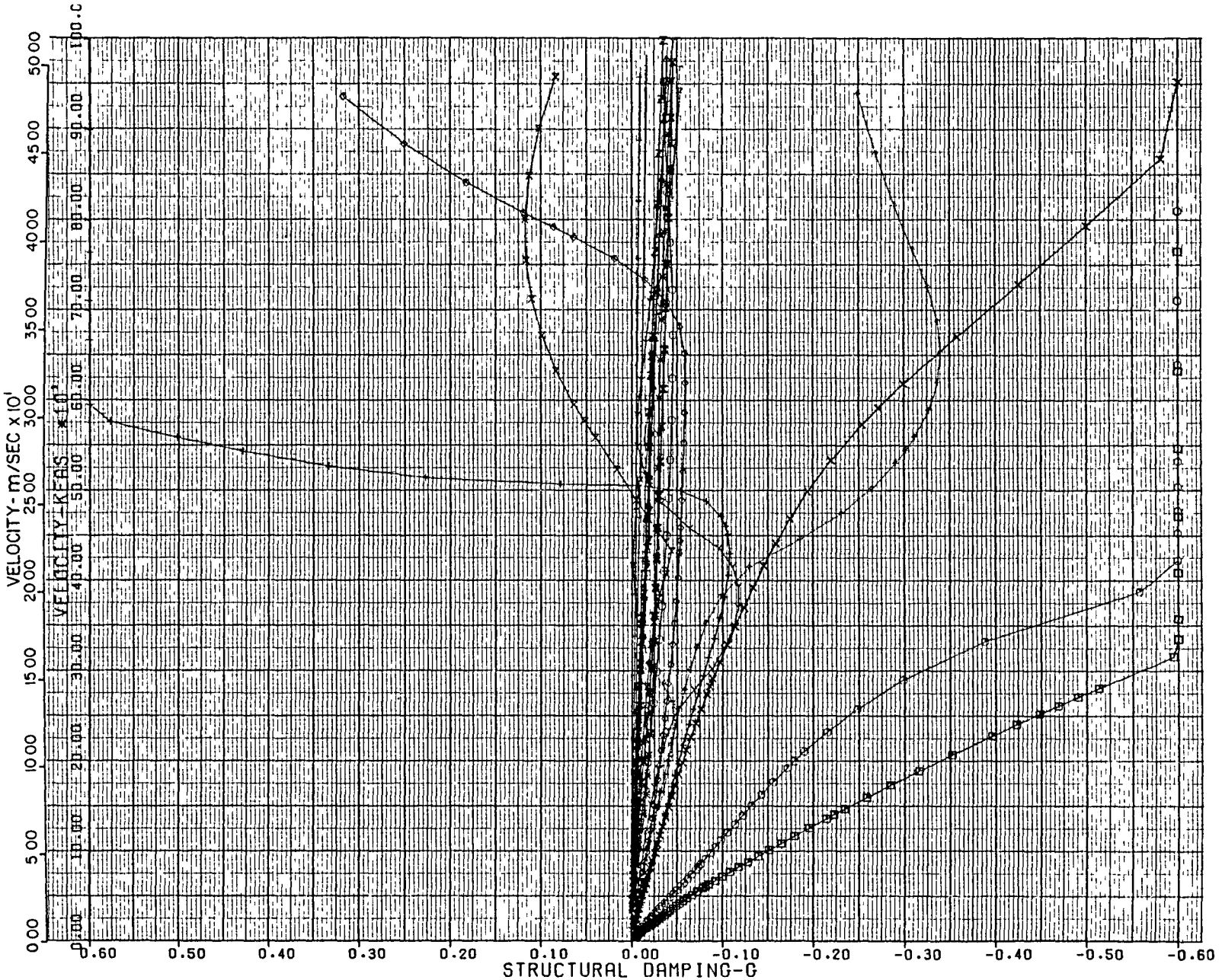

Figure D-96. Antisymmetric Velocity - Damping, Stiffness at 40,000 Ft 0.80 Mach, Zero Fuel - Two-Body MB2 Aircraft

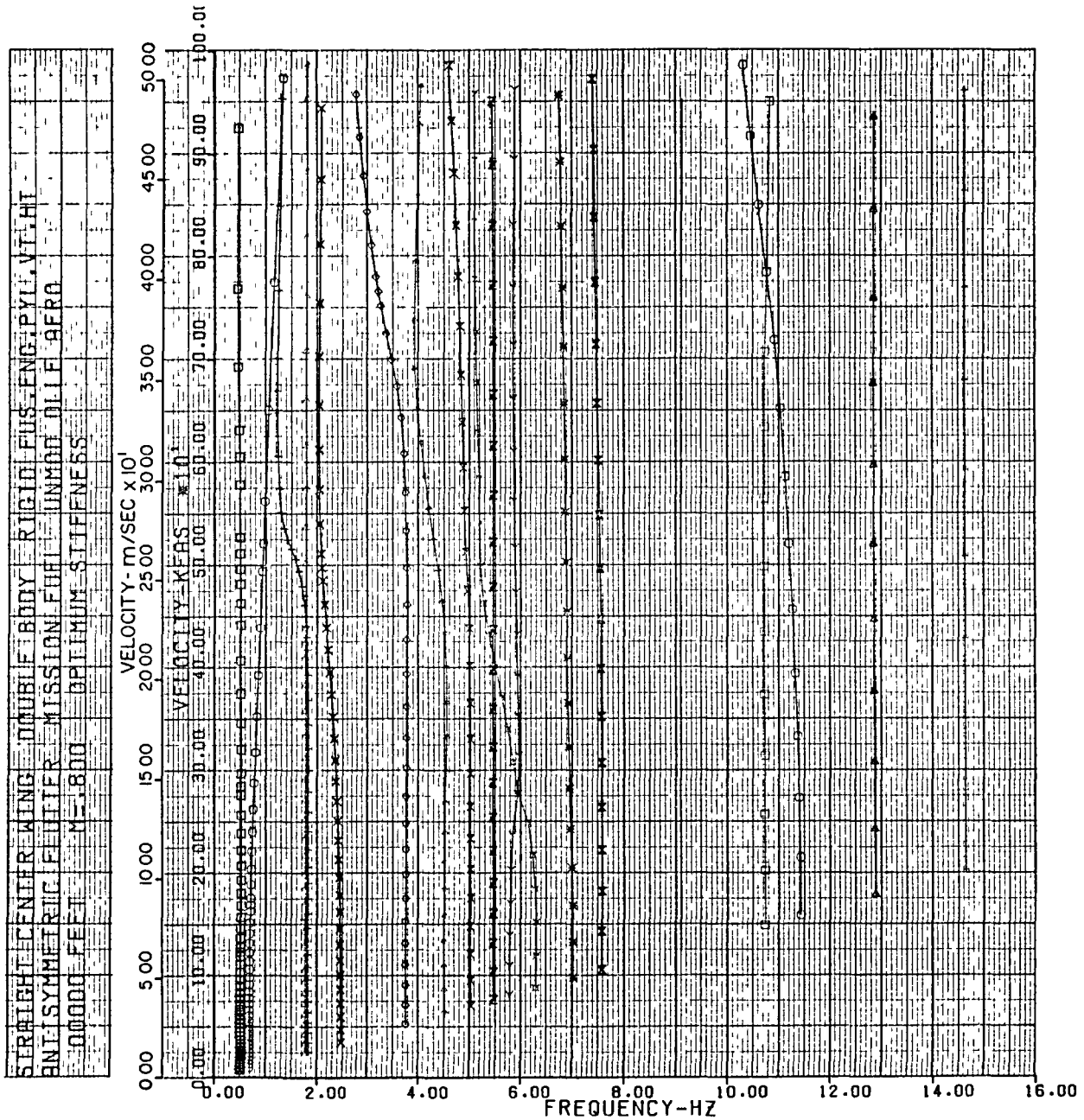

Figure D-97. Antisymmetric Velocity - Frequency, Stiffness at 0 Ft 0.80 Mach, Zero Fuel - Two-Body MB2 Aircraft

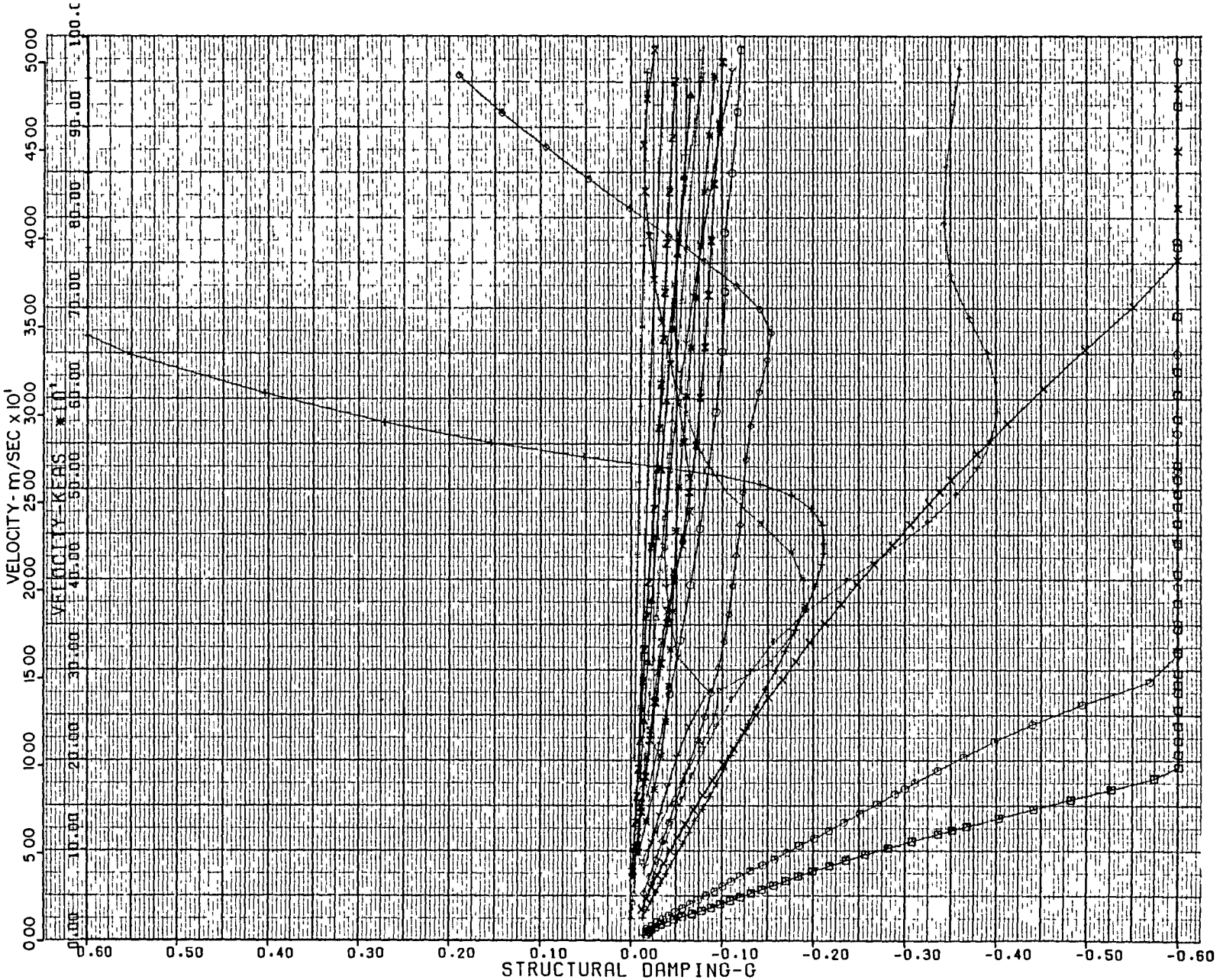

Figure D-98. Antisymmetric Velocity - Damping, Stiffness at 0 Ft 0.80 Mach, Zero Fuel - Two-Body MB2 Aircraft

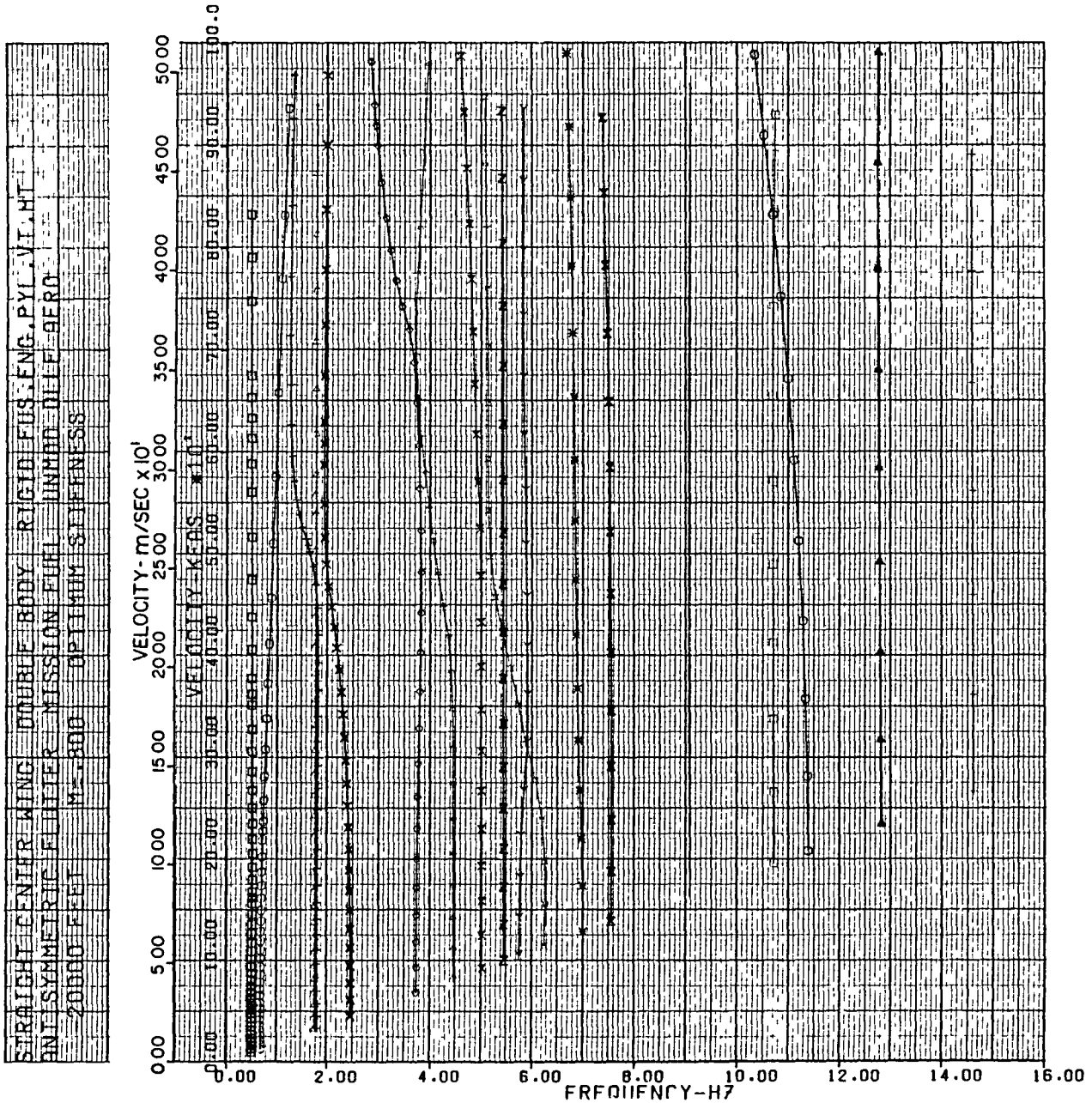

Figure D-99. Antisymmetric Velocity - Frequency, Stiffness at -20,000 Ft 0.80 Mach, Zero Fuel - Two-Body MB2 Aircraft

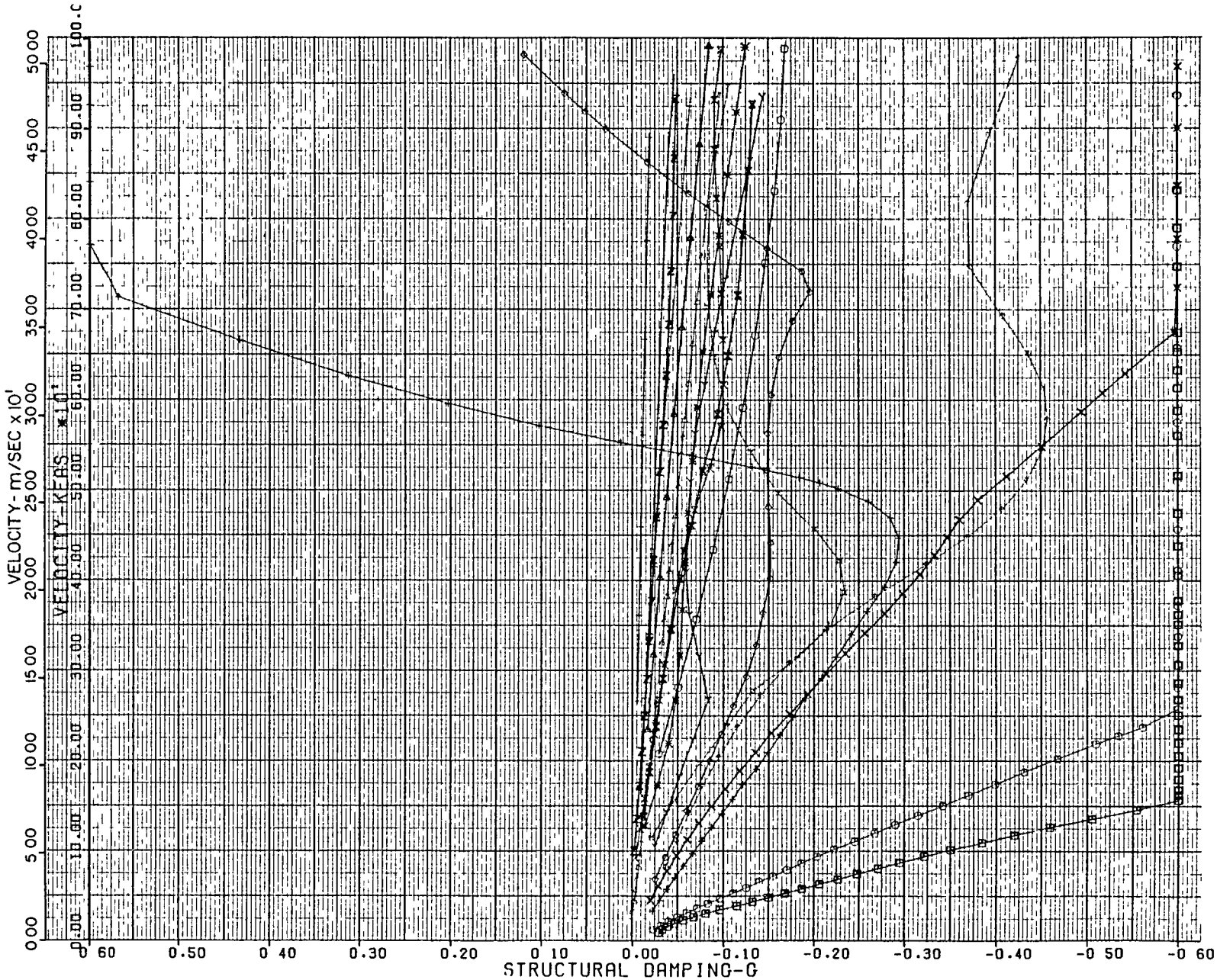

Figure D-100. Antisymmetric Velocity - Dampıng, Stiffness at -20,000 Ft
0.80 Mach, Zero Fuel - Two-Body MB2 Aircraft

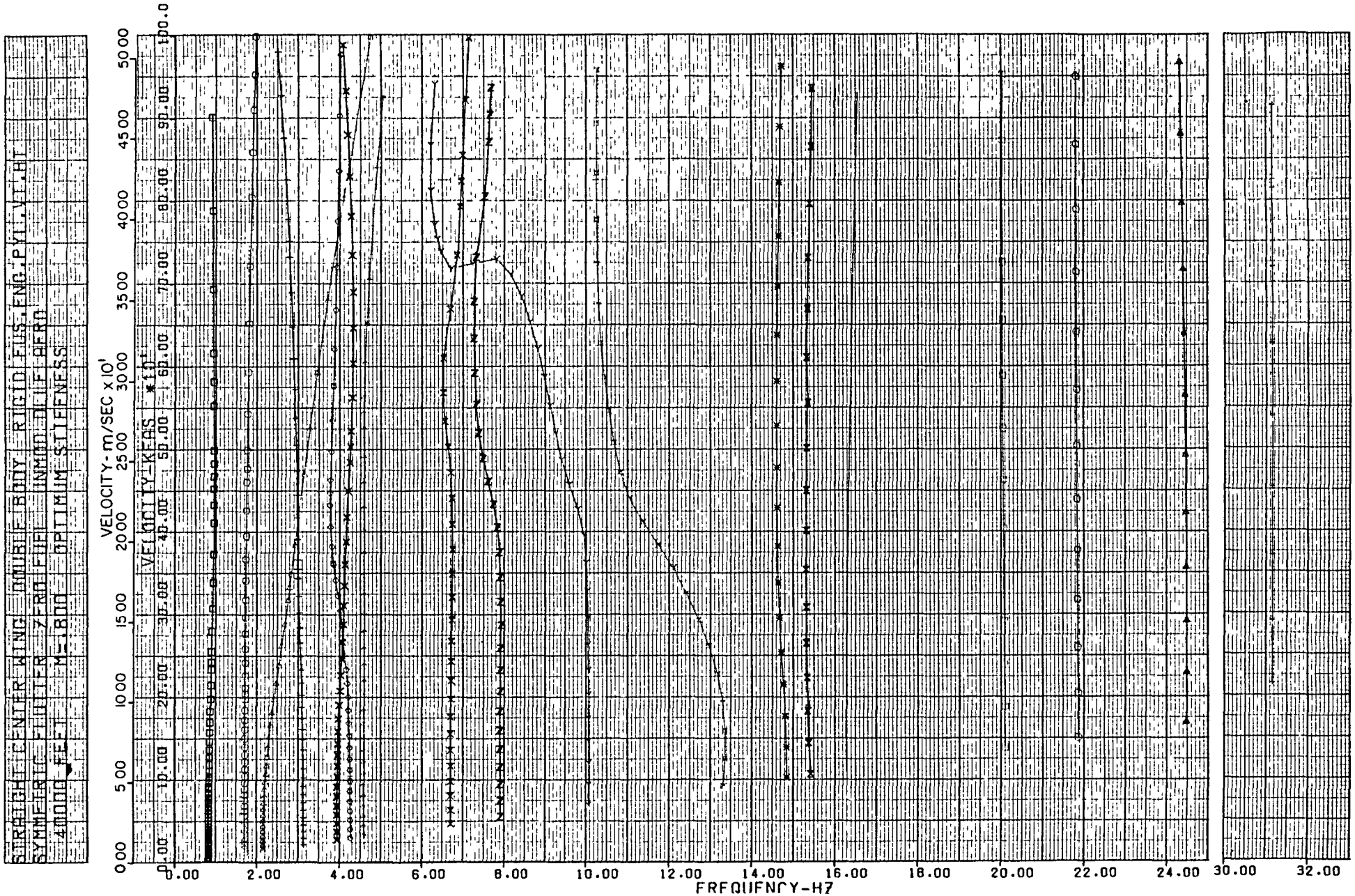

Figure D-101. Symmetric Velocity - Frequency, Stiffness at 40,000 Ft 0.80 Mach, Mission Fuel - Two-Body MB2 Aircraft

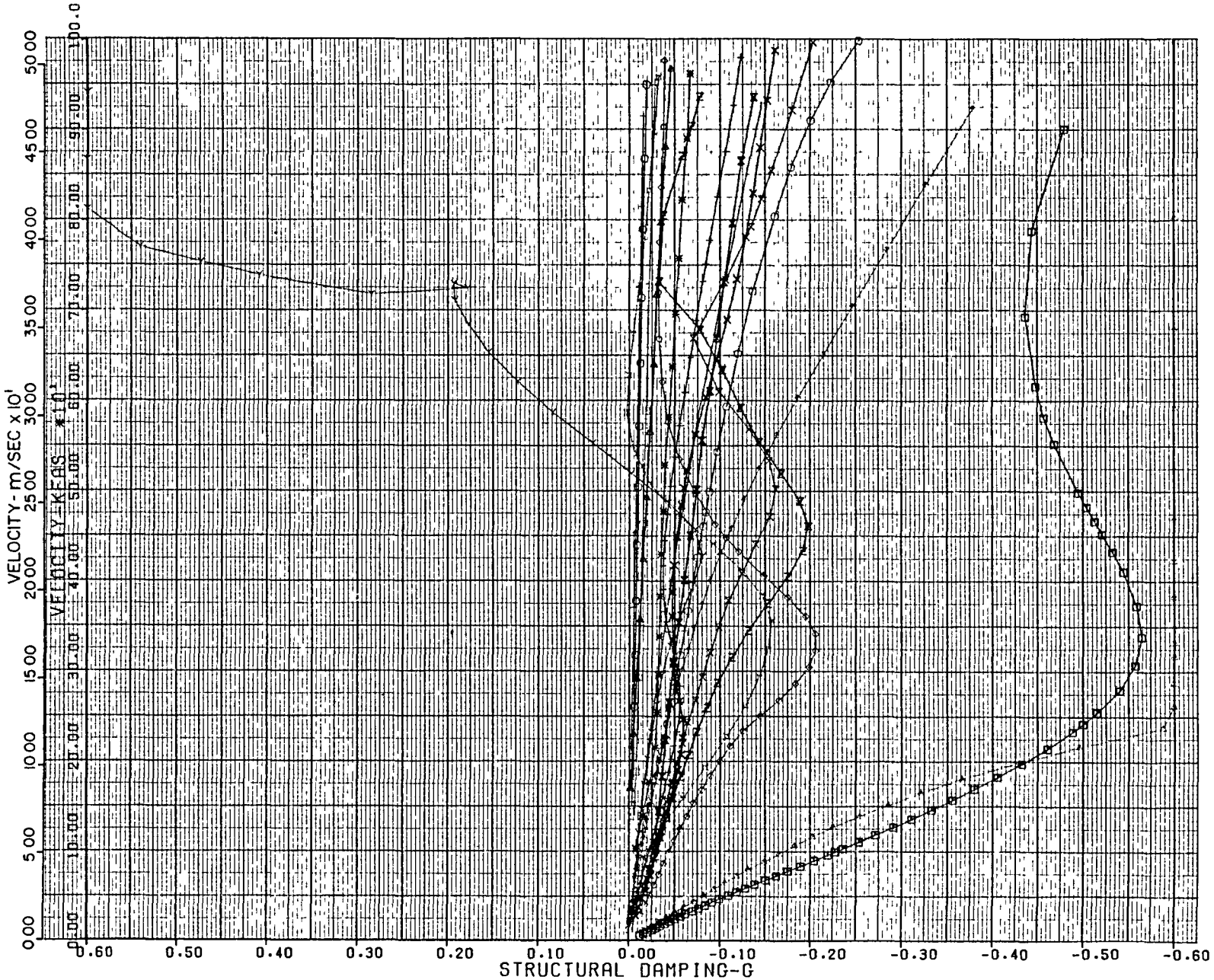

Figure D-102. Symmetric Velocity - Damping, Stiffness at 40,000 Ft 0.80 Mach, Mission Fuel - Two-Body MB2 Aircraft

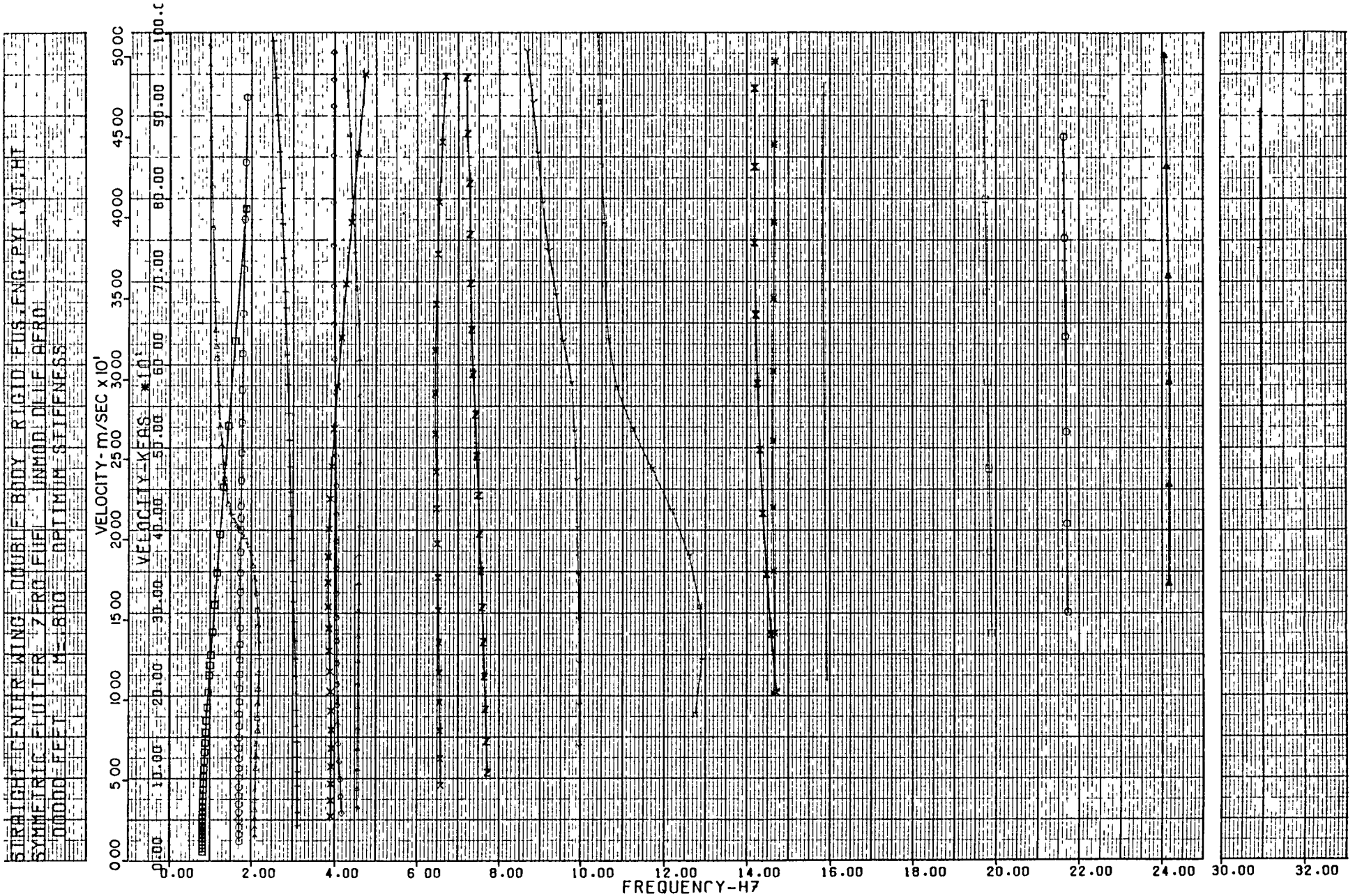

Figure D-103. Symmetric Velocity - Frequency, Stiffness at 0 Ft 0.80 Mach, Mission Fuel - Two-Body MB2 Aircraft

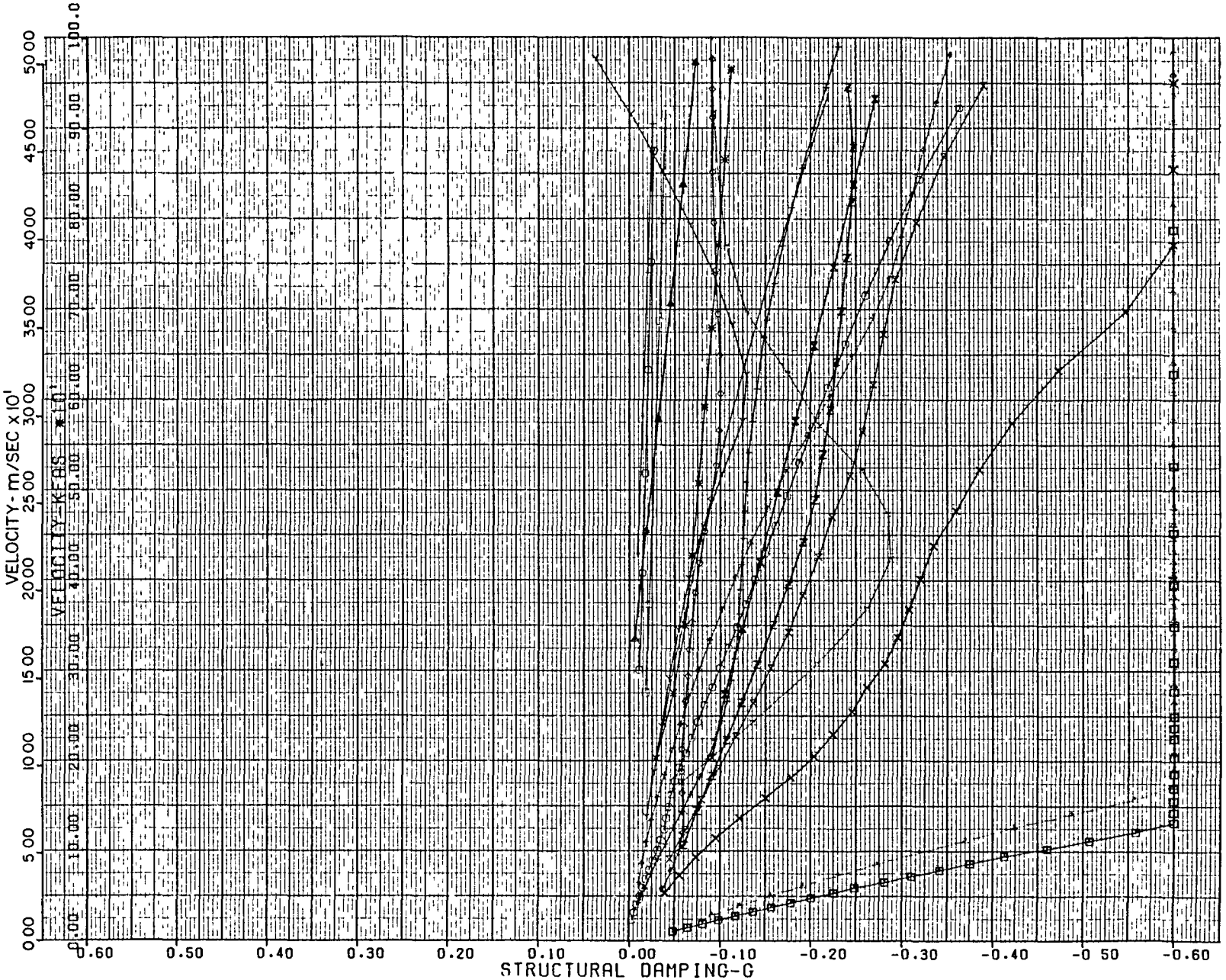

Figure D-104. Symmetric Velocity - Damping, Stiffness at 0 Ft 0.80 Mach, Mission Fuel - Two-Body MB2 Aircraft

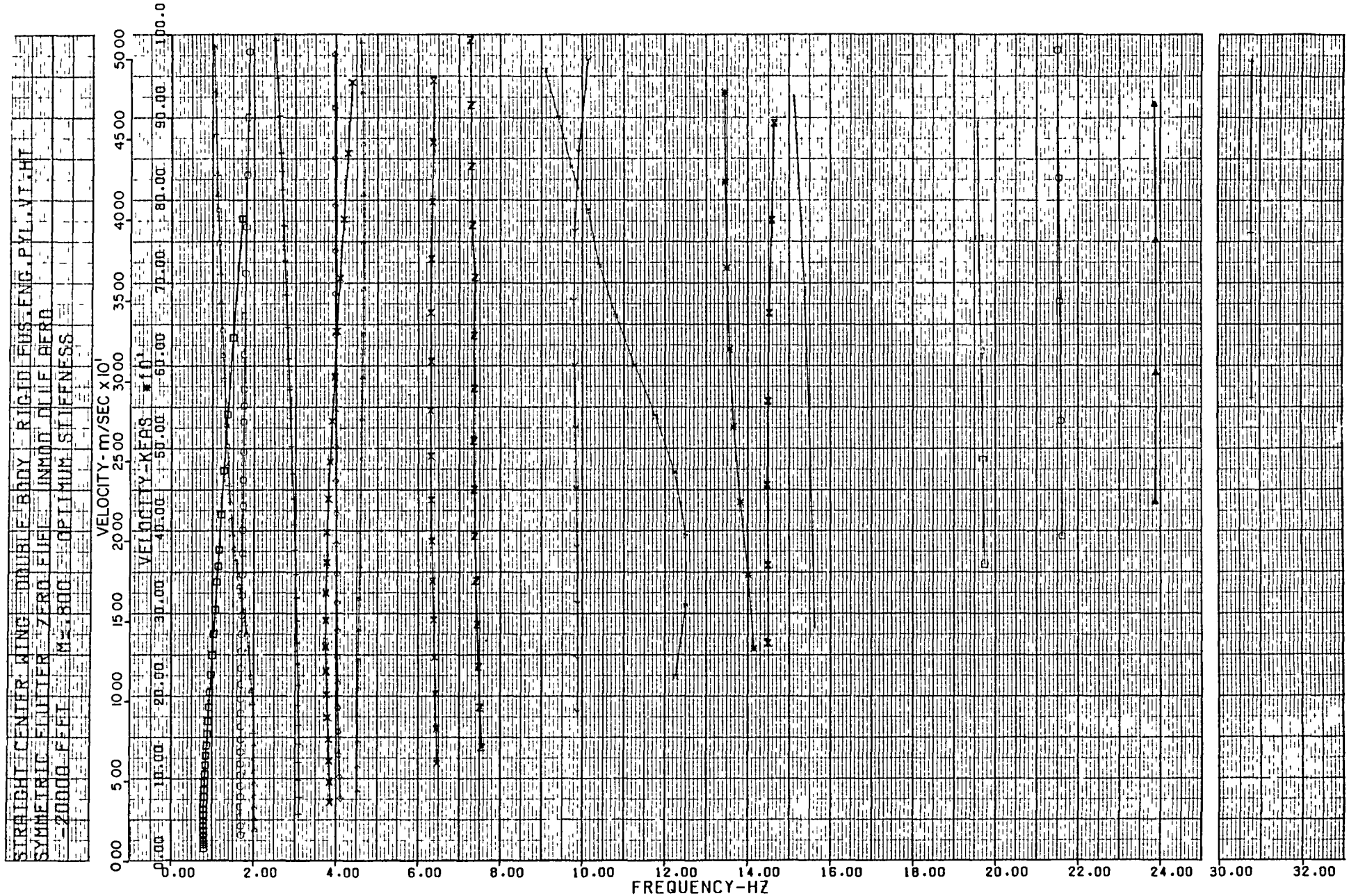

Figure D-105. Symmetric Velocity - Frequency, Stiffness at -20,000 Ft
0.80 Mach, Mission Fuel - Two-Body MB2 Aircraft

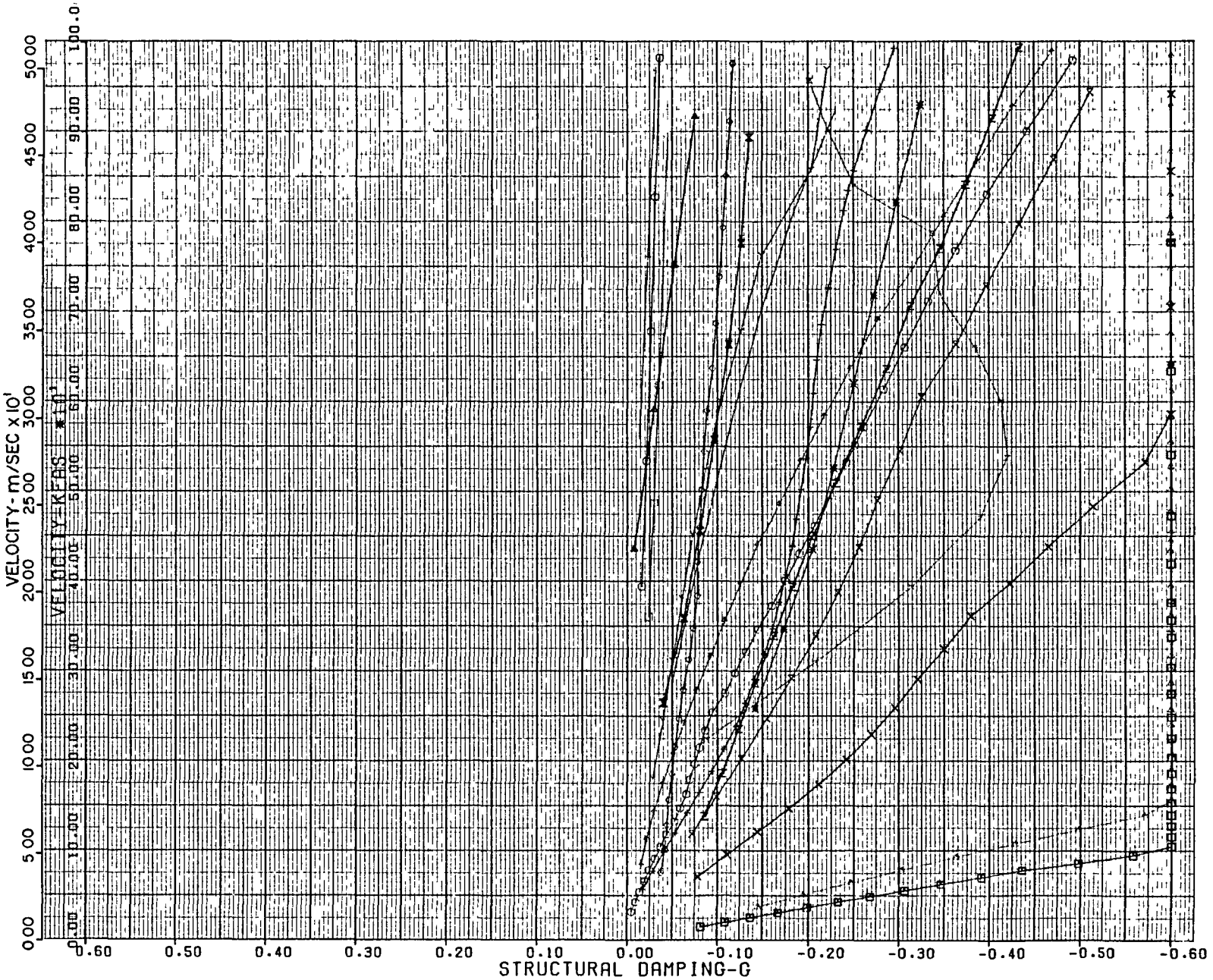

Figure D-106. Symmetric Velocity - Damping, Stiffness at -20,000 Ft
0.80 Mach, Mission Fuel - Two-Body MB2 Aircraft

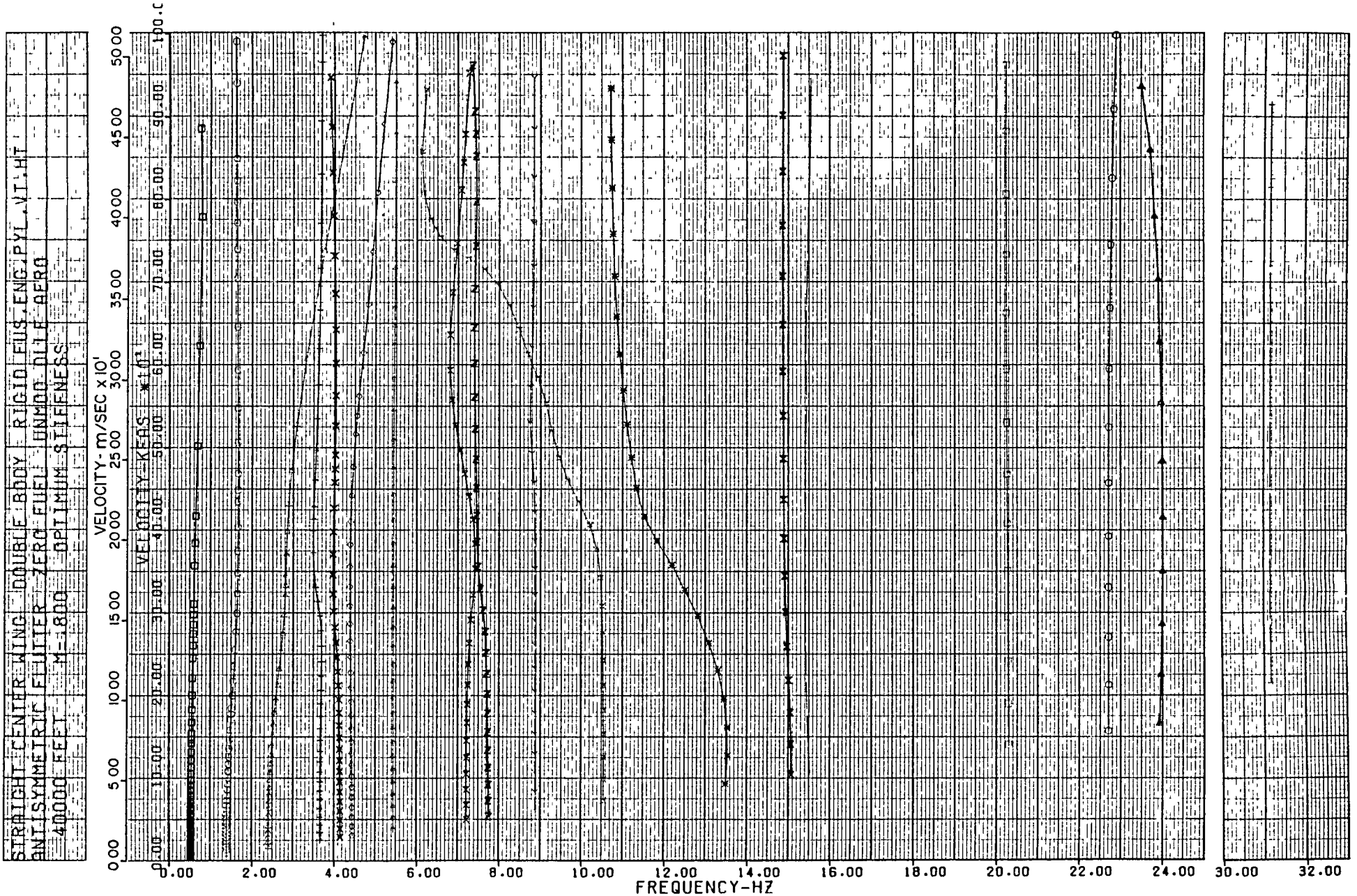

Figure D-107. Antisymmetric Velocity - Frequency, Stiffness at 40,000 Ft 0.80 Mach, Mission Fuel - Two-Body MB2 Aircraft

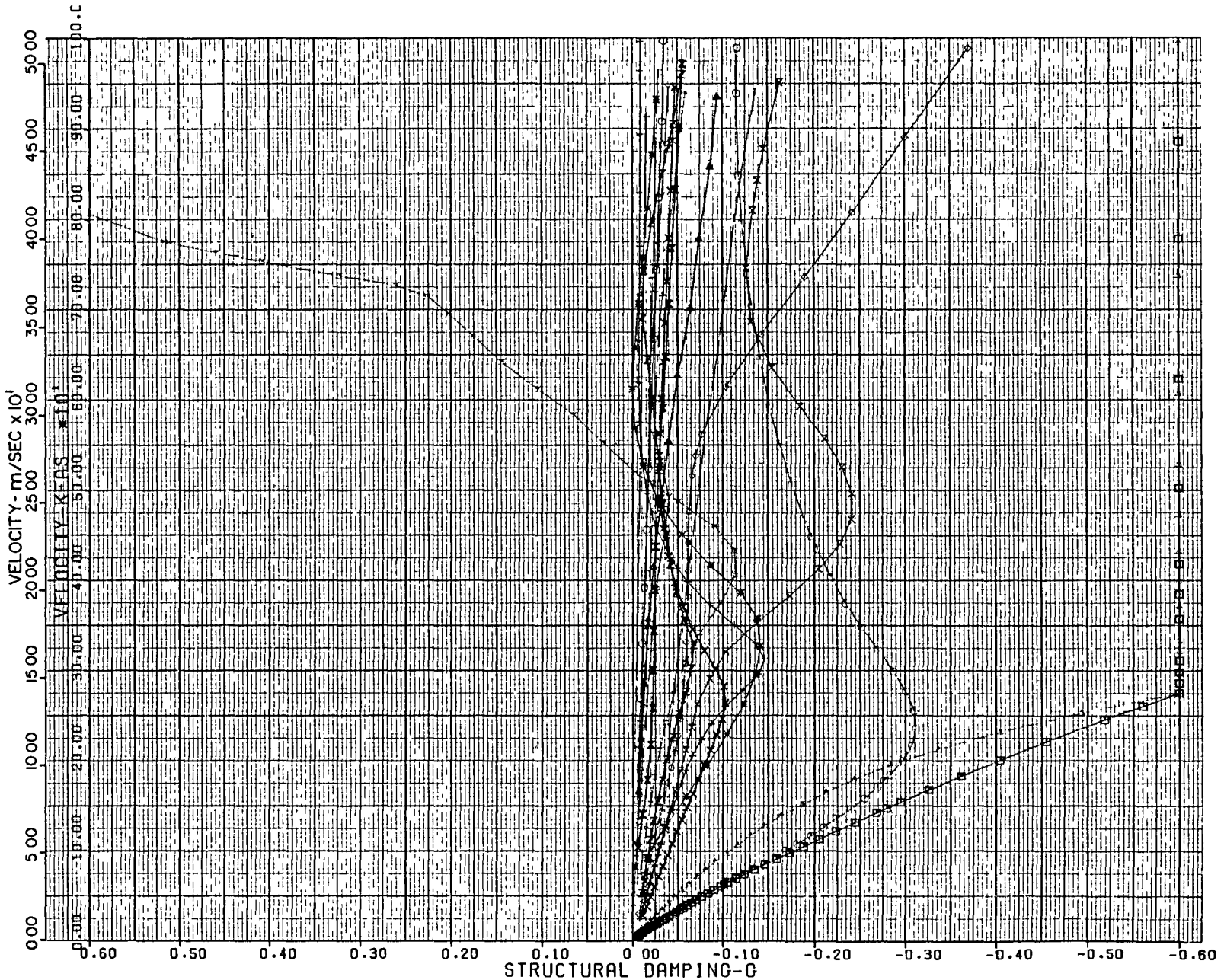

Figure D-108. Antisymmetric Velocity - Damping, Stiffness at 40,000 Ft 0.80 Mach, Mission Fuel - Two-Body MB2 Aircraft

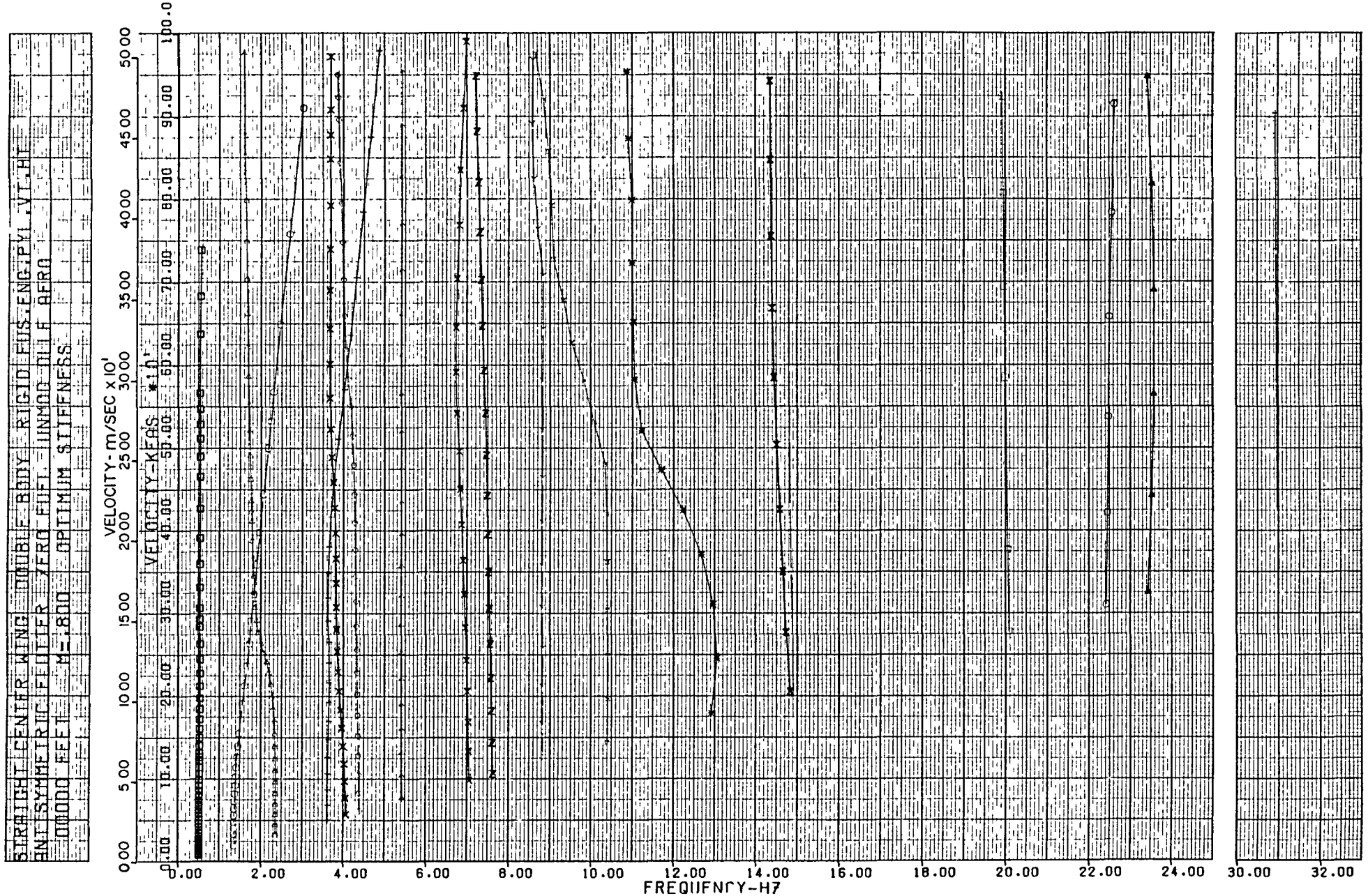

Figure D-109. Antisymmetric Velocity - Frequency, Stiffness at 0 Ft 0.80 Mach, Mission Fuel - Two-Body MB2 Aircraft

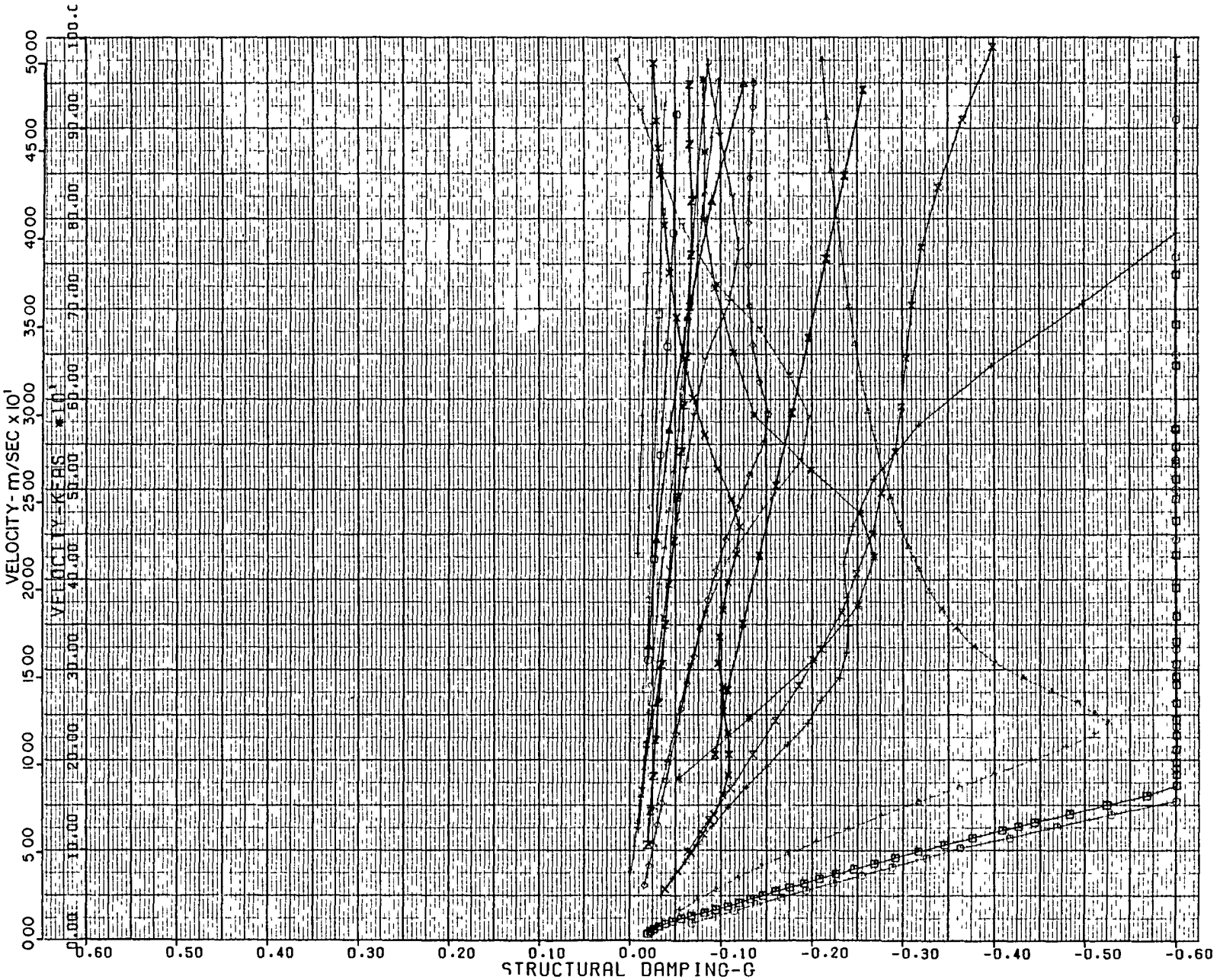

Figure D-110. Antisymmetric Velocity - Damping, Stiffness at 0 Ft 0.80 Mach, Mission Fuel - Two-Body MB2 Aircraft

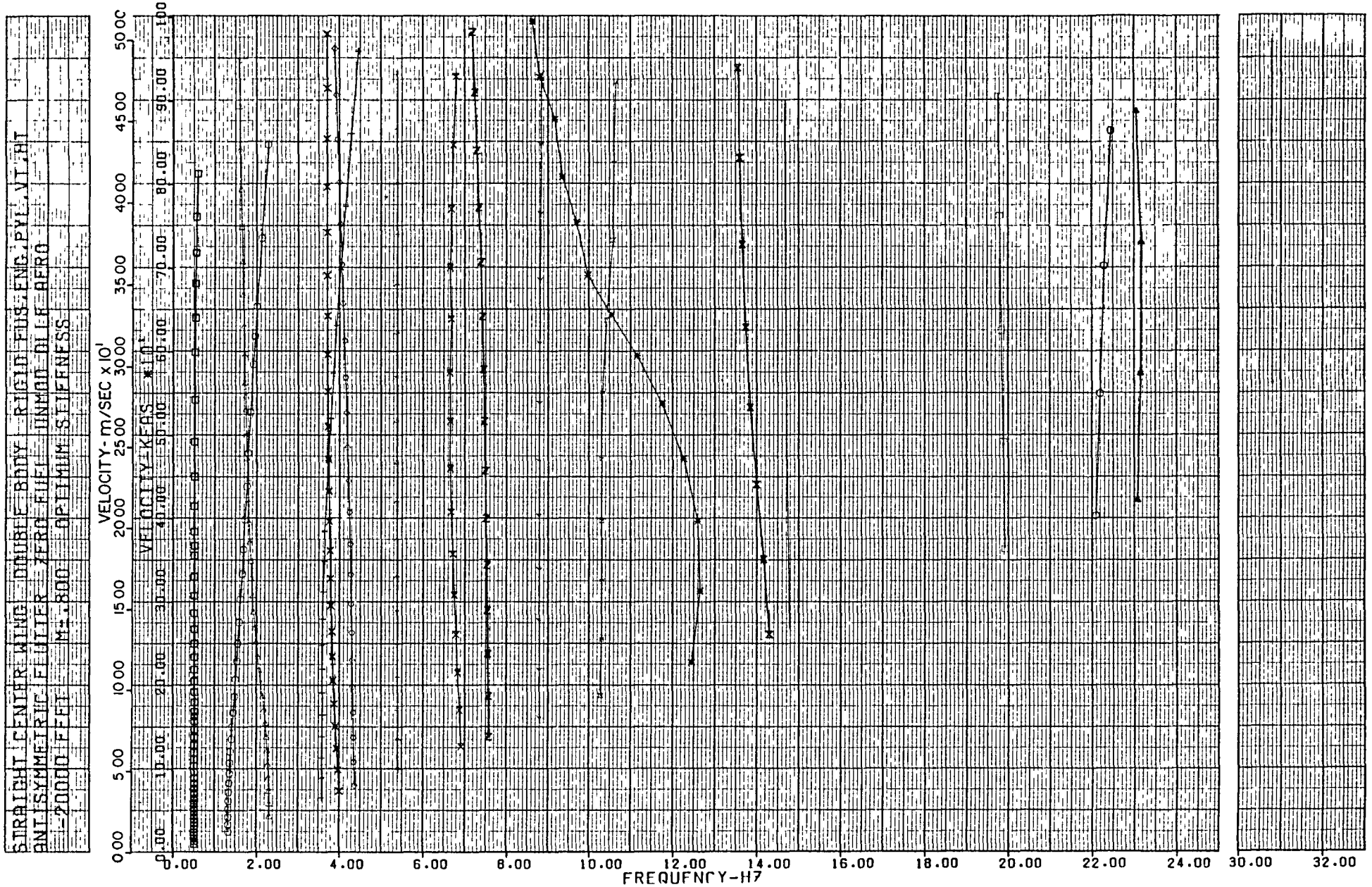

Figure D-111. Antisymmetric Velocity - Frequency, Stiffness at -20,000 Ft
0.80 Mach, Mission Fuel - Two-Body MB2 Aircraft

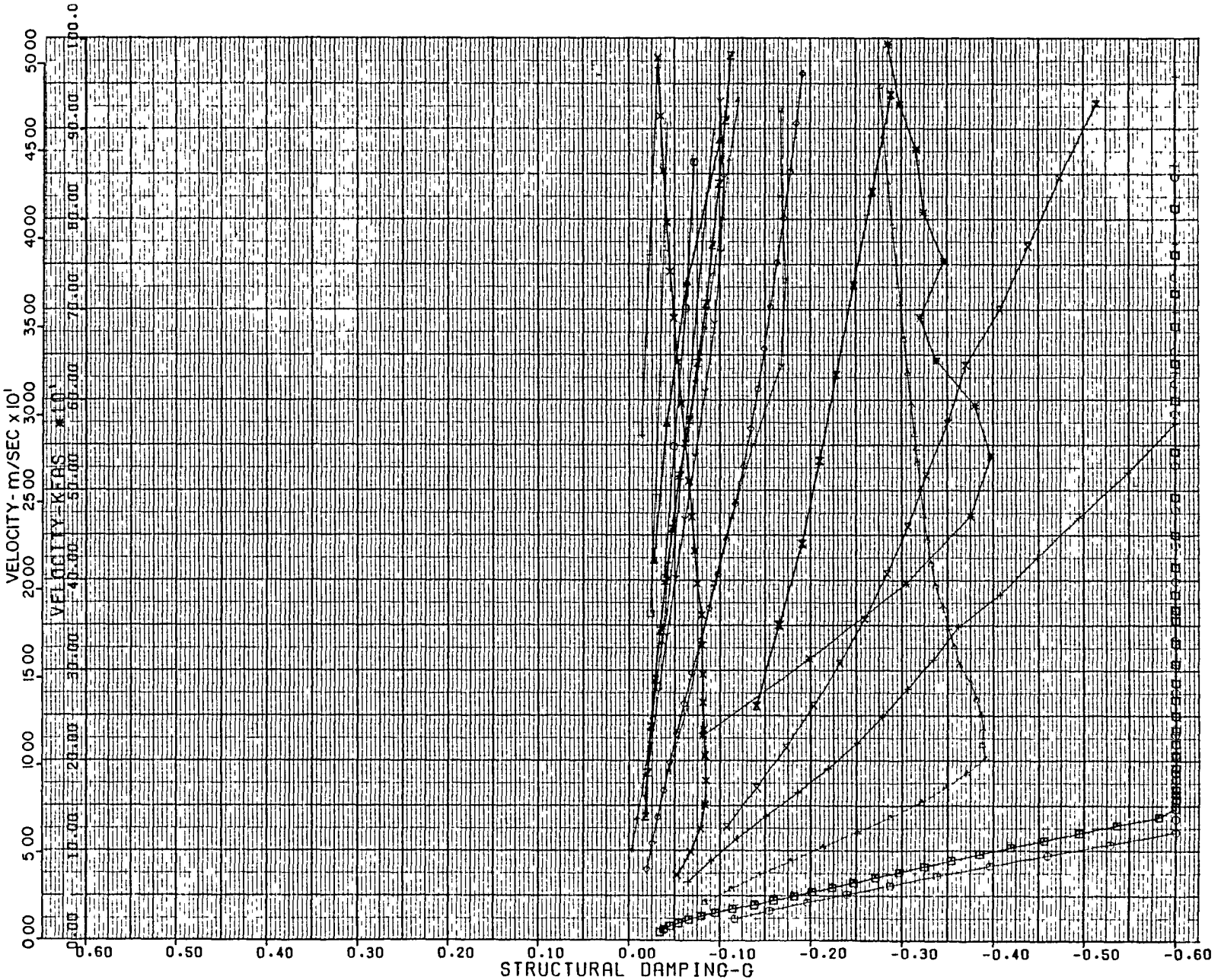

Figure D-112. Antisymmetric Velocity - Damping, Stiffness at -20,000 Ft 0.80 Mach, Mission Fuel - Two-Body MB2 Aircraft

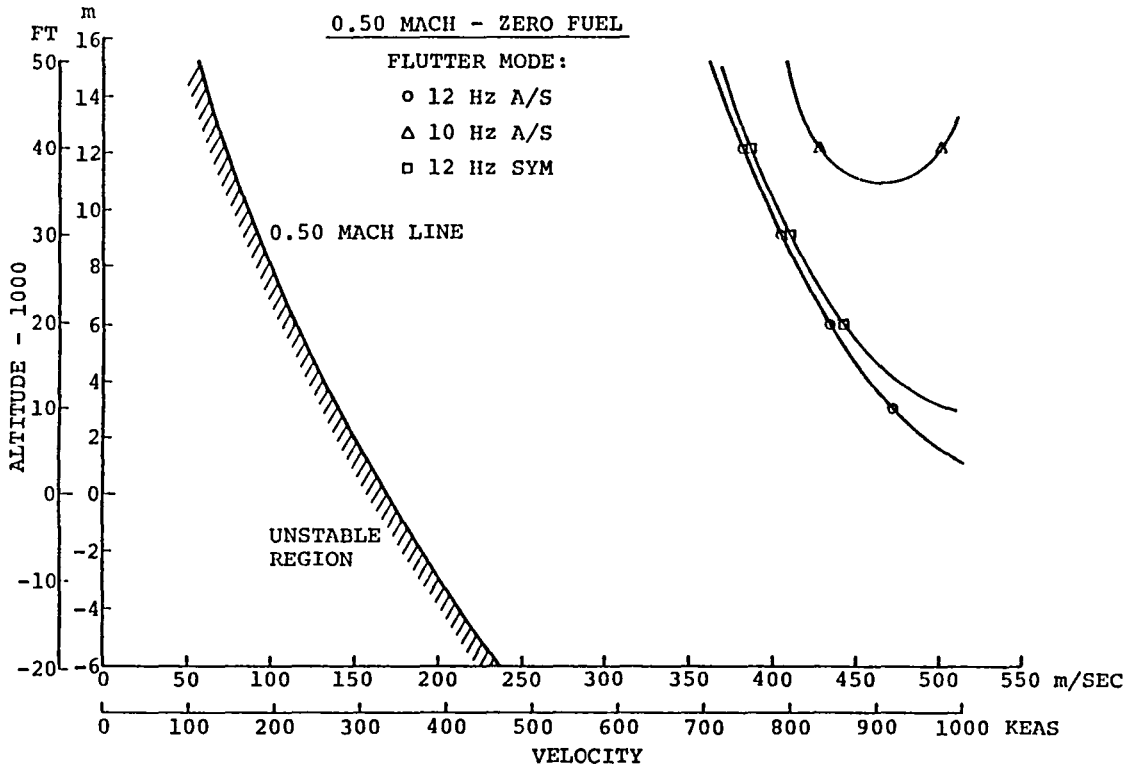

Figure D-113. Symmetric and Antisymmetric Flutter Velocities at Altitude - Single Body SBR Aircraft

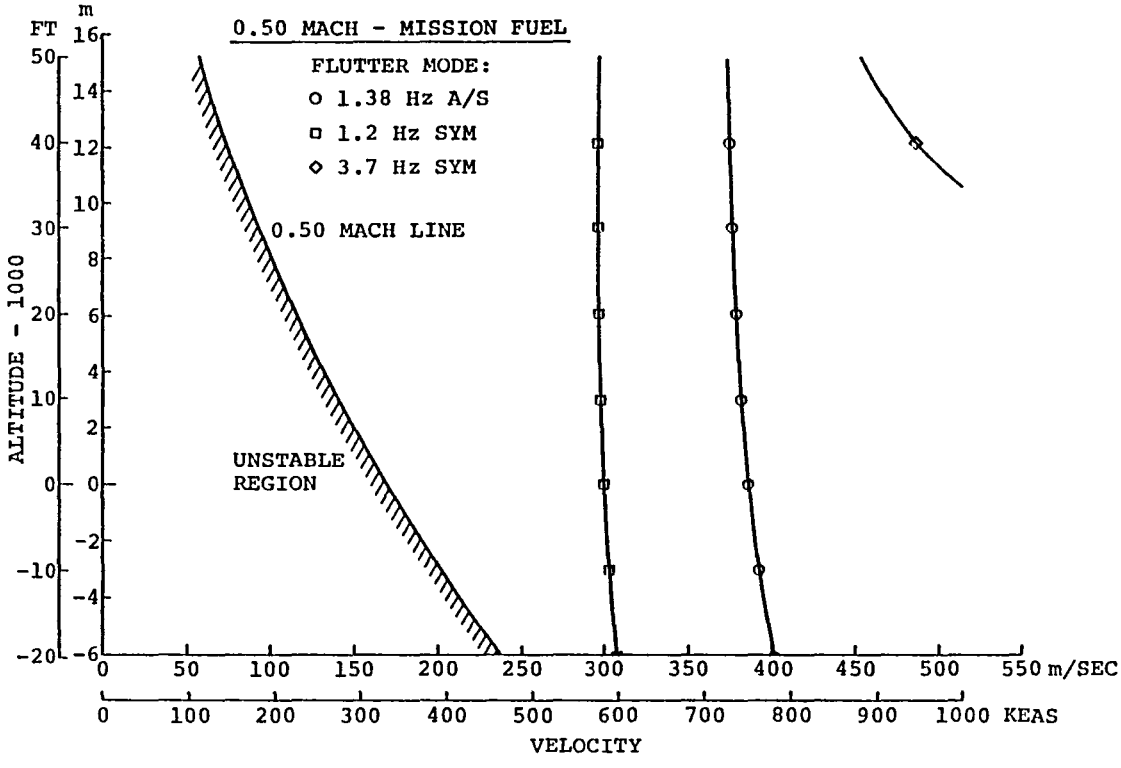

Figure D-114. Symmetric and Antisymmetric Flutter Velocities at Altitude - Single Body SBR Aircraft

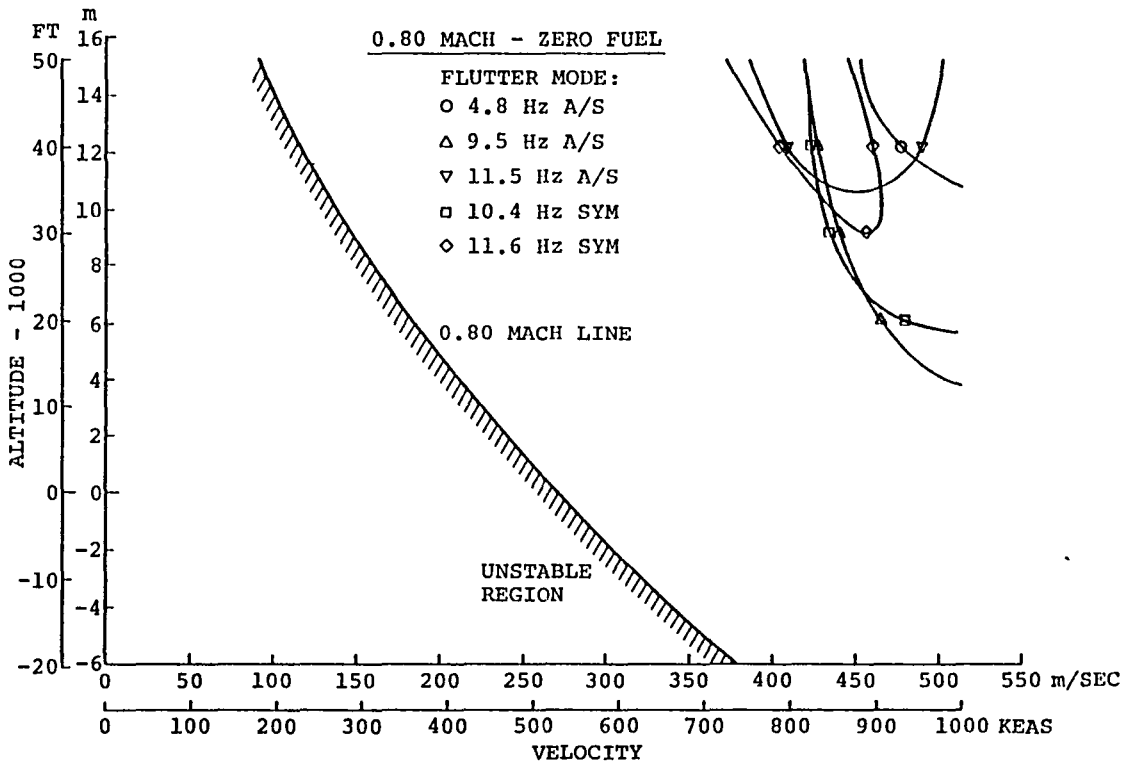

Figure D-115. Symmetric and Antisymmetric Flutter Velocities at Altitude - Single Body SBR Aircraft

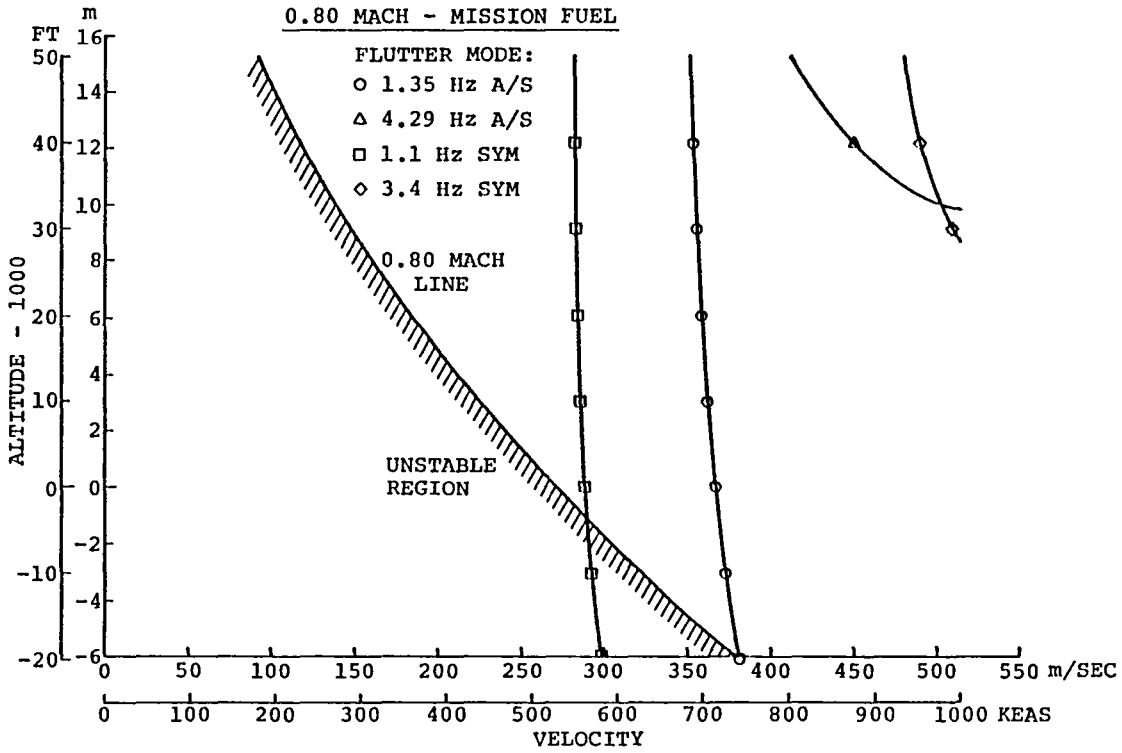

Figure D-116. Symmetric and Antisymmetric Flutter Velocities at Altitude - Single Body SBR Aircraft

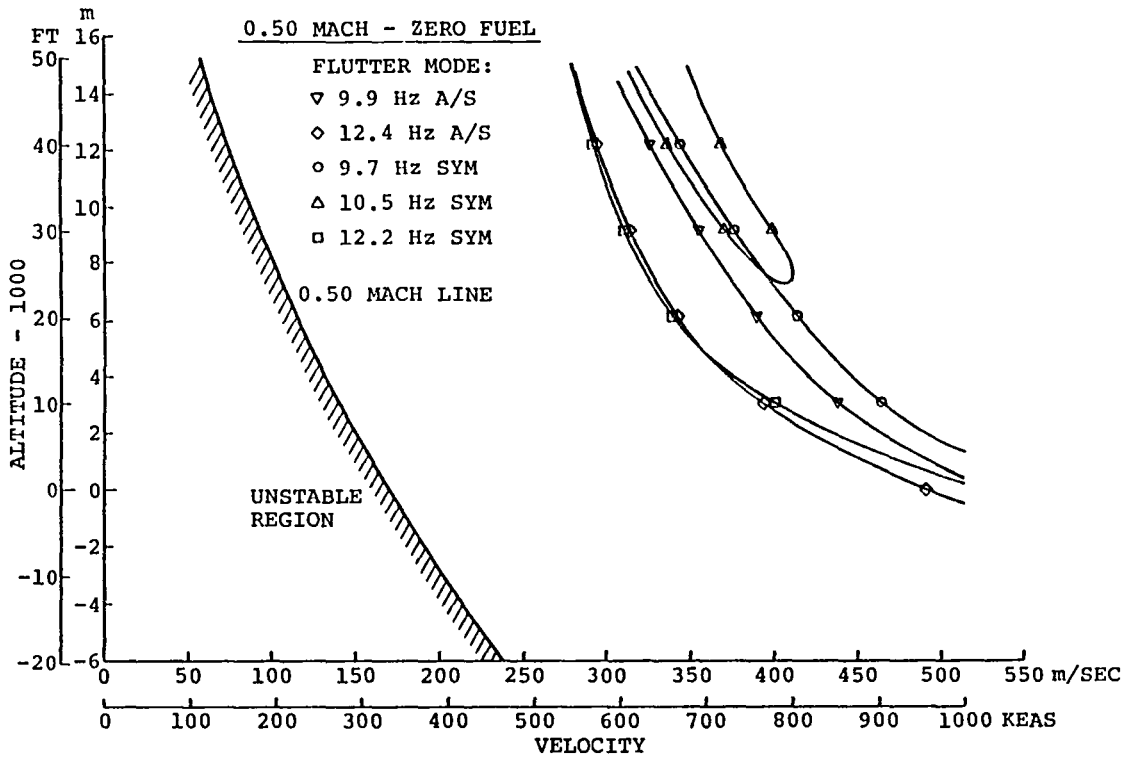

Figure D-117. Symmetric and Antisymmetric Flutter Velocities at Altitude - Two-Body MB1 Aircraft

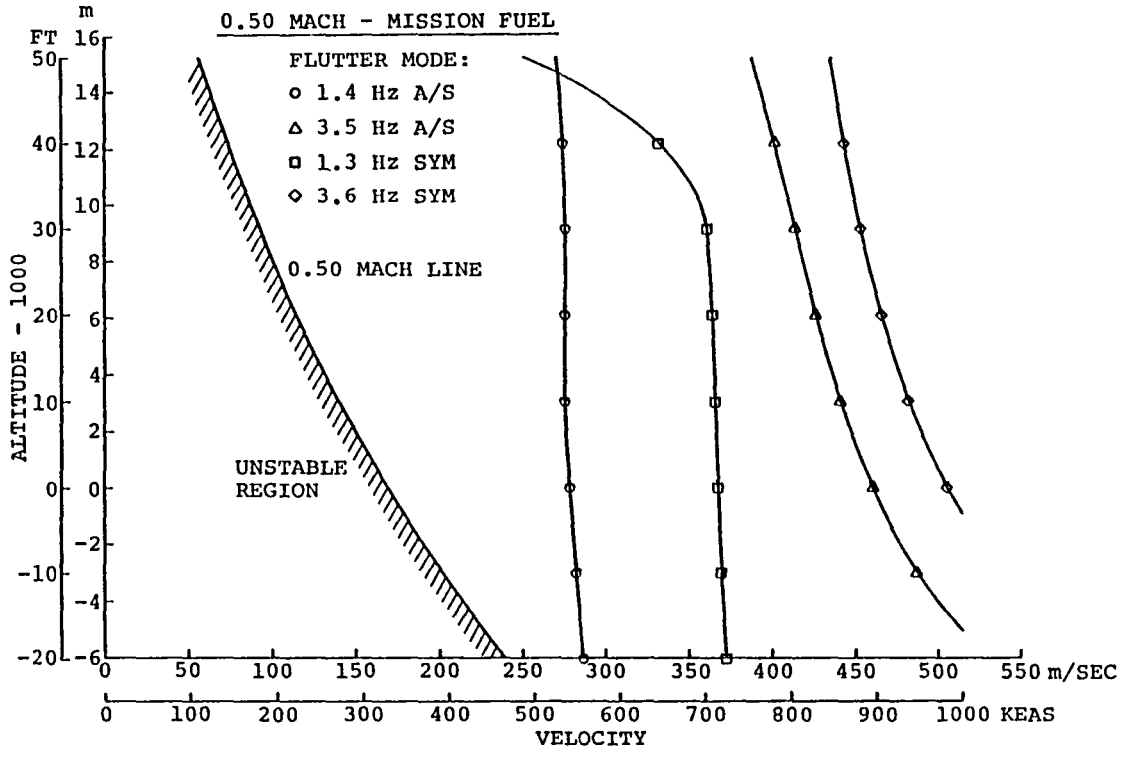

Figure D-118. Symmetric and Antisymmetric Flutter Velocities at Altitude - Two-Body MB1 Aircraft

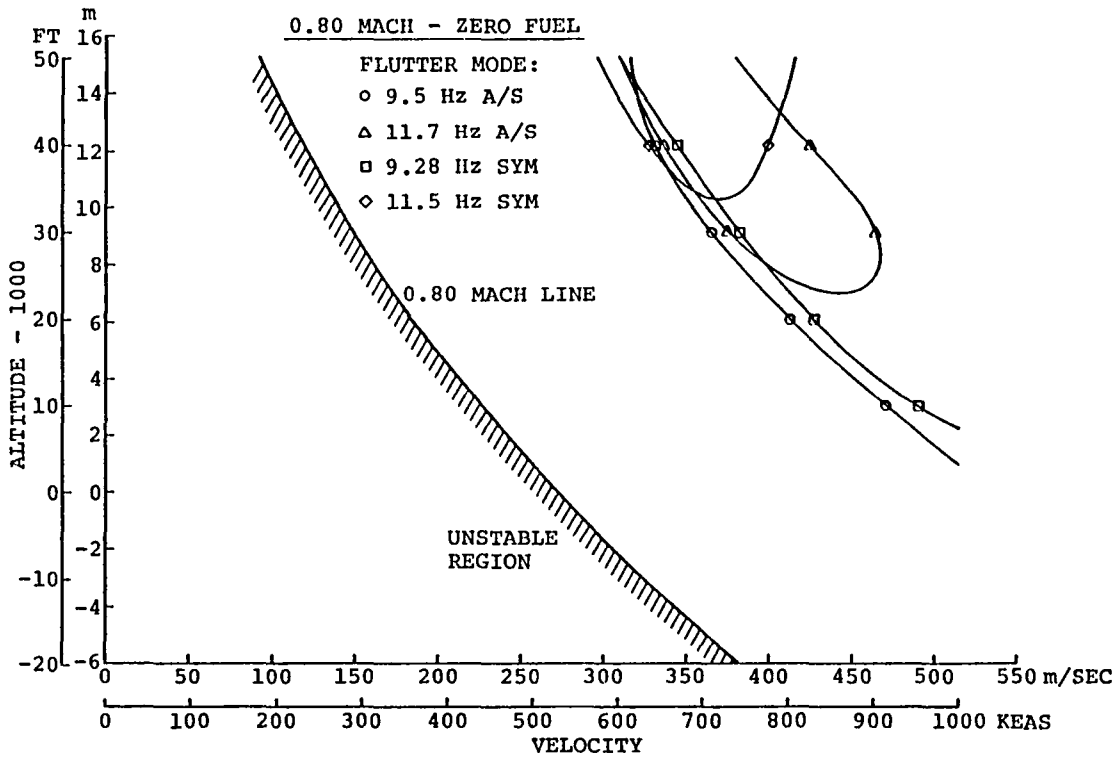

Figure D-119. Symmetric and Antisymmetric Flutter Velocities at Altitude - Two-Body MB1 Aircraft

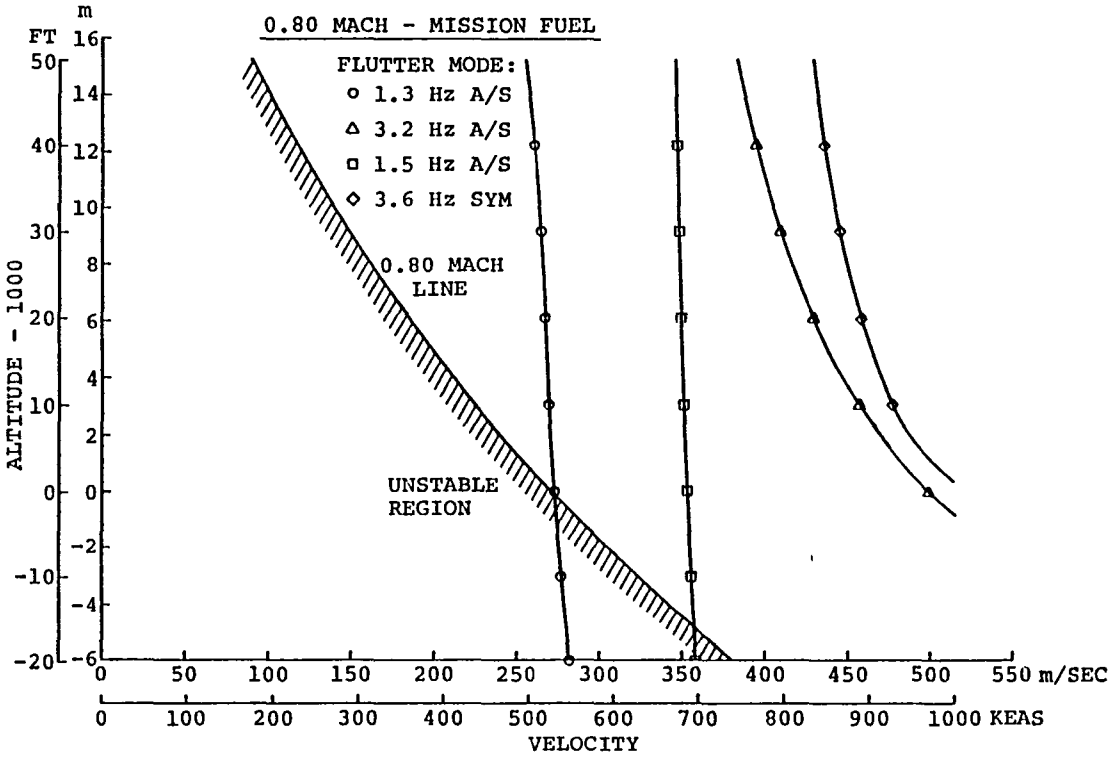

Figure D-120. Symmetric and Antisymmetric Flutter Velocities at Altitude - Two-Body MB1 Aircraft

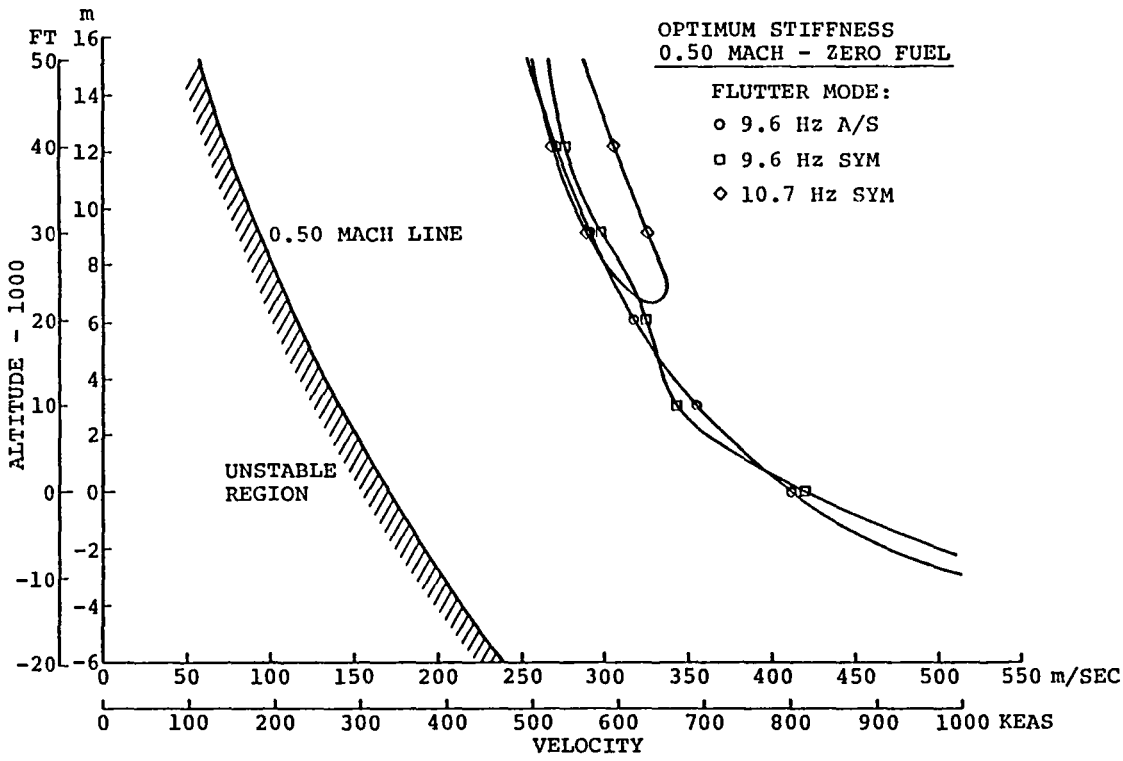

Figure D-121. Symmetric and Antisymmetric Flutter Velocities at Altitude - Two-Body MB2 Aircraft

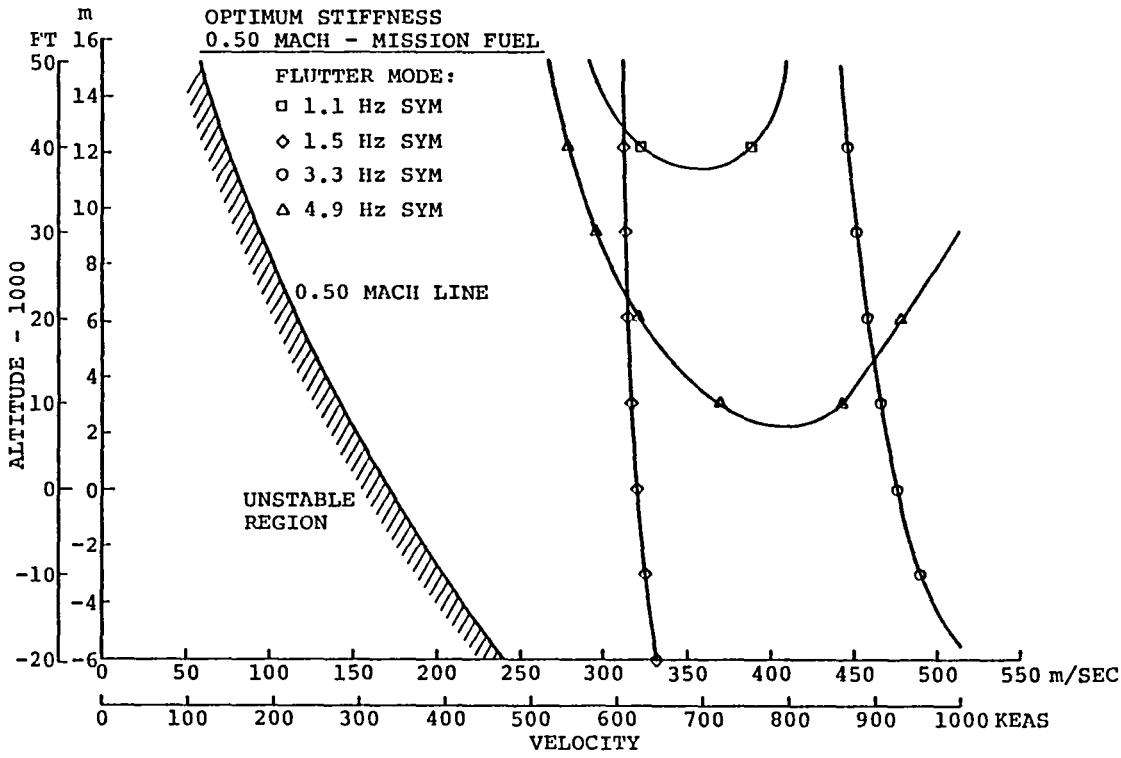

Figure D-122. Symmetric Flutter Velocities at Altitude Two-Body MB2 Aircraft

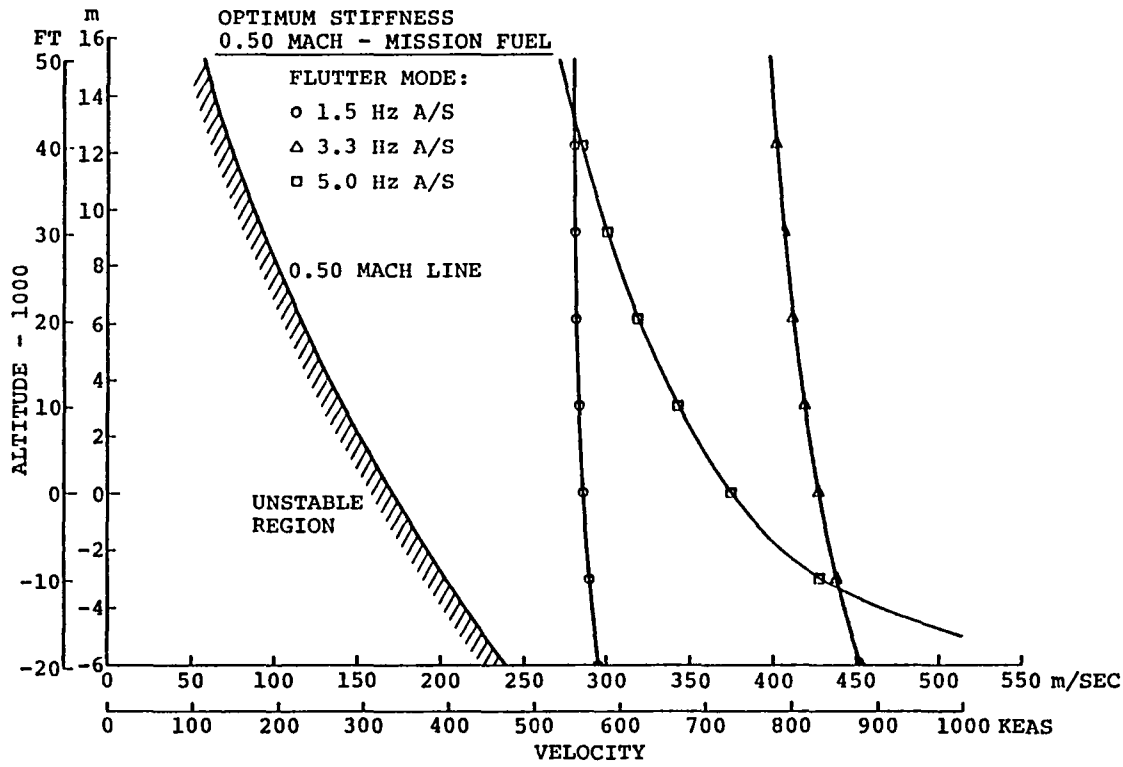

Figure D-123. Antisymmetric Flutter Velocities at Altitude Two-Body MB2 Aircraft

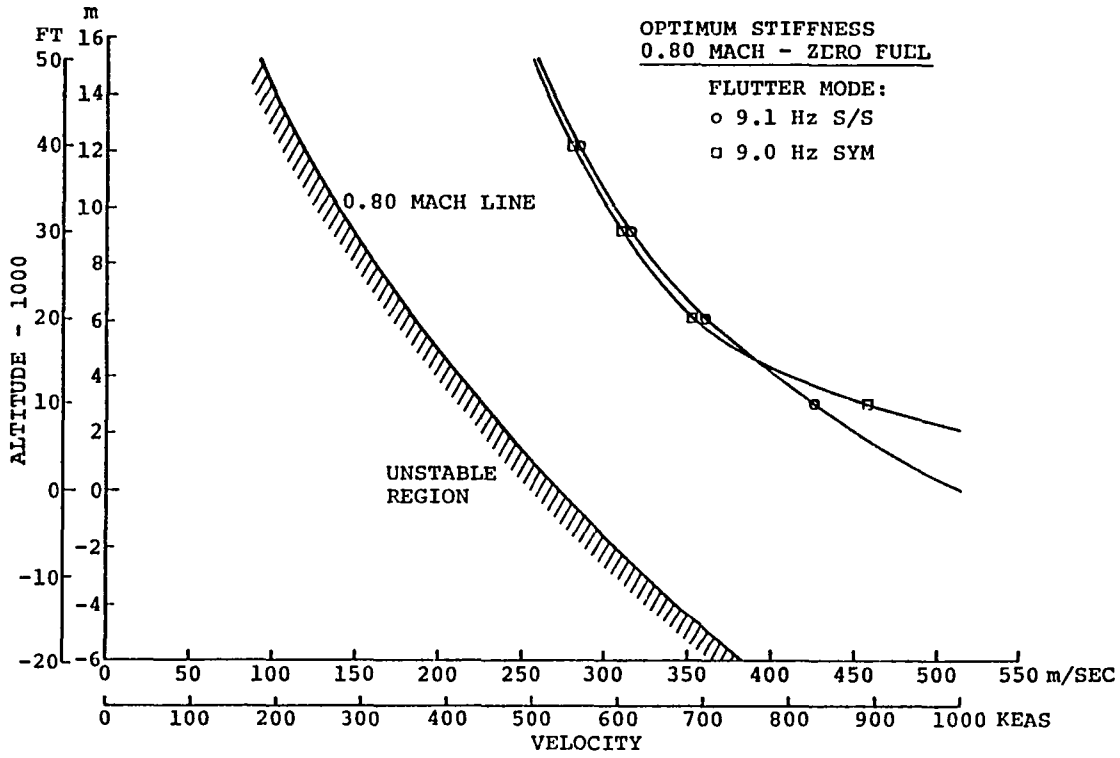

Figure D-124. Symmetric and Antisymmetric Flutter Velocities at Altitude - Two-Body MB2 Aircraft

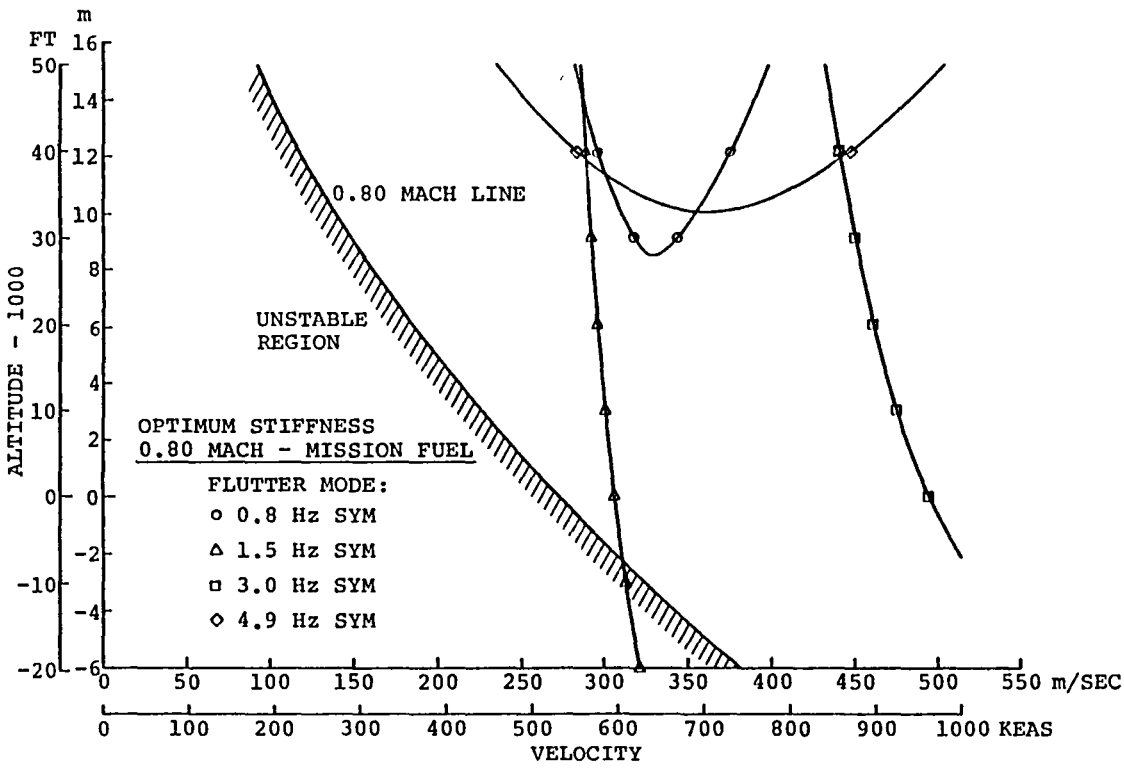

Figure D-125. Symmetric Flutter Velocities at Altitude Two-Body MB2 Aircraft

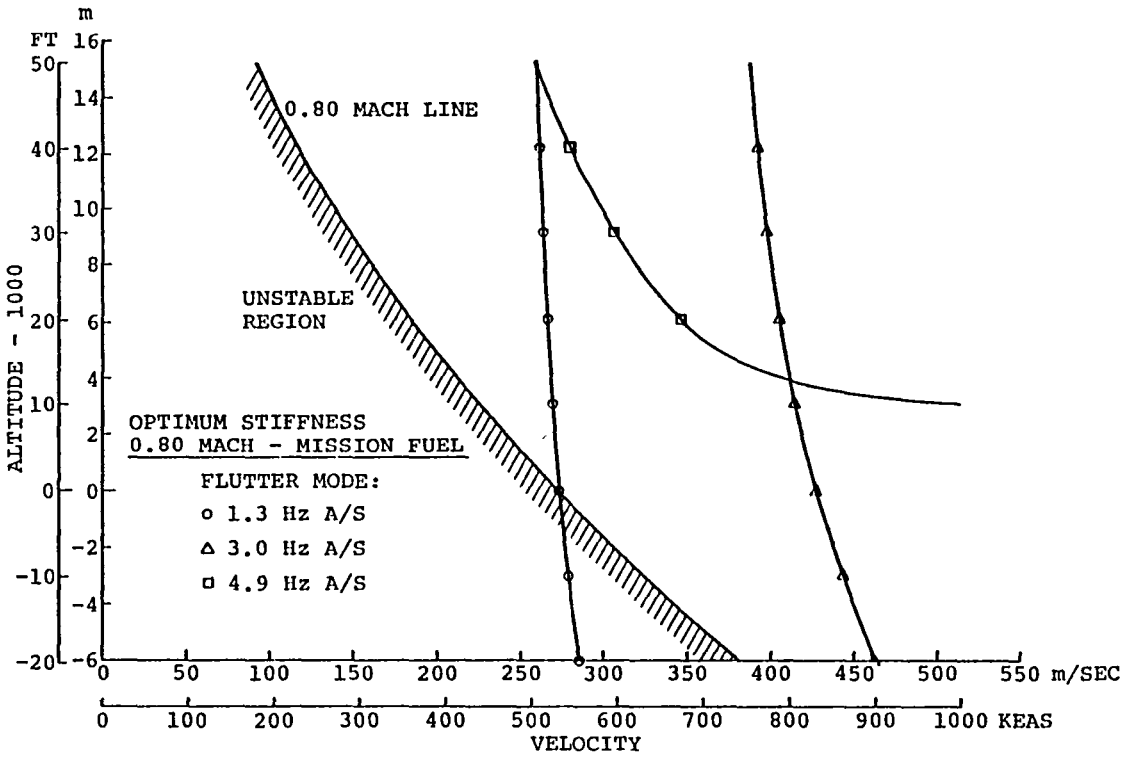

Figure D-126. Antisymmetric Flutter Velocities at Altitude Two-Body MB2 Aircraft

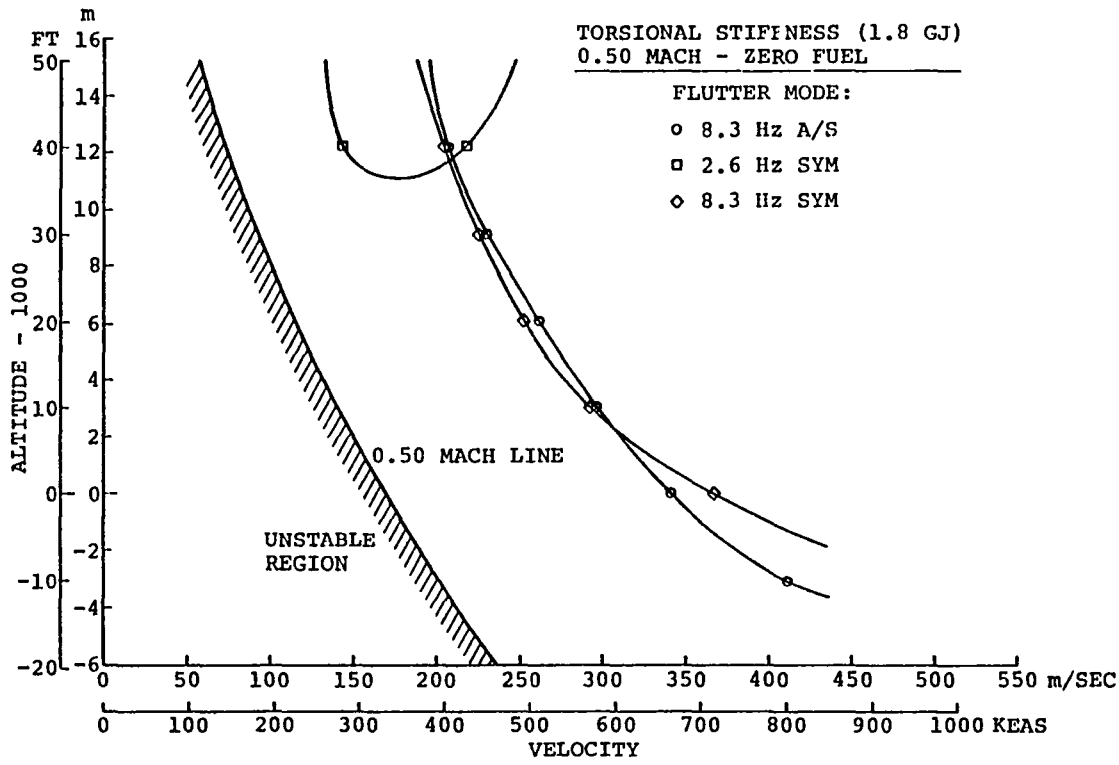

Figure D-127. Symmetric and Antisymmetric Flutter Velocities at Altitude - Two-Body MB2 Aircraft

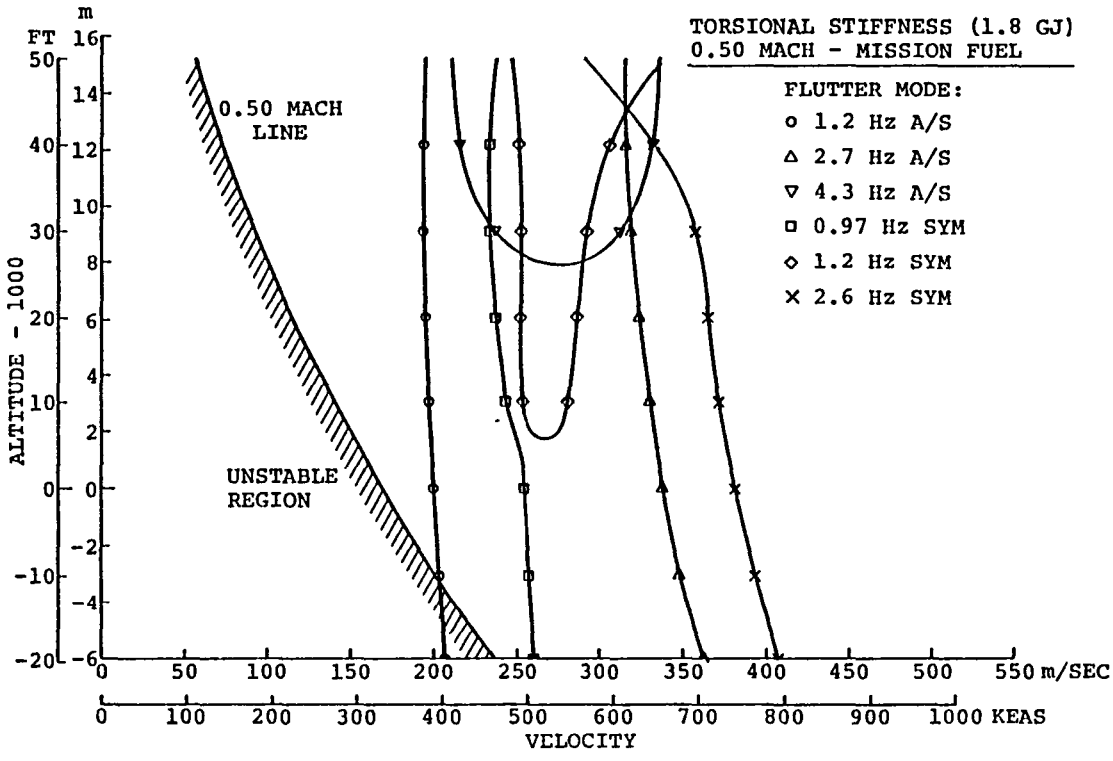

Figure D-128. Symmetric and Antisymmetric Flutter Velocities at Altitude - Two-Body MB2 Aircraft

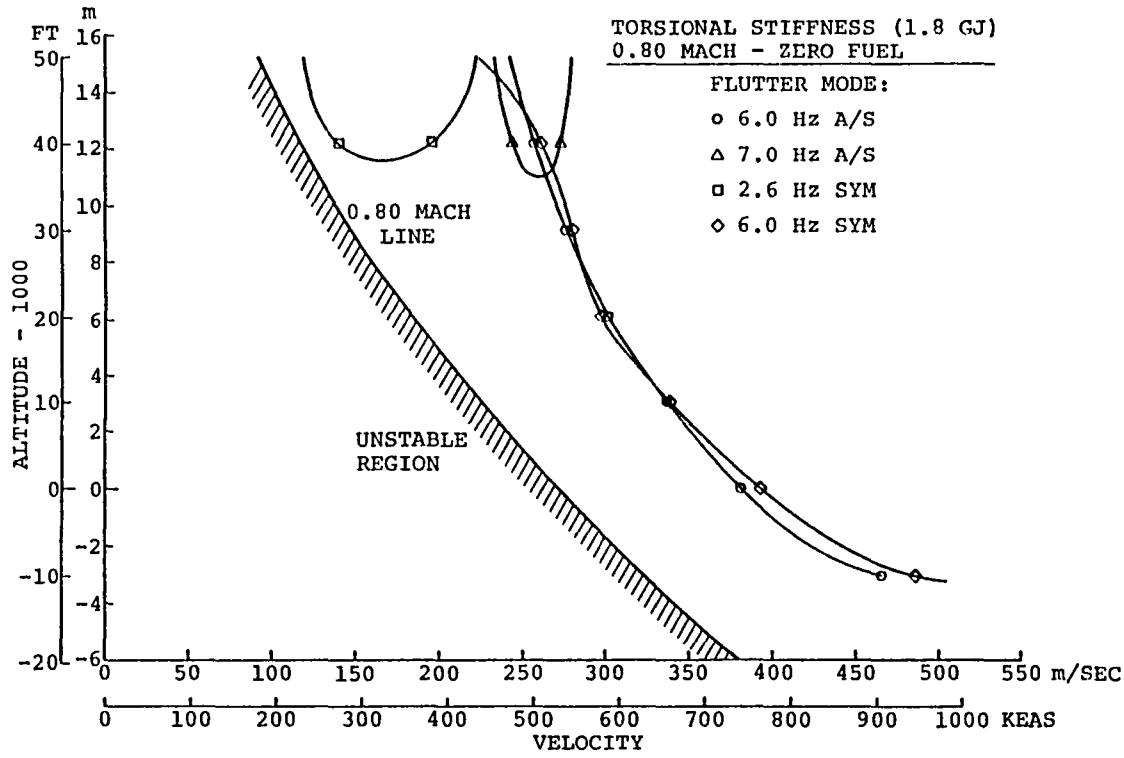

Figure D-129 Symmetric and Antisymmetric Flutter Velocities at Altitude - Two-Body MB2 Aircraft

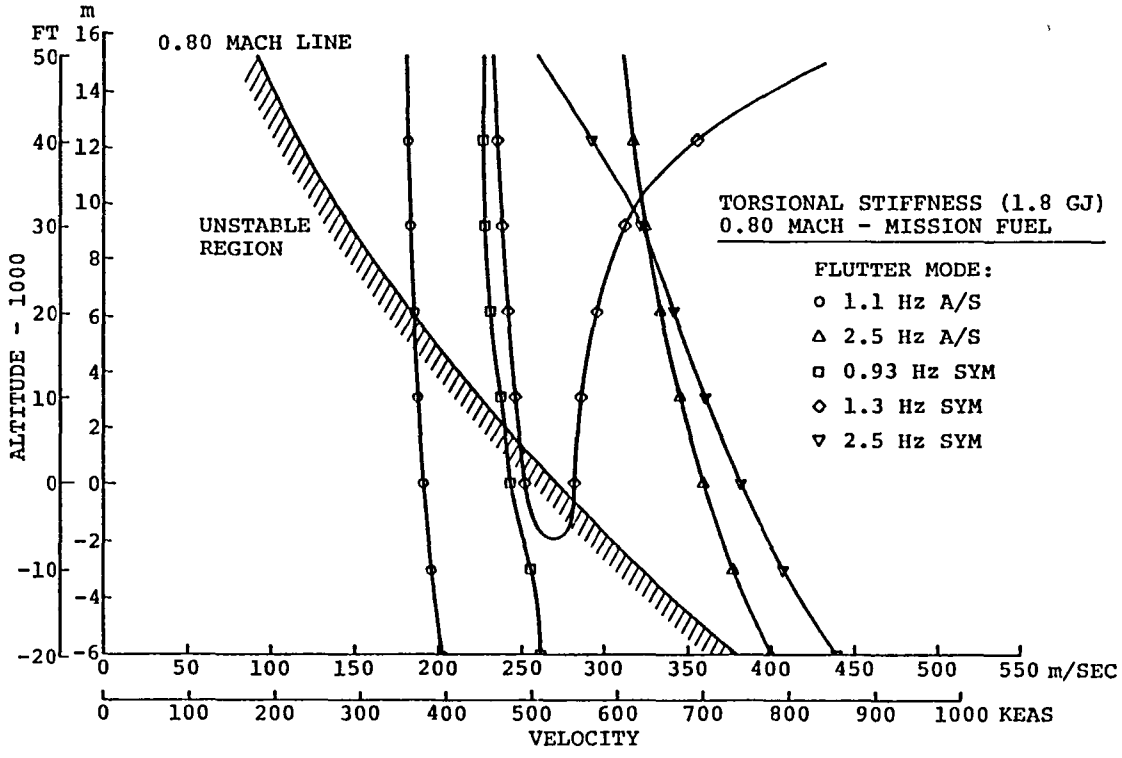

Figure D-130. Symmetric and Antisymmetric Flutter Velocities at Altitude - Two-Body MB2 Aircraft

Redistribution of stiffness values to increase the wing flutter velocity to its required level is accomplished using a flutter optimization computer program. An optimum set of stiffness values is defined when (1) flutter is outside the required 20 percent margin; (2) stiffnesses are at least those required for fatigue and fracture considerations and static, gust, taxi, and maneuver loads; (3) uniform flutter velocity derivatives for the unconstrained wing panels; and (4) stiffness changes, to obtain uniform derivatives, do not cause other flutter modes to become more critical. An ideal stiffness distribution is one where a change in flutter velocity for a change in weight is constant across the span. For instance, consider the case when one derivative is large for one wing panel and small for another, a lesser overall weight could be achieved by increasing the weight where the derivative is the largest and decreasing the weight by a larger amount for the smaller derivative so as to have the same flutter velocity with a lower value of weight. For the aircraft studied, such is not possible because of the four constraints noted above.

However, the least weight penalty is derived by choosing a path which restricted the total change in flutter velocity to 15 percent of the total velocity change required to be outside the 20 percent flutter margin. In this case, the total velocity change is defined as the difference between the required velocity and the flutter velocity for the initial condition which is less than the flutter margin requirements. As more weight, and thus stiffness, is added to the wing panels with the largest derivatives and lesser amounts of weight to the panels with the smaller derivatives, the values of the derivatives tend to be uniform. That is, the larger derivatives decrease in value and vice versa. As resizing steps were taken, in this case approximately seven, to move the flutter velocity outside the flutter margin envelope requirements, other flutter modes would become critical and another set of derivatives for this new mode needed to be considered for weight and stiffness changes. Thus, this smaller step size tends to account, as much as practical, for changes in critical flutter mode characteristics and derivative uniformity. Since many sets of flutter calculations are required in such an endeavor, a simpler mathematical model is used. This model includes modified unsteady strip theory aerodynamics for the wing, cantilevered wing bending, and torsion modes, and is used to optimize wing stiffness distributions at one fuel, cargo, symmetry, altitude, and Mach number. Cursory analyses for the other fuel, cargo, sym-

metry, and Mach number conditions, using this simpler mathematical model, are completed prior to computing a set of matched flutter boundaries.

APPENDIX E

FLIGHT SIMULATION DATA PACKAGE

The final evaluation of any aircraft design lies in the opinion of a pilot assigned to fly the design mission. Since there are possibly many unknown aspects of the routine usage of very large aircraft, a flight simulation effort is proposed. NASA-Langley is conducting such an experiment to investigate potential problem areas and to provide design criteria, if possible, associated with very large aircraft. The following data are provided to aid in this investigation for the moving base simulator at NASA-Langley. A comparison is to be made of five different very large aircraft designs shown in Figures E-1 through E-5. The first is the conventional single body aircraft with load carrying capabilities comparable to the multibody concepts developed. There are two, two-body designs, a three-body design, and a spanloader (taken from a previous study) used to study problems which may be configuration dependent as well as size dependent.

Tabulated data are presented in Figures E-6 through E-8 in a format for easy comparisons. General geometric and weight data are provided in Figure E-6. Stability and control derivatives are presented in Figure E-7. Incremental effects of ground proximity, ground spoilers, and flap effects are presented in Figure E-8. Figures E-9 through E-13 show maximum and minimum thrust capabilities for each configuration and Figure E-14 presents the common engine response characteristics to be used for all configurations. Drag polars are presented in Figures E-15 through E-19 for approach and landing flaps settings appropriate for each configuration.

These data are for the low-speed landing task which is considered critical from a design point of view. The previously described offset maneuver shown in Figure C-15 is an example of the typical tasks. Most studies vary the altitude and offset distances.

SPEED	0.80 MACH
PAYLOAD	350,000 kg (771,618 LB)
RANGE	6,482 km (3,500 NM)
OPERATING WT.	376,164 kg (829,300 LB)
GROSS WT.	959,665 kg (2,115,700 LB)
BLOCK FUEL	195,226 kg (430,400 LB)
ASPECT RATIO	9.21
DOC	7.09 ¢/AMgkm @ 34.34¢ PER LITER
	(11.91 ¢/AINM @ 1.30$ PER GAL.)

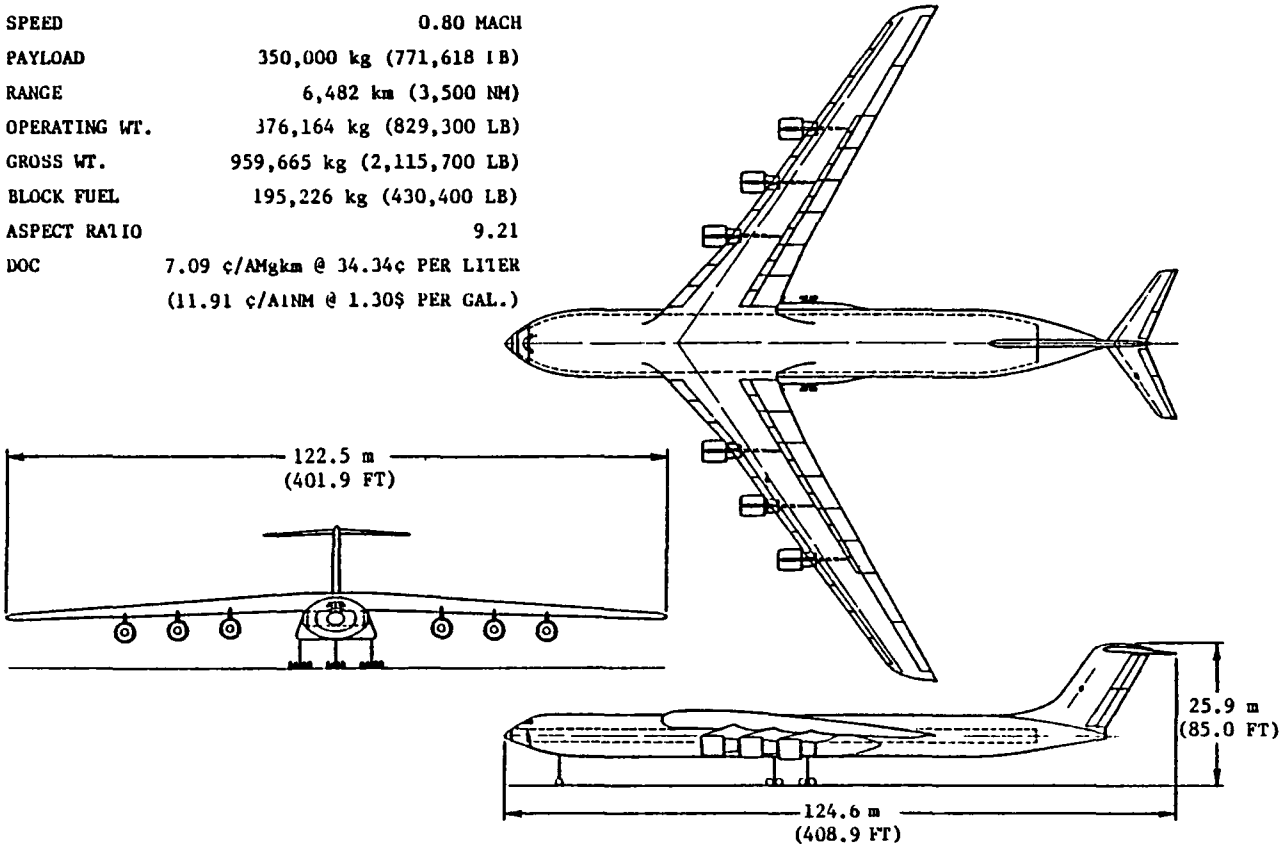

Figure E-1. Single Body Reference SBR Aircraft - Point Design

SPEED	0.80 MACH
PAYLOAD	350,000 kg (771,618 LB)
RANGE	6,482 km (3,500 NM)
OPERATING WEIGHT	323,547 kg (713,300 LB)
GROSS WEIGHT	893,214 kg (1,969,200 LB)
BLOCK FUEL	183,796 kg (405,200 LB)
ASPECT RATIO	9.70
DOC	6.47 ¢/AMgkm @ 34.34¢ PER LITER
	(10.87 ¢/ATNM @ 1.30$ PER GAL.)

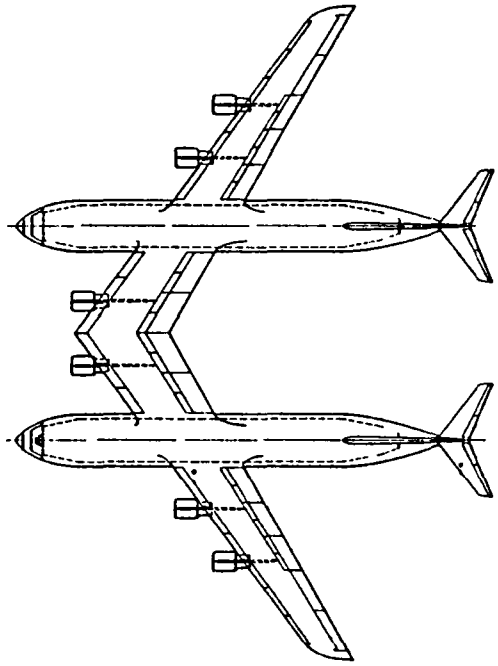

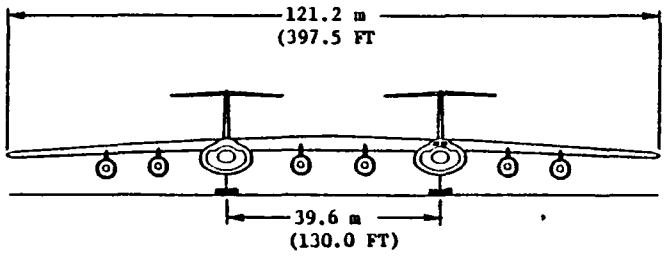

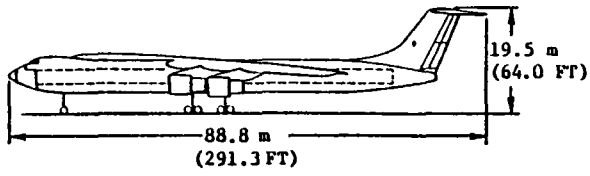

Figure E-2. Two-Body MB1 Aircraft - Point Design

SPEED	0.80 MACH
PAYLOAD	350,000 kg (771,618 LB)
RANGE	6,482 km (3,500 NM)
OPERATING WT.	346,091 kg (763,000 LB)
GROSS WT.	898,158 kg (1,980,100 LB)
BLOCK FUEL	168,827 kg (372,200 LB)
ASPECT RATIO	11.62
DOC	6.29 ¢/AMgkm @ 34.34¢ PER LITER
	(10.56 ¢/ATNM @ 1.30$ PER GAL.)

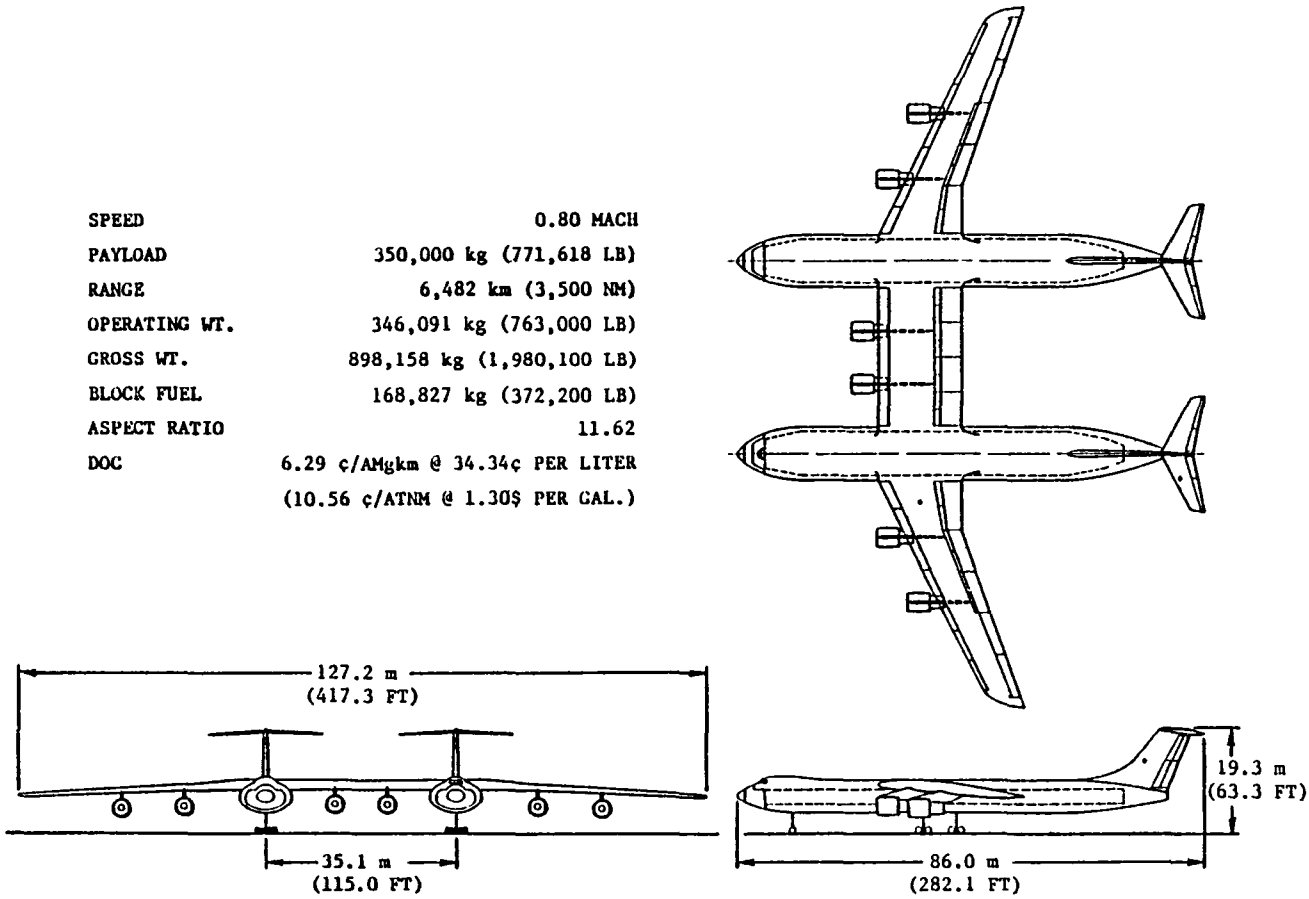

Figure E-3. Two-Body MB2 Aircraft - Point Design

SPEED	0.80 MACH
PAYLOAD	350,000 kg (771,618 LB)
RANGE	6,482 km (3,500 NM)
OPERATING WT.	338,845 kg (747,025 LB)
GROSS WT.	913,490 kg (2,013,900 LB)
BLOCK FUEL	187,904 kg (414,257 LB)
ASPECT RATIO	11.83
DOC	6.69 ¢/AMgkm @ 34.34¢ PER LITER
	(11.24 ¢/ATNM @ 1.30$ PER GAL.)

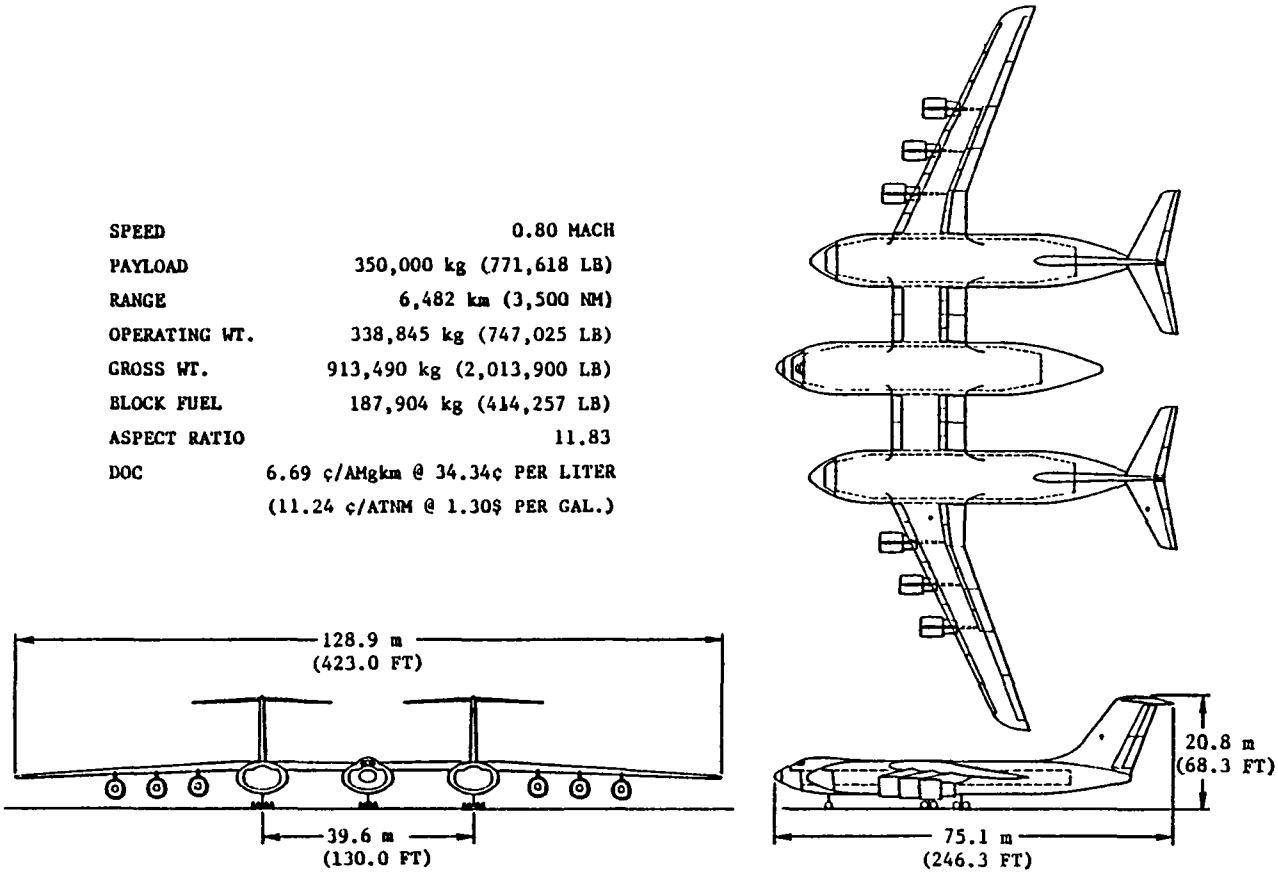

Figure E-4. Three-Body MB3 Aircraft - Point Design

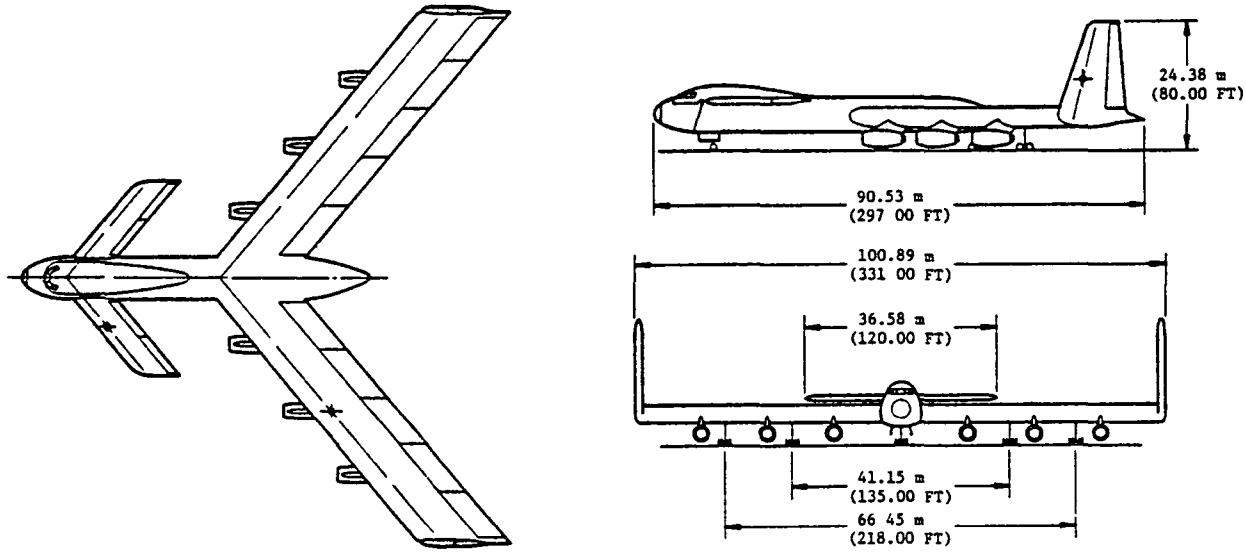

Figure E-5. Spanloader Aircraft - Canard

ITEM \ AIRCRAFT	SINGLEBODY SBR	TWO-BODY MB1	TWO-BODY MB2	THREE-BODY MB3	CANARD SPANLOADER
GROSS WEIGHT - kg (LB)	840,100 (1,852,100)	783,400 (1,727,100)	788,200 (1,737,700)	795,400 (1,753,600)	607,400 (1,339,000)
S REF - m^2 (FT^2)	1,618 (17,413)	1,454 (15,654)	1,458 (15,689)	1,352 (14,555)	1,724 (18,559)
b REF - m (FT)	120 17 (394.25)	118.77 (389.67)	125.12 (410.50)	130.23 (427.27)	101 (331)
$\bar{c}$ REF - m (FT)	14.88 (48.83)	13.00 (42.63)	12.62 (41.39)	11.24 (36.89)	17.15 (56.25)
CG - % $\bar{c}$	35	33	34	31	15
CG RANGE - % $\bar{c}$	34-42	33-46	34-43	21-44	3-15
INERTIAS $X10^{-6}$					
Ixx (ROLL) - kg-m^2 (SLUG FT^2)	286.5 (211,4)	540.8 (399.0)	502.7 (370.9)	485.3 (358.0)	
Iyy (PITCH) - kg-m^2 (SLUG FT^2)	432.7 (319.2)	209.0 (154.2)	194.1 (143.2)	106.9 (78.9)	
Izz (YAW) - kg-m^2 (SLUG FT^2)	707.4 (521.9)	744.0 (548.9)	658.9 (486.1)	584.2 (431.0)	
Ixz (PRODUCT) - kg-m^2 (SLUG FT^2)	8.77 (6.47)	3.51 (2.59)	5.26 (3.88)	5.79 (4.27)	
PILOT LOCATION FROM CG.					
X (FWD) - m (FT)	45.8 (150.4)	29.9 (98.0)	30.4 (99 7)	24.8 (81.3)	66.4 (217 7)
Y (LEFT) - m (FT)	0.9 (3.0)	20.7 (68.0)	18.4 (60.5)	0.9 (3.0)	0.9 (3.0)
Z (ABOVE) - m (FT)	2.3 (7.5)	1.8 (6.0)	1.8 (6 0)	1.8 (6.0)	3 0 (10.0)
ENGINE LOCATION FROM CG.					
INBD Y - m (FT)	19.5 (64.1)	5.9 (19.5)	4.8 (15.9)	31.9 (104.7)	12.6 (41 3)
Z (BELOW) - m (FT)	2.7 (8.8)	2.0 (6.4)	2.1 (7 0)	2 5 (8.2)	4 6 (15.0)
MIDDLE Y - m (FT)	29.3 (96.0)	32.4 (106.4)	32.6 (106.8)	31.5 (103.3)	25 3 (82.9)
Z (BELOW) - m (FT)	3.0 (9.8)	2.3 (7.4)	2.3 (7.6)	2.7 (8.8)	4.6 (15 0)
OUTBD Y - m (FT)	39.1 (128.3)	42.2 (138.3)	44.4 (145.7)	47.5 (156.0)	37.7 (123.8)
Z (BELOW) - m (FT)	3.3 (10.7)	2.7 (9.0)	2.9 (9.4)	2.9 (9.4)	4.6 (15.0)
LANDING GEAR HEIGHT-CG TO GROUND					
UNCOMPRESSED - m (FT)	10.3 (33.8)	7.8 (25.6)	8.0 (26.3)	6.6 (21.8)	7.3 (24.0)
COMPRESSED - m (FT)	9.7 (31.8)	7.2 (23.6)	7 4 (24.3)	6.0 (19 8)	6 7 (22.0)
TIRE SIZE - cm (IN)	132 x 51 (52 x 20)	132 x 51 (52 x 20)	132 x 51 (52 x 20)	132 x 51 (52 x 20)	132 x 51 (52 x 20)

Figure E-6. General Geometry and Weight Data - Point Design and Canard Spanloader Aircraft

ITEM \ AIRCRAFT	UNITS	SINGLEBODY	TWO-BODY		THREE-BODY	CANARD
		SBR	MB1	MB2	MB3	SPANLOADER
C_{L_α}	1/RAD	5.04	5.10	5.21	5 33	4 02
Cm_α (5% EFFECTIVE SM)	1/RAD	-0 252	-0.255	-0.261	-0 267	--
Cm_α (AT GIVEN CG)	1/RAD	0.0504 (-1% SM)	-0.255 (5% SM)	-0.0521 (1% SM)	-0 267 (5% SM)	-0 256 (7% SM)
Cm_α (At AFT CG, -8% SM)	1/RAD	0.403	0 408	0 417	0 426	--
Cm_α	1/RAD	-5.56	-3.64	-4.90	-7.32	-5 62
Cm_q	1/RAD	-25.5	-20.7	-16.4	-23.4	-19.2
Cm_{δ_e}	1/RAD	-0.925	-0.785	-0.788	-1.28	-0.420
$C_{L\,\delta e}$	1/RAD	0.216	0.202	0.206	0 353	0 176
$\delta_{e\ max}$	RAD (DEG)	±0.44 (±25)	±0 44 (±25)	±0 44 (±25)	±0.44 (±25)	±0.44 (±25)
Cmih	1/RAD	-2.42	-1.94	-1.83	-2.89	1 26
$C_{L_{i_H}}$	1/RAD	0.566	0.516	0.501	0 840	0 494
i H max	RAD (DEG.)	+0.12 to -0.09 (+7 to -5)	+0.16 to -0.09 (+9 to -5)	+0.19 to 0 (+11 to 0)	+0 12 to -0.14 (+7 to -8)	+0 07 to +0.35 (+4 to +20)
C_{n_β}	1/RAD	0.0981	0.0899	0.0734	0.0982	0 120
C_{l_β}	1/RAD	-0.139	-0 143	-0.131	-0 140	-0 178
C_{y_β}	1/RAD	-0.407	-0.567	-0.589	-0.942	-0 711
C_{n_p}	1/RAD	-0 0526	-0.0610	-0 0808	-0.0805	-0 000344
C_{l_p}	1/RAD	-0.473	-0.504	-0 642	-0 647	-0 354
C_{y_p}	1/RAD	0.164	0 186	-0.00596	-0 0209	0 00625
C_{nr}	1/RAD	-0.123	-0.0881	-0.0793	-0 0736	-0 0688
C_{l_r}	1/RAD	0.120	0.122	0.204	0.208	0.204
C_{y_r}	1/RAD	0	0	0	0	0
C_{n_r}	1/RAD	-0.0558	-0.0461	-0 0423	-0.0511	-0 0734
C_{l_r}	1/RAD	0 00463	0.00509	0.00479	0 0108	0 0128
C_{y_r}	1/RAD	0.123	0 129	0.128	0.204	0 275
$\delta_{r\ max}$	RAD (DEG)	±0.61 (±35)	±0.61 (±35)	±0.61 (±35)	±0 61 (±35)	±0.61 (±35)
$\delta_{a\ max}$	RAD (DEG)	±0.70 (±40)	±0.70 (±40)	±0.70 (±40)	±0.70 (±40)	±0.70 (±40)

Figure E-7. Stability Derivatives - Point Design and Canard Spanloader Aircraft

ITEM \ AIRCRAFT	SINGLEBODY SBR	TWO-BODY MB1	TWO-BODY MB2	THREE-BODY MB3	CANARD SPANLOADER
LANDING GEAR EFFECTS					
ΔC_D GEAR	0 0175	0 0175	0.0175	0.0175	0 0292
ΔC_m GEAR	-0.0082	-0 0082	-0 0082	-0 0082	-0.0137
GROUND EFFECTS					
ΔC_D GE	-0 03	-0 03	-0 03	-0.03	-0.03
$C_{L_\alpha GE}/C_{L_\alpha FA}$	1.186	1 186	1.186	1 186	1 186
$(dC_m/dC_l)GE/FA$ } Use Either Not Both	1.214	1.214	1 214	1 214	1 214
$\Delta C_{m_{GE}}$ } Use Either Not Both	-0.065	-0.065	-0 065	-0.065	-0.065
GROUND SPOILER EFFECTS					
ΔC_D GR SP	0.1220	0.1220	0.1220	0 1220	0.1220
ΔC_L GR SP	-0.8	-0.8	-0.8	-0.8	-0 8
(C_m Aero = 0 when ground spoilers are deflected)					
FLAP EFFECTS					
δ_{F_1} - RAD (DEG)	0.46 (26.1)	0 54 (31 1)	0.37 (21.4)	0.64 (36 9)	0 52 (30 0)
α_{ZL} - RAD (DEG)	-0.21 (-11.81)	-0 20 (-11 61)	-0 18 (-10.10)	-0.20 (-11 41)	-0.21 (-12.3)
CL_{max}	2.44	2.42	2.75	2 80	2.38
C_{MZL}	0.10	0.10	0.10	0.10	0 075
Vapp (1 $3V_s$) - m/SEC (KT)	25.7 (147 4)	77.6 (150.8)	72.9 (141.7)	75.4 (146.5)	63.3 (123 0)
C_l δ_a - 1/RAD	-0 112	-0 0914	-0.102	-0.100	-0 0857
Cn δ_a -1/RAD	-0.0055	-0.00342	-0 000747	-0 000720	-0 00115
δ_{F2} - RAD (DEG)	0 87 (50)	0.87 (50)	0.87 (50)	0.87 (50)	0 70 (40)
α_{ZL} - RAD (DEG)	-0 26 (-14 95)	-0.24 (-13.8)	-0.24 (-13.6)	-0.22 (-12 6)	-0.27 (-15.6)
$C_{L_{max}}$	2.78	2.65	3 24	2.97	2 5
$C_{m_{zl}}$	0.05	0.05	0.05	0.05	0.05
VApp (1 $3V_s$) - m/SEC (KT)	73.3 (142.5)	74.1 (144.1)	67.1 (130.5)	73.2 (142.3)	61.7 (120 0)
$C_{l_{\delta a}}$ - 1/RAD	-0.161	-0 125	-0.142	-0.139	-0.0966
$C_{n_{\delta a}}$ - 1/RAD	-0 0226	-0.0141	-0.00377	-0 00365	-0.00585

Figure E-8. Gear, Ground, Ground Spoiler, Flap Effects - Point Design and Canard Spanloader Aircraft

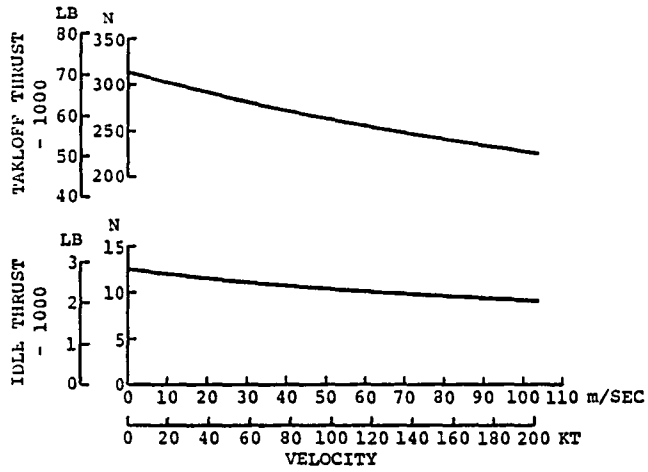

Figure E-9. Thrust Available per Engine - Single Body Reference Aircraft

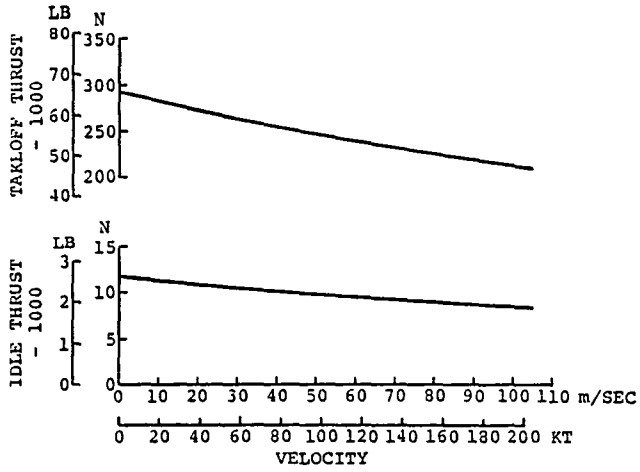

Figure E-10. Thrust Available per Engine - Two-Body MB1 Aircraft

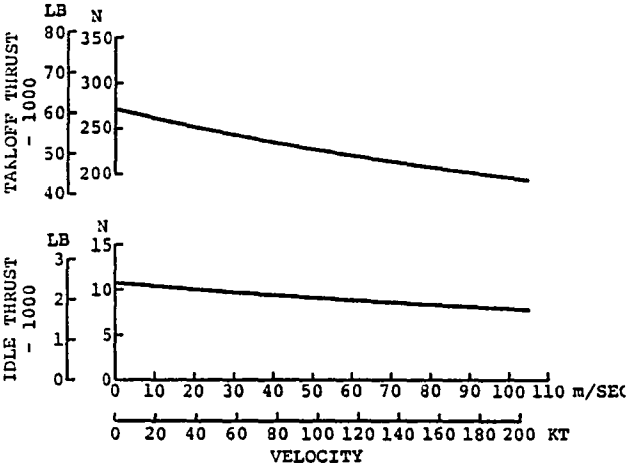

Figure E-11. Thrust Available per Engine - Two-Body MB2 Aircraft

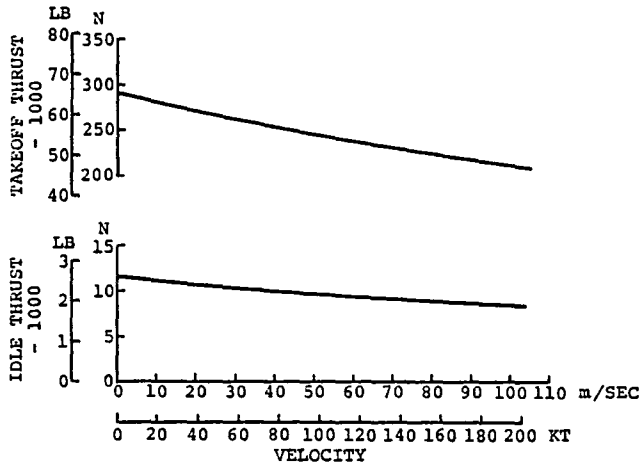

Figure E-12. Thrust Available per Engine - Three-Body MB3 Aircraft

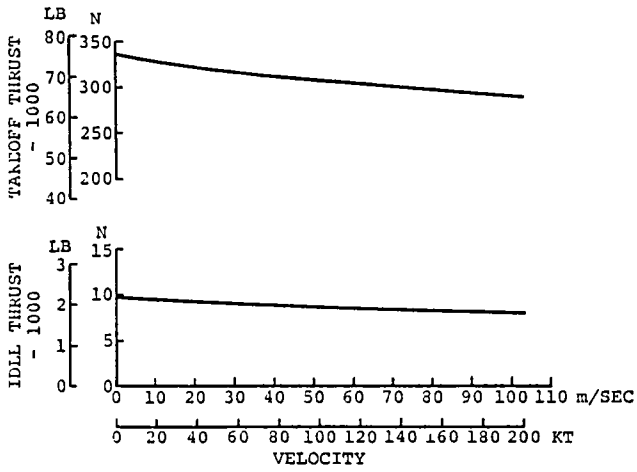

Figure E-13. Thrust Available per Engine - Canard Spanloader

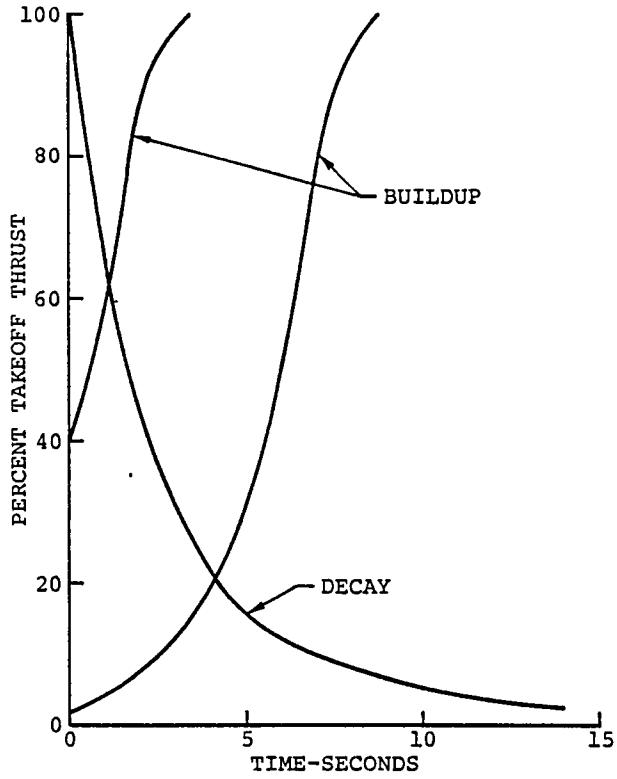

Figure E-14. Acceleration/Deceleration - Typical Advanced Technology Engine

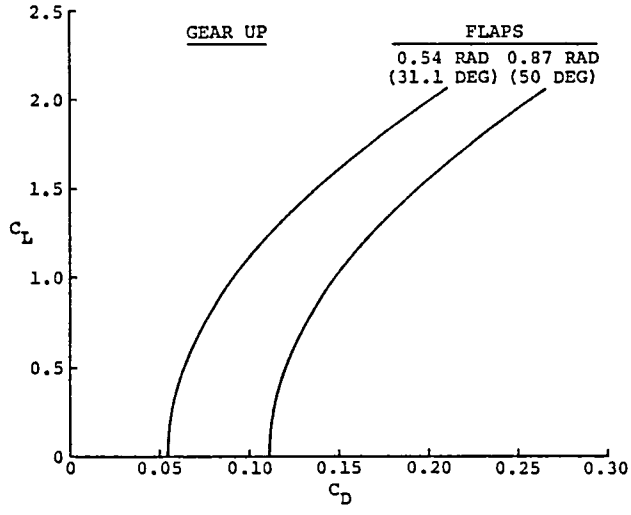

Figure E-15. Drag Polar - Approximate - Single Body Reference Aircraft

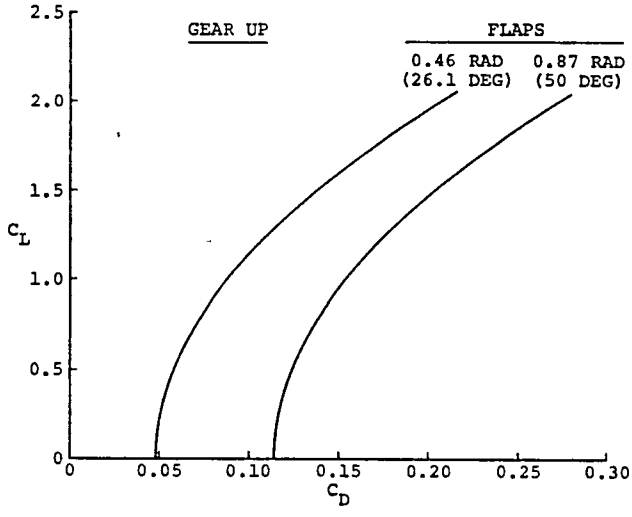

Figure E-16. Drag Polar - Approximate - Two-Body MB1 Aircraft

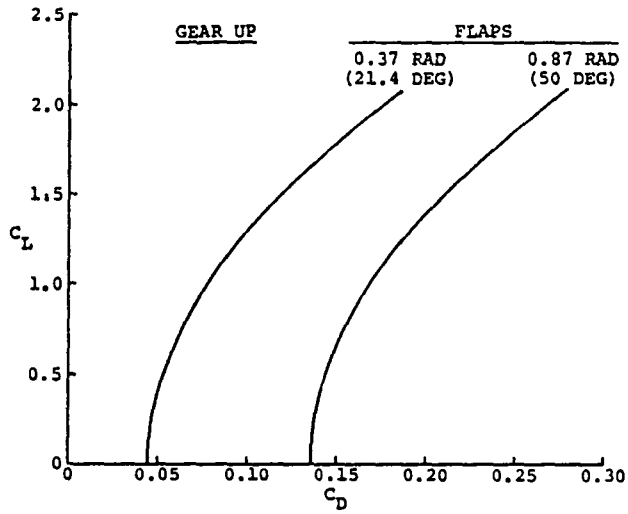

Figure E-17. Drag Polar - Approximate - Two-Body MB2 Aircraft

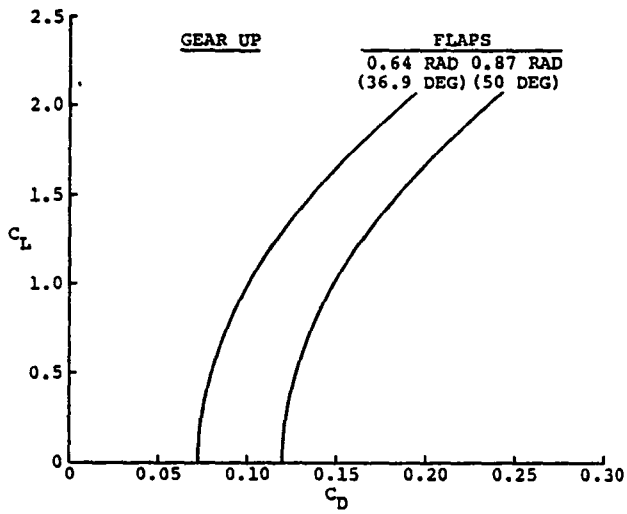

Figure E-18. Drag Polar - Approximate - Three-Body MB3 Aircraft

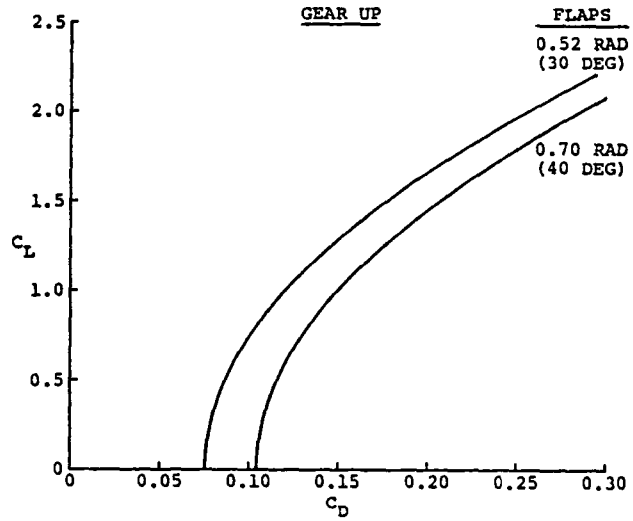

Figure E-19. Drag Polar - Approximate - Canard Spanloader

LIST OF SYMBOLS/ABBREVIATIONS

ACFT	Aircraft
ACQ	Acquisition
A_c/A_f	Fuselage Efficiency = $\frac{\text{container x-sec area x no. of sticks}}{\text{fuselage x-sec area}}$
AEDC	Arnold Engineering & Development Center
ALT	Altitude
AR	Aspect Ratio
ASTF	Aeropropulsion Systems Test Facility
ATA	Air Transport Association
ATNM	Available - Ton - Nautical Mile
b	Wing span
BF	Block fuel
BL	Baseline
BPR	Bypass Ratio
c	Chord
CAB	Civil Aeronautics Board
C_{D_c}	Compressibility Drag Coefficient
CG	Center of Gravity
CC_c1C	Unit lift
$CC_l/C_{av}C_L$	Spanwise lift distribution
$\bar{c}$	Mean aerodynamic chord
C_{av}	Average chord
C_L	Total wing lift coefficient
C_l	Section lift coefficient
℄	Centerline
CU FT	Cubic feet
D, d	Fuselage body diameter
D_f/b	Diameter fuselage/wing span
$d/[b/2]$	Body width to wing semispan ratio
DOC	Direct Operating Cost

e	Wing span efficiency
EA	Elastic axis
EPNdB	Equivalent Perceived Noise Level - Decibels
ETA	Engine power setting and Percent Body Location
FAR	Federal Aviation Regulation
FT	Feet
FVR	Fuel Volume Ratio
GAL	Gallon
GASP	Generalized Aircraft Sizing and Performance
GW	Gross Weight
Hz	Hertz (cycles/sec)
I	Moment of Inertia
k	1000
KEAS	Knots Equivalent Airspeed
KTAS	Knots True Airspeed
Kts	Knots
KWSS	Secondary Structure Weight per unit total wing area and Mach number
L/D_e	Fuselage Fineness Ratio (Length/Equivalent Dia.)
L/D	Lift/Drag
LB	Pounds
M	Mach number
M_c	Cruise Mach number
MAC	Mean aerodynamic chord

max	Maximum
MB1	Two-Body Aircraft (Straight Taper Wing)
MB2	Two-Body Aircraft (Unswept Center Section Wing)
MB3	Three-Body Aircraft
N_E	Number of Engines
N_{z_u}	Ultimate load factor for gross weight
N_z	Ultimate load factor
NM	Nautical mile
NP	Neutral Point
NWLO	Nosewheel liftoff at rotation speed
OW	Operating weight
OWE	Operating weight empty
P&WA	Pratt and Whitney Aircraft Company
P	Roll acceleration (radians/sec)
PLD	Payload
PSF	Pounds per square foot
PSI,	Pounds per square inch
R_e	Wing mounted nacelle, pylon, and engine weight to gross weight ratio
R_{fus}	Wing mounted fuselage, payload, and tail weight to gross weight ratio
RS_{ow}	Outer wing to total wing area ratio
RS_{iw}	Inner wing to total wing area ratio
R_{tax}	Taxi to maneuver load factor ratio
R_{zfw}	Zero fuel weight to gross weight ratio
RDT&E	Research & Development Test & Engineering
RFP	Request for proposal
RNG	Gust to maneuver load factor ratio
RT	Rated thrust

S	Wing area
S_f	Wing frontal area
S_h	Horizontal tail area
S_w	Total wing area
SBR	Single Body Reference
SFC	Specific fuel consumption
SM	Static margin
SOW	Statement of Work
SQ FT	Square feet
SS	Semispan
STA	Station
STR	Structure
T	Thrust
t/c	Thickness to chord ratio
$(t/c)_e$	Equivalent wing thickness ratio (%)
$(t/c)_{eff}$	Effective thickness to chord ratio
$(t/c)_{ow}$	Outer wing effective thickness ratio (%)
$(t/c)_{iw}$	Inner wing effective thickness ratio (%)
Takeoff F/O	Flyover noise point
Takeoff S/L	Sideline noise point
TBD	To be determined
T.C.	Trip cost
T.O.	Takeoff
T.O. WT	Takeoff weight
TOD	Takeoff distance
TS, T_s	Tension stress
$\bar{V}$	Tail volume coefficient
V_e	Equivalent airspeed
V_h	Horizontal tail volume coefficient
V_s	Stall speed

V_{sl}	Stall speed with landing flaps
VLM	Vortex lattice method
V_v	Vertical Tail Volume Coefficient
w	Distance between fuselages
W	Weight
W_G	Gross weight
W_{ss}	Weight - Secondary Structure
W_w	Wing weight
W_{zf}	Zero fuel weight
W/S	Wing loading
x/c	Point location along chord
Y	Lateral CG location consistent with W_{zf}
Y/SS	Fuselage (CG) lateral location to semispan ratio
Y/b	Fuselage (CG) lateral location to wing span ratio
$(\Delta n_t)_{LG}$	Incremental inner wing coefficient for 2.0g taxi due to landing gear location inboard of fuselage
ϵ_{ea}	Unit chord location of elastic axis
η	Body location in percent semispan and engine power setting
η_{al}	Unit spanwise location of wing airload
$(\eta_{al})_{ow}$	Unit spanwise location of outer wing airload
η_b	Unit spanwise location of planform break
η_e	Engine location
η_{fus}	Unit spanwise location of fuselage centerline
η_{lg}	Unit spanwise location of main landing gear
η_m	Unit spanwise location of total wing mean chord

$\bar{\eta}_a$	Correction factor for effective lift
$(\bar{\eta}_a)_{ow}$	Outer wing correction factor
$(\bar{\eta}_a)_{iw}$	Inner wing correction factor
$\bar{\eta}_e$	Unit spanwise loaction of engine CG
$\bar{\eta}_g$	Gust correction factor
$\bar{\eta}_t$	Taxi correction factor for 2.0g taxi
Λ	Wing sweep angle
$\Lambda_{c/z}$	Mid-chord sweep angle
Λ_{le}	Leading edge sweep angle
λ	Taper ratio
λ_b	Break chord ratio
λ_e	Equivalent taper ratio
λ_r	Total root chord to reference wing root chord ratio
$\bar{\lambda}$	Total wing average chord to reference wing root chord ratio
ϕ	Bank angle
$C_{L_{max}}$	Maximum lift coefficient
C_{L_α}	Lift curve slope
C_{M_α}	Pitching moment curve slope
$C_{M_{z_1}}$	Pitching moment at zero lift
$C_{M_{\dot{\alpha}}}$	Pitching moment due to α
C_{M_q}	Pitching moment due to q
$C_{M_{\delta_e}}$	Pitching moment due to elevator deflection
$C_{L_{\delta_e}}$	Lift due to elevator deflection
$C_{M_{i_H}}$	Pitching moment due to stabilizer incidence
$C_{L_{i_H}}$	Lift due to stabilizer incidence

C_{n_β}	Yawing moment due to sideslip
C_{l_β}	Rolling moment due to sideslip
C_{γ_β}	Side force due to sideslip
C_{n_p}	Yawing moment due to roll rate
C_{l_p}	Rolling moment due to roll rate
C_{γ_p}	Side force due to roll rate
C_{n_r}	Yawing moment due to yaw rate
C_{l_r}	Rolling moment due to yaw rate
C_{γ_r}	Side force due to yaw rate
$C_{n_{\delta_r}}$	Yawing moment due to rudder deflection
$C_{l_{\delta_r}}$	Rolling moment due to rudder deflection
$C_{y_{\delta_r}}$	Side force due to rudder deflection
$C_{l_{\delta_a}}$	Rolling moment due to aileron deflection
$C_{n_{\delta_a}}$	Yawing moment due to aileron deflection
S_{ref}	Aircraft reference area
b_{ref}	Aircraft reference span
$\bar{c}_{ref}$	Aircraft reference mean aerodynamic chord
CG	Center of gravity, % c
I_{xx}	Roll moment of inertia
I_{yy}	Pitch moment of inertia
I_{zz}	Yaw moment of inertia

I_{xz}	Product of inertia
δ_f	Wing flap deflection
δ_e	Elevator deflection
i_h	Horizontal stabilizer incidence
δ_r	Rudder deflection
δ_a	Aileron deflection
V_s	Stall speed
V_{App}	Approach speed
M	Mach number
β	Sideslip angle
$\ddot{\phi}$	Roll acceleration
$\ddot{\psi}$	Yaw acceleration
$\ddot{\theta}$	Pitch acceleration
p	Roll rate
$\dot{p}$	Roll acceleration
n	Load factor
α	Aircraft angle of attack
α_{zl}	Aircraft angle of attack for zero lift
$\dot{\alpha}$	Rate of aircraft angle of attack change
q	Pitch rate
r	Yaw rate
T_{30^o}	Time to achieve a 30^o bank angle using full lateral control input
T_{double}	Time to double amplitude for a pitch axis instability
SM	Static margin
ϕ_{osc}/ϕ_{avg}	Ratio of the oscillatory component to the average component of bank angle following a rudder-pedals-free impulse aileron input (see reference 3)

ψ_β	Phase angle in a cosine representation of the dutch roll sideslip component (see reference 3)
p_{osc}/p_{avg}	Ratio of the oscillatory component to the average component of roll rate following a rudder-pedals-free impulse aileron input (see reference 3)
$\Delta\beta_{max}$	Maximum sideslip excursion occurring within 2 seconds or one half-period of the dutch roll, whichever is greater, for a step aileron command (see reference 3)
k	Ratio of commanded roll performance to the applicable roll performance requirement (see reference 3)
$\omega_{n_{sp}}$	Short period natural frequency
δ_{sp}	Short period damping ratio
$\omega_{n_{dr}}$	Dutch roll natural frequency
δ_{dr}	Dutch roll damping ratio
τ_r	Roll mode time constant
$T_{\phi\ double}$	Spiral mode time to double bank angle

REFERENCES

1. Johnston, William M., et al., "Technical and Economic Assessment of Span-Distributed Loading Cargo Aircraft Concepts," NASA CR-145034 (prepared by Lockheed-Georgia Company), August 1976.

2. Whitlow, David H. and Whitener, P. C., "Technical and Economic Assessment of Span-Distributed Loading Cargo Aircraft Concepts," NASA CR-144963 (prepared by Boeing Commercial Airplane Company), June 1976.

3. "Technical and Economic Assessment of Span-Loaded Cargo Aaircraft Concepts," NASAA CR-144962 (prepared by McDonnell douglas Corporation), January 1976.

4. Whitehead, Allen H., Jr., "Preliminary Analysis of the Span-Distributed-Load Concept for Cargo Aircraft Design," NASA TM X-3319, Langley Research Center, December 1975.

5. Hess, John L., "Calculation of Potential Flow About Arbitrary Three-Dimensional Lifting Bodies," Naval Air Systems Command, MDC J5679-01 (prepared by Douglas Aircraft Company, McDonnell Douglas Corporation), October 1972.

6. Miranda, Luis R., Elliot, Robert D., and Baker, William M., "A Generalized Vortex Lattice Method for Subsonic and Supersonic Flow Applications," National Aeronautics and Space Administration, Report 2865 (prepared by Lockheed-California Company), December 1977.

7. "Military Specification, Flying Qualities of Piloted Airplanes," MIL-F-8785 (ASG)-4, August 1969.

8. Silvers, Charles L., and Withers, Clifton C., "Evaluation of the Flying Qualities Requirements of MIL-F-8785B(ASG) using the C-5A Airplane," Air Force Flight Dynamics Laboratory, AFFDL-TR-75-3 (prepared by Lockheed-Georgia Company), March 1975.

9. Moore, J. W., et al., "Peripheral Jet Air Cushion Landing System-Spanloader Aircraft," Volume 1, Air Force Flight Dynamics Laboratory, AFFDL-TR-79-3152 (prepared by Lockheed-Georgia Company), December 1979.

1 Report No.	2. Government Accession No	3. Recipient's Catalog No
NASA CR-165829		

4 Title and Subtitle	5 Report Date
MULTIBODY AIRCRAFT STUDY Volume II	December 1981 6 Performing Organization Code

7 Author(s)	8 Performing Organization Report No
J. W. Moore; E. P. Craven; B. T. Farmer; J. F. Honrath; R. E. Stephens; C. E. Bronson, Jr.; R. T. Meyer; and J. G. Hogue	LG81ER0259 10 Work Unit No

9 Performing Organization Name and Address	11 Contract or Grant No
LOCKHEED-GEORGIA COMPANY 86 South Cobb Drive Marietta, Georgia 30063	NAS1-15927 13 Type of Report and Period Covered Contractor Report Sept 1979 thru Sept 1981

12 Sponsoring Agency Name and Address	14
NATIONAL AERONAUTICS AND SPACE ADMINISTRATION Langley Research Center Hampton, Virginia 23665	

15 Supplementary Notes

NASA Program Manager: D. V. Maddalon

16 Abstract

The purpose of this report is to quantify and provide technical substantiation of the potential benefits of a multibody aircraft when compared to a single body aircraft. The analyses consist principally of a detailed point design analysis of three multibody and one single body aircraft, based on a selected payload of 350,000 kg (771,618 lb), for final aircraft definitions; sensitivity studies to evaluate the effects of variations in payload, wing semispan body locations, and fuel price; recommendations as to the research and technology requirements needed to validate the multibody concept.

Two, two-body, one, three-body, and one single body aircraft were finalized for the selected payload, with DOC being the prime figure-of-merit. When compared to the single body, the multibody aircraft showed a reduction in DOC by as much as 11.3 percent. Operating weight was reduced up to 14 percent, and fly-away cost reductions ranged from 8.6 to 13.4 percent.

Weight reduction, hence cost, of the multibody aircraft resulted primarily from the wing bending relief afforded by the bodies being located outboard on the wing.

Wind tunnel tests and flight simulation are recommended so as to better understand the aerodynamic characteristics in order to assure an acceptable level of risk in the design and development of a large multibody aircraft. For this same reason, further structural investigations are required in such areas as dynamic loads, load alleviation, unsymmetrical loadings, flutter, and material application.

17 Key Words (Suggested by Author(s))	18 Distribution Statement
Multibody, Two-Body, Three-Body, Single Body, Point Design, Wing Span Efficiency, Load Distribution, Vorlax, Hess	Unclassified-Unlimited

19 Security Classif (of this report)	20 Security Classif (of this page)	21 No of Pages	22 Price*
Unclassified	Unclassified	233	

*For sale by the National Technical Information Service, Springfield, Virginia 22161

End of Document